DOCTOR THESIS

PHYSICO-CHEMICAL PROPERTIES AND APPLICATIONS OF CONDUCTIVE ALUMINA WITH NANO-CARBON NETWORKS FABRICATED BY COMBINATION OF GELCASTING AND REDUCTIVE SINTERING

ゲルキャスティング法及び還元焼結法により創製した
ナノカーボンネットワークを有する導電アルミナの物理化学的特性とその応用

CHUNXI HAI

海 春喜

19513315

SEPTEMBER 2012

DOCTOR OF ENGINEERING

FRONTIER MATERIALS

NAGOYA INSTITUTE OF TECHNOLOGY

JAPAN

PHYSICO-CHEMICAL PROPERTIES AND APPLICATIONS OF CONDUCTIVE ALUMINA WITH NANO-CARBON NETWORKS FABRICATED BY COMBINATION OF GELCASTING AND REDUCTIVE SINTERING

ゲルキャスティング法及び還元焼結法により創製した

ナノカーボンネットワークを有する導電アルミナの物理化学的特性とその応用

CHUNXI HAI

海　春喜

19513315

SEPTEMBER 2012

TABLE OF CONTENTS

CHAPTER 1

INTRODUCTION

1.1. Applications and evaluation methods of electrically conductive porous ceramic

Electrically conductive ceramic combing the merits of ceramic and conductive candidate is a kind of functional composite with various potential applications, which is determined by its novel structure. Therefore, it is reasonable that electrically conductive ceramic composites have gained a surge of increased attentions as high performance heaters [1], catalysts [2-3], electrodes [4-8] etc. via different methods recently. Up to now, even though numerous possible applications are available for kinds of conductive ceramic composites, the most utilization is as heater and electrode, which is mainly determined by high accessible specific surface area, high effective and efficiency, good electrical conductivity etc. More, it is noticed that both heater and electrode are good energy converter or accelerator, by which various reactions can be progressed via different routes. This merit also actuates researchers to find a novel energy converter candidate with high effective and efficiency in order to meet the research demand.

- *Electrode*

Commonly, besides metal and semiconductor, composites with electrical conductivity are also good electrode candidates. Depending on different applications, electrode materials are also varied. Generally, various carbon forms are universally employed as electrodes by different modifying technologies. So far, these composites involve Pt/CNT, Pd/CNT (CNT means carbon nanotubes) [4], graphite nanosheets (GNS)/silicon oxycarbide (SiOC) [5], Hydroxyapatite (HA)/multi-walled carbon nanotubes (MWCNTs) [6], Nitrogen-containing carbon nanotubes (NCNT) [7], Iron Phthalocyanine (FePc)/Carbon [8] etc. By surface modification of carbonaceous substrates, selective reaction is possible to be designed. Based on the available techniques and materials, it is wondered if it is possible to develop a novel ceramic electrode candidate with electrical conductivity, physical-chemical stability and good mechanical strength.

- *Heater*

Conductive material especially that with porous form is also good heater meriting from high porosity induced high accessible specific surface area and thermal insulation of matrix. Usually, it is utilized for various organics decomposition or dehydrogenation. Transfer hydrogenation (TH) processing with stable hydrogen donors (e.g. 2-propanol) are highly advantageous methodologies in organic synthesis for the hydrogenation of a range of compounds which includes carbonyl compounds and related substrates [9-11]. These protocols are generally

simpler and more environmentally friendly as they avoid the use of molecular hydrogen (avoiding explosion risks, leaks and related hazards), high-pressure devices and favor mild reaction conditions that always lead to improved selectivity. Among such milder reaction conditions, these processes have been confirmed to be high efficient way for providing hydrogen generation system.

Especially, an extensive research on the generation of hydrogen by decomposition and reforming of alcohol at the aid of different methods has been reported [12-27]. These methods involve electrochemical evaluation (EE) [12-17], photo-catalytic evaluation (PE) [18-20], and microwave-assisted heating [21-24], ultra-high-vacuum (UHV) [25-26] etc. More, organic decomposition routes always change with different catalyst and evaluation method.

As heater, microwave-induced absorbents are good non-contacting heaters in many reactions. Microwave-assisted heating is regarded as more ideal method for various alcohol decompositions. In particular, microwave-assisted heating for various reactions have been intensively investigated during the last decades. Benefits of microwave-assisted heating are increased reaction rate and selectivity [28]. Microwave energy interacts with material at the molecular level. During the microwave heating of a dielectric, internal electric fields are generated within the material. Such fields can produce translation of electrons and ions and cause rotation of charged species. This movement can be opposed by friction, inertia and other forces that can lead to attenuation of the electric fields and to volumetric heating of the material. Either the ability of microwave electric field to polarize molecules or the ability of these molecules to follow the rapid reversal of the electric field, results in the conversion of electromagnetic energy to heat within the irradiated material.

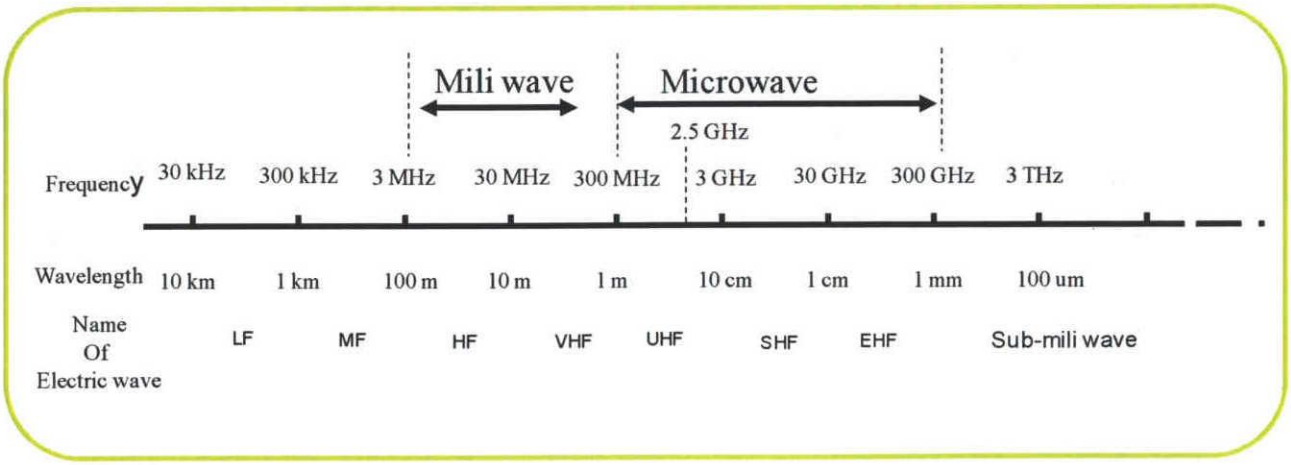

Fig. 1.1. Definition of electromagnetic wave

Herein, benefiting from these merits, it is plausible that a surge of interest has been attracted onto microwave absorbers in recent decades especially for organic dehydrogenation or decomposition [28-33]. Herein, it is devoted to developing various high effective and efficiency

microwave absorbents (Type of electromagnetic wave has been shown in Fig. 1.1) in this study.

As shown in Fig. 1.1, microwave is electromagnetic wave with wavelengths ranging from as long as one meter to as short as one millimeter, or equivalently, with frequencies between 300 MHz (0.3 GHz) and 300 GHz. So far, briefly speaking, classifying with absorbing mechanism, there are three kinds microwave absorbers. These absorbents include high magnetic loss materials, dielectric loss material and compound materials. Among the fast progress of microwave absorbents, the dielectric materials used for higher frequency regions have the increased demand. Many microwave active ceramics with high quality factor (Q, $Q=1/\tan\delta$) and relatively low dielectric constant (ε_r) as well as low temperature coefficient of resonant frequency have been extensively studied for such specific applications. In addition, the development of low-temperature-cofired ceramics (LTCC) for microwave applications has been paid an increased attention especially for designing multilayer materials with electrical performance employing kinds of internal metals (such as Ag/TiO_2) [36-37]. Wherein, it is reasonable that various multi-phases composites have been explored according to their applications in different fields and targets.

Furthermore, so far, the commonly utilized microwave-assisted organic decomposition catalysts include: (a) Carbon-support catalyst, such as oxidized carbon (D43/1) [29], Pt/Norit [21], Ni/MWNTs [32] etc., one of the important features of carbon support is its inertness, (b) Bimetallic catalysts, e.g. Co-Pd [25], (c) Metallic/Ceramic catalyst, e.g. Me/MgO [25], Cu/ZnO [30], Pt/CeO_2, Rh/CeO_2 and Pd/CeO_2 [34] etc. and (d) Ceramic catalyst, for example TiO_2 [33], mesoporous SiO_2 (MCM-41) [35] etc.

1.2. Limitations of energy converter and available solutions

Based on above analysis, it is facilitated to get a conclusion that high effective electromagnetic wave absorptive material at microwave frequency requires wider operating bandwidths, thinner in the dimension and low density. Complex permittivity ($\varepsilon= \varepsilon'-\varepsilon''$) and permeability ($\mu=\mu'-j\mu''$) of the absorbents play key roles in determining the absorption properties. It is well known that high efficiency absorber indicates high permeability and moderate permittivity. Metallic magnetic material (Co, Me, Cu, Ni, Pt, Pd, Ag etc.) always have large saturation magnetization. More, it is reasonable their permeability values could remain high at high frequencies according to Snoek limit [38]. However, the decreased permeability of metallic materials at low frequency due to the eddy current effect propels researchers to find novel absorbents with good magnetic/dielectric loss compound match.

Even though a series of absorbents with magnetic/dielectric loss match have been reported [25,32,30,34,37,38], it is still a challenge to discover a suitable absorbent which not only meets the demonstrated demand in practical application but also has various merits such as low cost, environmentally friendly, simple preparing technology etc. Simultaneously, it is regarded that ceramic bodies with electrical or thermal conductivity could resolve the difficulty we are facing

and their absorbability result from dielectric loss under microwave irradiation.

Up to now, benefiting from the considerably low density (3.2 $g \cdot cm^{-3}$), adjustable electrical resistivity, good oxidation resistance and super high temperature stabilities, SiC with various forms are the most commonly used absorbents [39-43]. However, high cost and too complicated preparing technology still inhibit the further extensive practical application. Therefore, it is so emergent and significant to develop a novel low cost ceramic-based absorbent with high effective and efficiency.

Although it was reported that sapphire (α-Al_2O_3) single crystals occupies the lowest microwave dielectric loss among all of the known crystal materials [44], Wei et al.[38], Liu et al. [45], Janes et al. [46] and Kaur group [47] also announced the possible application of α-Al_2O_3-based composites as microwave absorbers at the aid of some effective decoration ways. Herein, it would be very intriguing if an alumina related composite with good microwave capacity and electrical conductivity could be developed.

1.3. Preparing methods of Al_2O_3-based composite with electrical conductivity and microwave absorbability

It is noticed that most of alumina-matrix microwave absorbers are commonly modified with different ferrotype metallic particles as introduced in references [45-48]. These particles include Fe, Co, Pd, Cu, Pt etc. Furthermore, as-mentioned composites also announce their activity as electrocatalyst. Electrochemical and microwave activities can be enhanced by making suitable match between matrix and particles. More, it is interesting if it would be possible to develop a Al_2O_3 supported composite which not only has good functional activity but also can overcome some defects of ceramic such as insulation, fragility etc. Taking these factors into consideration, it is so emergent, significant and necessary for us to discover a novel multi-functional composite with electrical conductivity and microwave absorbability.

For electrically conductive ceramic material, so far, several methods have been attempted. Briefly, to overcome the electrical insulation of ceramic, metal or conductive oxides were commonly most reported. The key point of this method is making physical contacted a great number of cross-linked conductive pathways or networks allowing electron transferring vehicles, thereby forming high electrical conductivity.

Comparing with metallic additives, various carbon forms especially for graphite, carbon nanotubes (CNT) with graphitic structure are regarded as super-electrical conductor and dielectric loss microwave absorbents candidates [49-56]. Bockrath et al. [49] has reported the electrical properties of individual bundles or "ropes" of single-walled carbon nanotubes (SWNT). According to them, it was claimed that structure of SWNT (diameter and helicity) determines its conducting properties. Usually, a CNT can be imaged as a piece of rolled graphene creating a seamless cylinder (Fig.1.2 (A)). To a large part, good electrical conductivity merits from the peculiar electronic structure of graphene [50]. In graphene sheet, its band structure and the

hexagonal shape of its first Brillouin zone are discovered as displayed in Fig. 1.2 (B). It is noticed that the valence π and conduction π^* state are seen to join at six points lying at the Fermi energy (Fermi points). In the same graphene sheet, electron motion route changes with direction (Γ-K direction and K-points) encountering semiconductor-like band gap or metallic-like behaviors. More, meriting from the unconventional quantum Hall effect of various carbon forms with graphitic structure, graphene responses to magnetic field irradiation. Mechanism of graphene sheet microwave activity has been well discussed by Meera et al. [51]. A schematic of this situation is shown in Fig.1.3. In their principle, a monolayer graphene sheet is considered to be placed in the *XY* plane. A plane electromagnetic wave with wave vector q_0 is made incident at an arbitrary angle denoted by θ_0 with respect to the normal to the plane of the graphene sheet (along the Z axis). The incident wave is regarded as to be elliptically polarized, which is the most general way of considering a plane wave, with its electric field written as a linear combination of the two polarization directions, defined by the two unit vectors denoted by $\hat{u}_1$ and $\hat{u}_2$. The incident polarization is known as the aspect ratio of the incident polarization ellipse.

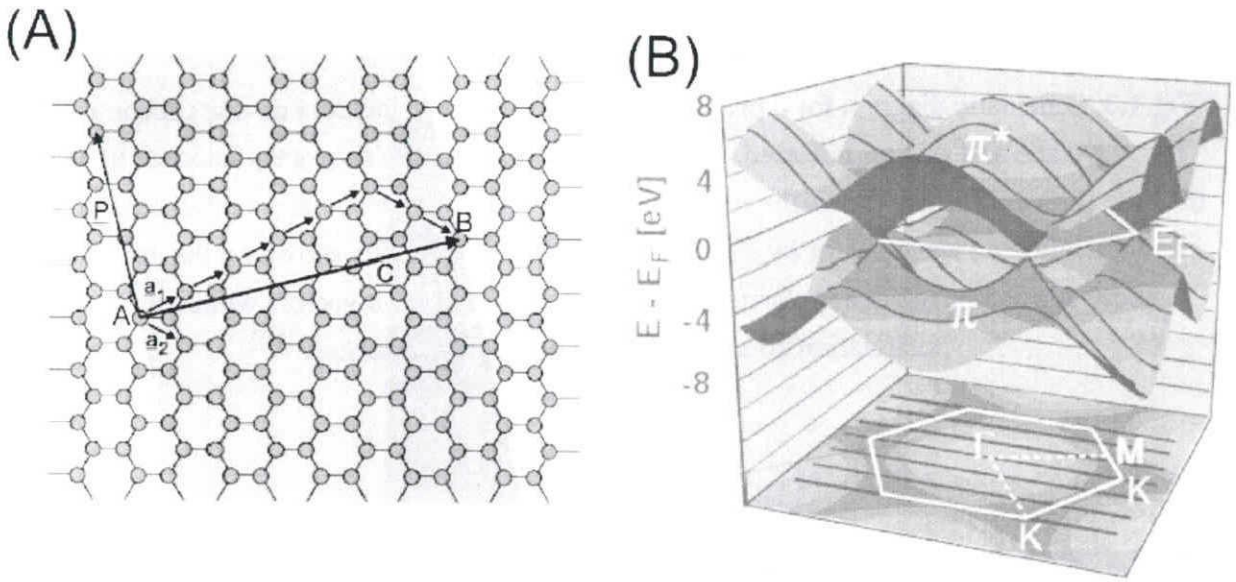

Fig.1.2. (A) Graphene sheet and (B) Top: Band-structure of the 2D graphene sheet (gray surface). The calence and condution band meet at six points (K-points) lying at the fermi energy. Bottom:The first brillion zone of graphene. The black lines represent the allowed states of a (3, 3) nanotube.[50]

According to the same principle, carbon with quasi-graphene structure is good microwave absorptive candidates. Simultaneously, it is intriguing to explore a novel electrical conductive alumina (CA) carbon/Al_2O_3 composite. To date, several techniques have been developed to fabricate Al_2O_3-based electrical composites [57-63]. These methods involve hot press [61], spark plasma [62], sol-gel [63] etc. However, it is still difficult to make uniform dispersed conductive networks (CN) in Al_2O_3 matrix. Various carbon forms acting as additive are facilitated to

agglomerate in composite leading to segregated conductive phase and weak bending strength.

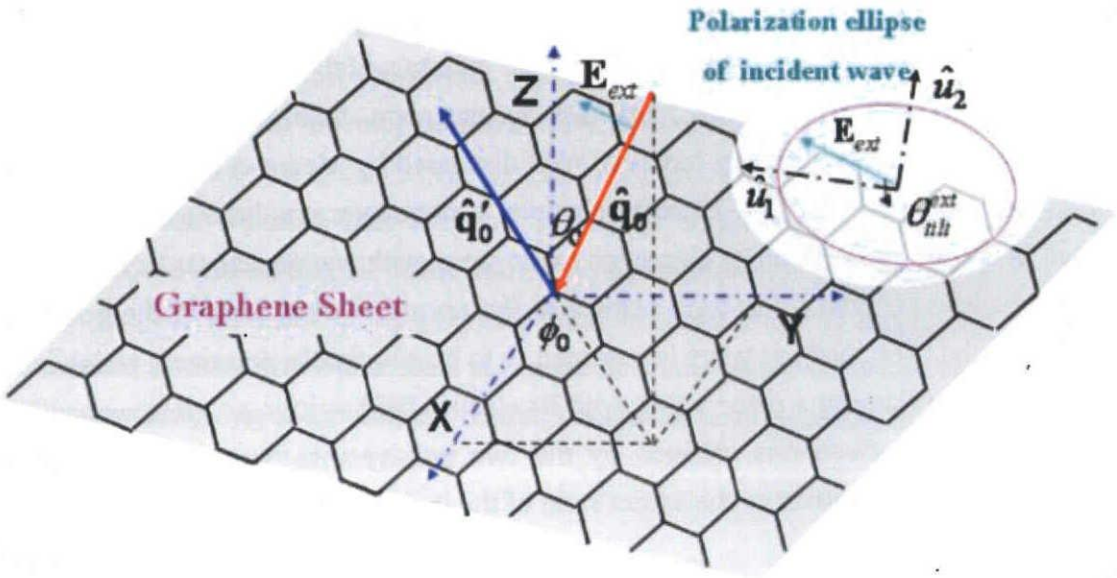

Fig.1.3. Schematic diagram for a plane electromagnetic wave incident on a graphene sheet in the $X\,Y$ plane and getting reflected. The red (downward) arrow shows the incident light and the blue (upward) arrow shows the reflected light, with the incident wave vector denoted by q^0 and the reflected wave vector by q'_0. The incident electric field is shown by the green (light grey) allow. The incident polarization ellipse and the two unit vectors which define the polarization components are also shown separately. [51]

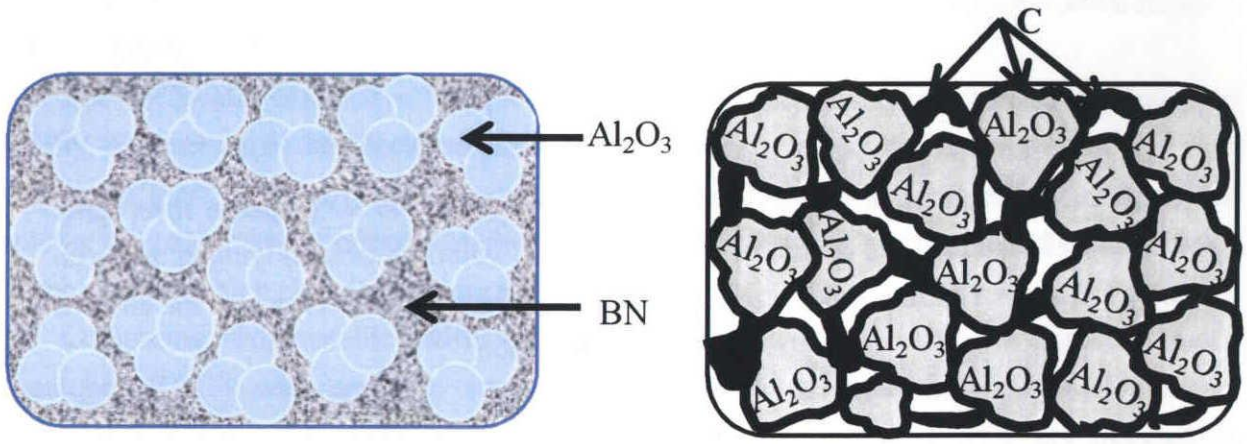

BN: Binder networks

(A) (B)

Fig. 1.4. Ideal models of microstructure by gelcasting and HTRS from (A) green body to (B) sintered body

Thus, that is certainly necessary to explore a new process that not only is simple and direct method, but also provides homogeneously dispersed conductive networks.

Then, as introduced in our group [64-65], electrically conductive alumina (CA) with two forms dense and porous, namely CDA and CPA, were fabricated by the combination of gel-casting and high temperature reductive sintering (HTRS) in argon atmosphere.

Gelcasting has been widely believed as a novel near-net-shape forming method derived from traditional ceramics and polymer chemistry [64-68]. This process is based on the polymerization of organic monomers and simultaneous solidification of concentrated slurry to green bodies. Especially, gelcasting provides a rapid forming cycle, good wet and dried strength making large parts at low cost. During gelcasting proceeding, polymerization of monomer (Methyacrylamide) was free radically initialized by ammonium persulfate. There are two available procedures in casting procedures, namely generation of free radicals by initiator and catalyst (Tetramethyl ethylene diamine) and polymerization of free radicals and monomer. By gelcasting, Al_2O_3 grains were cross-connected by polymer binder networks (as shown in Fig. 1.4 (a), BN means binder networks).

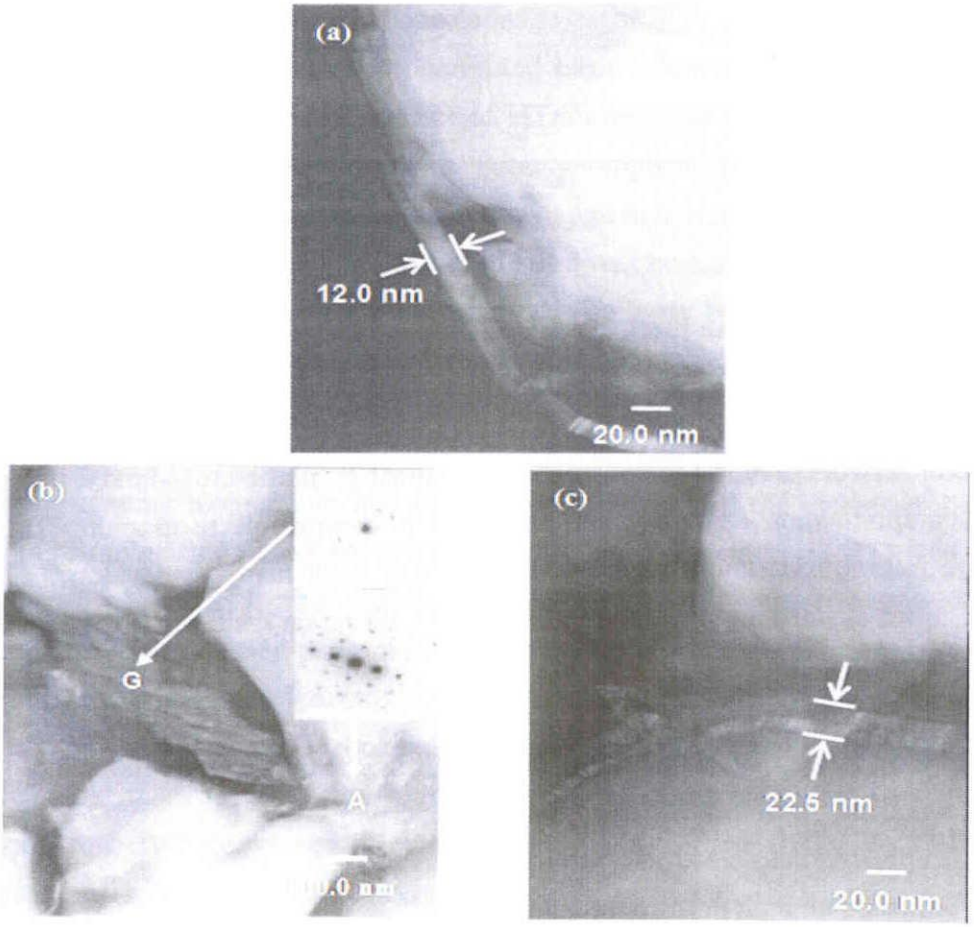

Fig. 1.5. TEM images of CA (G = Graphite, A =Alumina)

As-received alumina green bodies were reductively sintered in novel atmosphere resulting nano-carbon networks (NCN) with graphitic structure (as shown in Fig. 1.4 (b)) in CA. The NCN was converted from polymer binder networks via HTRS. And the graphitization degree of carbon changes with HTRS temperature as introduced by Kato et al. [69] CA sintered at 1700 °C in Ar owns good graphitic orientation as good as graphite. As shown in Fig. 1.5, morphologies of CA are shown. It is known that graphite and alumina co-exist in this binary composite. More, the graphitic structure of NCN is detected by Raman spectroscopy as shown in Fig. 1.6, which claims typical graphitic crystal structure of NCN in CA. The hexagonal electronic energy dispersive feature of two-dimensional graphene also has been reported by Skipa et al.[76].

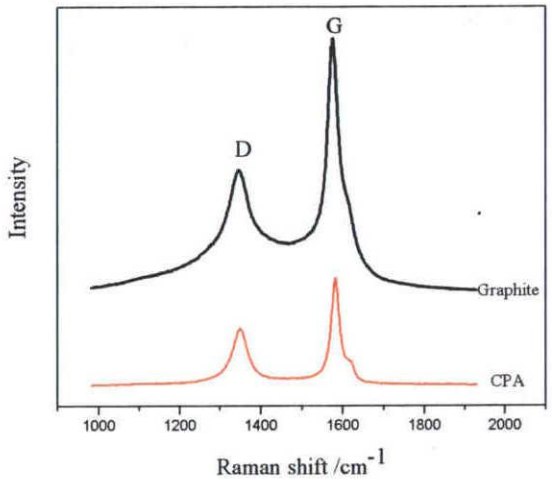

Fig. 1.6. Raman spectroscopy of CPA and Graphite reference

Nano-carbon networks (NCN) forms three-dimensional graphitic cross-linked paths in CA. Typically, high graphitization degree of carbon in CA is comparable to graphite. Taking this unique structure into consideration, various attempts have been made to develop its different potential applications as introduced in references [70-75]. Based on their study, several items are concluded as follows:

- Good isotropic electrical conductivity of CA meriting from NCN
- Physical and chemical stability in aggressive condition
- Possible application as electrode materials in fuel cells
- Three-dimensional high porosity composite
- Necessary of improving electro-activity via suitable methods

1.4. Thesis statement and Thesis organization

In this thesis, it is aimed at developing potential applications of electrically conductive alumina (CA) as energy converter by electrochemical and microwave irradiation methods. All of the attempts benefit from the unique graphitic nano-carbon networks (NCN) in CA. By discussing the physico-chemical properties of CA in much more detail, various vehicles have been proposed to enhance its performances. Then, this thesis is expected to explore available applications of CA by suitable structural or surface modifications.

Besides of this chapter, there are five chapters for arranging this thesis as follows:

In chapter 2, electrochemical activity of CPA was demonstrated. In order to increase its performances, briefly speaking, two methods had been conducted, that was covalent modification and heterogeneous particles decoration. It was supported that increased electrochemical activity of CPA by covalent functionalization was attributed to the increased hydrophilicity, by which larger real active surface was reached. Comparing with as-received CPA, Pt and Ni particles modification resulted in the enhanced behaviors. Finally, advantages and limits of CA as cell electrode were concluded.

In chapter 3, physico-chemical property and basic microwave absorption behavior of CA were investigated. By discussing the effect of HTRS temperature, porosity carbon content and size of CA, it was devoted to developing the potential application of CA as microwave absorber. By discussing different effect factors, microwave-assisted non-contacting heating of CA for non-polar paraffin liquid under microwave irradiation was investigated.

In chapter 4, considering the crystal structure similarity between NCN in CA and carbon nanotubes (CNT), another novel conductive alumina (CA, CNT/NCN/Al_2O_3 (CNT/CPA)) was fabricated employing CNT as structural modifying element. Before making CNT/Al_2O_3 slurry, as-received CNT was covalently pre-treated with concentrated acids at different conditions (investigating treating temperature and time), it was known that the increased dispersibility of CNT merited from grafted functional groups. By the same gelcasting and HTRS in Ar with CPA, CNT/CPA was fabricated. In this chapter, it was expected to make a CNT reinforced ternary composite (CNT/NCN/ Al_2O_3) with enhanced microwave absorptive absorbability. The related influence factors have been well discussed.

In chapter 5, surface modifications of substrates were completed by uniformly dispersed Pt nanoparticles by microwave-assisted irradiation method. Substrates were CPA and CNT/CPA. Briefly speaking, two components, namely Al_2O_3 and carbon (NCN or CNT/NCN) with three-dimensional graphitc structure were available in matrices. Al_2O_3 grains were microwave transparent while carbon was microwave active. Then, it was possible to realize the selective deposition of Pt nanoparticles on matrix. Moreover, comparing with conventional heating method, more simple, ultrafine and selective deposition of Pt nanoparticles on substrate was

arrived by microwave irradiation. Benefiting from the metal/dielectric loss match in as-received composites, the increased microwave absorptive heating performance of multi-phase composite was achieved.

Finally, in chapter 6, the concluding remarks of the present work were stated and the future directions of this research work were recommended.

1.5. Thesis innovations and significances

✧ ***(Innovations)***

- Enhanced electro-chemical activity of CPA was developed via methods
- Microwave absorbability of binary dielectric electrically conductive alumina (CA) was discovered
- Potential application of CA as passive heating Elements (PHEs) for non-polar liquid was explored
- A novel conductive porous alumina (CPA) structurally modified by CNT was fabricated, which has enhanced microwave absorptive behavior
- Ultrafine Pt nanoparticles was anchored on substrates (CPA and CNT/CPA) via microwave irradiation method
- Increased microwave-assisted heating behaviors of metal/dielectric loss match composites (Pt/CPA and Pt/CNT/CPA) were demonstrated

✧ ***(Significances)***

- Confirming the feasible way for conductive alumina (CA) with increased electro-chemical performance
- Demonstrating the possible application of conductive alumina (CA) as electromagnetic wave absorbent at microwave region.
- Announcing the feasibility of CNT reinforced ternary composite with enhanced absorptive performance
- Claiming the high efficiency way for preparing metal/dielectric composite employing CPA and CNT/CPA as substrate via microwave irradiation method
- Exploring the potential application of CA as microwave-assisted non-conductive heater

References

[1]. D. R. Hahn, Electrical Overseas/Electrostatic Discharge Symposium Proceedings, *EOS-17*, Phoenix, Arizona, September, **1995**, 154-161.

[2]. Yindee Suttisawat, Satoshi Horikoshi, Hideki Sakai, Masahiko Abe, Hydrogen production from tetralin over microwave-accelerated Pt-supported activated carbon, *Int. J. hydrogen energy*, 35, **2010**, 6179-6183.

[3]. Takashi Ohshima, Yoshiki Miyamoto, Junji Ipposhi, Yasuhito Nakahara, Masaru Utsunomiya and Kazushi Mashima, Platinum-Catalyzed direct amination of allylic alcohols under mild conditions: Ligand and Microwave effects, Substrate scope and Mechanistic study, *J. Am. Chem. Soc.*, 131, **2009**, 14317-14328.

[4]. Dominik Eder, Carbon Nanotube-Inorganic Hybrids, *Chem. Rev.*, 110. **2010**, 1348-1385.

[5]. Fang Ji, Ya-Li Li, Jianming Feng, Dong Su, Yangyang Wen, Yan Feng and Feng Hou, Electrochemical performance of graphene nanosheets and ceramic composites as anodes for lithum batteries, *J. Mater. Chem.*, 19, **2009**, 9063-9067.

[6]. Changjian Lin, Huijuan Han, Fang Zhang, Aimin Li, Eelctrophoretic deposition of HA/MWNTs composite coating for biomaterial application, *J. Mater. Sci: Mater. Med.*, 19, **2008**, 2569-2574.

[7]. Shankhamala Kundu, Tharamani Chikka Nagaiah, Wei Xia, Yuemin Wang, Stefan Van Dommele, Johannes Hendrik Bitter, Monika Santa, Guido Guundmeier, Michael Bron, Wolffang Schuhmann and Martin Muhler, Eletcrocatalytic activity and Stability of Nitrogen-containing Carbon Nanotubes in the oxygen reduction Reaction, *J. Phys. Chem. C*, 113, **2009**, 14302-14310.

[8]. A. A. Tanaka, C. Fierro, D. Scherson and E. B. Yeager, Electrocatalytic Aspects of iron phthalocyanine and its μ-Oxo Derivatives dispersed on high surface area carbon, *J. Phys. Chem.*, 91, **1987**, 3799-3807.

[9]. R. Noyori and S. Hashiguchi, Asymmetric Transfer Hydrogenation catalyzed by chiral Ruthenium complexes, *Acc. Chem. Res.*, 30, **1997**, 97-102

[10]. V. Cadierno, J. Francos, J. Gimeno and N. Nebra, Ruthenium catalyzed reduction of allylic alcohols: An efficient isomerization/transfer hydrogenation tandem process, *Chem. Commun.*, **2007**, 2536-2538.

[11]. Tamao Ishida, Noriko Kawakita, Tomoki Akita and Masatake Haruta, One-pot N-alkylation of primary amines to secondary amines by gole clusters supported on porous coordination polymers, *Gold Bulletin*, 42(4), **2009**, 267-274.

[12]. Wenzhen Li, Changhai Liang, Weijiang Zhou, Jieshan Qiu, zhenhua Zhou, Gongquan Sun and Qin Xin, Preparation and Characterization of Multiwalled carbon nanotubes-supported platinum for cathode catalysts of direct methanol fuel cells, *J. Phys. Chem. B*, 107, **2003**, 6191-6299.

[13]. Weilin Xu, Changpeng Liu, Wei Xing, Tianhong Lu, A novel hybrid based on carbon nanotubes and heteropolyanions as effective catalyst for hydrogen evolution, *Electro. Commun.*,

9, **2009**, 180-184.
[14]. Gang Wu, Yongsheng Chen, Boqing Xu, Remarkable support effect of SWNTs in Pt catalyst for methanol electrooxidation, *Electro. Commun.*, 7, **2005**, 1237-1243.
[15]. Zhaolin Liu, Xing Yi Ling, Bing Guo, Liang Hong, Jim Yang Lee, Pt and PtRu nanoparticles deposited on single-wall carbon nanotubes for methanol electro-oxidation, *J. Power Sources*, 167, **2007**, 272-280.
[16]. Yuehe Lin and Xiaoli Cui, Platinum/Carbon Nanotube Nanocomposite Synthesized in supercritical Fluid as electrocatalysts for low-temperature fuel cells, *J. Phys. Chem. B*, 109, **2005**, 14410-14415.
[17]. Gang Wu, Li Li, Jinghong Li, Bo-qing Xu, Methanol electrooxidation on Pt particles dispersed into PANI/SWNT composite films, *J. Power Sources*, 155, **2006**, 118-127.
[18]. Shu Yin, Tsugio Sato, Photocatalytic activity of platinum loaded fibrous titania prepared by selvothermal process, *J. Photochem. Photobiol.* A, 169, **2005**, 89-94.
[19]. Peter Claus, Sabine Schimpf, Rainer Schödel, Peter Kraak, Wolfgang Mörke, Dieter Hönicke, Hydrogeneration of crotonaldehyde on Pt/TiO_2 catalysts: Influence of the phase composition of titania on activity and intramolecular selectivity, *Appl. Catal. A*, 165, **1997**, 429-441.
[20]. Wendong Wang, Philippe Serp, Philippe Kalck, Joaquim Luís Faria, Photocatalytic degradation of phenol on MWNT and titania composite catalysts prepared by a modified sol-gel method, *Appl. Catal. B*, 56, **2005**, 305-312.
[21]. P. Tolmacsov, A. Gazsi, F. Solymosi, Decomposition and reinforming of methanol on Pt metals supported by carbon Norit, *Appl. Catal. A*, 362, **2009**, 58-61.
[22]. Hideki Kurihara and Tatsuhiko Yajima, Decomposition of waste organic solvents by liquid-phase atmospheric pressure microwave plasma generated using carbon felt pieces impregnated with NaCl, *Bull. Chem. Soc. Jpn.*, 81(5), **2008**, 656-658.
[23]. Ya-Fen Wang, Yen-Sheng You, Cheng- Hsien Tsai, Lin-Chi Wang, Production of hydrogen by plasma-reforming of methanol, *Int. J. Hydrogen energy*, 35, **2010**, 9637-9640.
[24]. Lifeng Wang, Jian Zhang, Dang Sheng Su, Yanyan Ji, Xuejing Cao and Fengshou Xiao, Simple preparation of honeycomb-like Macrostructured and Microporous Carbons with high performance in oxidative dehydrogenation of ethylbenzen, *Chem. Mater.*, 19, **2007**, 2894-2897.
[25]. H. Borchert, B. Jürgens, T. Nowitzki, P. Behrend, Yu. Borchert, V. Zielasek, S. Giorgio, C. R. Henry, M. Bäumer, Decomposition of methanol by Pd, Co and bimetallic Co-Pd catalysts: Acombined study of well-defined systems under ambient and UHV conditions, *J. Catal.*, 256, **2008**, 24-36.
[26]. Tobias Nowitzki, Holger Borchert, Birte Jürgens, Thomas Risse, Volkmar Zielasek, and Marcus Bäumer, UHV studies of methanol decomposition on mono- and bimetallic CoPd Nanoparticles supported on thin Alumina films, *Chem. Phys. Chem.*, 9, **2008**, 729-739.
[27]. Cuiyu Niu, Jiao Jiao, Bin Xing, Guichang Wang, Xianhe Bu, Reaction mechanism of methanol decomposition on Pt-based model Catalysts: A theoretical Study, *J. Comput. Chem.*,

31(10), **2010**, 2023-2037.

[28]. Maria Jose Gracia, Juan Manuel Campelo, Elia Losada, Rafael Luque, Jose Maria Marinas and Antonio Angel Romero, Microwave-assisted versatile hydrogenation of carbonyl compounds using supported metal nanoparticles, *Org. Biomol. Chem.*, 7, **2009**, 4821-4824.

[29]. Grzegorz S. Szymaáski, Catalytic destruction of methyl tertiary butyl ether (MTBE) using oxidized carbon, *Catal. Today*, 137, **2008**, 460-465.

[30]. Kwang-Deog Jung, Oh-Shim Joo, Sung-Hwan Han, Sung-Jin Uhm, and In-Jae Chung, Deactivation of Cu/ZnO catalyst during dehydrogenation of methanol, *Catal. Lett.*, 35, **1995**, 303-311.

[31]. Yucheng Huang and Zhaoxu Chen, Density functional investigation of methanol dehydrogenation on Pd-Zn Surface alloy, *Langmuir*, 26(13), **2010**, 10796-10802.

[32]. Tianchun Zou, Haipeng Li, Naiqin Zhao, Chunsheng Shi, Electromagnetic and microwave absorbing properties of multi-walled carbon nanotubes filled with Ni nanowire, *J. Alloys Compd.*, 496, **2010**, L22-L24.

[33]. Satoshi Horikoshi, Masahiko Abe, Nick Serpone, Influence of alcoholic and carbonyl functions in microwave-assisted and photo-assisted oxidative mineralization, *Appl. Catal., B*, 89, **2009**, 284-287.

[34]. George Avgouropoulos, Isotropic transient study of methanol decomposition over noble metal/ceria catalysts, *Catal. Commun.*, 10, **2009**, 682-686.

[35]. Yi-Shijue Lin, Meng-Tso Chen, Yu-Feng Lin, Yi-shung Pang, Hong-Ping Linand Jong-Liang Lin, Photochemistry catalyzed by copolymer-templated mesoporous SiO_2: Decomposition of methanol and fomic acid, *J. Phys. Chem. B*, 110, **2006**, 14809-14815.

[36]. Bo Li, Shuren Zhang, Ying Yuan, Xiaohua Zhou, Longcheng Xiang, Dielectric properties and microstructure of TiO_2 modified (ZnMg)TiO_3 microwave ceramics with CaO-B_2O_3-SiO_2, *J. Mater. Sci.*, 44, **2009**, 4993-4998.

[37]. Huagang Wang, Hideaki Takashima, Yozo Miyakawa, Yoshinori Kanno, Development of catalyst materials being effective for microwave sterilization, *Science and Technology of Advanced Materials*, 6, **2005**, 921-926.

[38]. Jianqiang Wei, Jianbo Wang, Qingfang Liu, Liang Qiao, Tao Wang and Fashen Li, Enhanced microwave absorption properties of Fe_3Al/Al_2O_3 fine particle composites, *J. Phys. D: Appl. Phys.*, 43, **2010**, 115001/1-115001/5.

[39]. Zengyong Chu, Haifeng Cheng, Yongjiang Zhou, Qiang Wang, Jun Wang, Anistropic microwave absorbing properties of oriented SiC short fiber sheets, *Mater. Des.*, 31, **2010**, 3140-3145.

[40]. M. Izawa, T. Koseki, Y. Kamiya, T. Toyomasu, Characteristics of a SiC microwave absorber for a damp cavity, *Rev. Sci. Intrum.*, 66(2), **1995**, 1910-1912.

[41]. E. Mouchon, PH. Colomban, Properties and r.f.-microwave conductivity of SiC (and/or mullite) fiber reinforced Nasicon matrix composites, *J. Mater. Sci.*, 31, **1996**, 323-334.

[42]. Dong-Lin Zhao, Fa Luo, Wan-cheng Zhou, Microwave absorbing property and complex

permittivity of nano SiC particles doped with nitrogen, *J. Alloys Compd.*, 490, **2010**, 190-194.
[43]. Zehua Zhou, Shouhong Tan and Dongliang Jiang, Yu Yi, Microwave absorption properties of β-SiC-C composites with solid phase sintering at X band, *Surface Rev. Lett.*, 12, **2005**, 799-807.
[44]. Nicolas A. Shtin, José Mauricio Lopez Romero and Eugenen Prokhorov, Theory of fundamental microwave absorption in sapphire (α-Al_2O_3), *J. Appl. Phys.*, 106, **2009**, 104115/1-104115/9.
[45]. X. G. Liu, D. Y. Geng and Z. D. Zhang, Microwave-sbsorption properties of FeCo microspheres self-assembled by Al_2O_3-coated FeCo nanocapsules, *Appl. Phys. Lett.*, 92, **2008**, 243110/1-243110/3.
[46]. Robert Janes, Kaushai K. Singh, Jane Blunt and Peter P. Edwards, Low-field Microwave absorption in mechanical mixes of superconducting YBa_2Cu_{7-x} with Al_2O_3 and $BaPbO_3$, J. Chem. Soc. *Faraday Trans.*, 86 (22), **1990**, 3289-3830.
[47]. Manmeet Kaur, R.M. Kadam, M.K. Bhide, M.V. Rane, Y. Babu, M.D. Sastry, I.K. Gpoalakrishnan and J.V. Yakhmi, Microwave absorption studies of diluted high-temperature superconductors: delineation of superconductor junctions, *Philos. Mag. B*, 81, **2001**, 267-277.
[48]. Chundi Cao, Keith L. Hohn, Study of reaction intermediates of methanol decomposition and catalytic partial oxidation on Pt/Al_2O_3, *Appl. Catal. A*, 354, **2009**, 26-32.
[49]. Marc Bockrath, David H. Cobden, Paul L. McEuen, Nasreen G. Chopra, A. Zettl, Andreas Thess, R. E. Smalley, Single-Electron Transport in ropes of carbon nanotubes, *Science*, 275 (28), **1997**, 1922-1925.
[50]. Phaedon Avouris, Molecular Electronic with Carbon Nanotubes, *Acc. Chem. Res.*, 35, **2002**, 1026-1034.
[51]. V. Meera and Girish S. Setlur, Conductivity tensor of graphene through reflection of microwave measurements, *J. Phys. D: Appl. Phys.*, 42, **2009**, 055403/1-055403/10.
[52]. Hao-Bin Zhang, Qing Yan, Wen-Ge Zheng, Zhixian He and Zhongzhen Yu, Yough Graphene-Polymer microcellar foams for Electromegnetix interfluence shielding, *ACS Appl. Mater. Interfaces*, 3, **2011**, 918-924.
[53]. Hua Bai, Chun Li and Gaoquan Shi, Functional Composite Materials based on chemically Converted Graphene, *Adv. Mater.*, 23, **2011**, 1089-1115.
[54]. Xuchun Gui, Wei Ye, Jingquan Wei, Kunlin Wang, Ruitao Lv, Hongwei Zhu, Feiyu Kang, Jialin Gu and Dehai Wu, Optimization of electromagnetic matching of Fe-filled carbon nanotubes/ferrite composites for microwave absorption, *J. Phys. D: Appl. Phys.*, 42, **2009**, 075002/1-075002/5.
[55]. B. Corzilius, K.-P. Dinse and K. Hata, Single-wall carbon nanotubes and peapods investigated by EPR, *Phys. Chem. Chem. Phys.*, 9, **2007**, 6063-6072.
[56]. Ester Vázuqez and Maurizio Prato, Carbon Nanotubes and Microwaves: Interaction, Response and Applications, *ACS Nano*, 3(12), **2009**, 3819-3824.
[57]. V. P. Veedu, A. Cao, X. Li, K. Ma, C. Soldano, S. Kar et al., Multifunctional composites

using reinforced laminae with carbon-Nanotube forests, *Nat. Mater.*, 5(6), **2006**, 457-62.

[58]. G. Zhan, J. D. Kuntz, J. Wan, A. K. Mukherjee, Single-wall carbon nanotubes as attractive toughening agents in alumin-based nano-composites, *Nat. Mater.*, 2, **2003**, 38-42.

[59]. B. W. Sheldon, W. A. Curtin, Tough to test, *Nat. Mater.*, 3, **2004**, 505-506.

[60]. C. Du, Pan N. Preparation of single-walled carbon nanotube reinforced magnesia films, *Nanotechnology*, 15, **2004**, 227-31.

[61]. J. Fan, D. Zhao, M. Wu, Z. Xu, J. Song, Preparation and Microstructure of Multi-wall Carbon Nanotubes-Toughened Al_2O_3 Composite, *J. Am. Ceram. Soc.*, 89(2), **2006**, 750-753.

[62]. M. Estili, A. Kawasaki, H. Sakamoto, Y. Mekuchi, M. Kuno, T. Tsukada, The homogenerous dispersion of surfacantsless, slightly disordered, crystalline, multiwalled carbon nanotubes in α-alumina ceramics for structural reinforcement, *Acta. Mater.*, 56, **2008**, 4070-4079.

[63]. V. G. Gavalas, R. Andrews, D. Bhattacharyya, L. G. Bachas, Carbon Nanotube Sol-Gel Composite Materials, *Nano. Lett.*, 1(12), **2001**, 719-721.

[64]. R. L. Menchavez. M. Fuji. M. Takahashi, Electrically Conductive dense and porous alumina with In-situ-synthesized Nanoscale carbon networks, *Adv. Mater.*, 20, **2008**, 2345-2351.

[65]. R. L. Menchavez, M. Fuji, T. Yamakawa, T. Endo, M. Takahashi, Investigation of phase composition in dense and porous gelcast alumina sintered under argon atmosphere, *Mater. Sci. Forum.*, 561-565, **2007**, 2123-2126.

[66]. Xiu Wang, Zhi-peng Xie, Yong Huang, Yi-Bing Cheng, Gelcasting of silicon carbide based on gelation of sodium alginate, *Ceram. Int.*, 28, **2002**, 865-871.

[67]. Manjiang Dong, Xiaojian Mao, Zhaoquan Zhang, Qian Liu, Gelcasting of SiC using epoxy resin as gel former, *Ceram. Int.*, 35, **2009**, 1363-1366.

[68]. Rabah Mouazer, Ivo Thijs, Steven Mullens and Jan Luyten, SiC foams produced by gelcasting: Synthesis and Charaterization, *Adv. Eng. Mater.*, 6, **2004**, 340-343.

[69]. Tomoaki Kato, Takashi Shirai, Masayoshi Fuji and Minoru Takahashi, Graphitization behavior of polymer in the gelcasted alumina by sintering, *J. Ceram. Soc. Jpn.*, 117, **2009**, 992-995.

[70]. J. Liu, H. Watanabe, M. Fuji, M. Takahashi, Electrocatalytic evolution of hydrogen on porous alumina/gelcast-derived-carbon network composite electrode, *Electrochem. Commun.*, 10, **2008**, 922-925.

[71]. J. Liu, R. L. Menchavez, H. Watanabe, M. Fuji, M. Takahashi, Highly conductive alumina/NCN composite electrodes fabricated by gelcasting and reduction-sintering-An electro-chemical behavior study in aggressive environments, *Electrochima. Acta*, 53, **2008**, 7191-7197.

[72]. C. Hai, H. Watanabe, T. Shirai, M. Fuji, M. Takahashi, F. Wang, Modifying the surface of the electrically conductive porous alumina, *Mater. Lett.*, 63, **2009**, 1320-1322.

[73]. C. Hai, J. Liu, H. Watanabe, M. Fuji, F. Wang, M. Takahashi, Surface Activation of Conductive Porous Alumina by Deposition Nickel Particles, *J. Am. Ceram. Soc.*, 92, **2009**, S38-S41.

[74]. C. Hai, H. Watanabe, T. Shirai, M. Fuji, F. Wang, J. Liu and M. Takahashi, Chemical reductive preparation of Ni decorated conductive porous alumina composite and its electro-performance in alkaline solution, *Ceram. Trans.*, 219, **2009**, 249-254.

[75]. Xuhui Zhao, Masayoshi Fuji, Takashi Shirai, Hideo Watnabe, Minoru Takahashi, Electrocatalytic activity of the conductive alumin/NCN Composite electrode by electrode-deposting NiCu particles for methanol oxidation, *J. Am. Ceram. Soc.*, 94, **2011**, 1167-1172.

[76]. T.Skipa, Modification of the Electronic properties of Carbon Nanotubes by bunding, Temperature, B- and N-doping: a Resonance Raman Study, *Forschungszentrum Karlsruhe GmbH, Karlsruhe*, **2006**.

CHAPTER 2

SURFACE MODIFICATION OF ELECTRICALLY CONDUCTIVE POROUS ALUMINA (CPA) VIA CHEMICAL METHODS AND ELECTROCHEMICAL STUDIES

2.1 Introduction

Electrically conductive porous alumina abbreviated as CPA has been paid a surge of attention since its discovery because of its outstanding instinctive properties and sorts of potential applications in various fields [1-3] especially as fuel cells. CPA was fabricated by gelcasting and reductive sintering in Ar atmosphere. At the aid of reductive sintering, polymer networks formed in gel-casted green body can be converted to be inner-connected carbon [1]. Comparing with conductive ceramics prepared by other conventional methods, such as impregnating metal elements (Cr, Mg) into alumina [4] or employing conductive component as a host matrix [5], as-fabricated CPA has been confirmed to be a novel material with convenient, low cost, good physical and chemical properties. In CPA, the mechanical strength and thermal stability are attributed to porous alumina matrix, and the conductivity is derived from the nano-carbon networks (NCN) along the alumina grains. NCN is converted from polymer by high temperature reductive sintering (HTRS) in Ar. Moreover, due to the existence of nano-carbon, physical and chemical stability and ideal mechanical strength, many potential applications also can be expected, such as catalyst support, electrode and capacitor and so on. In our group, relative study reported by Liu et al. [3] also announces the potential application of conductive alumina (CA) as electrodes in fuel cells.

So far, various methods have been reported for fabricating suitable electrode material employing different substrates [11-15]. Among kinds of available surface modifying routes for carbonaceous materials [6-10], anchoring oxygen-functional groups at the aid of pre-treatment employing mixed acids has been confirmed to be one of the most effective methods for developing further investigations, by which the intact carbon crystal structure (hexagon) can be partly replaced by various oxygen-functional groups, which ascribes to the enhancement of hydrophilicity of acid-treated ones. Herein, in this chapter, we would like to introduce the available surface modification technology for broad applications in cells. Briefly speaking, two ways were involved for surface modification, namely covalent and hetorogeneous modification.

2.2. Experimental Procedures

2.2.1. Surface modification of CPA

2.2.1.1. Fabrication of CPA

Electrically conductive porous alumina (CPA) was prepared using gelcasting and high

temperature reductive sintering (HTRS) under inert atmosphere (Ar) [1-3]. The mixture of premix solution containing methacrylamide, N,N′-methylenebisacrylamide, alumina powder (AL 160SG-4, Showa Denko, Japan) with mean particle size of 0.60 μm with solid loading of 54 vol% and ammonium polycarboxylate acid (Chukyo Yushi, Japan) as a dispersant were ball-milled for 24 h, followed by degassing, mechanical foaming, adding ammonium peroxodisulfate (Initiator) and N,N,N′,N′,-tetramethylethylenediamine (catalyst) into the slurry to initiate polymerization and to form gel-green body. The well-dried green body was sintered at 1700 °C for 2h in a gas-tight furnace under argon atmosphere. Through the reductive sintering, nano-carbon networks can be formed along the porous alumina grains [1], which is responsible for the electrical conductivity of resulted ceramics. The conductive porous alumina (CPA) has 0.72 wt% of pyrolyzed carbon measured by TG/DTA. The bending strength is about 20~30 MPa and the bulk porosity is about 66.23 %. For further investigation, as-prepared CPA was cut into small plates (15 mm×20 mm×2 mm).

2.2.1.2. Covalent modification of CPA

The CPA plates were immersed into mixed acids (H_2SO_4/HNO_3=3:1, v/v) subjected to ultrasonication for 60 min, followed by extensive washing with distilled water until the pH reached netural. As-resulted sample was denoted as pre-treated CPA. Pre-treating condition was optimized by different pre-treating time for 15 min, 30 min, 90 min and 120 min at room temperature.

2.2.1.3. Preparing Pt/CPA and Ni/CPA composites

3.094 g of pre-treated-60 min CPA was soaked into 10 ml of $Ni(AC)_2$ (0.027 M) solution and evaporated at 60 °C for 24 h. Finally, as-resulted sample was refluxed in 20 ml 0.4 M N_2H_4 aqueous solution at 75 °C for 3h, followed by thoroughly washing and drying and the obtained sample was named as Ni/CPA.

1.028 g of pre-treated-60 min CPA was soaked into 5 ml of H_2PtCl_6 (0.006 M) ethanol solution followed by evaporation at 60 °C for 24 h. Finally, as-received Pt^{4+}/CPA were refluxed in EG at 140 °C for 1 h and followed by thoroughly washing with distilled water and drying at 90 °C for 24 h. Wherein, the CPA plates modified with Pt nanoparticles are denoted as Pt/CPA.

2.2.1.4. Characterization

The pre-treated CPA plates were characterized by field-emission scanning electron microscope (FE-SEM, JEOL, JSM7000F) equipped with electron diffraction X-ray spectroscopy (EDS, JEOL, JSM7000F), X-ray diffraction (XRD, RINT, Rigaku, Japan), X-ray photoelectron spectroscopy (XPS, Surface Science Instruments, United Kingdom, SSX-100) and Raman

spectroscopy (JEOL, NRS-3100) employing graphite (KGR-3, Akechi Ceramics (Co., Japan)) as reference.

2.2.2. Evaluation of Electrochemical Performances of CPA-based composites

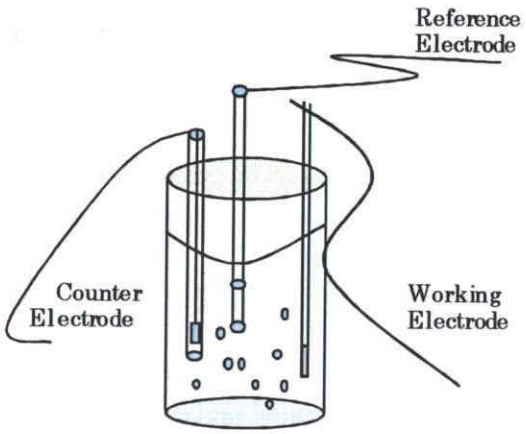

Fig. 2.1 Three electrodes electrochemical test cells

Electrochemical performances of CPA-based composites were investigated by employing a potentiostat/galvanostat system (HZ–5000, HOKUTO DENKO) at room temperature. In this test, a typical three-electrode system has been constructed. This system was consisted of a working electrode of CPA (with/without pre-treatment), Ni/CPA and Pt/CPA, a counter electrode of a platinum plate and a reference electrode of Ag/AgCl electrode with statured KCl (Fig.2.1). Different electrolytes 0.5 M H_2SO_4 and 1 M NaOH were employed for performance evaluation.

2.3. Results and Discussion

2.3.1. Effects of pre-treatment on CPA

2.3.1.1. Physico-chemical property of pre-treated CPA

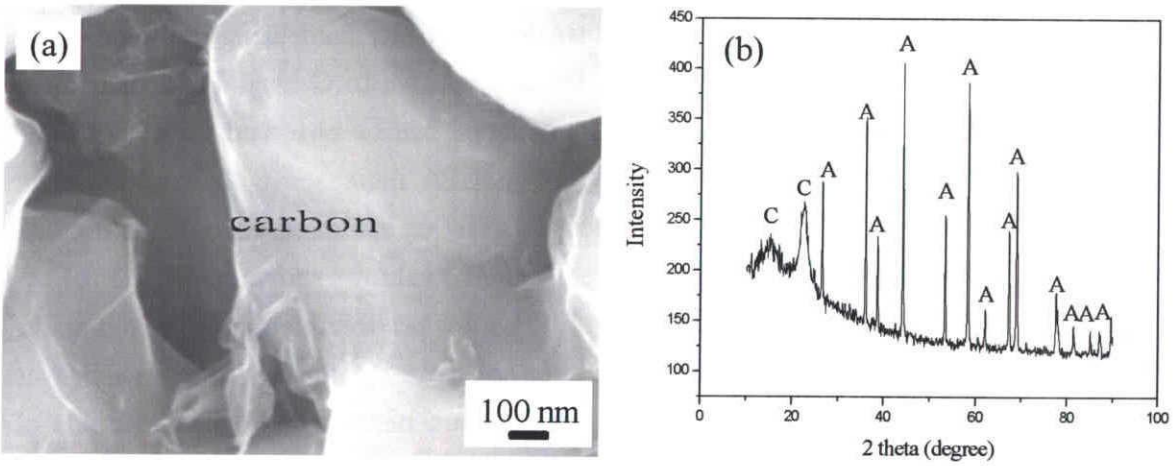

Fig. 2.2. (a) FE-SEM image of as-fabricated CPA (b) XRD pattern of as-fabricated CPA (C: carbon, A: Alumina)

FE-SEM image of as-prepared CPA is displayed in Fig. 2.2 (a). There are inner-connected nano-carbon networks (NCN) along alumina grains. The NCN converted from polymer monomer by reductive sintering contributes to the electrical conductivity of the ceramics. As introduced in our previous studies [1-3], the formed networks were confirmed to be graphite, which makes more desired applications become reality by some efficient methods. And according to the XRD patterns as shown in Fig. 2.2 (b), the detected peaks at 16° and 23° reflect the existence of carbon in CPA, while other peaks in this pattern reflect alumina phase. The absence of other diffraction peaks in the detected materials indicates that during the fabricating process, others phases did not occur expect purified alumina and pyrolyzed carbon converted from polymer.

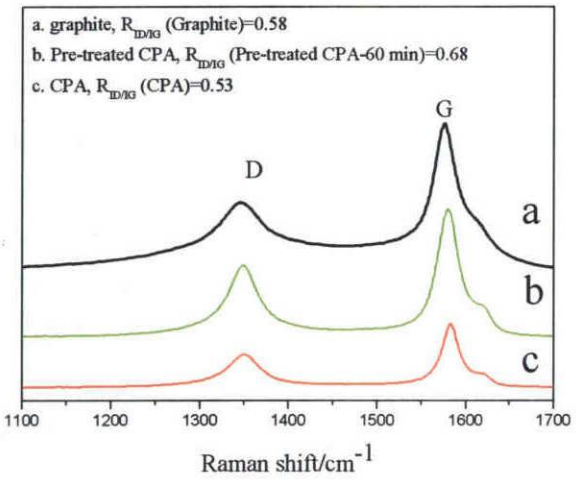

Fig. 2.3. Raman spectra of conductive porous alumina (a) graphite (b) Pre-treated CPA (c) as-fabricated CPA (R: the intensity ratio of D band and G band)

Raman spectra is commonly regarded as an efficient way to characterize structure of various carbonaceous materials with conjugated and C-C double band [6,7,16]. Fig.2.3 shows Raman spectroscopy of CPA with/without surface pre-treatment-60 min employing graphite as reference. There are obvious Raman peaks for graphite structure material around 1350 cm $^{-1}$ and 1575 cm $^{-1}$, which also can be annotated as D band and G band, respectively. By comparing the Raman spectra of CPA with/without pre-treatment-60 min with graphite, useful information can be arrived as follows: (a) the existence of graphite can be verified in as-fabricated CPA (with/without) acid-treatment. (b) by comparing the intensity of D band relative to G band for as-fabricated CPA and acid-treated CPA (Fig. 2.3 (b) and (c)), a larger one can be observed for acid-treated CPA, which means that defects of graphite structure in CPA increases with acid-treatment because the intensity of D band of graphite is opposed to the intact extent of hexagonal structure, this conclusion also can be confirmed by the increased R (I_D/I_G) value as shown in Fig.2.3 (c).

As confirmed by Wong et al.[6] and Kotov et al. [7], after pre-treatment with mixed acids, the intact hexagonal of carbon was destructed resulting sp^3 from sp^2 to C-C band, which was aroused by the reaction between mixed acids and nano-carbon networks (NCN) and kinds of oxygen-functional groups can be introduced onto the graphite defects resulting enhanced hydrophilicity. Optimum pre-treating condition was reached by discussing different treating time for 15 min, 30 min, 60 min; 90 min and 120 min, respectively. However, due to the unique structure of CPA, it is difficult to determine the suitable condition.

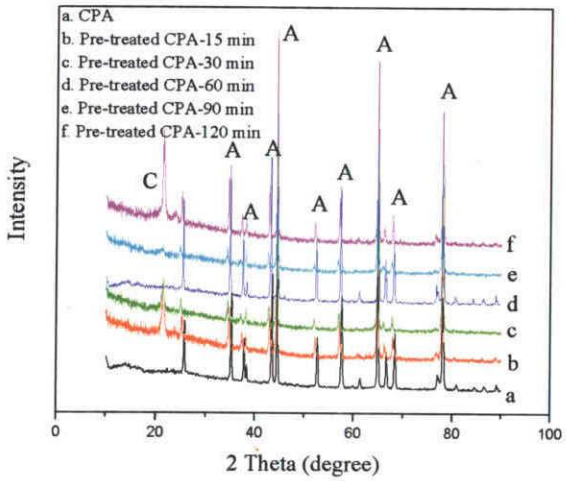

Fig. 2.4. XRD patterns of pre-treated CPA with different time (a) CPA, (b) 15 min, (c) 30 min, (d) 60 min,(e) 90 min and (f) 120 min

Table 2.1. Analysis results from Raman spectroscopy

Sample	Half width of G band	$R_{ID/IG}$
Graphite	-------	0.58
CPA	24	0.53
Pre-treated CPA-15 min	29	0.80
Pre-treated CPA-30 min	29	0.69
Pre-treated CPA-60 min	**30**	**0.68**
Pre-treated CPA-90 min	30	0.81
Pre-treated CPA-120 min	25	0.77

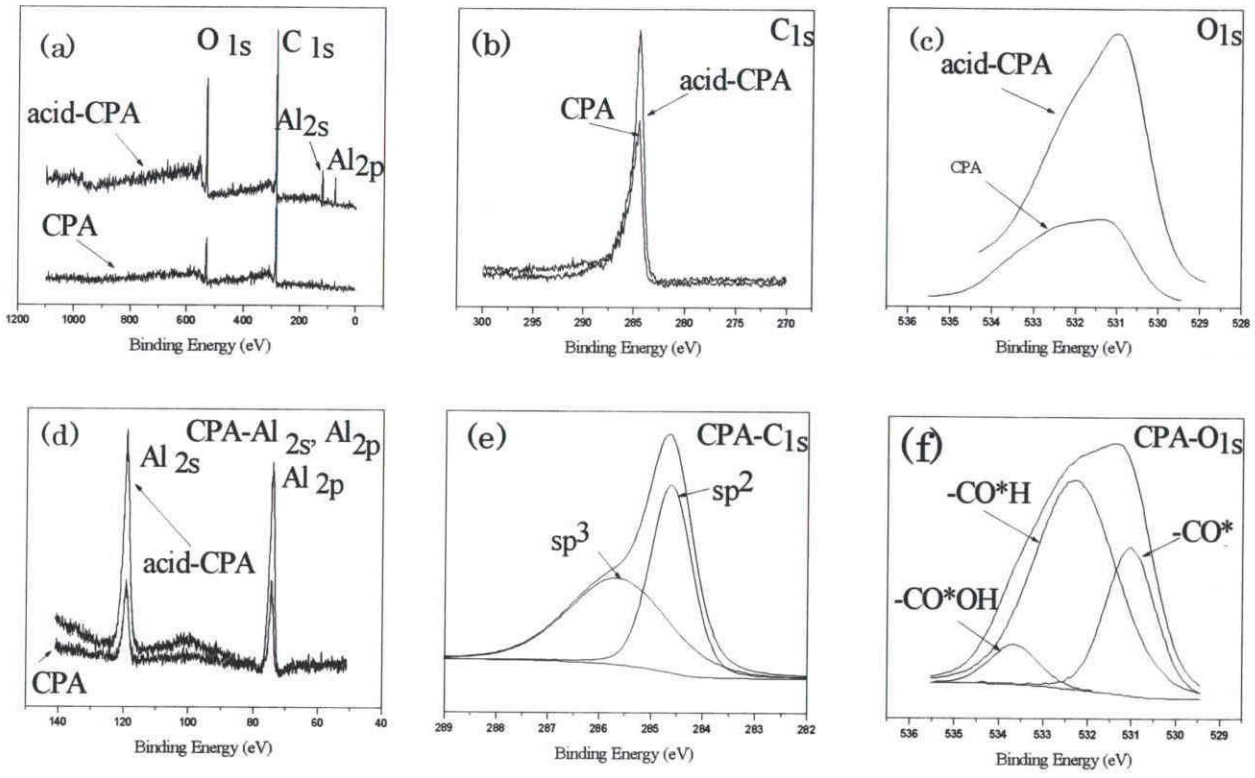

Fig. 2.5. XPS spectra of (a) a special region of 0~1100 eV, (b) C_{1s}, (c) O_{1s}, (d) Al_{2s}, Al_{2p} (e) the deconvoluted C_{1s} of as-fabricated CPA and (f) the deconvoluted O_{1s} of as-fabricated CPA

As shown in Fig. 2.4, it is known that no obvious crystal change occurs during pre-treatment. The increased surface defects of CPA with increased treating time as shown in Table 2.1 indicates more covalent modification has been arrived. However, it is worried that too aggressive treating condition will totally destruct NCN in CPA, which is the key point we should avoid. Usually, for graphitic carbonaceous, there are two evaluation ways to determine the modification effects, namely, half width of G band and calculated surface defects ($R_{ID/IG}$). It is noticed that pre-treated CPA-60 min owns the highest G band half width and increased surface defects without carbon destruction, which is regarded as optimum condition. Later, pre-treated CPA means pre-treated CPA-60 min.

According to XPS spectra of as-fabricated CPA and acid-CPA as shown in Fig. 2.5, The C (1s) signal at 284.8 eV, O (1s) at 543.1 eV, Al (2s) at 121.2 eV and Al (2p) at 78 eV for investigated samples is well in agreement with references introduction [17-21] as shown in Fig. 2.5 (a). Since XPS is sensitive to the surface components, the evidently enhanced O (1s), C (1s) Al (2s) and Al (2p) (Fig. 2.5 (b), (c) and (d)) peaks intensity displayed by XPS spectroscopy imply that acid-treatment has roused the surface changes by introducing functional groups and removing impurities. As shown in (e) and (f), the deconvoluted C (1s) and O (1s) peaks of as-fabricated CPA imply the presence of C and O with different bonding structure. The C1s of as-fabricated CPA displays a maximum centered at 284.6 eV and the deconvoluted spectrum gave two peaks which can be confirmed to be sp^2 graphitic (C-C, C-H, at 285±0.2 eV) and sp^3 (-CO-, at 286.4±0.2 eV). Moreover, the deconvoluted spectrum of O 1s also indicate oxygen-functional groups such as –CO*OH (533.4±0.2 eV), -CO*H (532.1±0.2 eV) and –CO* (530.6±0.2 eV) and defects can be expected on as-fabricated CPA [17-20], namely the well-structured 3-dimensional nano-carbon networks in CPA were partly destructed by some groups and instinctive defects [17,18].

2.3.1.2. Electrochemical performances of CPA with/without pretreatment

To investigate the electrical performance of CPA with/without pre-treatment, cyclic voltammetry (CV) has been employed in 0.5 M H_2SO_4 solution between -0.3 V and + 1.3 V at a scan rate of 20 mV/s. In Fig.2.6, a broader time window for as-fabricated and acid-treated CPA (Fig. 2.6 (b) and (c)) can be seen as compared with graphite classical electrode material (Fig. 2.6 (a)). This result indicates that the porous structure ascribes to the enhancement of electrical performance. Subsequently, as introduced in the former studies [10,11], the enlarged time window in cyclic voltammetry curve is attributed to introducing oxygen-functional hydrophilic groups on the surface of CPA both outer and inner surface leading to higher electrical double layer. As compared with un-treated one Fig. 2.6 (b), chemical pretreatment with concentrated mixed acids Fig. 2.6 (c) can not only dramatically increase the hydrophilicity of the material, which facilitate to penetration of electrolyte into the inner porous chamber, but also ascribe to the increased surface charges meriting from the enlarged chamber inner-volume. Moreover, in

comparison between as-fabricated CPA (b) and acid-treated CPA (c) as shown in Fig. 2.6, there is a positive shift in the range from +0.3 to +0.8 V, which is presumably due to Faradaic pseudocapacitances associated with oxygen-containing surface functional groups on the carbon support materials [9].

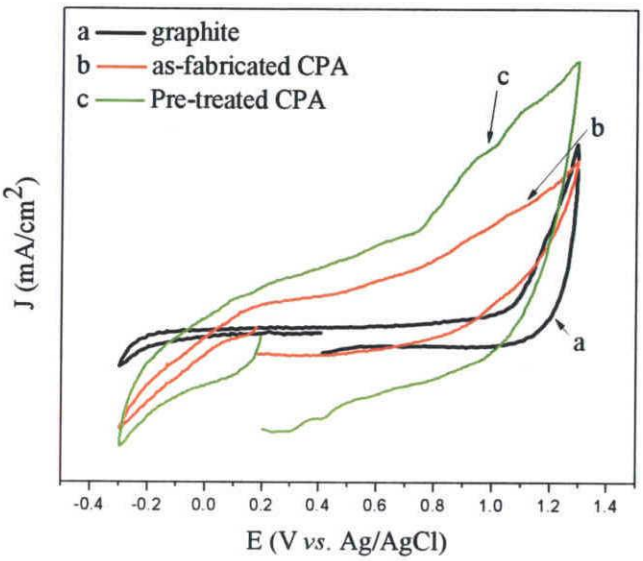

Fig.2.6. Cyclic voltammograms (CV) of (a) graphite, (b) as-fabricated CPA and (c) acid- CPA in 0.5 M H_2SO_4 with a scan rate of 20 mV/s (*vs.* Ag/AgCl)

2.3.2. Effects of surface modification with Pt and Ni nanoparticles

2.3.2.1. Physico-chemical property of Pt/CPA and Ni/CPA

The changes of morphology in this work are shown in Fig. 2.7. Nano-carbon connects each other forming conductive networks in CPA, which exist along the bone structure of CPA as shown in Fig. 2.7 (a) and (d). By comparing with (a) and (d) images, as shown in Fig. 2.7 (b) and (e), it is obvious that Ni nanoparticles has been successfully deposited onto the surface of CPA with smaller particles size and little coagulation. It is interesting that Pt nanoparticles also has been uniformly deposited onto the surface of CPA and higher selectivity is available.

The role of acid-treatment for particles dispersion was investigated by precipitating Pt and Ni nanoparticles onto as-received CPA. As-resulted specimens are named as Ni-untreated CPA and Pt-untreated CPA. Fig. 2.8 shows the morphologies of Pt/CPA and Ni/CPA with/without pre-treatment, by which we can get a conclusion that pre-treatment plays an important role for decreasing particles size and uniform distribution. According to the introduction of formers [21,22], various functional groups can be introduced on to the surface of CPA by acid pre-treatment, which can serve as the active sites for particles growth. These groups belong to hydrophilic.

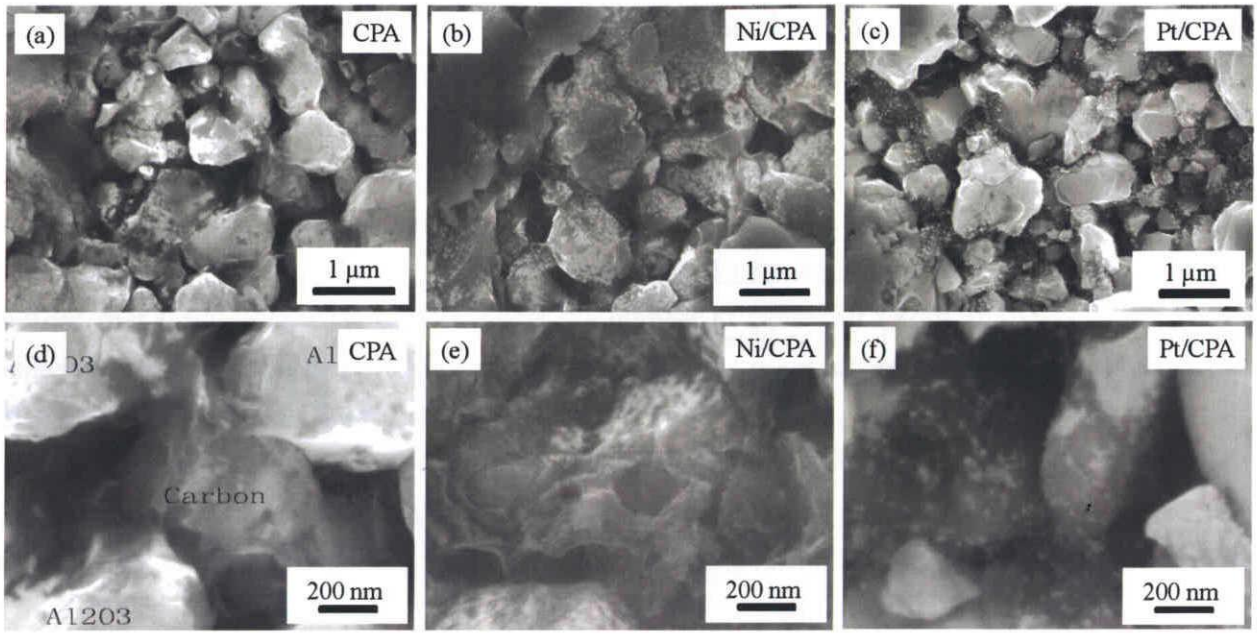

Fig. 2.7. FE-SEM images of (a) CPA, (b) Ni/CPA, (c) Pt/CPA with low magnification and (d) CPA, (e) Ni/CPA, (f) Pt/CPA with high magnification

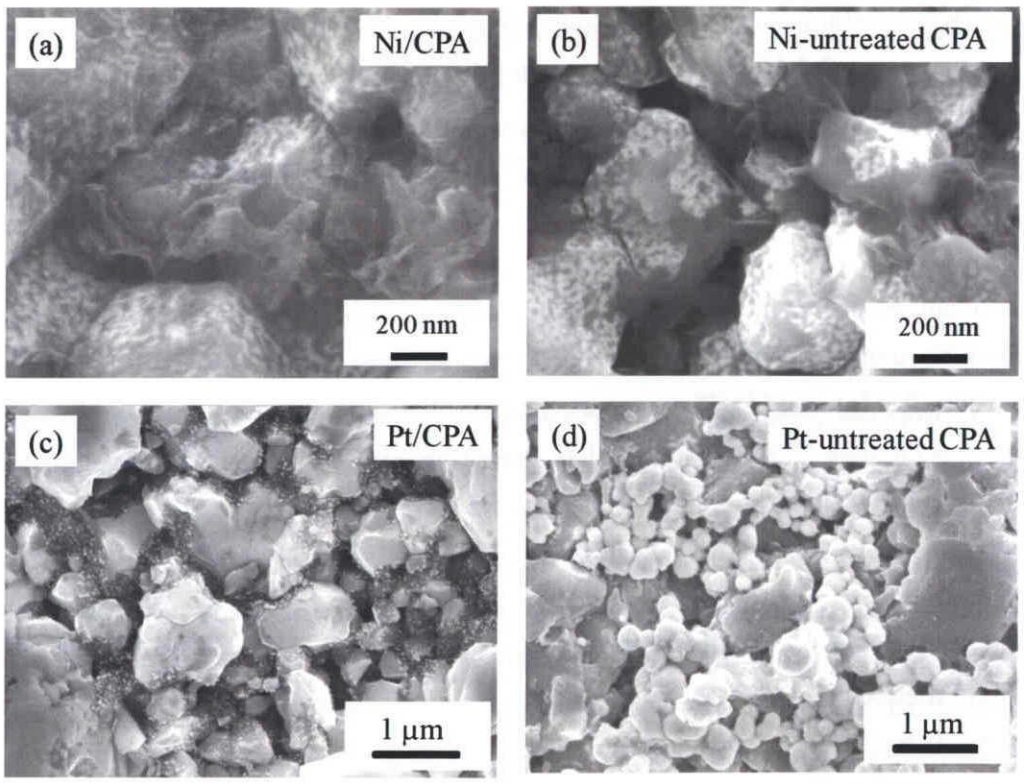

Fig. 2.8. FE-SEM images of (a) Ni/CPA (b) Ni-untreated CPA (c) Pt/CPA and (d) Pt-untreated CPA

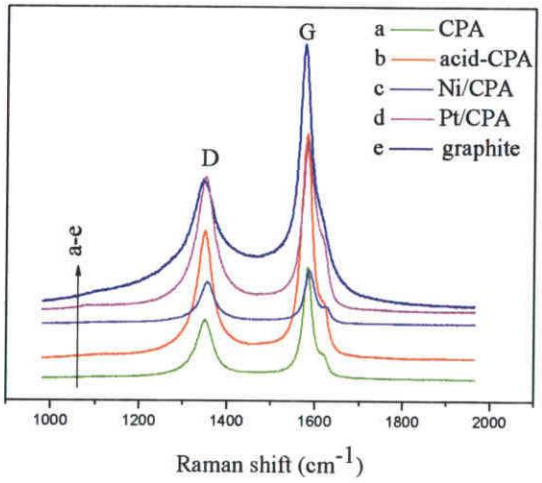

Fig. 2.9. Raman spectroscopy of (a) CPA (b) Acid-CPA (c) Ni/CPA (d) Pt/CPA and (e) graphite

Table 2.2. Surface defects analysis results

Samples	I_D/I_G
Graphite	0.58
CPA	0.53
Acid-CPA	0.68
Ni/CPA	0.79
Pt/CPA	0.84

Fig. 2.9 shows the Raman spectrum of as-prepared CPA, acid-CPA, Ni/CPA and Pt/CPA employing graphite as a reference. According to the appearance of typical peaks around 1575 cm^{-1} and 1350 cm^{-1} for CPA-based composites comparing with graphite [6], graphitic structure of NCN in CPA is confirmed. After surface modification via different methods, increased surface defects are available especially for Pt/CPA and Ni/CPA (I_D/I_G, as displayed in Table 2.2), which may be mainly result from covalent modification (sp^2 converts to sp^3 hybrid style) and nanoparticles deposition leading increased specific surface.

Table 2.3. EDS analysis results

Sample	Al (%)	O (%)	C (%)	Metal (wt %)		
				Total (wt %)	001 spot (wt %)	002 spot (wt%)
Ni/CPA	61.36	29.27	5.17	2.55	0.92	2.92
Pt/CPA	55.91	31.44	5.27	7.13	7.13	0

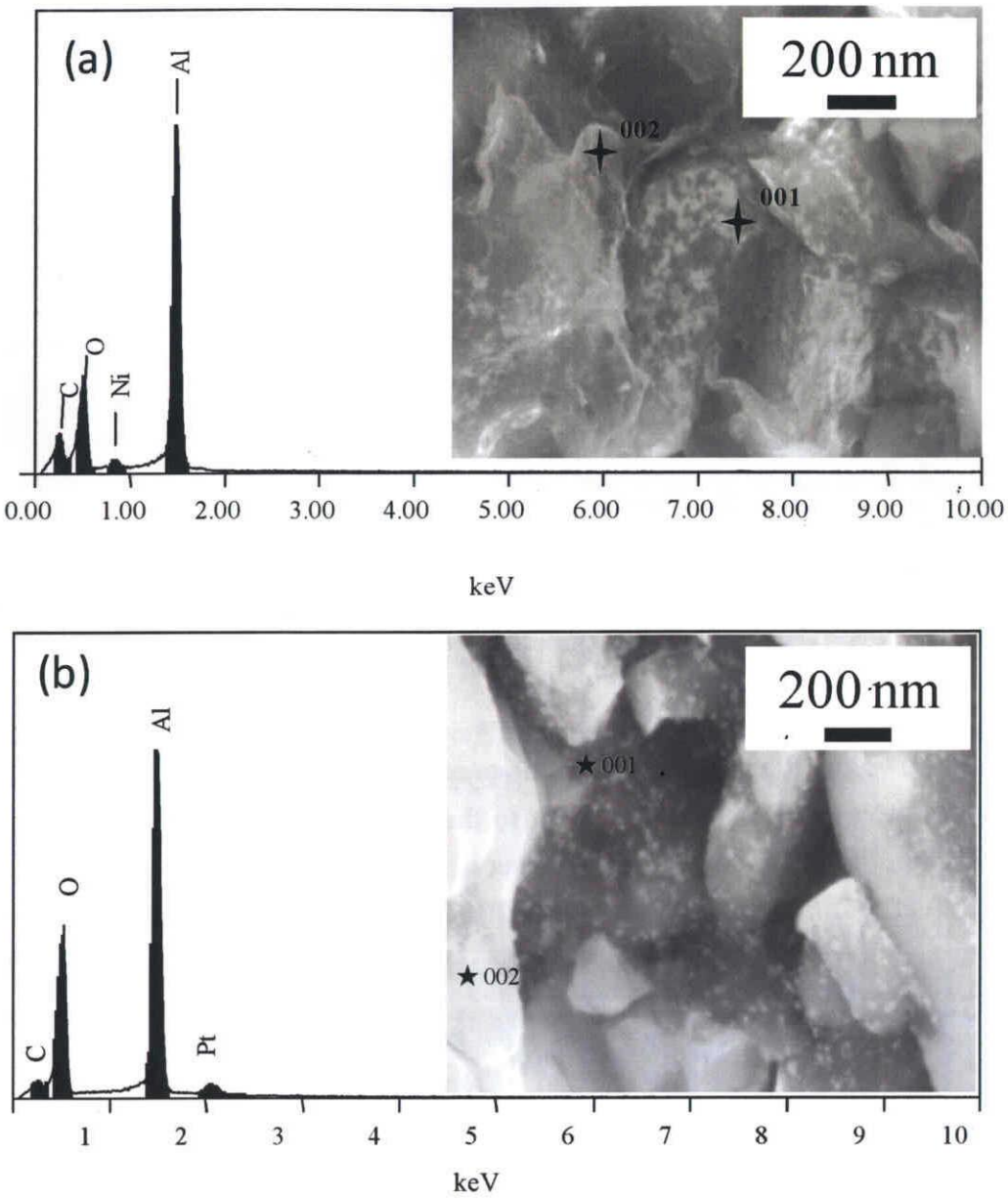

Fig. 2.10. EDS spectrum results of (a) Ni/CPA and (b) Pt/CPA

Fig. 2.10 shows the EDS analysis results. As displayed in Fig. 2.10 (a) and (b), selective deposition of Ni and Pt nanoparticles is proved by multi-spot analysis. It is noticed that there are two kinds surfaces in CPA, that is NCN surface and alumina grains surface. In order to investigate the different depositing situation, different surfaces were detected. 001 means the deposited metallic nanoparticles on NCN in CPA, while 002 implies the amount of deposited particles on alumina grains. As supported in Table 2.3, Ni nanoparticles not only deposits onto the NCN surface but also anchors onto the alumina surface. Contrast, Pt nanoparticles is mainly deposited onto NCN surface, higher selectivity is available.

Taking Pt/CPA preparing procedures for example, the fabrication schematic is shown in Fig. 2.11. Briefly speaking, three steps were involved for making metal/CPA. (a) Surface pre-treating, by which various surface defects on NCN with graphitic structure are available. These defects include five- or seven-membered rings in the carbon networks instead of normal ring, sp^3-hybridized defects (H or OH) and vacancies in the carbon lattice [6]. Pre-treating of CPA attributes to increased sp^3-hybridized defects (-COOH, -COH etc.) [23]. (b) Absorption of Pt^{4+} onto substrate via electrostatic interaction and (c) Chemical reduction of Pt^{4+} to Pt particles. The same schematic applies for Ni/CPA composite.

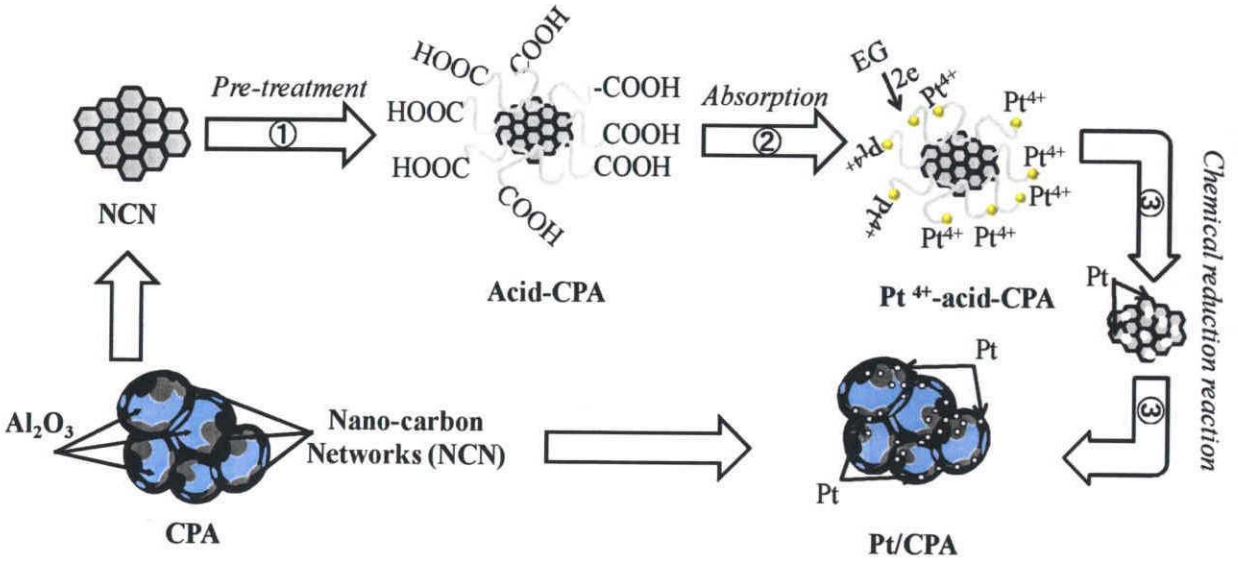

Fig.2.11. Schematic representation of preparing Pt/CPA via chemical reductive reaction

2.3.2.2. Electrochemical performances of Pt/CPA and Ni/CPA

2.3.2.2.1. Electrochemical performances of Pt/CPA and Ni/CPA in alkaline electrolyte

a). *Measurement of electrochemical surface area*

Electrochemical surface area was examined by a potential step method. Before measuring, the tested electrodes were electro-activated at their open-circuit potential and kept for at least 5 min for stabilization, followed by stepping immediately of potential up to -10 mV and maintained for 250 ms [24]. As-resulted chronoampermetric curves for tested electrodes obtained in 1 M NaOH solution are shown in Fig. 2.12 and the calculated double layer capacitances for employed electrodes were listed in Table 2.4, respectively. Usually, the double layer capacitance of pure mercury is used as reference, for which the typical value C^* is 20 μF cm^{-2}. Compared with graphite electrodes, the increased electrochemical surface area is attributed to the appearance of nano-carbon networks (NCN) along the connected alumina grains. Moreover, a

highest specific surface also can be expected for Ni/CPA because of the deposition of Ni nanoparticles.

Table 2.4. Characteristic values of the measured double layer capacitance and real surface area on studied electrodes in 1 M NaOH aqueous at room temperature

Electrode Materials	C ($\mu F\ cm^{-2}$)	S_a (cm^2)
Graphite	20623	1031.2
As-fabricated CPA	106590	5329.5
Ni/CPA	426661	21333.5

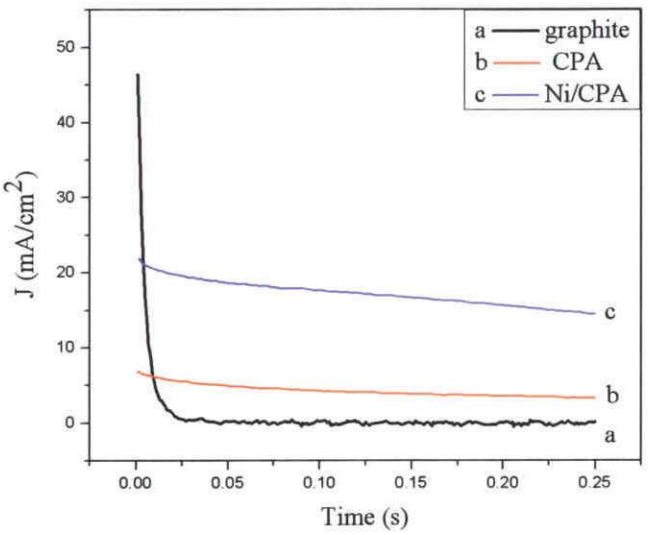

Fig.2.12. Chronoampermetric curves for different electrode: (a) graphite; (b) as-fabricated CPA and (c) Ni/CPA

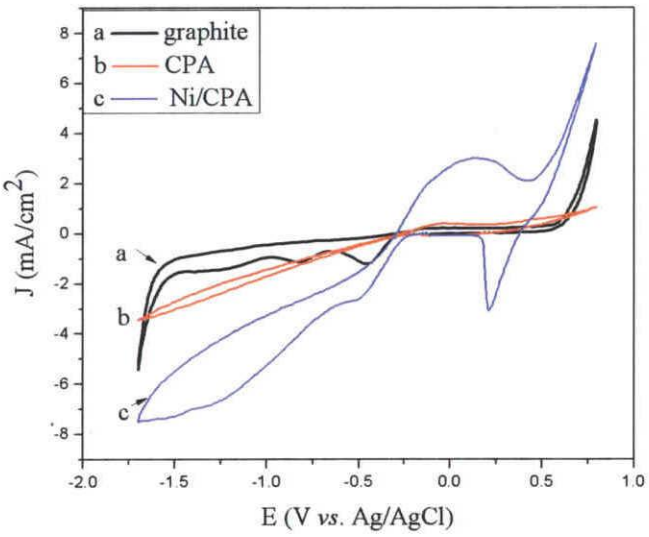

Fig.2.13. Cyclic voltammetric curves of different electrodes in 1 M NaOH solution at scan rate of 2 mV/s (a) graphite; (b) as-fabricated CPA and (c) Ni/CPA

b). Electrocatalytic reduction of oxygen on electrodes

In Fig. 2.13, the cyclic voltammograms (CV) involving the potential range for oxygen reduction reaction (ORR) was displayed with a scanning rate of 2 mV/s. By comparing with graphite electrode, two obvious typical oxygen reduction peaks around -430 mV and -820 mV can be observed for employed electrodes except as-fabricated CPA between the potential range from 0.8 V to -1.7 V. Simultaneously, slightly positive shifts are attributed to the higher catalytic activity and higher specific area [25-27]. Besides the peaks mentioned above, it is a most obvious differences between Ni/CPA and other electrodes that appearance of reductive peak around +210 mV, which is as good as those reported for nano-Pt/MWCNTs/GCE [26] and others. It is obvious that the nano-Ni functionalized CPA can increase the activity of ORR greatly, which is attributed to the reductive reaction of O_2 toward OH^-.

Another important evaluation of electro-catalytic performance for ORR is their stability at given working potentials. Further tests of ORR rates under potentionstatic conditions were conducted at +0.45 V in 1 M NaOH as shown in Fig. 2.14. Apparently, the Ni/CPA is advantageous over other electrodes by developing the highest current density, which indicates that the electrode fabricated from CPA were electrochemical stability for ORR in alkaline solutions.

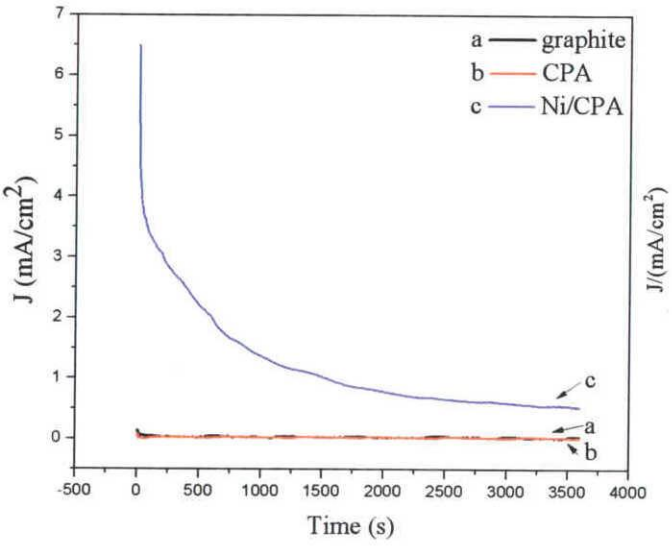

Fig. 2.14. Current-time plots when poised at 0.45 V vs. SCE in 1 M NaOH aqueous solution for (a) graphite; (b) as-fabricated CPA; (c) Ni/CPA

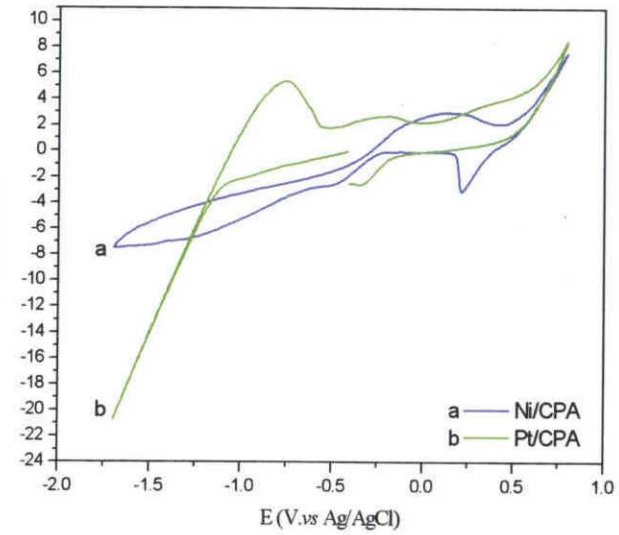

Fig. 2.15. Cyclic voltammetric curves of different electrodes in 1 M NaOH solution at scan rate of 2 mV/s (a) Ni/CPA; (b)Pt/CPA

Moreover, comparing Ni/CPA and Pt/CPA in the same measurement condition, much more increased electrochemical activity is available for Pt/CPA as supported in Fig. 2.15. Higher

current density and increased time window in CV curves prove this conclusion. And the enhanced performance is attributed to the higher surface selective deposition especially on NCN as claimed in Fig. 2.8 (c).

Fig. 2.16 investigates the effect of electrolyte. Increased electrochemical activity of Pt/CPA in acidic electrolyte announces the improved activity of Pt/CPA toward ORR than in alkaline solution. Then it is necessary to investigate the electro-activity of Pt/CPA in 1 M of H_2SO_4.

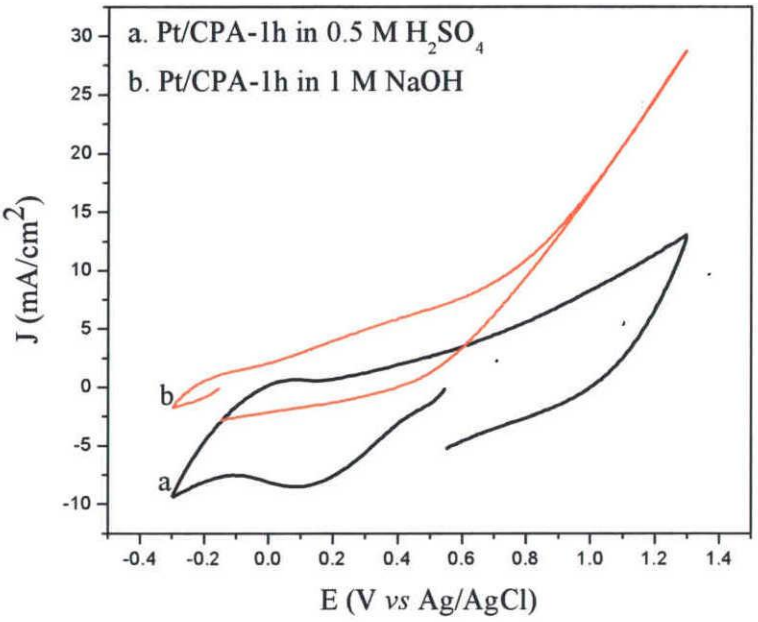

Fig. 2.16. Cyclic voltammetric curves of Pt/CPA in different electrolytes (a) 0.5 M H_2SO_4 and (b) 1 M NaOH solution at scan rate of 2 mV/s

2.3.2.2.2. Electro-chemical performances of Pt/CPA in acidic electrolyte

a). *Measurement of electrochemical surface area*

For porous electrode, it is commonly regarded that the most informative in situ characterization of electrodes about its surface areas can be obtained by potential step method in a solution. The chronoampermetric charge Q is proportional to the number of surface active area. This kind of information is very useful since electrochemical surface is one of the crucial parameters to characterize performance of electrodes in their preparation and application. During the potential step measurement, the initial potential for the tested electrode was its open-circuit potential, and kept for at least 5 min for stabilization, and then the potential stepped immediately up to -10 mV and maintained for 250 ms.

Table 2.5. Characteristic values of the measured double layer capacitance and real surface area on studied electrodes in 0.5 M H_2SO_4 aqueous at room temperature

Electrode Materials	C ($\mu F\ cm^{-2}$)	S_a (cm^2)
Graphite	243	1219.9
As-fabricated CPA	137945	6397.3
Pre-treated-CPA	117217	5860.9
Pt/CPA	611396	30569.8

It is valuable to investigate the real surface change before and after decorating with metallic Pt nanoparticles. Because of deposition of Pt nanoparticles, by employing the same potential step methods, the calculated real specific surface is 30569.8 cm^2 which is much higher than other electrodes. It is believed that the increased specific surface is attributed to the deposited small Pt nanopartiles with little agglomeration. This result is also in agreement with the Raman analysis results.

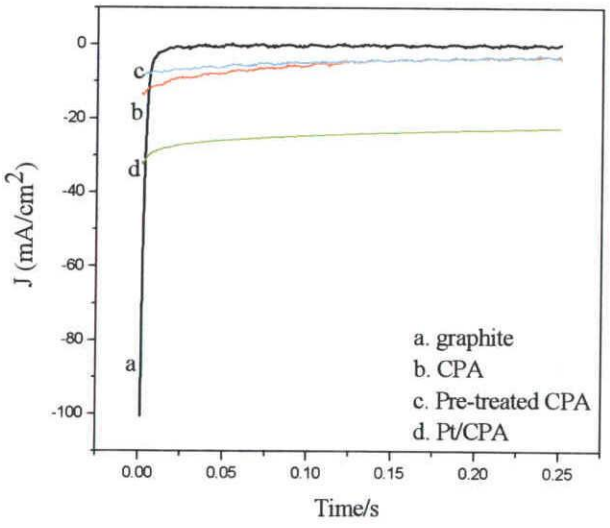

Fig. 2.17. Chronoampermetric curves for different electrode: (a) graphite; (b) as-fabricated CPA; (c) Pre-treated CPA and (d) Pt/CPA-1h in 0.5 M H_2SO_4

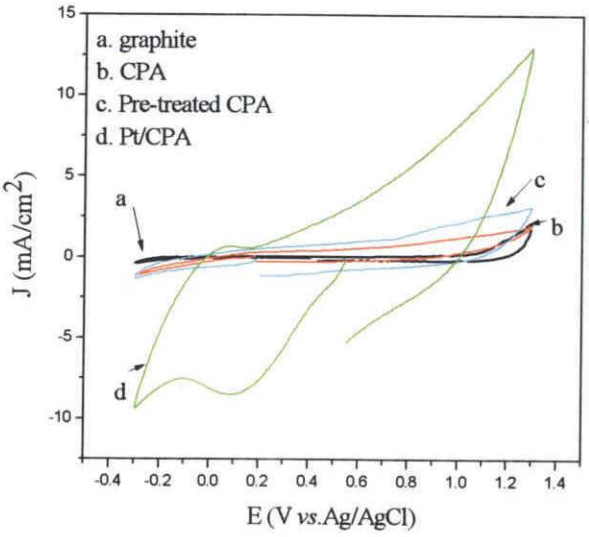

Fig. 2.18. Cyclic voltammograms (CV) of (a) graphite, (b) as-fabricated CPA and (c) Pre-treated CPA and (d) Pt/CPA in 0.5 M H_2SO_4 with a scan rate of 20 mV/s

b). Electro-catalytic reduction of oxygen reductive reaction (ORR) on electrodes

Fig. 2.18 shows the CV curves of graphite, as-received CPA, pre-treated CPA and Pt/CPA. We have reported that surface pre-treatment with mixed acids resulted in increased electrochemical activities of pre-treated CPA comparing with commonly utilized graphite electrode. The enhanced performance is attributed to grafted functional groups by covalent modification. As-received and pre-treated CPA display electro-catalytic activities toward oxygen reductive reaction (CRR), which can be proved by similar slopes of the reductive current with decreasing potential from -0.3 V to -0.2 V. Moreover, ORR occurred at potentials of -0.1 V- +0.4 V for Pt/CPA (Fig. 2.18 (d)). It is believed that the ORR activity of the Pt/CPA at more positive potentials is attributed to Pt (5-d orbital vacancies) nanoparticles deposition. Enhanced performance of Pt/CPA can be rapidly increased current and enlarged time window as shown in Fig. 2.18, Meng et al., [28] reported the ORR activity of Pt/C at potentials of + 0.7 V. Pt/CNT /CHIT was also claimed to be ORR activity electro-catalysts at the same measurement condition and the ORR activity occurred at + 0.1 V [29]. Then, by surface modification, it was confirmed in this study that as-fabricated Pt/CPA has a potential application in fuel cells.

2.3.2.2.3. Electro-chemical performances of Pt/CPA for methanol decomposition

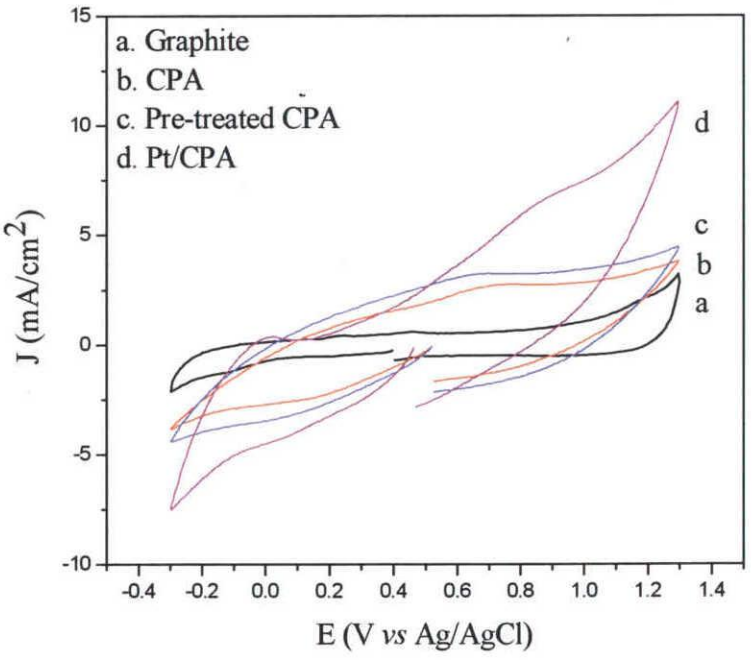

Fig. 2.19. Cyclic voltammograms (CV) of Pt/CPA in (a) graphite (b) as-fabricated CPA (c) pre-treated CPA (d) Pt/CPA in 0.5 M CH_3OH + 0.5 M H_2SO_4 with a scan rate of 20 mV/s

By the previous investigations, it is known that as-fabricated Pt/CPA has electro-activity toward ORR, its electro-chemical activity towards methanol oxidation is investigated in Fig.2.19. Although no obvious oxidation peaks, as fabricated Pt/CPA electrodes displays an increased performance toward methanol electro-oxidation comparing with other electrodes, which can be proved by the increased current density and the appearance of widen peaks around 0.74 V [30,32].

2.4. Conclusions

In this chapter, surface of as-received CPA was modified by chemicals and metallic particles followed by exploring its potential applications as electrode in fuel cells. As-involved electro-chemical activities of them in different conditions were evaluated and several conclusions are listed as follows:

- ✧ Pre-treatment permits the enhanced electro-chemical performance of CPA, which merits from the increased hydrophilic of as-received CPA.
- ✧ Electro-activity of CPA-based composites toward ORR.
- ✧ Electro-activity of CPA can be increased by preparing heterogeneous Pt/CPA and Ni/CPA.
- ✧ Activity of Pt/CPA toward methanol in acid medium.

However, even though Pt/CPA announced the possible and enhanced activity toward methanol decomposition or oxygen reductive reaction, limited NCN amount, part-destructive of NCN by too aggressive condition, high electrical resistivity inhibited the further investigation of CPA as electrodes for energy conversion. Then, it is necessary to explore the other potential application considering its unique structure.

References

[1]. R. L. Menchavez. M. Fuji. M. Takahashi, Electrically Conductive dense and porous alumina with In-situ-synthesized Nanoscale carbon networs, *Adv. Mater.*, 20, **2008**, 2345-2351.

[2]. R. L. Menchavez, M. Fuji, H. Taroaki, M. Takahashi, Electrically conductive gelcast porous alumina sintered under argon atmosphere, *Mater. Lett.*, 61, **2007**, 754 -756.

[3]. J. Liu, R. L. Menchavez, H. Watanabe, M. Fuji, M. Takahashi, Highly Conductive Alumina/NCN Composites Electrodes Fabricated by Gelcasting and Reduction Sintering-An Electrochemical Behavior Study in Aggressive Environments, *Electrochima. Acta*, 53, **2008**, 7191-7197.

[4]. K. L. Gavrilov, S. J. Bennison, K. R. Mikeska and R. Levi-setti, Role of magnesia and silica in alumina microstructure evolution, *J. Mater. Sci.*, 38(19), **2003**, 3965-3972.

[5]. M. Takahashi, T. Mizuno, Y. Shiroki, T. Yokoyama, H. Abe, M. Naito, Porous alumina with double-layered structure fabricated by pore-controlled in situ solidification, *Ceram. Trans.*, 112, **2001**, 559-564.

[6]. S. Banerjee, T. Hemraj-Benny, S. S. Wong, Covalent Surface Chemistry of Single-Walled Carbon Nanotubes, *Adv. Mater.*, 17, **2005**, 17-29.

[7]. Z. Tang, N. A. Kotov, One-Dimensional Assembilies of Nanoparticles: Preparation, Properties and Promise, *Adv. Mater.*, 17, **2005**, 951-962.

[8]. X. Hu, T. Wang, L. Wang, S. Guo, S. Dong, A General Route to Prepare One- and Three-Dimensional Carbon Nanotube/Metal Nanoparticle Composite Nanostructures, *Langmuir*, 23, **2007**, 6352-6357.

[9]. G. Wu, Y. S. Chen, B. Q. Xu, Remarkable support effect of SWNTs in Pt catalyst for methanol electrooxidation, *Electrochem. Commun.*, 7, **2005**, 1237-1243.

[10]. B. Fang, L. Binder, A novel carbon electrode materials for highly improved EDLC performance, *Electrochim. Acta*, 52, **2007**, 6916-6921.

[11]. Jianshe Wang, Xiaozhi Deng, Jingyu Xi, Liquan Chen, Wentao Zhu, Xinping Qiu, Promoting the current for methanol electro-oxidation by mixing Pt-based catalysts with CeO_2 nanoparticles, *J. Power Sources*, 170, **2007**, 297-302.

[12]. Jianbo Xu, Kaifeng Hua, Genzhi Sun, Cheng Wang, Xiangyu Lv, Yujiang Wang, Electrooxidation of methanol on carbon nanotubes supported Pt-Fe alloy electrode, *Electro. Commun.*, 8, **2006**, 982-986.

[13]. Kalayil Manian Manesh, Padmanabhan Santhosh, Anantha Iyengar Gopalan, Kwang-Pill Lee, Electrocatalytic Dioxygen Reduction at Glasssy Carbon Electrode Modified with Polyaniline Grafted Multiwall Carbon Nanotube Film, *Electroanalysis*, 18, **2006**, 1564-1571.

[14]. Chu Youqun, Ma Chunan, Zhu Yinghong, Electrocatalytic reduction of oxygen on carbon nanotubes electrode, *Acta Phys. Chim. Sin.*, 20(3), **2004**, 331-335.

[15]. Yongyan Mu, Hanpu Liang, Jinsong Hu, Li Jaing and Lijun Wan, Controllable Pt Nanoparticle Deposition on Carbon Nanotubes as an Anode Catalyst fr Direct Methanol Fuel Cells, *J. Phys. Chem. B.*, 109, **2005**, 22212-22216.

[16]. K. N. Kudin, B. Ozbas, H. C. Schniepp, R. K. Prud'homme, A. I. Aksay, R. Car, Raman spectra of graphite oxide and functionalized graphene sheets, *Nano Lett.*, 8, **2008**, 36-41.

[17]. Z. Tang, N. A. Kotov, One-dimensional Assembilies of Nanoparticles: Preparation, Properties and Promise, *Adv. Mater.*, 17, **2005**, 951-962.

[18]. R. Loscutova, A. R. Barron, Coating single-walled carbon nanotubes with cadmium chalcogenides, *J. Mater. Chem.*, 15, **2005**, 4346-4353.

[19]. N. M. Rodriguez, P. E. Anderson, A. Wootsch, U. Wild, R. Schl o¨gl, Z. Paál, XPA, EM, and Ctalytic Studies of the Accumulation, 197, *J. Catal.*, **2007**, 365-377.

[20]. J. T. Titantah, D. Lamoen, Sp^2/sp^3 characterization of carbon materials from first-principles calculations: X-ray photoelectron versus high energy electron energy-loss spectroscopy techniques, *Carbon*, 43, **2005**, 1311-1316.

[21]. R. Loscutova, A. R. Barron, Coating single-walled carbon nanotubes with cadmium chalcogenides, *J. Mater. Chem.*, 15, **2005**, 4346-4353.

[22]. M. Olek, T. Büegeb, M. Hilgendorff, and M. Giersig, Quantum Dot Modified Multiwall Carbon Nanotubes, *J. Phys. Chem. B*, 110, **2006**, 12901-12904.

[23]. Z. Xia, L. Riester, W.A. Curtin, H. Li, B.W. Sheldon and J. Laing, Direct observation of toughening mechanisms in carbon nanotube ceramic matrix composite, *Acta. Mater.*, 52, **2004**, 931-944.

[24]. A. Burian-Blajeni, A. G. Kimball, L.S.Robblee, G. L. Kahanda and M. Tomkiewica, *J. Electrochem. Soc.*, 134, **1987**, 2367.

[25]. Y. Lin, X. Cui, X. Ye, Electrocatalytic reactivity for oxygen reduction of palladium-modified carbon nanotubes synthesized in supercritical fluid, *Electrochem. Commun.*, 7, **2005**, 267-274.

[26]. Yanhui Xu, Xiangqin Lin, Selectively attaching Pt-nano-clusters to the open ends and defect sites on carbon nanotubes for electrochemical catalysis, Electrochim. Acta, 52, **2007**, 5140-5149.

[27]. A. Choi, H. Jeong, S. Kim, S. Jo, S. Jeon, Electrocatalytic reduction of dioxygen by cobalt porphyrin-modified glassy carbon electrode with single-walled carbon nanotubes and nafion in aqueous solutions, *Electrochim. Acta.*, 53, **2008**, 2579-2584.

[28]. H. Meng and P. Shen, Tungsten Carbide Nanocrystal promoted Pt/C Electrocatalysts for oxygen reduction, *J. Phys. Chem. B*, 109, **2005**, 22705-22709.

[29]. M. Yang, Y. Yang, H. Yang, G. Shen, R. Yu, Layer-by layer self-assembled multilayer films of carbon nanotubes and platinum nanoparticles with polyelectrolyte for the fabrication of biosensors, *Biomater.*, 27, **2006**, 246-255.

[30]. C. Coutanceau, M. J. Croissant, T. Napporn, C. Lamy, Electrocatalytic reduction of dioxygen at platinum particles dispersed in a polyaniline film, *Electrochim. Acta.*, 46, **2000**, 579-588.

[31]. King-Tsai Jeng, Chun-Ching Chien, Ning-Yih Hsu, Shi-Chern Yen, Shean-Du Chiou, Su-Hsine Lin, Wan-Min Huang, Performance of direct methanol fuel cell using carbon nanotube-supported Pt-Ru anode catalyst with controlled composition, *J. Power Sources*, 160, **2006**, 97-104.

[32]. Ahmad Nozad Golikand, Mehdi Asgari, Mohammad Ghannadi Maragheh, Saeed Shahrokhian, Ethaol electrooxidation on a nickel electrode modified by nickel-dimethylglyoxime complex formed by electrochemical synthesis, *J. Electroanal. Chem.*, 588, **2006**, 155-160.

CHAPTER 3

MICROWAVE-INDUCED HEAT PERFORMANCE OF CONDUCTIVE ALUMINA (CA) AND POTENTIAL APPLICATION AS PASSIVE HEATING ELEMENTS (PHES)

3.1 Introduction

21th Century is an epoch for developing various energy saving materials, which are especially highlighted by a surge of attracted interests in electromagnetic absorbing material [1]. Rooting from its defects (electromagnetic interference etc.) and merits (low energy consumption etc. [2]), an increased of attention has been devoted to exploring various microwave absorbing materials for meeting different practical applications. However, up to now, even though ferrite absorbent (such as Fe, Ni, FeCo, $BaCo_2Fe_{16}O_{27}$ and Fe_3B[1-4]) is noted as good candidates for microwave absorbents meriting from large saturation magnetization and Snoek's limit at high frequencies, their further developments are stilled inhibited by the eddy current effect leading to the decreased permeability at high frequency. Herein, that is reasonable that extensive studies on varied dielectric loss absorbents have been reported in recent decades, which mainly involve ceramic (SiC [5-7], $Pr_xY_{1-x}TiTaO_6$ etc.[8]) and various carbonaceous forms such as carbon nanotubes (CNT) [9-10]. Although various magnetic/dielectric loss composites (Ag/CNT, Ni/CNT, Fe/CNT [11-12], $FeCo/Al_2O_3$ [13], $(ZnMg)TiO_3$–TiO_2 (ZMT–TiO_2) [14] etc.) have been exposed to be effective absorbers and it was concluded that their effectiveness were determined by the component and structure of dielectric materials, few literatures are about microwave transparent α-Al_2O_3-based absorbers with low cost, electrical conductivity, thermal stability and corrosive resistivity.

CNT with unique graphitic structure is commonly regarded as effective microwave absorber in the range of 2.0-20 GHz [15] and the absorbing ability changes with irradiated energy. Good absorbing efficiency is attributed to polarization of six-member graphite structure under electromagnetic wave radiation. Cao et al. [16] have confirmed that carbon fiber/silica has microwave absorbability in the range of 8.2-12.4 GHz at temperatures between 30 °C and 600 °C. However, besides of cost and preparing technology inhibitions, poor affinity of carbon and ceramic also blocks the further researching steps in exploring carbon/ceramic composite as high capacitive electromagnetic absorbent. Therefore, it would be very intriguing that if a novel carbon/ceramic microwave absorber without limits listed above could be developed.

Electrically conductive alumina (CA) with two forms: dense/porous (CDA or CPA) prepared by the combination of gel-casting and high temperature reductive sintering (HTRS) in Argon is regarded as good candidate in various potential applications, which is determined by its unique structure [17]. As shown in former studies, by reductive sintering in Ar, the well gelled polymer in green body can be converted to be three-dimensional conductive networks with graphitic structure resulting electrical conductivity of CDA and CPA [18-19]. Herein, in this

chapter, by investigating the basic property of CA, microwave-induced heat performance and application as passive heating Elements (PHEs) were demonstrated. In order to well understand the microwave activity of CA, effects of HTRS temperature (CDA-1400 °C and CDA-1700 °C), porosity resulted from mechanical forming (CPA-1700 °C and CDA-1700 °C) and NCN amount (CPA-1700 °C, PA-1700 °C (PA: Porous Alumina) and CDA-1700 °C) were well discussed based on Raman spectroscopy, density and porosity analysis and morphology observation via FE-SEM.

3.2. Experimental Procedures

3.2.1. Preparation of CA

3.2.1.1. Slurry preparation and casting process

Alumina powder (AL 160SG-4) with mean particle size (D50) of 0.60 μm was supplied by Showa-Denko Cooperation. Premix solution was initially prepared before making slurry. Monomer (Methacarylamide, MAM, 3.2 wt% based on slurry mass), dispersant (Ammonium Polycarboxylate, APC, Seruna D-305, Chukyo Yushi, Osaka, Japan, 0.87 wt% based on added alumina powder) and cross-linker (N,N′-Methylenebiscarylamide, MBAM, 1.05 wt% based on slurry mass) were employed to make aqueous pre-mix solution. Then Al_2O_3 powder up to 80 wt% solid-loading was added in three steps followed by ball-milling for 24 h. As-resulted ceramic slurry was firstly degassed in ice ultrasonic bath followed by casting by injecting initiator (Ammonium preoxodisufate, APS, 1.03 μL per gram of as-resulted slurry) and catalyst (N,N,N′,N′-Tetramethylenediamine, TMEDA, 0.17 μL per gram of as-resulted slurry). High porosity body CPA was formed with the same slurry, which was initially treated with surfactant sodium polyoxyethylene Lauryl Ether Surfate (Mw=400 $g \cdot cm^{-1}$, 1.74 μL per gram of as-resulted slurry) followed by mechanical stirring in glove box filled with nitrogen gas. All of the related chemicals employed for preparing CA are listed in Table 3.1.

Table 3.1. Chemicals utilized in this study for preparing CA

Chemicals	Suppliers	Function	Composition (wt %)
Alumina Powder (AL 160SG-4, D_{50}=*0.50 μm.*)	Showa Denko, Tokyo, Japan	Powder	80.00
Distilled Water	----------	Solvent	15.05
Seruna D-305	Chuyo Yushi Co. LTD	Dispersant	0.70
Methacrylamide	Kanto Chemical Co. INC	Monomer	3.20
N, N'-methyrenebrsacrylamide	Kanto Chemical Co. INC	Cross-linker	1.05

3.2.1.2. Drying and Sintering process

Two procedures were conducted to get well dried green body without cracks.

a). Humidity controlled drying was finished in 4 days with 10 wt% decrease per day.

b). Constant weight of green body was arrived at 150 °C to ensure moisture removal.

As-resulted well dried green body was sintered in furnace equipped with digital controller with a constant flow of N_2 (99.99 % purity). The holding time at 1700 °C was 2 h. In order to investigate the effect of HTRS temperature on microwave absorbability, as-fabricated CDA green body was sintered at 1400 °C and 1700 °C for 2h, respectively. Effect of high porosity of CA was investigated by comparing CDA and CPA sintered at 1700 °C for 2h. In order to investigate the effect of NCN amount, CPA green body was firstly degreased at 400 °C for 10 h and followed by HTRS at 1700 °C for 2h, as-resulted sample was named as PA-1700 °C. Therefore, four kinds of samples namely, CDA-1400 °C, CDA-1700 °C, CPA-1700 °C and PA-1700 °C were available in this research.

3.2.2. Electromagnetic wave absorbability measurement

3.2.2.1 Confirmation of microwave absorbability

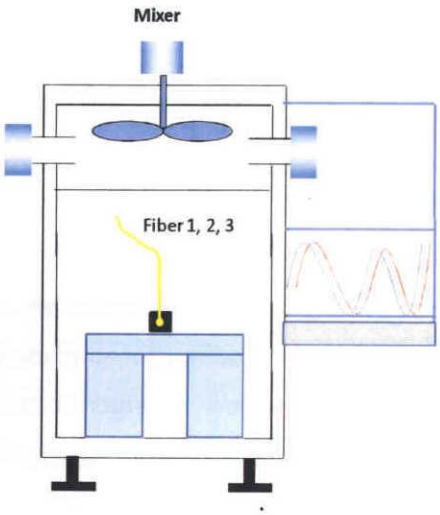

Fig. 3.1. A schematic diagram of microwave irradiation

CA cubic (10 mm × 10 mm ×10 mm) was prepared for microwave-induced heat behaviors investigation. Double mode continuous microwave irradiation with different energy 150 W, 450 W, 750 W and 1050 W were utilized to monitor microwave-induced heat performance of detected materials on MWK-B-3.0 apparatus supplied by Takasago Industry Co., Ltd. This equipment is consisted of a 2.45 GHz microwave magnetron. The schematic chat of absorption measurement by microwave equipment is shown in Fig. 3.1.

Absorptive Efficiency irradiated by microwave at 2.45 GHz with different energies was calculated from equation (1). Incident and reflective powers were automatically recored on microwave apparatus as mentioned above.

$$\text{Absorptive Efficiency} = \frac{\text{Incident power (W)} - \text{Reflective power (W)}}{\text{Incident power (W)} \times a \times b \times c} \times 100 \qquad (1)$$

a, b,c indicates length (cm), width (cm) and height (cm) of specimens

3.2.2.2 Application as Passive Heating Elements (PHEs)

In order to monitor PHEs behaviors, 20 ml of non-polar solvent liquid paraffin (LP, Wako Pure Chemical Industries. Ltd. Japan) was microwave-assisted heated by CDA-1700 °C and CPA-1700 °C cubes (10 mm×10 mm×10 mm), respectively. As-constructed heating systems were irradiated at 750 W by the same apparatus as mentioned in 3.2.2.1.

3.2.3. Characterization

Morphologies of composites were observed by field-emission scanning electron microscopy (FE-SEM, JSM-7600R, Jeol, Corp.). Nano-carbon in composites were evaluated via Raman spectroscopy (NRS-3100, JASCO, Corp.) comparing with reference graphite (KGR-3, Akechi Ceramics (Co., Japan)). Porosity and density of CA were measured on SGM-300 P (Shimadzu Corp.) equipped with meter balance (AEG-320, Shimadzu Corp.) according to Archimedes principle. On average, three specimens were employed to evaluate Porosity and density of as-resulted samples.

3.3. Results and Discussion

3.3.1. Effect of HTRS Temperature

3.3.1.1. Physico-Chemical Analysis

It was proved that HTRS accelerates the conversion and graphitilization of carbon in electrically conductive alumina (CA) [17-20]. As shown in Fig.3.2 (a), electronic crystal structure of carbon in CDA with different sintering temperature (CDA-1400 °C and CDA-1700 °C) is detected by Raman spectroscopy via employing standard graphite as reference. Quasi-graphitic structure of carbon in CA is supported by disorder induced mode and not a Γ-point phonon (D band) around 1350 cm^{-1} and tangential displacement mode (G band) around 1580 cm^{-1} [21]. Both calculated surface defects ($R_{ID/IG}$: Intensity ratio of D band and G band in Raman spectroscopy) and half width of G band ($(\Delta\upsilon_{1580\ cm^{-1}})$) calculated from Raman spectroscopy confirm the graphitization degrees are comparable to graphite. By comparing CDA-1400 °C with CDA-1700 °C, the increased temperature of HTRS eventually accelerates the graphitization processing of carbon in CA composite. This was proven by the reduced surface defects of CDA sintered at higher HTRS temperature ($R_{ID/IG}$(CDA-1400 °C)=1.26>$R_{ID/IG}$ (CDA-1700 °C)=0.35) or decreased half width of G band ($\Delta\upsilon_{1580\ cm^{-1}}$) of CDA sintered at increased HTRS temperature ($\Delta\upsilon_{1580\ cm^{-1}}$(CDA-1400 °C)=80>$\Delta\upsilon_{1580\ cm^{-1}}$(CDA-1700 °C)=22).

While in Fig.3.2 (b) and (c), effect of HTRS on sintered ceramic body is observed comparing CDA-1400 °C and CDA-1700 °C, respectively. All of the FE-SEM images in this study were directly taken from the cut specimen surface without any conductive coating. Results display that HTRS of CDA-1700 °C attributes to increased alumina grain size than CDA-1400°C.

As reported by Rahaman [22], during high temperature sintering (HTS), in order to reduce the surface free energy, coarsening procedure and densification procedure should be present. Coarsening process mainly attributes to micro-structural change without shrinkage and densification process results in increased grain size by removing trapped material from grain boundary. In addition, it is confirmed that polymer binder networks (BN) in well gelled CA green body, namely trapped material, was converted to NCN in CA by HTRS [17]. Simultaneously, growth of alumina grains were inhibited by BN. Furthermore, effect of HTRS temperature on graphitization process was also discussed by Kato et al. [20] It was concluded that: (a) when T>900 °C (T means HTRS temperature), BN was converted to amorphous carbon. This was corrected by stable carbon content (around 0.7 wt %) in sintered body at different temperatures; (b) When T=1400 °C, formation of graphitization was started as supported by the decreased $R_{ID/IG}$ evaluation in Raman spectroscopy and in this study we can conclusion that (c) When T>1400 °C, acceleration of good graphite orientation is achieved as confirmed in Fig.3.2 (a).

Table 3.2. Density and porosity analysis results by Archimedes principle

Materials	Bulk Density ($g \cdot cm^{-3}$)	Open Porosity (%)	Close Porosity (%)	Total Porosity (%)
CDA-1400 °C	2.28	41.46	------	41.46
CDA-1700 °C	3.31	12.37	------	12.37
CPA-1700 °C	1.32	63.85	2.38	66.23

Then, based on the above analysis results, when T<1400 °C, coarsening process occupies leading role in HTRS. This can be validated by HTRS induced shrinkage ratio of CDA-1400 °C (0.5 v%). Instead, when 1400 °C<T<1700 °C, it is replaced by densification process. The densification procedure is confirmed by increased bulk density ($\rho_{bulk\ density}$ (CDA-1400 °C)=2.28 $g \cdot cm^{-3} < \rho_{bulk\ density}$ (CDA-1700 °C)=3.31 $g \cdot cm^{-3}$, Table 3.2), increased HTRS resulted shrinkage ratio of CDA-1700 °C (21 v%) and alumina grain size of CDA-1700 °C as shown in FE-SEM images (Fig.3.2 (b) and (c)). More, HTRS attributes to the improved graphite orientation of NCN ($R_{ID/IG}$(CDA-1400 °C)=1.26>$R_{ID/IG}$(CDA-1700 °C)=0.35) in CA. According to these analysis results, change of alumina green body during HTRS processing is proposed in Figure 3.2 (d). Generally, for carbon-induced conductive composite, both electron and phonon transport results

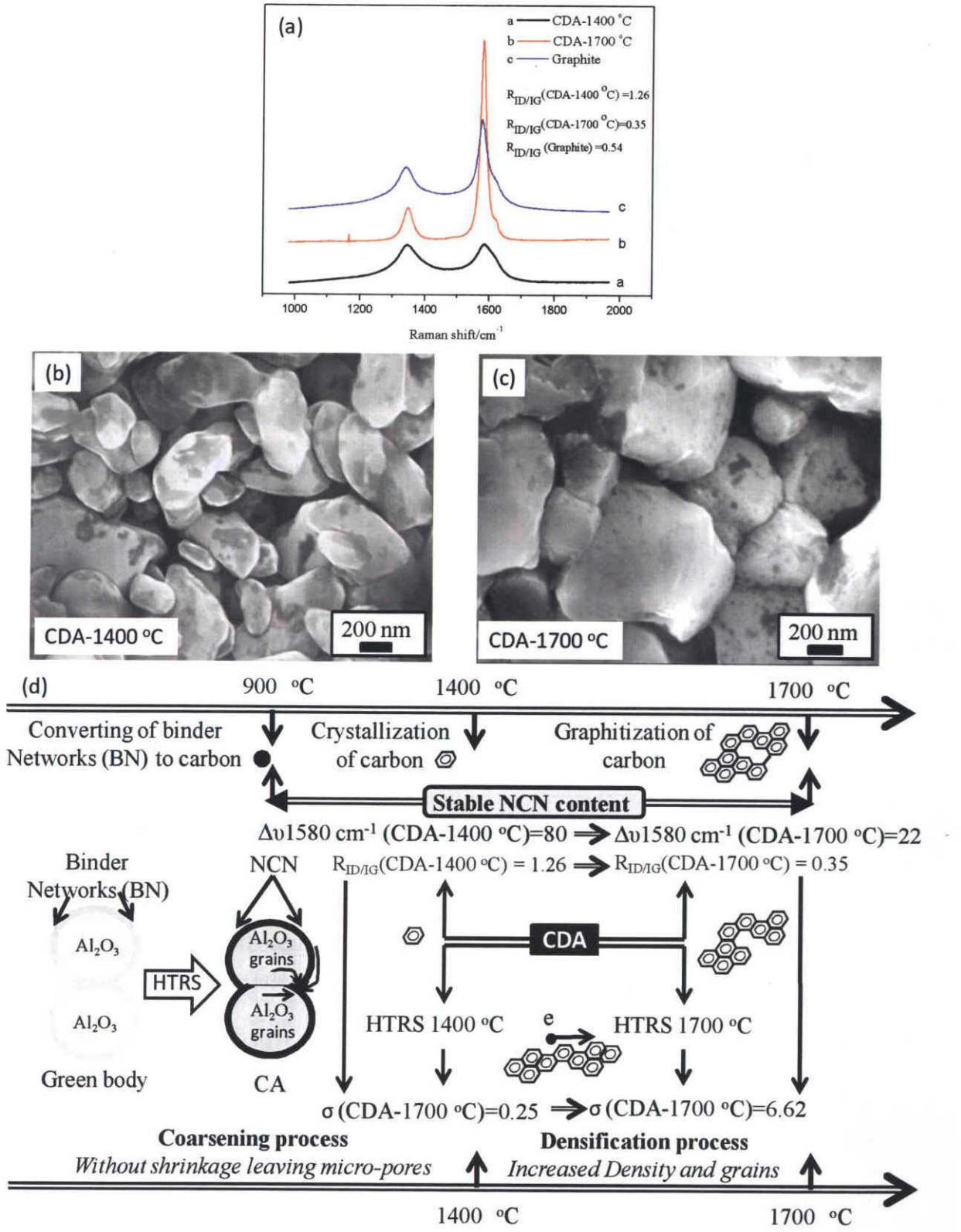

Fig. 3.2. (a) Raman spectroscopy of CDA-1400 °C and CDA-1700 °C employing graphite as standard reference; FE-SEM secondary electron image (SEI) images of (b) CDA-1400 °C and (c) CDA-1700°C with high resolution and (d) Schematic illustration between densifying and coarsening procedures micro-structure changes of CA via high temperature reductive sintering (HTRS) resulting graphitization of binder networks (BN)

Table 3.3. Electrical conductivity [17,22] and graphitilization degree evaluations of NCN in composites by Raman spectroscopy

Materials	Electrical Conductivity ($S \cdot cm^{-1}$)	Surface Defects ($R_{ID/IG}$)	$\Delta\upsilon_{1580\ cm^{-1}}$
CDA-1400 °C	0.25	1.26	80
CDA-1700 °C	6.62	0.35	22
CPA-1700 °C	2.84	0.48	25

in the conductivity of materials. In our case, higher HTRS leads to the increased electrical conductivity, which merits from the enhanced graphitilization degree of NCN.

3.3.1.2.Electromagnetic wave Absorption Evaluation

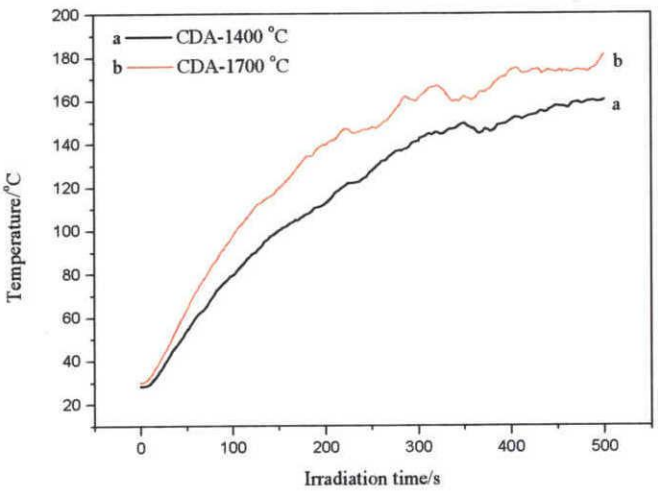

Fig.3.3. Temperature-irradiation time curves of CDA sintered atdifferent temperature (a) CDA-1400 °C and (b) CDA-1700 °C

Microwave irradiation has attracted considerable attentions in recent years as an environmental friendly process. Especially, developing various microwave absorbers with high effective and efficiency and low cost plays an important role [24]. α-Al_2O_3 is commonly regarded as one of the lowest microwave dielectric loss materials among all known ceramic crystal oxides, which is related to finite life time of thermal phonons [25]. However, as shown in Fig.3.3, both CDA-1400 °C and CDA-1700 °C display microwave absorptive behaviors under irradiating at 750 W, which is attributed to the polarized NCN in CDA. And at the varied HTRS condition of CDA with the same carbon content (0.7 wt%), the microwave-induced heat behaviors

difference of them are resulted from different graphite orientation of NCN in CDA. Better graphite orientation, better performances. Increased temperatures of monitored samples indicate that microwave transparency of alumina was resolved.

It was noticed in the former section that the difference among the monitored samples with varied microwave capacity was not only NCN graphitization, also porosity. Therefore, it is plausible to inveatigate the effect of poroisty on property and microwave activity of CA.

3.3.2. Effect of Porosity

3.3.2.1. Physico-Chemical Analysis

Porosity of ceramic body is commonly analyzed according to Archimedes principle. Mechanical forming at the assistance of surfacant (sodium polyoxyethylene Lauryl Ether Surfate) induces high porosity of CPA-1700 °C up to 66.23 % as listed in Table 3.2. Contrast, that of CDA-1700 °C is 12.37 % (which is attributed from HTRS).

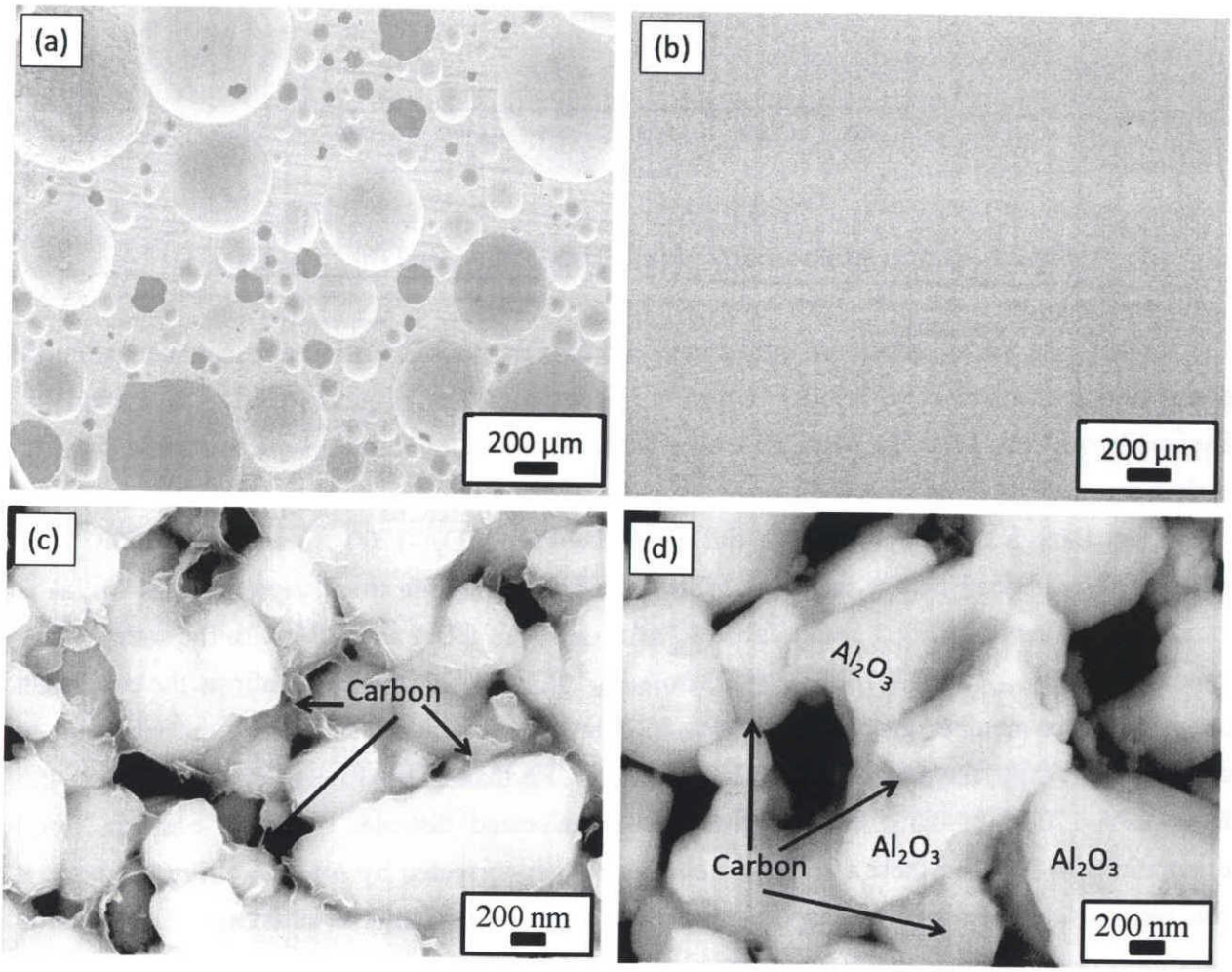

Fig.3.4. FE-SEM secondary electron image (SEI) low magnification images of (a) CPA-1700 °C and (b) CDA-1700°C and compo high magnification images of (c) CPA-1700 °C and (d) CPA-1700 °C

As shown in Fig.3.4 (a), sizes of mechanically induced pores in CPA-1700 °C belong to micrometers and crossed-linked pores permit high porosity of CPA-1700 °C. This was validated by the open porosity analysis using Archimedes principle as shown in Table 3.2. Similarly, few pores are observed in CDA-1700 °C (Fig.3.4 (b)). Micro-structure features of CDA-1700 °C and CPA-1700 °C as shown in high resolution compo images (Fig.3.4 (c) and (d)), an observable co-existence of alumina grains and carbon in composite forms is available.

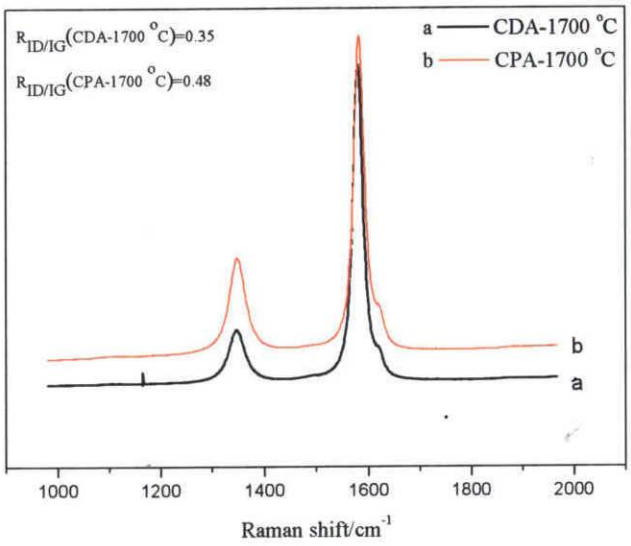

Fig.3.5. Raman spectroscopy of (a) CDA-1700 °C and (b) CPA-1700 °C

In this case, nano-carbon not only covers alumina grains surface but also connects alumina grains acting as conductive bridges, which forms nano-carbon networks (NCN) in composite. Especially, in CPA-1700 °C, more fiber-like NCN during alumina grains are available. Briefly, carbon forms cross-connected 3-dimensional graphite sheet in CA.

Even though the only structure difference between CDA-1700 °C and CPA-1700 °C is porosity, it is noticed that at the same HTRS condition, graphite orientation of NCN in CA is varied as confirmed in Fig.3.5 and Table 3.3. $\Delta\upsilon_{1580\ cm^{-1}}$ of CDA and CPA with the same HTRS condition ($\Delta\upsilon_{1580\ cm^{-1}}$ (CDA-1700 °C)=22, $\Delta\upsilon_{1580\ cm^{-1}}$ (CPA-1700 °C)=25) confirms the equivalent integrity of six-member graphitic structure in composites, which results from the vibration of carbon [21]. While, the enhanced surface defects of CPA than CDA ($R_{ID/IG}$(CPA-1700 °C)=0.48> $R_{ID/IG}$(CPA-1700 °C)=0.35) benefits from either enhanced disorder or non Γ-phonon. Good orientations of NCN in these two specimens have been corrected by $\Delta\upsilon_{1580\ cm^{-1}}$. Furthermore, it was reported that, competing with other carbon forms with graphitic structure, the intensified D band in carbon nanotubes (CNT) was attributed to double-resonance scattering-induced D band which was most related to phonon process [26-27]. Herein, the increased defect concentration of CPA-1700 °C is derived from intensified phonon process attributing to fiber-like NCN nets. Comparing with CDA-1700 °C, increased surface defect of CPA-1700 °C ($R_{ID/IG}$(CPA-1700°C)=

0.48>$R_{ID/IG}$(CDA-1700 °C)=0.35) attributes to the decreased conductivity of them ($\sigma_{CDA\text{-}1700\ °C}$=6.62 S•cm^{-1}>$\sigma_{CPA\text{-}1700\ °C}$=2.84 S•cm^{-1}) [17,20].

3.3.2.2. Electromagnetic wave Absorption Evaluation

Even though a number of materials can be heated by electromagnetic wave at high frequency, ceramic and carbon belonging to dielectric heating materials have the ability in polarization and non-polarization at high frequency electric field or relaxation and resonance process by altering magnetic field or conductivity paths [7-10]. Microwave-induced performances of CDA-1700 °C and CPA-1700 °C by changing irradiating powers at 2.45 GHz are confirmed by increased temperature curves of specimens as shown in Fig.3.6 (a) and (b).

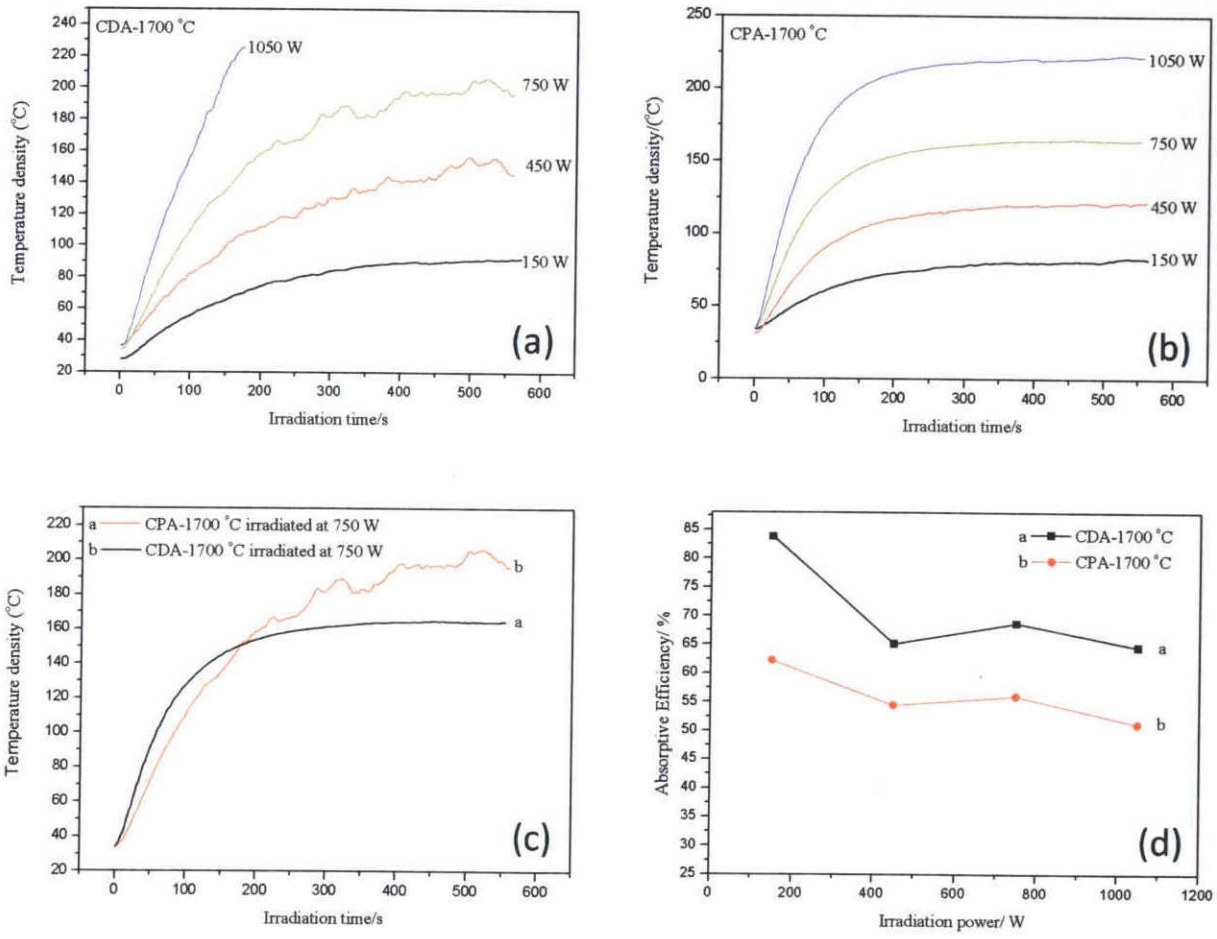

Fig. 3.6. Temperature-irradiation time curves of (a) CDA-1700 °C and (b) CPA-1700 °C irradiating with different microwave energy; (c) comparison of CDA-1700 °C and CPA-1700 °C irradiated at 750 W and (d) Absorptive efficiencies of CDA-1400 °C and CDA-1700 °C with different irradiation powers

Generally, with the same irradiation condition (such as irradiating at 750 W, Fig. 3.6 (c)), microwave absorbability of CDA-1700 °C exhibits higher than that of CPA-1700 °C, which is attributed to the enhanced absorptive efficiency of CDA-1700 °C as shown in Fig. 3.6 (d). It is noticed that with different irradiation powers at 2.45 GHz, absorptive efficiency of CDA-1700 °C and CPA-1700 °C decrease with the increased irradiation energy and keep stable when irradiation power is higher than 450 W. Electromagnetic wave absorptive behavior of CNT with the same graphite structure indicates the length independency of "perfect" CNT and microwave absorbability [9]. It has been confirmed that, in CDA with different HTRS condition, better NCN orientation indicates the enhanced heat behavior. Then, proposing the same NCN graphite orientation (because of the similar $\Delta\upsilon_{1580\ cm^{-1}}$ of composites ($\Delta\upsilon_{1580\ cm^{-1}}$(CDA-1700 °C)=22, $\Delta\upsilon_{1580\ cm^{-1}}$ (CPA-1700 °C)=25)) in CDA and CPA at the same HTRS condition, it is concluded that lower NCN amount resulting from high porosity of CPA up to 66.23 % attributes to the weaker absorbability of CPA than CDA at the same HTRS condition. Herein, chemical inert and microwave sensitive material CA-1700 °C with different forms (CDA-1700 °C and CPA-1700 °C) have been experimentally proven in this study.

3.3.3. Effect of nano-carbon networks (NCN) amount

3.3.3.1 Physico-Chemical Analysis

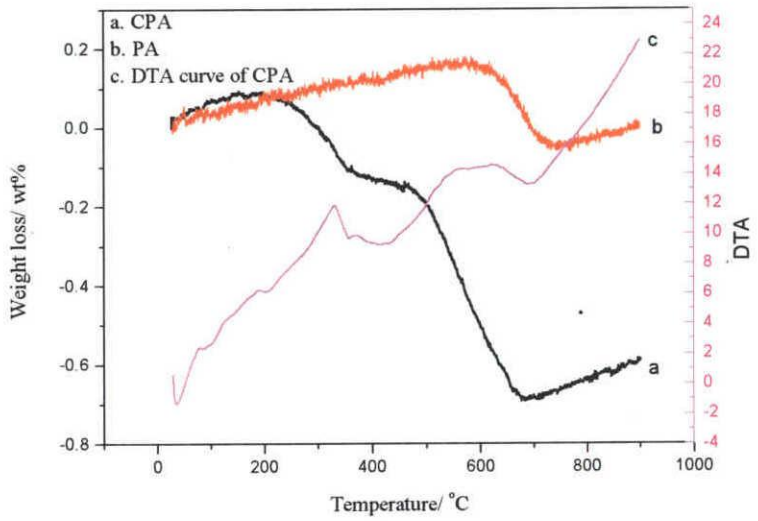

Fig.3.7. Thermal analyses of CPA with/without degreasing (a) TG curve of CPA-1700 °C in oxygen atmosphere; (b) TG curve of PA-1700 °C in oxygen atmosphere and (c) DTA curve of CPA-1700 °C in oxygen atmosphere

Microwave absorptive ability of CA meriting from the polarization of NCN has been confirmed in former sections. Both graphitic orientation and amount of NCN in composites influence the absorbing performances.

The increased graphitic orientation of NCN (as proved by comparing CDA-1700 °C and CDA-1400 °C) attributes to the enhanced absorbing behaviors. Wherein, it is necessary to discuss the role of NCN amount in composite for their polarization performances. For comparing, PA-1700 °C was employed. Then, two kinds of porous composites with varied carbon content are available in this investigation namely PA-1700 °C (0.15 wt %) and CPA-1700 °C (0.72 wt %) as shown in Fig. 3.7.

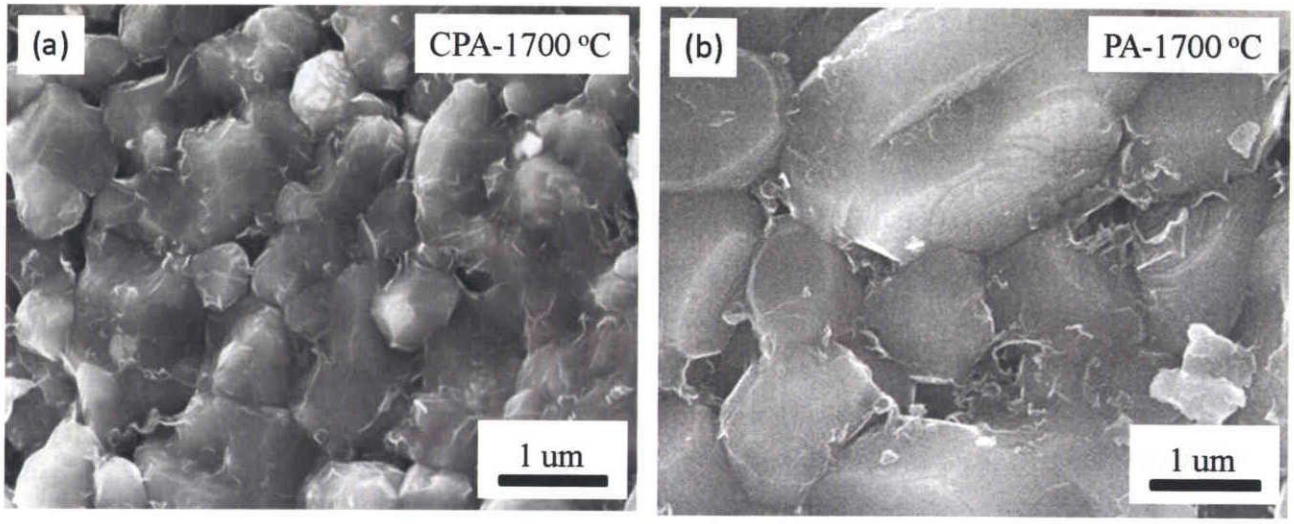

Fig. 3.8. FE-SEM images of (a) CPA-1700 °C and (b) PA-1700 °C

Fig.3.8 (a) and (b) FE-SEM images support that the decreased BN in green body attributes to the increased Al_2O_3 grain size, which is in accordance with our proposal in Fig. 3.2 (d). Herein, it is feasible to conclude that densification processing also can be accelerated by degreasing, which can be proven by density analysis as displayed in Table 3.4. Furthermore, the varied density and porosity of PA-1700 °C also verify the inhibition of BN for alumina grain growth during HTRS.

Table 3.4. Density and porosity analysis results by Alchimedes principle

Materials	Bulk Density ($g \cdot cm^{-3}$)	Apparent Density ($g \cdot cm^{-3}$)	Real Density ($g \cdot cm^{-3}$)	Open Porosity (%)	Closed Porosity (%)	Total Porosity (%)
CPA-1700 °C	1.32	3.65	3.91	63.85	2.38	66.23
PA-1700 °C	1.91	2.45	3.88	22.04	28.67	50.71

3.3.3.2. Electromagnetic Absorption Evaluation

As shown in Fig.3.9 (a), even though NCN content in PA-1700 °C is only 0.15 wt%, microwave absorptive performance is as good as CPA-1700 °C. Perhaps its performance is not directly determined by NCN amount. Then, the relationship between the monitored temperature difference ($\Delta T=T_t-T_0$, $t_{(irradiation\ time)}$=540 s) and amount of NCN in investigated composites cubic with dimension (10 mm×10 mm×10 mm) are investigated. These samples were irradiated at 750 W.

As displayed in Fig.3.9 (b), comparing with as-received Al_2O_3 powder, CA composites own good microwave activity meriting from NCN polarization at microwave irradiation. By comparing CDA-1700 °C, CPA-1700 °C and PA-1700 °C each other, it is facilitated to conclude that these varied behaviors are determined by both NCN orientation and NCN amount. Especially, the changed temperature difference ratio (ΔT(CDA-1700 °C)/ΔT(CPA-1700 °C), ΔT(CDA-1700 °C)/ΔT(PA-1700 °C) and ΔT(CPA-1700 °C)/ΔT(PA-1700 °C)) of each two samples are 1.330, 1.330 and 0.998, respectively. The calculated carbon contents of these three pairs are 2, 6 and 3. While the graphitic orientation of them (Obtained from the detected surface defects value from Raman spectroscopy) are 1.4, 1.14 and 0.8. While, the similar evaluation results are available via $\Delta\upsilon_{1580\ cm^{-1}}$ of composites, which is 1.13, 1.11 and 0.96 for the evaluation pairs mentioned above. Then, based on various parameter proportions, it is facilitated to reach a conclusion that microwave absorbability of specimens with the same size is relatated with the graphitilization degree of NCN rather than NCN amount. Unvaried microwave performance of CPA-1700°C and PA-1700 °C (Fig. 3.9 (b)) is a good proof of it.

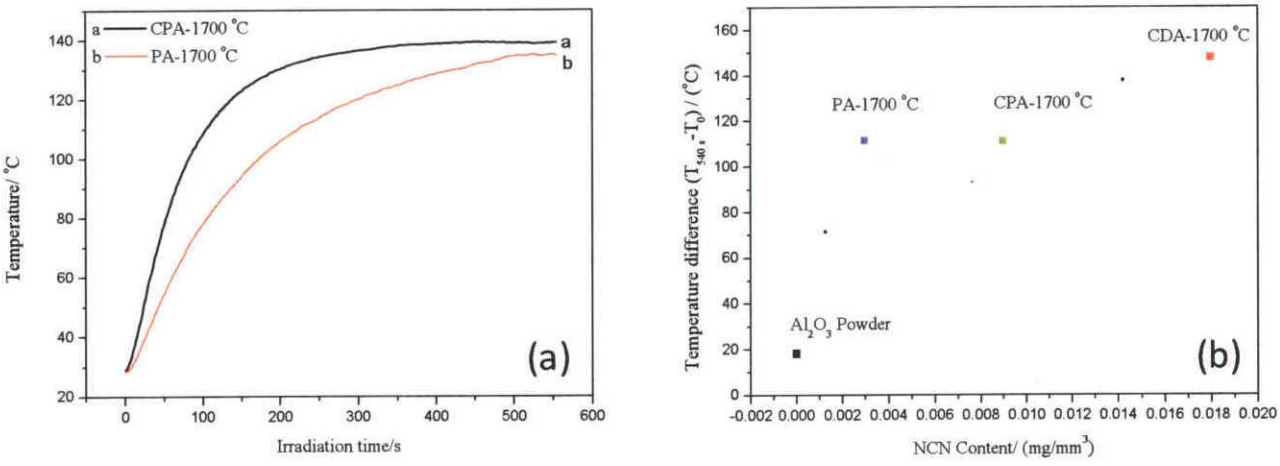

Fig.3.9. (a) Temperature-irradiation time curves of CPA-1700 °C and PA-1700 °C; (b) Correlation plot between temperature difference and NCN Content in Al_2O_3, CDA-1700 °C, CPA-1700 °C and PA-1700 °C

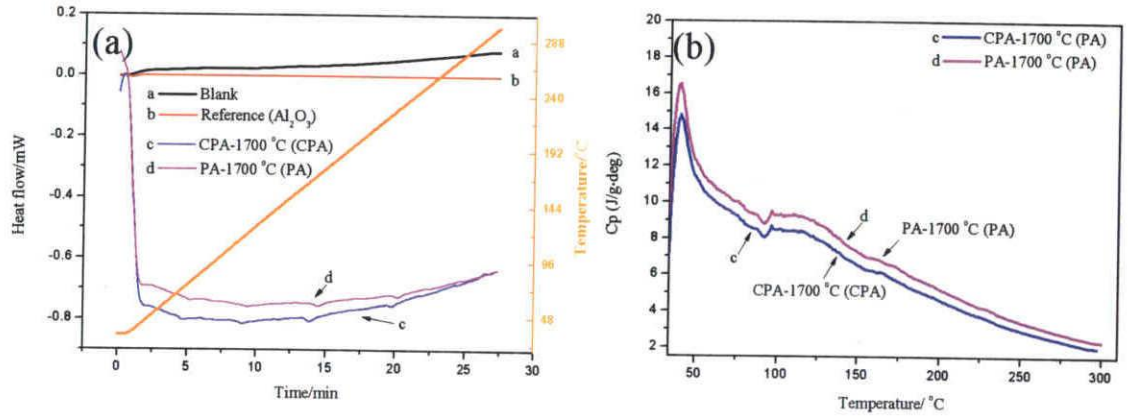

Fig. 3.10. (a) DSC analysis results of as-fabricated composites and (b) Calculated specific heat capacity of composites

By monitoring the heat performances of CA as discussed above, it is reasonable to get a conclusion that at the assistance of microwave irradiation, meriting from polarization of NCN in CA with graphitic structure, good microwave capacity of CA is verified. This summary can be confirmed by temperature-irradiation time curves as displayed in Fig. 3.3, Fig. 3.6 and Fig. 3.9 (a). More, before arriving a saturated temperature, all of them own temperature increasing slope, which belongs to the feature of dielectric loss materials as microwave absorbent [27,28]. In Fig. 3.10, we are trying to explain this phenomenon via thermodynamic. Employing Al_2O_3 (T2X05Q) as reference, at the same experimental condition, the sharply decreased DSC curves of CPA-1700 °C and PA-1700 °C as shown in Fig. 3.10 (a) is an effective proof for their thermal capacity. And the released energy keeps stable with time increase. Simultaneously, the calculated specific heat capacity (Cp ($J/g \cdot cm^{-3}$)) of composites as displayed in Fig. 3.10 (b) make this conclusion valid. Moreover, the decreased specific heat capacity of CA as increased temperature also seems plausible to explain the feature detected temperature-irradiation time curve. For the same amount of specimens, lower specific heat capacity equals to the increased temperature change via microwave radiation.

3.3.4. CPA size dependence on Electromagnetic Absorption Evaluation

In order to investigate the size depency of CA microwave absorbability, as-fabricated CPA-1700 °C was cut into cubes with different sizes as shown in Table 3.5.

All of these samples were irradiated at 750 W. Fig.3.11 (I) displays the temperature change monitored by thermo-fiber. By which it is understood that temperature increases with sample size, but not direct depends on that. This conclusion is supported by (II) detected by thermocouple equipped in microwave apparatus.

Table 3.5. Physical property of CPA cubes with different sizes

Materials	Size (mm)	Volume (cm^{-3})	Weight (g)
CPA-1	8.70×9.99×8.68	0.75	2.10
CPA-2	22.72×9.99×8.70	1.98	3.94
CPA-3	22.03×24.45×9.45	5.09	11.32
CPA-4	24.66×33.69×9.31	7.74	19.44
CPA-5	23.11×24.55×21.94	12.45	27.52

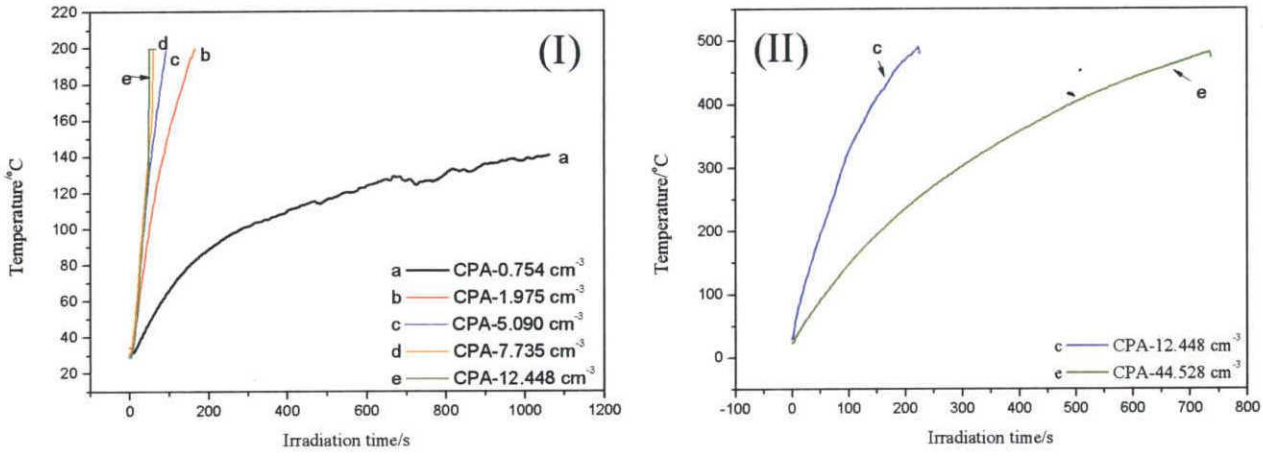

Fig. 3.11. Temperature-irradiation time curves of CPA with different sizes (I) monitored by fiber and (II) monitored by thermal-couple

3.3.5. Application as Passive Heating Elements (PHEs)

Performance of passive heating elements (PHEs) was investigated by increased temperature of non-polar solvent via microwave irradiation. Disadvantages of invasive heating methods involve varied polarity of the heated solvent, contamination of reaction system etc.[28] As reported in our studies, CA with two forms prepared by the combination of gel-casting and high temperature reductive sintering at 1700 °C not only have good thermal and chemical stability in

aggressive conditions [18,19], but also overcome the microwave transparency of α-Al_2O_3, which permits CA-1700 °C as an ideal candidate for developing PHEs in microwave-assisted experimental system.

In order to confirm the PHEs flexibilities, CA-1700 °C cubes (10 mm × 10 mm × 10 mm) were put into 20 ml non-polarized solution liquid paraffin followed by microwave irradiation at 2.45 GHz with output power of 750 W. As shown in Fig. 3.12 (a), non-polar solvent without CA-1700 °C cannot be heated at microwave irradiation at all and the slight temperature increase is attributed to glass container. Contrast, liquid paraffins are rapidly heated to higher temperature at the aids of microwave absorber CA-1700 °C (CDA-1700 °C and CPA-1700 °C). Even though only 1 cm^3 of absorbers are employed in very short irradiation time, increased temperatures of microwave transparent solvent support good PHEs performance of CA-1700 °C.

Furthermore, by comparing PHEs performances of CDA-1700 °C and CPA-1700 °C as displayed in Fig.3.12 (a), in accordance with previous section, higher absorption of CDA-1700 °C attributes to higher monitored temperature. However, when the detected temperature is lower than 40 °C, heating speed of CPA-1700 °C is faster than CDA-1700 °C (Fig.3.12 (b)). Meriting from high porosity of CPA-1700 °C, increased contact surface between CPA-1700 °C and solvent at the initial step and quicker thermal flow benefiting from high porosity attribute to this behavior.

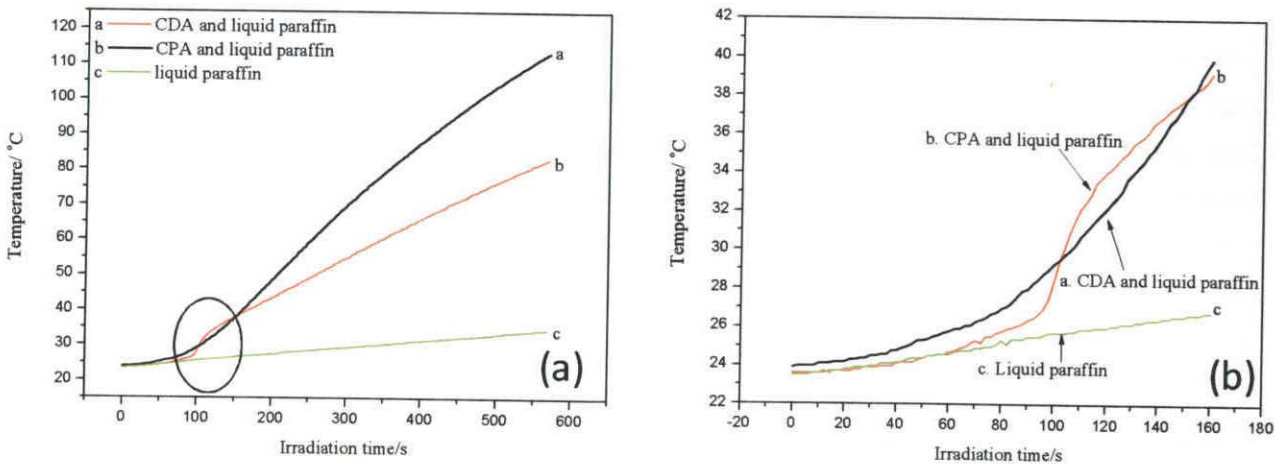

Fig.3.12. Temperature-irradiation time curves of CDA-1700°C and CPA-1700°C for investigating passive heating elements (PHEs) performances in liquid paraffin (a) Large-scale investigation (b) Enlarged curves of circled part in (a)

By investigating the physico-chemical and electromagnetic wave absorptive property of CDA-1700 °C and CPA-1700 °C, we can get understood that both electrical conductivity and microwave capacity are influenced by NCN in CA. Good electrical conductivity merits from

graphite orientations of NCN in CA. However, microwave absorbability is mainly related with graphite orientation of NCN and porosity. This scheme is shown in Figure 3.13. Based on these features, it is feasible to design other research direction.

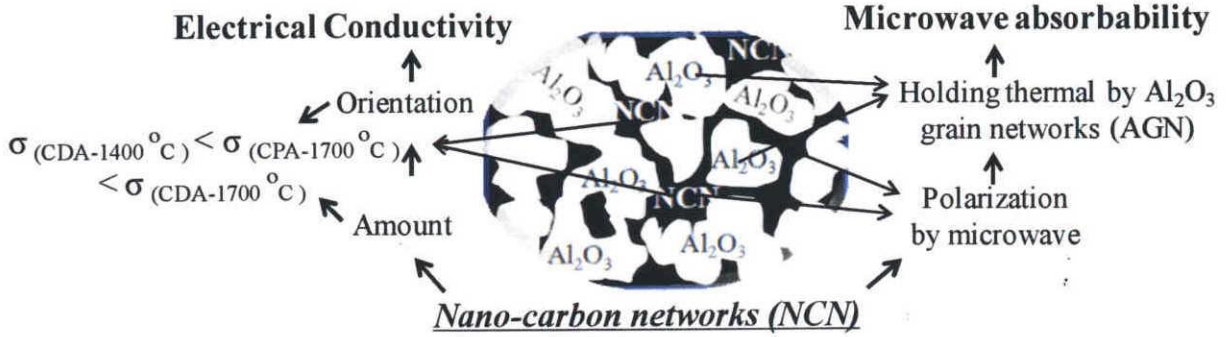

Fig. 3.13 Schematic diagram of relationship between electrically conductivity and thermal conductivity for CA

3.4. Conclusions

Novel electromagnetic wave absorbability of CA-1700 °C with dense and porous two forms (abbreviated as CDA-1700 °C and CPA-1700 °C) were confirmed in this chapter, by which microwave transparence of alumina was effectively resolved. As confirmed by characterization results, NCN converted from well-gelled polymer binder networks (BN) was obtained by HTRS. As-resulted NCN with graphitic structure in CA was responsible for good electrical conductivity and microwave absorbing performance. By discussing the influence of HTRS temperature, porosity and carbon amount, respectively, it is concluded that graphite orientation of NCN in composites play the most important role. And absorptive behaviors change with size of irradiated specimens. Furthermore, the investigated PHEs performances of CDA-1700 °C and CPA-1700 °C for microwave transparent non-polarized solvent liquid paraffin claim their potential application as non-contacting heater.

References

[1]. Jiangqiang Wei, Jianbo Wang, Qingfang Liu, Liang Qiao, Tao Wang, and Fashen Li, Enhanced microwave absorption properties of Fe_3Al/Al_2O_3 fine particle composites, *J. Phys. D: Appl. Phys.*, 43, **2010**, 115001/1-115001/5.

[2]. Maria Jose Gracia, Juan Manuel Campelo, Elia Losada, Rafael Luque, Jose Maria Marinas and Antonio Angel Romero, Microwave-assisted versatile hydrogenation of carbonyl compounds using supported metal nanoparticles, *Organic&Biomolecular Chemistry*, 7, **2009**, 4821-4824.

[3]. C. Sudakar, G. N. Subbanna and T. R. Kutty, Hexaferrite-Foco nanocomposite particles and their electrical and magnetic properties at high frequencies, *J. Appl. Phys.*, 94 (9), **2003**, 6030-6033.

[4]. Liang Qiao, Xianghua Han, Bo Gao, Jianbo Wang, Fusheng Wen and Fashen Li, Microwave absorption properties of the hierarchically branched Ni nanowire composites, *J. Appl. Phys.*, 105, **2009**, 053911/1-053911/4.

[5]. Zengyong Chu, Haifeng Cheng, Yongjiang Zhou, Qiang Wang, Jun Wang, Anisotropic microwave absorbing properties of oriented SiC short fiber sheets, *Mater. Des.*, 31, **2010**, 3140-3145.

[6] M. Izawa, T. Koseki, Y. Kamiya, T. toyomasu, Characteristics of a SiC microwave absorber for damped cavity, *Rev. Sci. Instrum.*, 66(2), **1995**, 1910-1912.

[7]. Donglin Zhao, Fa Luo, Wan-Cheng Zhou, Microwave absorbing property and complex permittivity of nano SiC particles doped with nitrogen, *J. Alloys compd.*, 490, **2010**, 190-194.

[8]. H. Padma Kumar, James T. Joseph, J. K. Thomas, K. Joy, Sam Solomon, Composites and solid solutions of Pr-Y titanium tantalite microwave ceramics, *J. Mater. Sci: Mater. Electron.*, 20, **2009**, 551-554.

[9]. Ester Vázzquez, Maurizio Prato, Carbon Nanotubes and Microwaves: Interactions, Responses and Applications, *ACS Nano*, 3(12), **2009**, 3819-3824.

[10]. B. Corzilius, K. P. Dinse and K. Hata, Single-wall carbon nanotubes and peapods investigated by EPR, *Phys. Chem. Chem. Phys.*, 9, **2007**, 6063-6072.

[11]. Xuchun Gui, Kunlin Wang, Jinquan Wei, Ruitao Lü, Qinke Shu, Yi Jia, Chen Wang, Hongwei Zhu, Dehai Wu, Microwave absorbing properties and magnetic properties of different carbon nanotubes, *Sci. China, Ser. E*, 52(1), **2009**, 227-231.

[12]. Ruitao Lv, Feiyu Kang, Jialin Gu, Xuchun Gui, Jinquan Wei, Kunlin Wang and Dehai Wu, Carbon nanotubes filled with ferromagnetic alloy nano-wires: Lightweight and wide-band microwave absorber, *Appl. Phys. Lett.*, 93, **2008**, 223105/1-223105/3.

[13]. X. G. Liu, D. Y. Geng and Z. D. Zhang, Microwave-absorption properties of FeCo microspheres self-assembled by Al_2O_3-coated FeCo nanocapsules, *Appl. Phys. Lett.*, 92, **2008**, 243110/1-243110/3.

[14]. Bo Li, Shuren Zhang, Ying Yuan, Xiaohua Zhou and Longcheng Xiang, Dielectric properties and microstructure of TiO_2 modified $(ZnMg)TiO_3$ microwave ceramics with

$CaO-B_2O_3-SiO_2$, *J. Mater. Sci.*, 44, **2009**, 4993-4998.
[15]. Peng Zhihua, Peng Jingcui, Peng Yanfeng, Ou Yangyu, Ning Yantao, Investigation of the microwave absorbing mechanisms of HiPco carbon nanotubes, *Physica E*, 40, **2008**, 2400-2405.
[16]. Maosheng Cao, Weili Song, Zhiling Hou, Bo Wen, Jie Yuan, The effects of temperature and frequency on the dielectric properties, electromagnetic interference shielding and microwave-absorption of short carbon fiber/silica composite, *Carbon*, 48, **2010**, 788-796.
[17]. R. L. Menchavez, M. Fuji, M.Takahashi, Electrically Conductive dense and porous alumina with In-situ-synthesized Nanoscale carbon networs, *Adv. Mater.*, 20, **2008**, 2345-2351.
[18]. J. Liu, H. Watanabe, M. Fuji, M. Takahashi, Electrocatalytic evolution of hydrogen on porous alumina/gelcast-derived-carbon network composite electrode, *Electrochem. Commun.*, 10, **2008**, 922-925.
[19]. C. Hai, H. Watanabe, T. Shirai, M. Fuji, M. Takahashi, F. Wang, Modifying the surface of the electrically conductive porous alumina, *Mater. Lett.*, 63, **2009**, 1320-1322.
[20]. T. Kato, T. Shirai, M. Fuji and M. Takahashi, Graphitization behavior of polymer in the gelcasted alumina by sintering, *J. Ceram. Soc. Jpn.*, 117(9), **2009**, 992-99.
[21]. Ying Tian, Delphine Chassaing, Albert G. Nasibulin, Paola Ayala, Hua Jiang, Anton S. Anisimov and Esko I. Kauppinen, Combined Raman spectroscopy and Transmission electron microscopy studies of a nanobud structure, *J. Am. Chem. Soc.*, 130, **2008**, 7188-7189.
[22]. M.N. Rahaman, Ceramic Processing and Sintering (Materials and Engineering, 10), *New York. Basel: Marcel Dekker, INC*; **1995**.
[23]. P. F. Fulvio, R. T. Mayes, X. Wang, S. M. Mahurin, J. C. Bauer, V. Presser, J. Mcdonough, Y. Gogotsi and S. Dai, "Brick-and-Motar" Self-Assembly Approach to Graphitic Mesporous Carbon Nanoparticles, *Adv. Funct. Mater.*, 21, **2011**, 2208-2214.
[24]. Doris Dallinger, Muhammed Irfan, Amra Suljanovic, and C. Oliver Kappe, An investigation of wall effects in microwave-assisited ring-closing materials and cyclotrimerization reactions, *J. Org. Chem.*, 75, **2010**, 5278-5288.
[25]. Nicolas A. Shtin, José Mauricio Lopez Romero and Eugene Prokhorov, Theory of fundamental microwave absorption in sapphire (α-Al_2O_3), *J. Appl. Phys.*, 106, **2009**, 104115.
[26]. C. Thomsen and S. Reich, Double resonant Raman scattering in Graphite, *Phys. Rev. Lett.*, 85 (24), **2000**, 5214-5217.
[27]. Christian Thomsen, Stephanie Reich and Janina Maultzsch, Resonant Raman spectroscopy of nanotubes, *Phil. Trans. R. Soc. Lond. A*, 362, **2004**, 2337-2359.
[28]. Tahseen Razzaq, Jennfer M. Kremsner and C. Oliver Kappe, Investigation the existence of Nonthermal/Specific microwave effects using silicon carbide heating elements as power modulators, *J. Org. Chem.*, 73, **2008**, 6321-6329.

CHAPTER 4

STRUCTURAL MODIFICATION OF CONDUCTIVE POROUS ALUMINA EMPLOYING CARBON NANOTUBES AND ELECTROMAGNETIC WAVE ABSORABILITY INVESTIGATIONS

4.1 Introduction

In chapter 3, we have confirmed the good electromagnetic wave-induced heat performance of CA. By discussing the influence of nano-carbon networks (NCN) graphitilization degree, mechanical forming resulted high porosity and NCN amount, several useful conclusions are listed as follows:

a). Nano-carbon networks (NCN) converted from well-gelled biner networks (BN) via HTRS has graphitic electronic crystal structure and its microwave-induced heat performance can be controlled by different HTRS temperature, which leads to the varied graphitilization degree of NCN in CA.

b). NCN-induced Electrical conductivity and microwave-induced heat performance increases with improved orientation.

It is noticed that in CA namely CDA and CPA (in this chapter CDA and CPA mean that HTRS temperature is 1700 °C), highly graphitized NCN not only leads to the good electrochemical performances as demonstrated in Chapter 2 [1-4], but also results in the good electromagnetic wave absorbability as introduced in Chapter 3. Due to the more fiber-like NCN in CPA, the increased non-Γ phonon processing attributes to the increased surface defects than CDA as supported by Raman spectra evaluation in Chapter 3. More, it was reported that phonon determines the thermal behaviors of materials. Furthermore, for most of high porosity composite, both non-conductivity and brittleness of ceramics has suspended their different potential applications. So far, for reinforcement technology, incorporating components leading to the increased fracture toughness are believed to be more effective methods than reducing critical flaw size [5-10].

High-performance composites with good bending strength are always reinforced by whiskers, polymers with high elastic modulus [11-12] and nanofibers with high long-diameters ratio [6-8] etc. Carbon nanotubes (CNT), with high tensile strength ranging from 20-100 GPa and 1 TPa as elastic modulus, is commonly used as reinforcement in brittle materials [8-13]. In CNT-reinforced ceramic matrix composites, induced energy is absorbed by highly flexible elastic nanotubes, which results in the increased strength of composites. In addition to the good mechanical properties, CNT also possesses superior thermal and electrical properties. CNT has a good thermal stability up to 750 °C in air and 2800 °C in vacuum [10]. As reported in references [10-17], fracture toughness and strength of composites can be enhanced by incorporating with CNT. And the involved fabrication technologies include hot press [10], spark plasma spray (SPS)

[14], sol-gel [15] etc.

Although CNT is confirmed to be effective reinforcement for various matrices, materials fabrication difficulties have limited the further research on this topic. Aqueous gelcasting is commonly regarded as an effective way in shaping by chemical route [16]. Wet-technology with sufficient mixing supplies opportunity for making uniformly dispersed ceramic and CNT slurry. And the poor dispersibility of CNT in aqueous medium was solved by surface pre-treatment with mixed concentrated acids, which is mainly attributed to the enhanced surface defects. Usually, for CNT, two kinds of defects are available: (a). Instinctive defects resulted from the end caps of fibers with high activity and sidewall defected sites, which involve pentagon-heptagon pairs called Stone-wales defects, sp^3-hybridized defects and vacancies in the lattice [17]. (b). Manually induced defects by physical and chemical ways at the ends and sidewall of carbon nanotubes (CNT). Therefore, taking these factors into consideration and comparing with non-covalent functional methods with less destruction, covalent modification is believed to be much more effective technique because of the higher degree of tunability of tubes through reactions onto π-conjugated skeleton [18]. So far, universally used covalent reagents involve strong acids [19], oxygen gas, $K_2Cr_2O_7/H_2SO_4$ [17] etc.

Herein, in this chapter we would like to introduce the effect of carbon nanotubes (CNT) on conductive porous alumina composite namely CNT/CPA by the combination of gel-casting and HTRS in Ar. In order to increase hydrophilic of as-received CNT from company, commonly utilized mixed-acids (H_2SO_4:HNO_3=3:1, v/v) were employed and optimum pre-treating condition in aqueous was concluded by comparing the influences of temperature and time. Effects of CNT on microwave absorptive behaviors were investigated by increasing CNT amount and degreasing of as-received green body. Furthermore, in order to well understand the influence of filler graphitilization degree, carbon black (CB), highly graphitilized CNT (HGCNT) were employed.

4.2 Experimental procedures

4.2.1 Experimental steps for preparing composite

4.2.1.1 Surface pre-treatment of as-received CNT

0.5 g of CNT supplied by showa denko (VGCF-X®) was added into 60 ml of mixed acids (H_2SO_4/HNO_3=3:1, v/v) and refluxed at 40 °C, 50 °C, 60 °C, 70 °C and 80 °C respectively for 6h followed by thoroughly washing and drying at 60 °C in vacuum oven overnight to obtain the optimum pre-treating temperature. Moreover, in order to gain the most suitable treating time at optimum temperature, 2h, 4h, 6h, 7h and 8h also had been conducted.

4.2.1.2 Fabrication of CNT/CPA Composite

Table 4.1 shows the chemicals used for making CNT/alumina slurry. These chemicals were directly used without any further purification processing.

a). CNT/Alumina slurry Preparation and Gelcasting process

To prepare 1000 g of CNT/Alumina slurry, included steps are listed as follows:

- 1 g of pre-treated CNT and 150.5 g of distilled water were placed in ultrasonic bath at room temperature for 20 min to form a stable black CNT suspension.
- Dispersant, monomer and cross-linker listed in Table 4.1 and CNT suspension were well-mixed by ball-milling for 8h (milling ball is 800 g of Al_2O_3 with diameter of 5 mm). This mixture was denoted as pre-mix solution.

Table 4.1. Chemicals used for making CNT/Alumina slurry

Chemicals	Suppliers	Function	Composition (w %)
CNT	Showa Denko, Tokyo, Japan	Filler	0.10
Alumina Powder (AL 160SG-4, D_{50}=0.50 μm.)	Showa Denko, Tokyo, Japan	Powder	79.90
Distilled Water	Nagoya Institute of Technology	Solvent	15.05
Seruna D-305	Chuyo Yushi Co. LTD	Dispersant	0.70
Methacrylamide	Kanto Chemical Co. INC	Monomer	3.20
N, N'-methyrenebrsacrylamide	Kanto Chemical Co. INC	Cross-linker	1.05

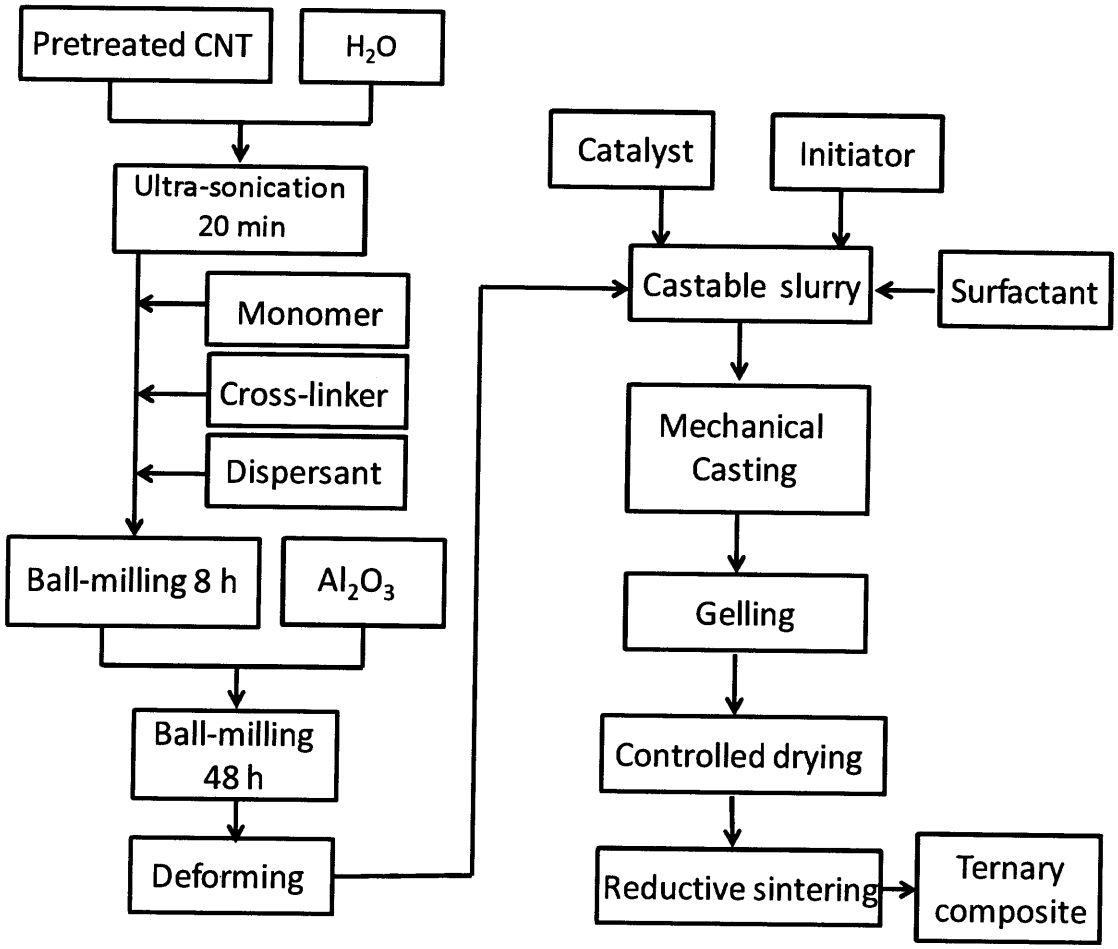

Fig. 4.1. Processing flow sheet of CNT/CPA (CNT/NCN/Alumina) ternary composite

- 800 g of alumina powder (AL 160SG-4, D_{50}=0.50 μm) was added into the pre-mixed solution by three times. Gray CNT/Alumina slurry without bulky agglomeration can be obtained after ball-milling for 48 h.
- As-resulted CNT/Alumina slurry was firstly vacuum-pumped in ultra-sonication bath at 0 °C-2 °C to remove the trapped air bubbles without evaporation of water. Secondly, slurries were treated with desired amount of surfactant (Latemul AD-25, 4μL/gram) and mixed manually with a spoon under nitrogen atmosphere inside a glove box.
- The surfactant treated slurry was subsequently added with initiator in 10 wt% solution (Ammonium preoxodisufate, 8.24 μL per 1g of slurry) and catalyst (N,N,N′,N′-Tetramethylenediamine, 1.36 μL per 1g of slurry), followed by mechanically forming for 3 min inside the nitrogen-filled glove box using hand mixer at full speed. The final foamed slurry was poured into a Teflon mold and kept for one night to obtain the well gelled green body.

b). Drying and Sintering schedule

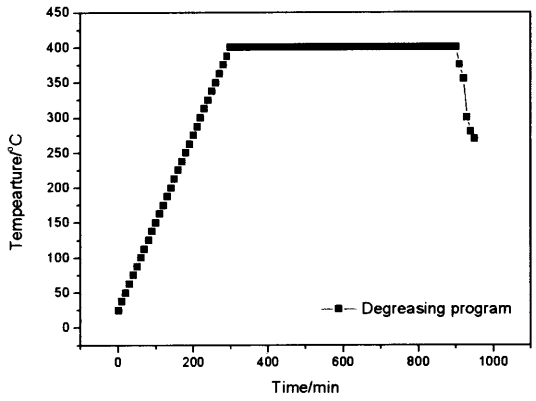

Fig. 4.2. Degreasing program for preparing PA and CNT-0.3 wt%-PA

The controlled humidity drying of well gelled green body was implemented in 4 days from 90 wt% to 60 wt%, and was dried in vacuum at 150 °C until a constant weight was achieved. This dried sample was reductive sintered at 1700 °C for 2 h in argon, by which a ternary (CNT-0.1wt%/NCN/Alumina (CNT-0.1 wt%-CPA)) composite was obtained. Amount of added CNT was 0.1 wt %. A detail of processing flow is shown in Fig. 4.1. For comparing, binary composite CPA (NCN/ Alumina) was also prepared.

In order to investigate the role of CNT on physic-chemical property and absorptive performance of composites, CNT/CPA composites with different CNT amount were prepared, namely CNT-0.3 wt%-CPA and CNT-0.4 wt%-CPA. More, CNT-0.3 wt%-PA was also prepared by degreasing firstly and followed by reductive sintering at the same condition with others. The degreasing program is shown in Fig. 4.2.

Influence of filler graphitic orientation on monitored properties of composite was conducted via different carbon forms with varied graphitization degree employing the same fabrication method. These carbonaceous include carbon black (CB), highly graphitilized CNT (HGCNT). As-resulted composite was denoted as HGCNT-0.1 wt%-CPA and CB-0.1 wt%-CPA.

4.2.2. Electromagnetic wave absorbability measurement

CNT-0.1 wt%-CPA, CNT-0.3 wt%-CPA, CNT-0.4 wt%-CPA, CPA, HGCNT-0.1 wt%-CPA and CB-0.1 wt%-CPA cubic (10 mm×10 mm×10 mm) were prepared for microwave absorbability measurement. Double mode continuous microwave irradiation with different energy 150 W, 450 W, 750 W and 1050 W were utilized to monitor the microwave absorbability of detected materials on MWK-B-3.0 apparatus supplied by Takasago Industry Co., Ltd. This equipment is consisted of a 2.45 GHz microwave magnetron.

4.2.3. Characterization

4.2.3.1. Functionalization of as-received CNT

Fourier Transform Infrared (FT-IR, FT/IR-6200, JASCO, Corp.) spectrometer was employed to detect the surface change of CNT with/without pre-treatment. ζ-Potential analysis and size distribution of CNT with/without pre-treatment measured by Zetasizer Nano Series (Malvern Instrument Ltd.) were employed to monitor the effect of treating conditions and to investigate the chemical functional modification route. Crystal structure of sample was characterized by Raman spectroscopy (NRS-3100, JASCO, Corp.) and X-ray diffraction (XRD, RINT, Rigaku, Japan, CuKα, 40keV, 20mA)

0.03 mg/ml of black CNT aqueous solutions with/without treatment were prepared for ζ-Potential and size-distribution measurement. These solutions were centrifuged at 15,000 rpm for 3h followed by decanting the brown transparent supernatant into small glass bottle with caps. Then as-resulted solutions were utilized to evaluate ζ-potential and size distribution after adjusting pH value by NaOH and HCl.

4.2.3.2. Characterization of CNT/CPA Composite

Structures of the composites were observed by field-emission scanning electron microscopy (FE-SEM, JEOL, JSM7600R). The electronic crystal structure of carbon was monitored by Raman spectroscopy (NRS-3100, JASCO, Corp.). Body density and apparent porosity of composites were measured according to Archimedes principle (SGM-300 P, Shimadzu Corp.) equipped with meter balance (AEG-320, Shimadzu Corp.). Mechanical behaviors were examined using a three-point bending technique (AGS-G, Shimadzu Corp., span=20 mm, cross head speed =0.5mm/min). And the tested samples were prepared by cutting sintered bulk sample into desired dimension (40mm×4mm×3mm) using diamond blade. On average, three measurements were conducted for each sample and at least three specimens were utilized for density and mechanical strength evaluations. 4-Probe method was utilized to get electrical conductivities of composites. X-ray diffraction (XRD, RINT, Rigaku, Japan, CuKα, 40keV, 20mA) and TG/DTA (TG 8120, Rigaku Thermo Plus, Japan, 20 mg of crushed sample powder) were also employed.

4.3. Results and Discussion

4.3.1 Surface pre-treatment of as-received CNT

Two impact factors (time and temperature) are briefly discussed in this study. CNT-A-I °C-6h means that CNT is treated at different temperature for 6h (I means 40 °C, 50 °C, 60 °C, 70 °C and 80 °C). CNT-A-60 °C-II h means that CNT is covalently modified at 60 °C with different time (II means 2h, 4h, 6h, 7h and 8h).

Strong acids are widely regarded as an efficient way to purify and shorten as-produced CNT [20-23]. Increased solubility of treated CNT is mainly attributed to the increased amount of functional groups at active sites of CNT. It is believed that stability of CNT aqueous is relative to electrostatic interactions [24-25]. ζ-Potential result of CNT as a function of pH with different treating temperature and time are shown in Fig. 4.3 and Fig. 4.4. Isoelectric point (IEP) of as-received CNT is around pH=4.27 and poor solubility is confirmed (-15 mV<ζ-potential<+15 mV), which is attributed to the strong Van Der Waals (VDW) attraction forces between CNT and water [26].

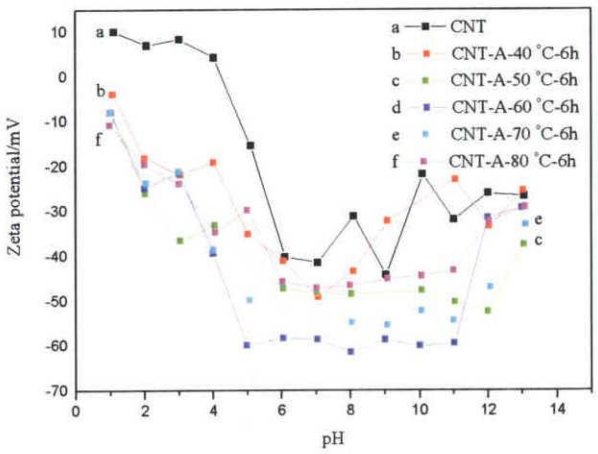

Fig. 4.3. ζ-potential of (a) CNT, (b) CNT-A-40 °C -6h, (c) CNT-A-50 °C -6h, (d) CNT-A-60 °C -6h, (e) CNT-A-70 °C -6h and (f) CNT-A-80 °C -6h as a function of pH in aqueous solutions

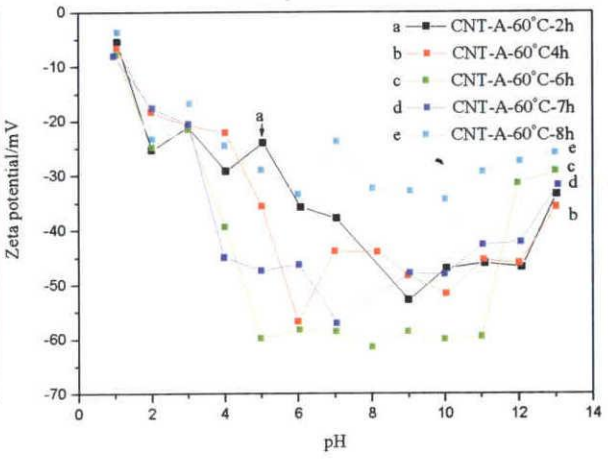

Fig. 4.4. ζ-potential of (a) CNT-A-60 °C-2h, (b) CNT-A-60 °C -4h, (c) CNT-A-60 °C -6h, (d) CNT-A-60 °C -7h and (e) CNT-A-60 °C -8h as a function of pH in aqueous solutions

As shown in Fig. 4.5, as-received VGCF can be shortened by mixed acids by changing treating conditions. Size decreases with increased treating temperature and time. Furthermore, when pre-treatment time is 8h, some aggregation blocks seem formed, which is promoted by Van Der Waals interactions among shortened CNT 1-dimensional nanoparticles. This result is in agreement with the studies of formers [28-29]. As shown in Fig. 4.6, size evaluation of CNT-A-60 °C-6h confirms stability of as-prepared CNT in aqueous solution.

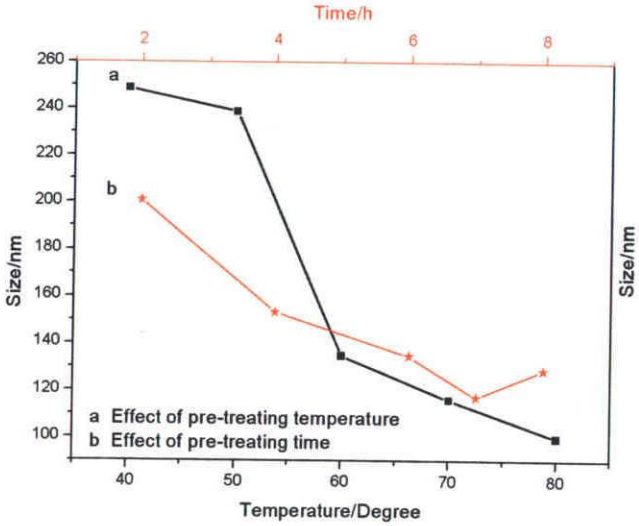

Fig. 4.5. Size distributions of CNT with/without acid-treatment (a) effect of pre-treating temperature and (b) effect of pre-treating time

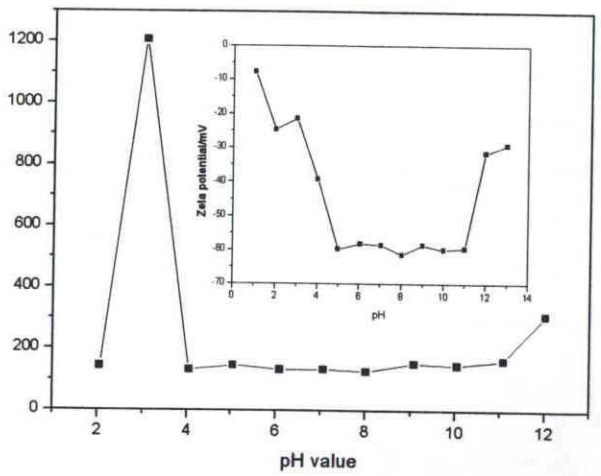

Fig. 4.6. Size distribution of CNT-A-60 °C-6 h as a function of pH in aqueous solutions

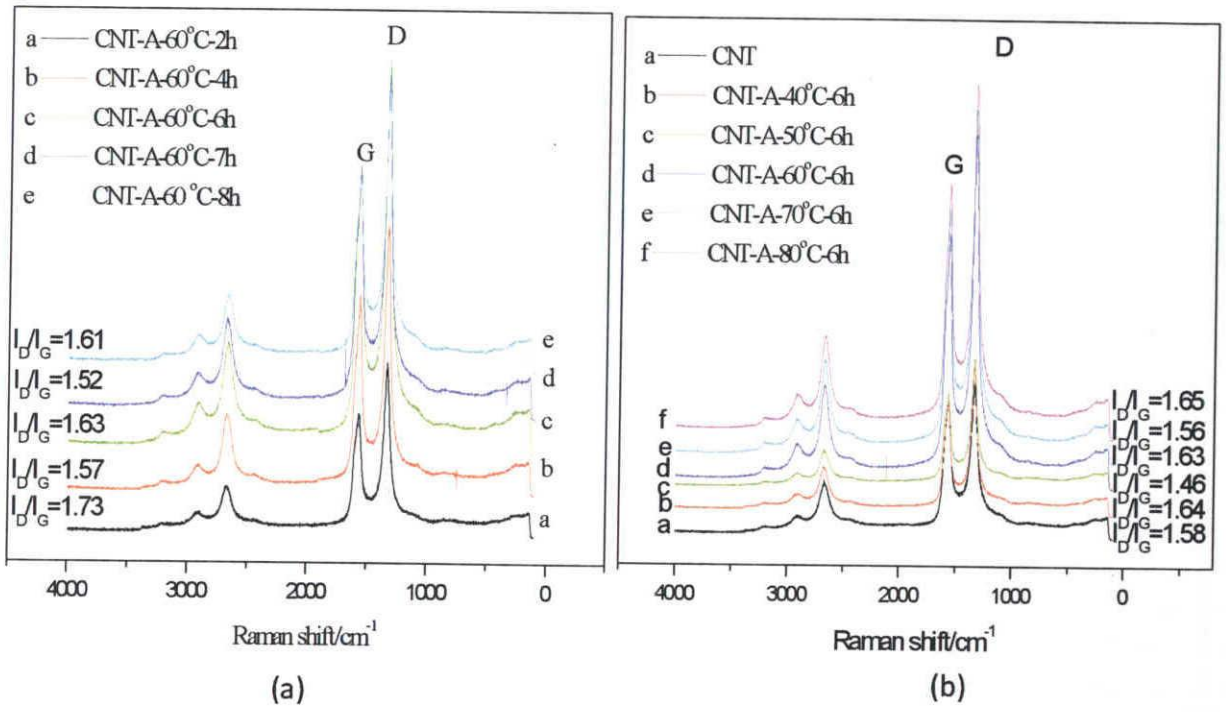

Fig. 4.7. Raman spectroscopy of acid-treated CNT by investigating (a) the effect of pre-treating temperature and (b) the effect of pre-treating time

In Fig. 4.7, Raman spectroscopy results have been shown to detect the effects of pre-treating temperature and time, which can be effectively reflected by intensity ratio of D band and G band. By acid-treatment, at the initial step (when pre-treating temperature is lower than 60 °C and time is less than 6h at 60 °C), the increased intensity ratio of D band and G band is mainly attributed to the instinctive and induced surface defects (byproducts, catalyst [29-31] and band destruction induced defects). Moreover, when treating temperature is higher than 60 °C or treating time is longer than 6 h, varied surface defects are probably due to the surface erosion resulting the bared new inner layer of CNT. This is also a reasonable reply to why lower ζ-potentials are obtained with higher temperature and longer time.

As confirmed by negative forward increase of ζ-potential as changing treating conditions, it is no doubt that negative functional groups have been grafted onto the surface of CNT. As shown in Fig. 4.8, detected absorbent band at 1574 cm^{-1} of as-received CNT is assigned to be carbon skeleton [32]. The appearance of 3461 cm^{-1} and 1084 cm^{-1} are reflected by the stretching vibration of –OH and C-O-C group, which mean that negative hydrophilic groups have been introduced onto the surface of CNT.

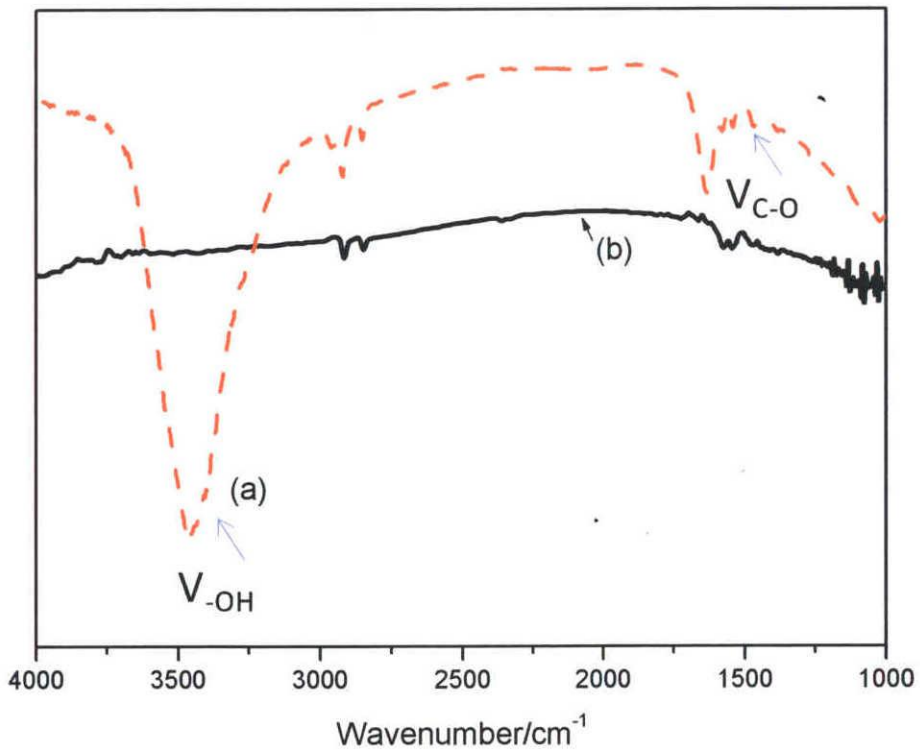

Fig.4.8. FT-IR spectrum of (a) CNT and (b) CNT-A-60 °C-6h

Although we have tried to conduct surface modification of CNT by concentrated acids, it is also interested whether the bone structure of CNT is destructed by the aggressive condition or not. XRD patterns of CNT with different pre-treating conditions as shown in Fig. 4.9 (a) confirm that bone graphitic structure of CNT is maintained. And the dispersibility of treated CNT (which can stand longer than 3 month) is increased by comparing with as-received CNT (which only undergo several hours) as shown in Fig. 4.9 (b).

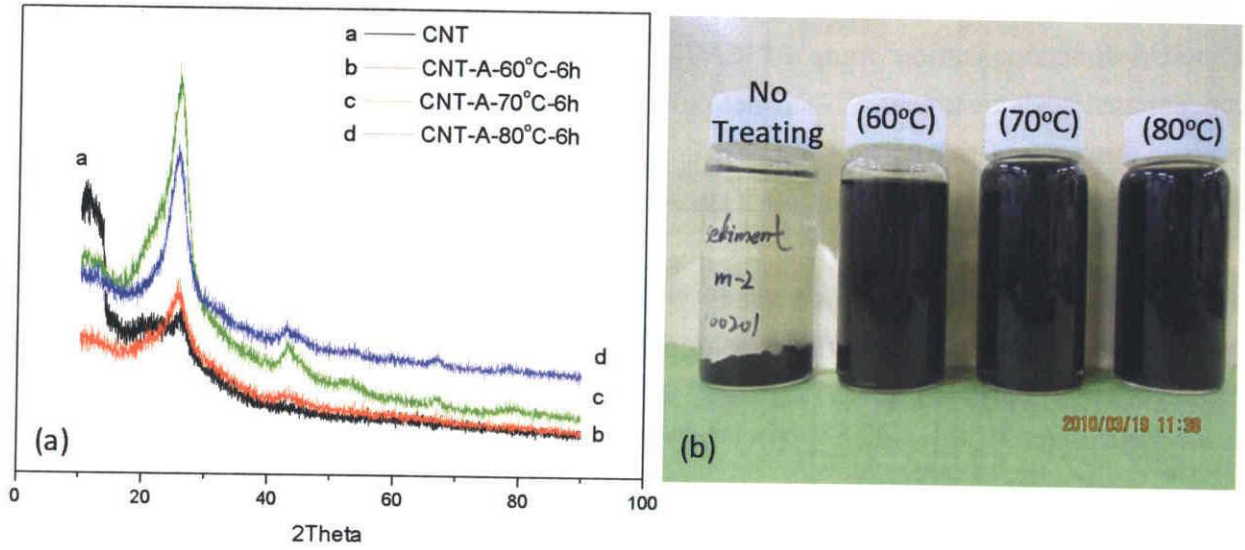

Fig.4.9. (a) XRD patterns of pre-treated CNT (b) photography of pre-treated CNT in water (3 month)

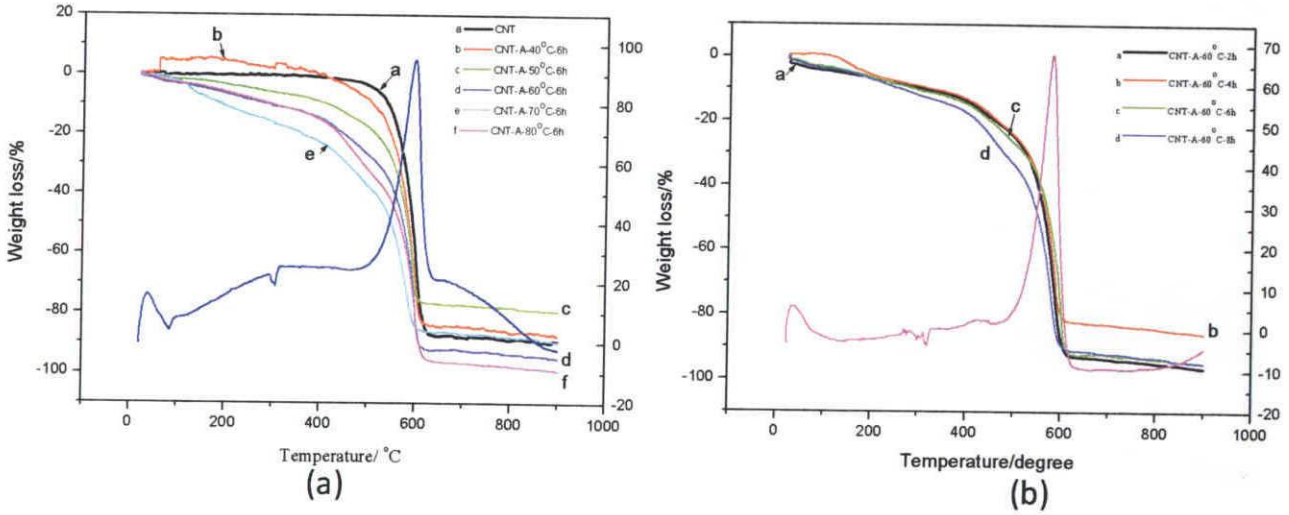

Fig.4.10. TG/DTA analysis curves of CNT with different conditions (a) effect of pre-treating temperature and (b) effect of pre-treating time

Furthermore, it has been proved in former references [20-22], surface covalent modification accelerates not only grafting functional groups leading increased workability, but also purification process of as-received CNT. The same conclusion also was obtained in this study as shown in Fig. 4.10. And the increased carbon content merits from pre-treatment.

Based on the above introduction, we can summarize that by mixed acids treatment, negative functional groups can be grafted onto the surface of CNT and the optimum pre-treating condition is 60 °C for 6h, which can be supported by the highest and most stable ζ-potential compared with other conditions and increased surface defects detected by Raman spectroscopy. In this case, chemical functionalization route of CNT has been proposed as shown in Fig. 4.11. By concentrated acids treatment, CNT is not only grafted by functional groups and purified, but also become thinner and shorter till total destruction as supported by characterization results. When treating temperature is lower than 60 °C or time is less than 6h at 60 °C, increased stabilities of CNT in water is mainly attributed to the increased surface negative charges and defects induced by functional groups. The contrast trendy with more aggressive conditions is resulted from the naked layer. Furthermore, darkest solution color of treated CNT (pictures of potential measurement samples in Fig. 4.11) at 60 °C for 6h also verifies its best dispersibility.

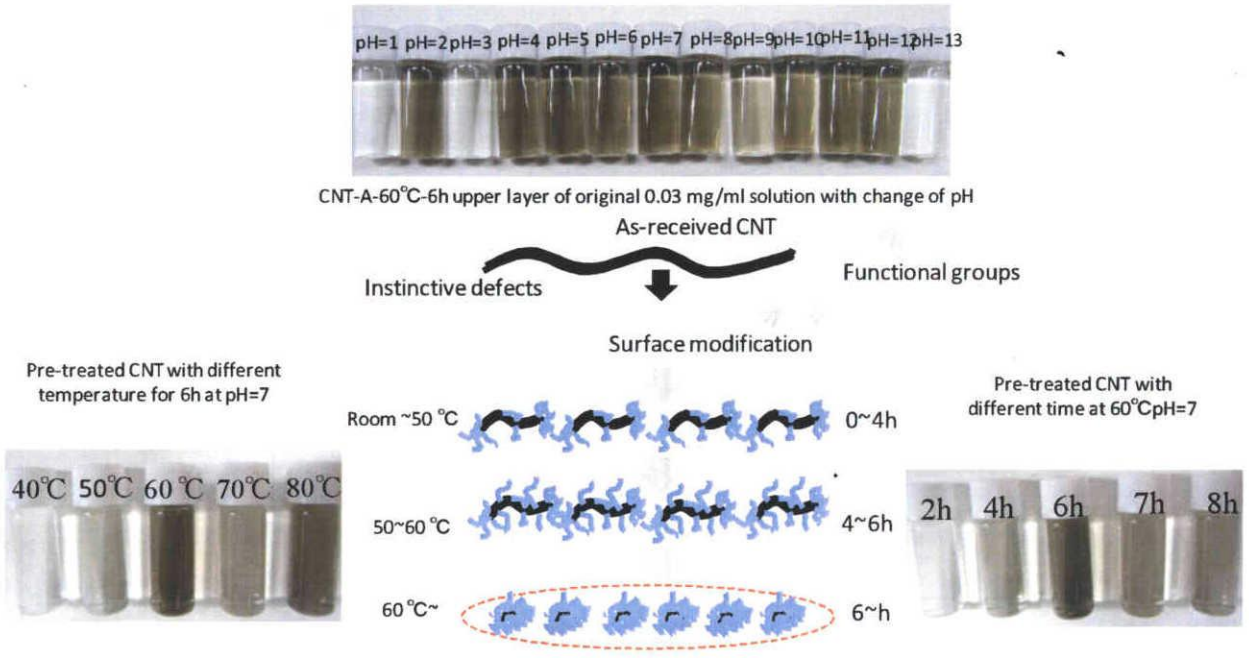

Fig.4.11. The proposed chemical functional routes of CNT by acid-treatment

4.3.2. Fabrication of CNT-0.1 wt%-CPA composite

4.3.2.1.Physico-chemical property of CNT-0.1 wt%-CPA

Table 4.2. Properties of sintered composites at 1700 °C in argon

Samples	Bulk Density ($g \bullet cm^{-3}$)	Apparent density ($g \bullet cm^{-3}$)	Real density ($g \bullet cm^{-3}$)	Open porosity (%)	Closed porosity (%)	Porosity (%)
CPA	1.32	3.65	3.91	63.85	2.38	66.23
CNT-0.1 wt%-CPA	1.44	3.78	3.90	61.88	1.24	63.13

As shown in Table 4.2, although only 0.1 wt% of pre-treated CNT was added, comparing with CPA, porosity and bulk density of fabricated ternary composite have a slight change, which implies that CNT is uniformly dispersed in ceramic matrix [33-35]. All of these tests were repeated at least three times.

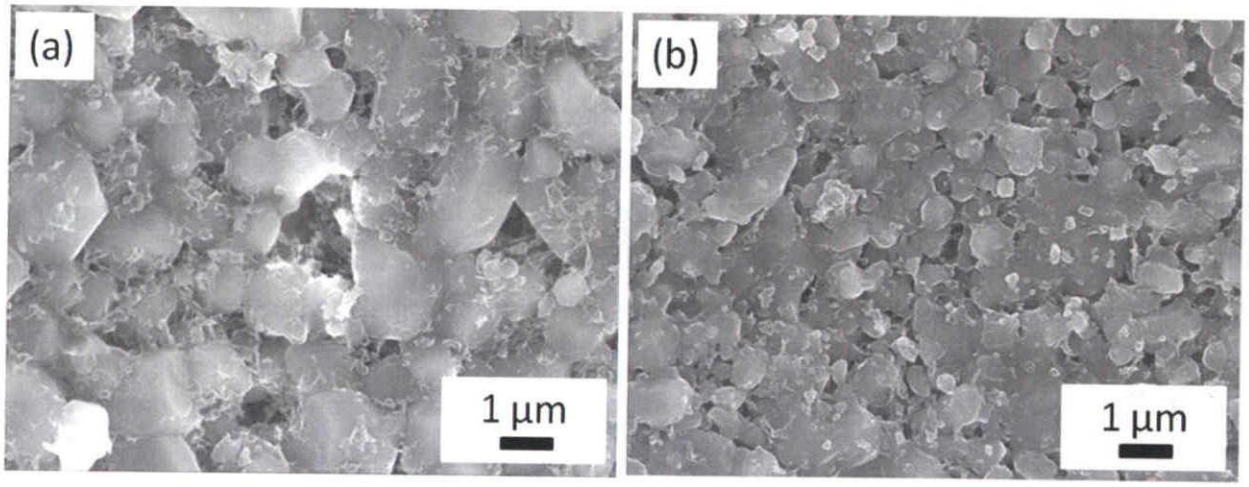

Fig. 4.12. FE-SEM images of (a) CNT-0.1 wt%-CPA (CNT/NCN/Alumina) ternary composite (b) CPA (NCN/Alumina) binary composite with low magnification

In Fig. 4.12, it is observed that inner-connected alumina grains form porous ceramic bone body and reductive sintering-converted carbon co-exists with ceramic grains leaving the unique carbon/Alumina structure. Comparing with CPA (Fig. 4.12 (b)), CNT-reinforced ternary composite (Fig. 4.12 (a)) occupies an increased alumina grain size in sintered body.

As introduced by Rahaman group [35], during ceramic sintering, to reduce surface free

energy, either densification or coarsening of the microstructure can be accomplished. Menchavez et al. [36-37] also reported the hinder of binder networks (BN) for grain growth in CPA. Therefore, the increased alumina grain in ternary composite is attributed to CNT which results in the thinner graphitized carbon coating on the surface of alumina particles.

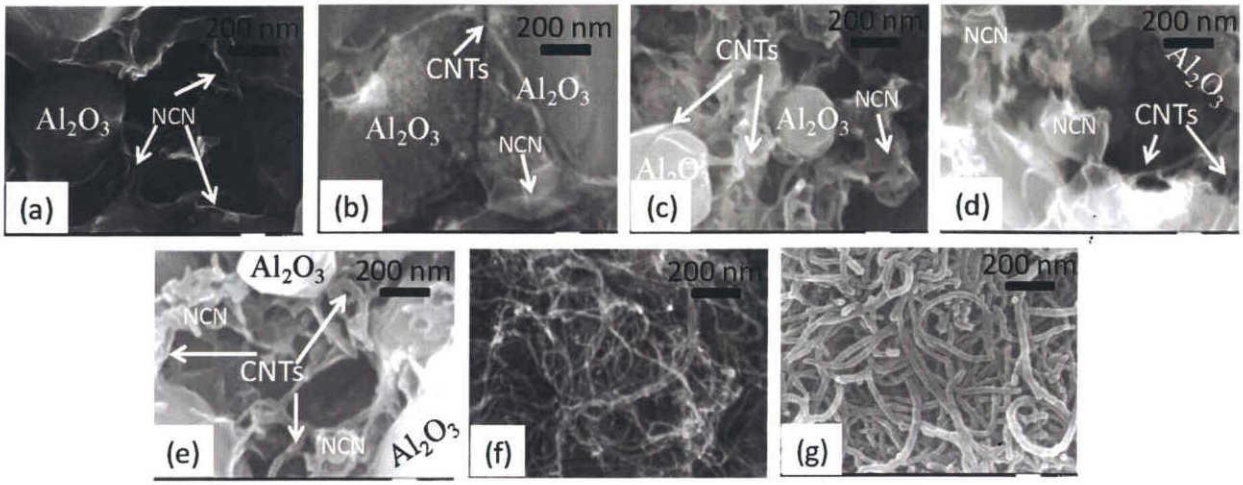

Fig. 4.13. FE-SEM images of (a) CPA (NCN/alumina), (b)-(e) CNT-0.1 wt%-CPA (CNT/NCN/alumina), (f) as-received CNT and (g) Al_2O_3/CNT with high magnification

As displayed in Fig. 4.13 (a), in CPA (NCN/alumina) composite, high temperature sintering of gel-casted body in novel atmosphere results in the inner-connected nano-carbon paths, which not only cover alumina grains, but also exist among alumina grains boundaries forming three-dimensional conductive bridges. These three-dimensional nano-carbon networks can not only undergo aggressive conditions, but also supply various potential applications in many fields, such as electrodes or catalysts [3-4].

In Fig. 4.13 (b)-(e), high magnification images of ternary composite are displayed to investigate the micro-structure of composite. Various co-existing ways of main components can be verified by these images. CNT acts as bridge (Fig. 4.13 (b)) and NCN is adhered onto the surface and boundaries of CNT and alumina grains. In Fig. 4.13 (c), alumina grain is surrounded by inner-crossed CNT mesh, which indicates good affinity of CNT and alumina. In Fig. 4.13 (d) and (e), conductive networks are formed by cross-linked CNT and NCN. This result is in accordance with the reported studies in other groups using CNT as reinforcing material [8,15,38] by different technologies.

Increased diameter of CNT in CNT-0.1 wt%-CPA is observed (as shown in Fig. 4.12 (b)-(e)) by comparing with as-received CNT in Fig. 4.13 (f), which results from attachment of Al_2O_3 particles during making CNT/alumina slurry by electrostatic interaction. This conclusion is confirmed by FE-SEM image and X-ray diffraction Pattern (XRD, UltimaIV R285-BS, Rigaku, Japan) of Al_2O_3/CNT as shown in Fig. 4.13 (g) and Fig. 4.14 (I), respectively. (Al_2O_3/CNT

composite was prepared by only injecting ultra-sonicated 1 g/L of Al_2O_3 dispersions into pre-treated 0.5 g/L of CNT aqueous solution without adding any other chemicals followed by aggressive stirring for 24 h and vacuum drying at 60 °C). The morphology features of them were also supported by STEM images as shown in Fig. 4.14 (I, III), which has the same magnification.

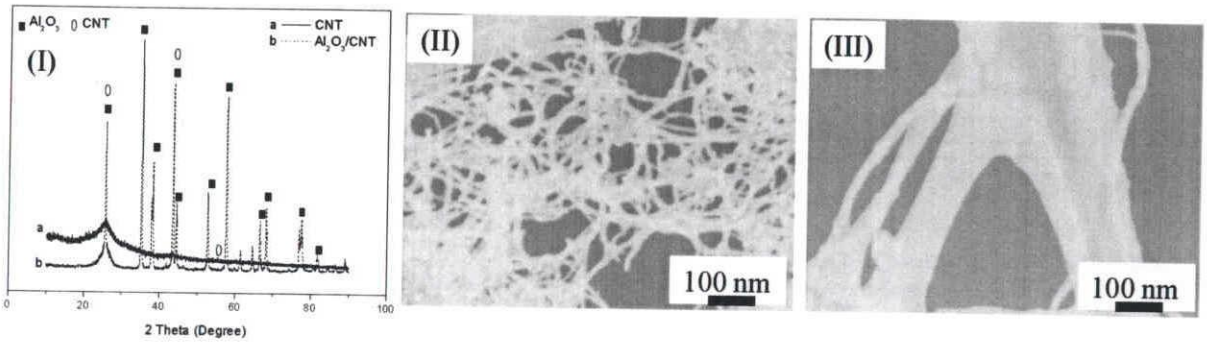

Fig. 4.14. (I) X-ray diffraction Patterns of (a) CNT and (b) Al_2O_3/CNT and STEM images of (II) CNT and (III) Al_2O_3/CNT

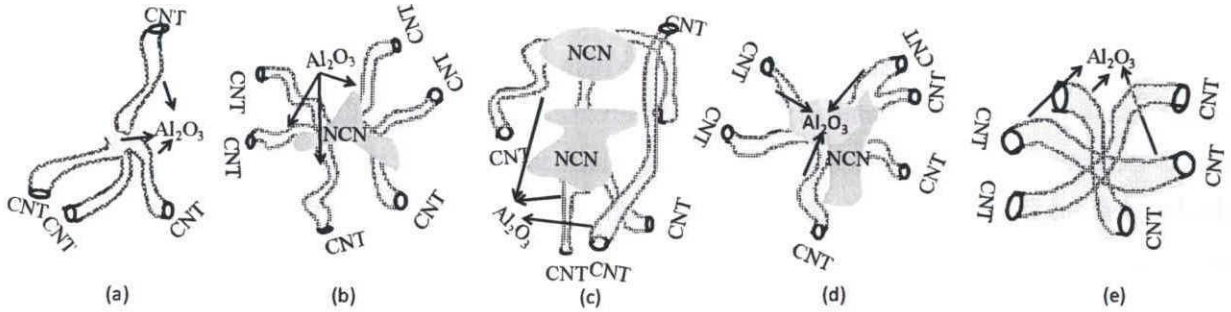

Fig. 4.15. Proposed snapshots of co-existence way of components in ternary

In Fig. 4.15, co-existence style of components in ternary composite is proposed based on morphology observation results in Fig. 4.13 and Fig. 4.14 (II) and (III). Generally, it is noticed that three main components in ternary composite (CNT covered with alumina nanoparticles (named as Al_2O_3/CNT), reductive sintering converted NCN and alumina grains (abbreviated as alumina)) co-exist in four different situations: (a) Al_2O_3/CNT-alumina co-junction (Fig. 4.15 (a)), (b) Al_2O_3/CNT-NCN co-junction (Fig. 4.15 (b) and (c)), (c) Al_2O_3/CNT-alumina-NCN (Fig. 4.15 (d)) and (d) Al_2O_3/CNT mesh between alumina boundaries (Fig. 4.15 (e)). The cross-linked micro-structure of as-prepared composite permits the enhanced contact between insulator alumina and conductor carbon, which indicates the possibile of varied property.

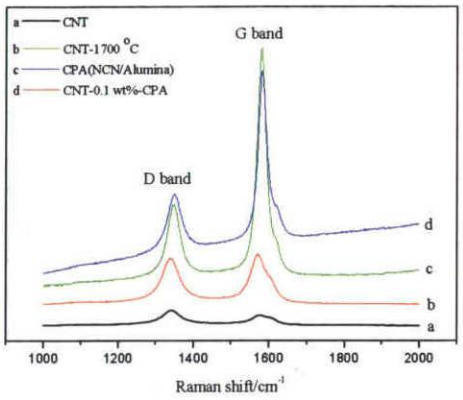

Fig. 4.16. Raman spectroscopy of (a) CNT (b) CNT-1700 °C (c) CPA (NCN/Alumina) and (d) CNT-0.1 wt%-CPA

Table 4.3. Surface defects analysis results from Raman spectroscopy Fig. 4.16

Materials	$\Delta\upsilon_{1580}$/ cm^{-1}	I_D/I_G
CNT	79	1.59
CNT-1700 °C	61	0.98
CPA	25	0.48
CNT-0.1 wt%-CPA	27	0.59

Raman spectroscopy, which is universally regarded as an effective characterization method especially for different carbonaceous forms, was employed to detect the variation of carbon in monitored composites. As introduced in references [24,30-31,39-41], surface defects induced D band, around 1350 cm^{-1} and C-C stretch modes at 1570 cm^{-1} identified to G band are employed to investigate the electronic crystal structure of carbon forms with graphitic structure. As shown in Fig. 4.16, comparing with CNT, CPA (NCN/alumina) and CNT-0.1wt%-CPA (CNT/NCN/alumina) have higher graphitization degree, which is confirmed by the increased G band intensities (Fig. 4.16 (a), (c) and (d)) and the decreased half band width of G band ($\Delta\upsilon_{1580}$) and surface defects as listed in Table 4.3. Surface defects of CNT, CNT-0.1wt%-CPA and CPA calculated from D band and G band intensity ratio (I_D/I_G) are 1.59, 0.59 and 0.48, respectively. Comparing with CPA (NCN/Alumina), the increased defect of ternary composite is attributed to the added CNT. And in order to investigate the effect of reductive sintering for CNT at 1700 °C in Ar, as-received CNT from company was also sintered at the same condition with composites, as-resulted CNT was named as CNT-1700 °C. By comparing CNT and CNT-1700 °C as shown in Fig. 4.16 (a) and (b), it is noticed that both increased typical graphitic structure peaks and decreased surface defect of CNT-1700 °C (I_D/I_G(CNT-1700°C)=0.98<I_D/I_G(CNT)=1.59) confirm the further graphitization of CNT during reductive sintering instead of destruction, which implies the good thermal stability of CNT at high temperature. And the same conclusion was reported by Fan et al. [10].

From the former analysis, it is noticed that thermal stability of CNT at high temperature reductive sintering (HTRS) plays an important role for making composite. Raman spectroscopy as shown in Fig. 4.16 supports its stability in novel atmosphere. By HTRS, graphitization degree of CNT can be accelerated as proved by decreased surface defects. Fig. 4.17 claims that by HTRS, carbon content decreases from 89 wt% to 82 wt% without bone structure destruction. This conclusion can be confirmed by the increased pyrolysis temperature of CNT-1700 °C as

shown in Fig. 4.17 (a) and (b), which indicates the increased crystallization of carbon. This is in accordance with Raman spectroscopy evaluation result.

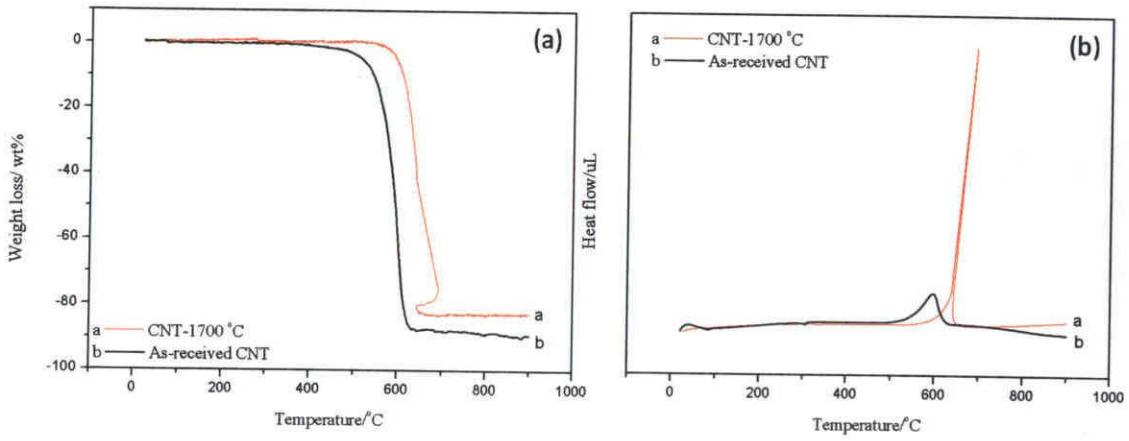

Fig.4.17. (a) Thermogravimetry (TG) curves and (b) DTA curves of samples in oxygen atmosphere

Structure stability of CNT has been confirmed by monitored XRD patterns as shown in Fig. 3.18. Alongside the diffraction pattern of as-received CNT and CNT-1700 °C, diffraction peak around 25° is assigned to graphite (002) peak [42]. Appearance of this peak indicates the graphite sheet crystal structure of CNT. And it is noticed that even though it is thermal treated at high temperature up to 1700 °C, the bone structure of CNT is remained implying the good thermal stability of CNT in novel atmosphere, the same conclusion is arrived in other group [10].

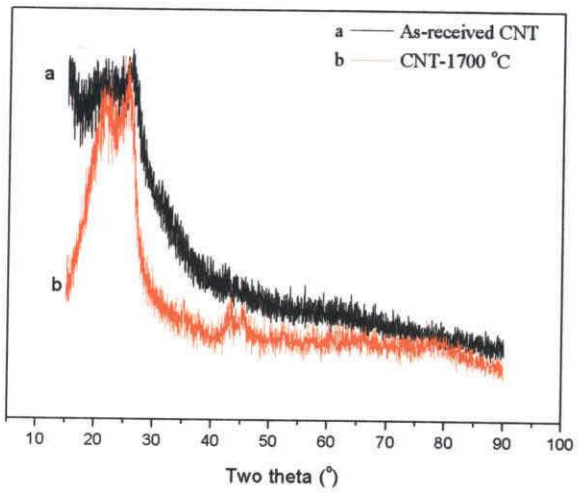

Fig. 4.18. XRD pattern of CNT-1700 °C and as-received CNT

Fiber-formed CNT is a good candidate for degradation of brittleness cracks resulting increased mechanical strength [34,35,38]. We have reported flexural strength of CPA (20 to 23 MPa) measured by three-point bending technique [36-37]. By the same technique, as-fabricated ternary composite CNT-0.1wt%-CPA is 38 MPa, 1.9 times as much as that of CPA. For this high bulk porosity ceramics (as shown in Table 4.2), CNT effectively increases the flexural strength by acting as bridge or mesh as confirmed in Fig. 4.13. In ceramic-based composites, Du et al.

[43], Javey et al. [44-45] have reported that the added CNT can increase strength by absorbing the strain energy. In our study, the same principle applies.

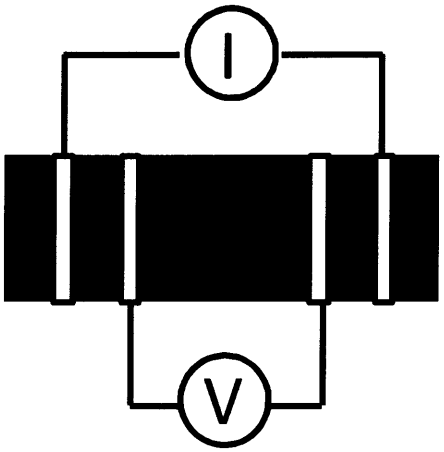

Fig. 4.19. Diagram of electrically conductivity measurement by four-probe method

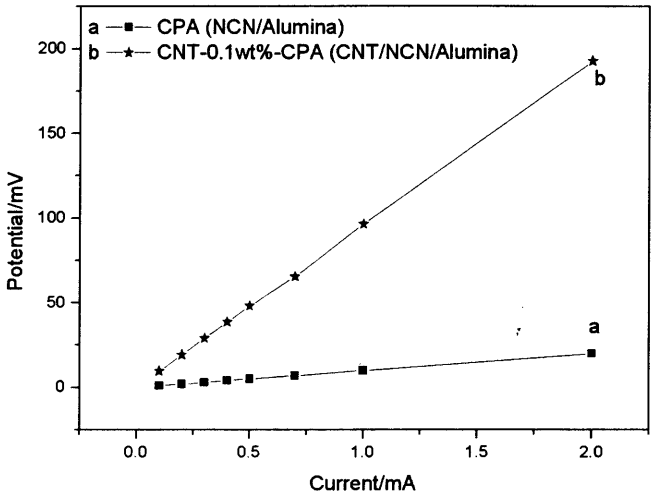

Fig. 4.20. Potential-current curves of (a) CPA (NCN/Alumina) and (b) CNT-0.1 wt%-CPA

Four-probe method electrical conductivity measurement (Fig. 4.19) result is shown in Fig. 4.20. Both two composites show an omhic behavior curves. Good contacts between electrodes and samples are confirmed by linear relationship of voltage and current. It is understood that a decrease of electrically conductivity of CNT-0.1 wt%-CPA by comparing with CPA. Although many researchers have devoted to exploring electrical conductive ceramics by doping CNT with different methods so far, no sensible contribution can be observed, which is in agreement with the reported result by Tatami et al. [46]. Isotropic electrically conductivity (σ) of CNT/ graphitized carbon/alumina decreases from that of CPA (2.18 S•cm) to 0.08 S•cm. For this behavior, as we have known, both carbon amount and carbon graphitization degree result in electrical conductivity. Even though only 1 gram of pre-treated CNT has been employed to reinforce CPA, increased suspended conductive net-paths in composite resulting from CNT is responsible for this behavior.

In order to explain this performance, weight loss of green bodies and sintered bodies have been conducted. However, because it is too difficult to detect the existence of CNT in ternary composite with little content, CNTs-0.3 wt %-CPA green body was employed. As shown in Fig. 4.21, CNT pyrolysis temperature is around 500 °C-600 °C and polymer pyrolysize around 300 °C-450 °C, however, CNT has no obvious contribution to weight loss of specimens. As shown in Fig. 4.22, carbon content in CNT/CPA and CPA is 0.75 wt % and 0.71 wt %, respectively. Furthermore, it is noticed that CNT attributes to different carbon content in different layers of

CNT/CPA specimens as displayed in Fig. 4.22, which implies that CNT moved to upper surface of green body during gel-casting. One cut specimen was divided into three layers for this investigation as shown in Fig. 4.23.

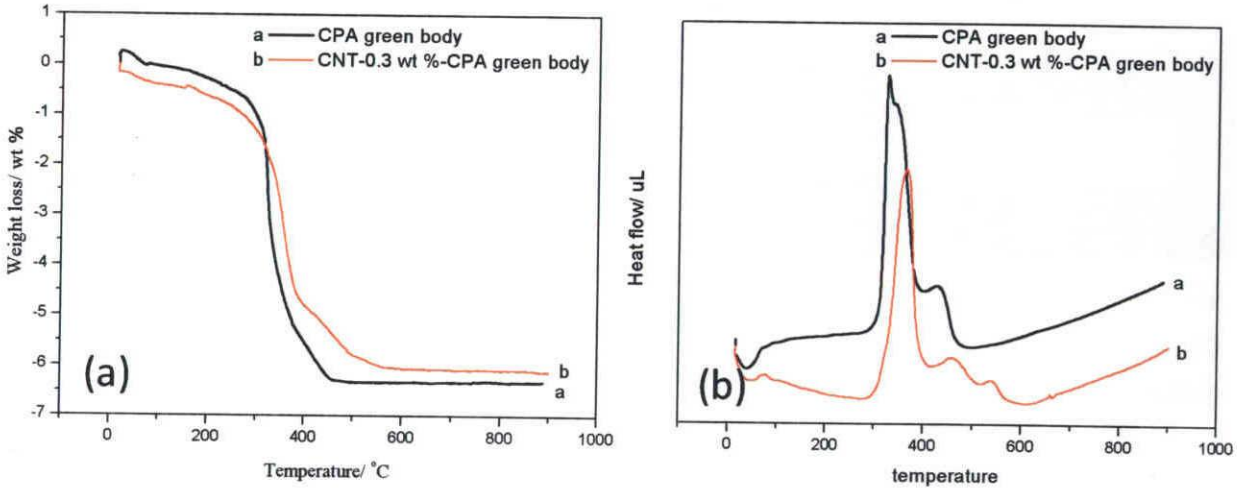

Fig. 4.21. (a) TG and (b) DTA analysis results conducted in oxygen atmosphere

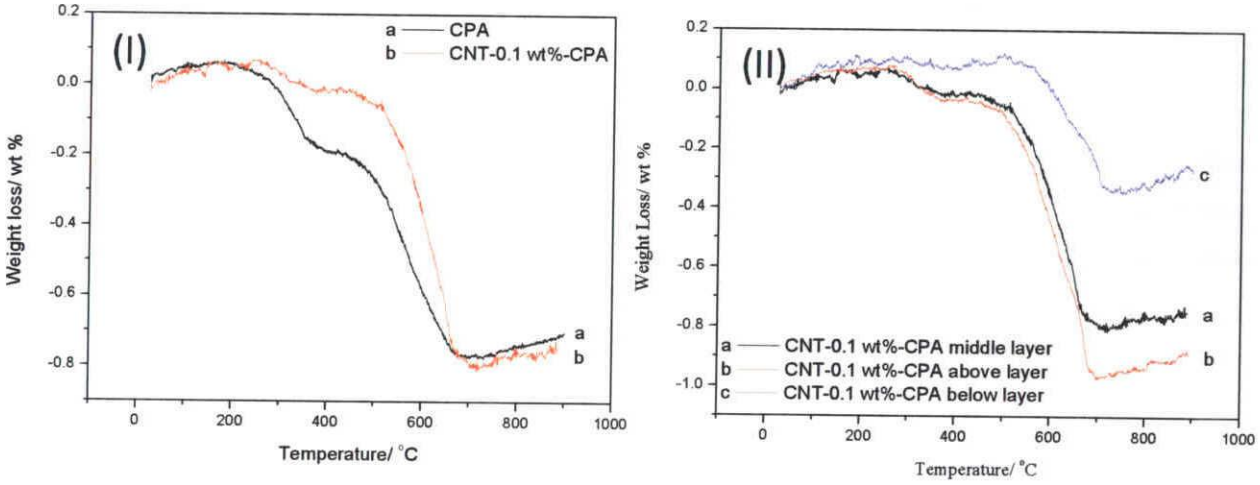

Fig. 4.22. TG analysis of (I) (a) CPA and (b) CNT-0.1 wt%-CPA and (II) (a) CNT-0.1 wt%-CPA middle, (b) CNT-0.1 wt%-CPA above layer and (c) CNT-0.1 wt%-CPA below layer conducted in oxygen atmosphere

The varied CNT amount in different part and weaker graphitization degree of carbon (CNT/NCN) also explain weaker electrical conductivity of CNT-0.1 wt%-CPA (CNT/NCN/Alumina) by comparing with commonly utilized CPA. More, CNT-induced increased grain size of Al_2O_3 leads to the interrupted carbon networks, which permits the

decreased electrical conductivity.

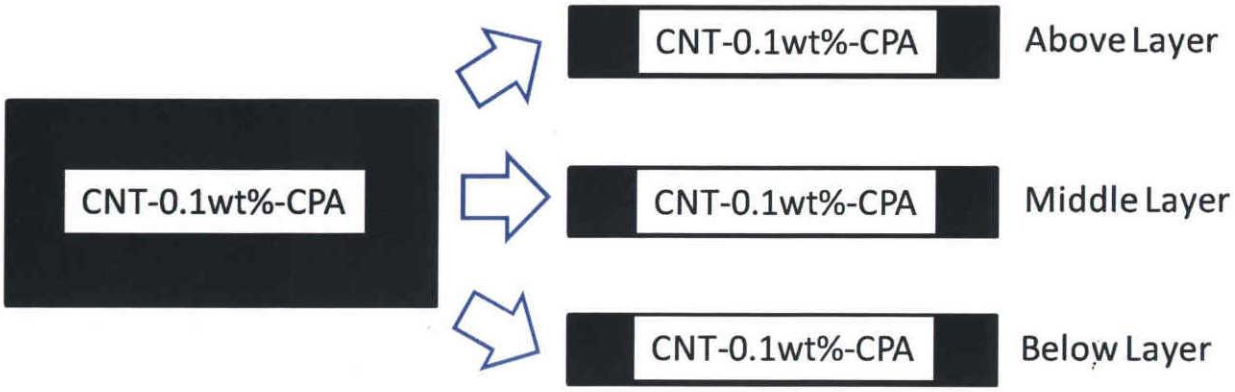

Fig. 4.23. Proposed CNT-0.1 wt%-CPA samples preparation for TG/DTA analysis

4.3.2.2 Electromagnetic wave absorbability of CNT-0.1 wt%-CPA ternary composite

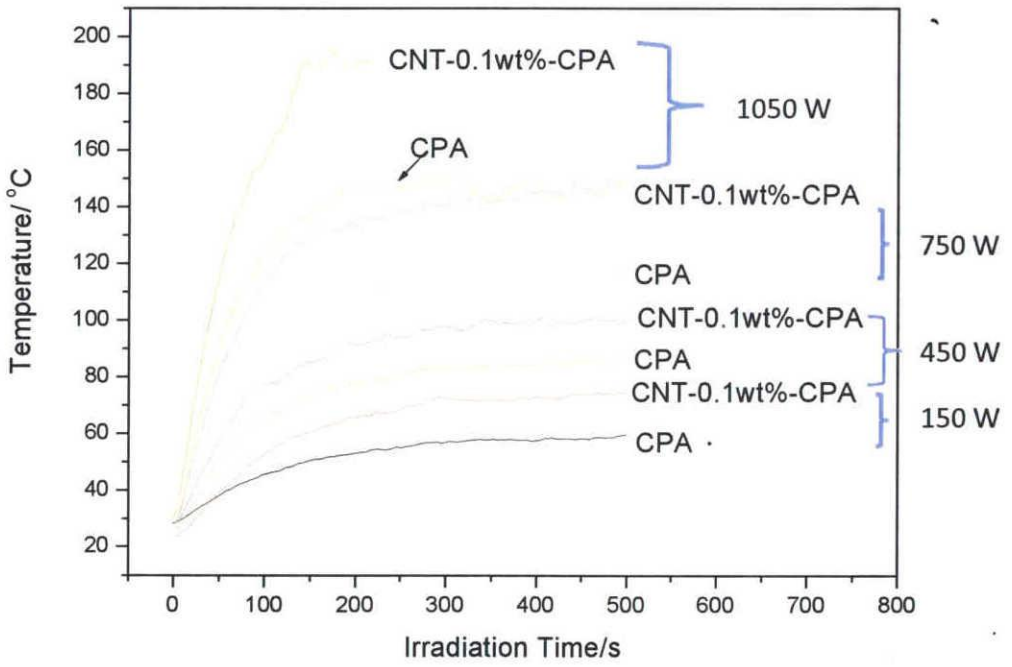

Fig. 4.24. Temperature-irradiation time curves of CNT-0.1 wt%-CPA irradiated with various output energy by comparing with CPA

In chapter 3, it had been confirmed that CPA owns good electromagnetic wave absorbability, which not only overcomes microwave transparency of Al_2O_3, but also announces a novel microwave absorbent in materials fields as electromagnetic absorber. It was understood that absorbability of CPA merited from the polarization of NCN which has graphitic electronic crystal structure as confirmed in Fig. 3.5. In this chapter, microwave-induced heat behavior of CNT modified composite CNT-0.1wt%-CPA (namely CNT/NCN/Alumina) was reported. As shown in Fig. 4.24, electromagnetic wave absorbability of CNT/CPA was detected. By comparing with CPA, it is noticed that CNT-0.1 wt%-CPA has higher absorbability than CPA at the same irradiation powers, which means that CNT resulted absorbability is not directly related with graphitization degree of carbon in this ternary composite. As introduced by Mao et al., [47], microwave absorbability is not only related with electron but also phonon. The increased phonon intensity induced by CNT attributes to this performance as confirmed by the increased surface defects in Table 4.3. More, Vázquez et al. [48] reported that CNT with higher impurities owns stronger absorptions than 'perfect' one benefiting from impurities-induced localized superheating and heating performance of CNT is little related with its length. In this study, the same principle applies as confirmed by Raman evaluation in Fig. 4.16. In a word, the intensified phonon accelerates increased D intensity leaving higher heating performances [50].

Briefly, there are three factors involved for influencing microwave absorbing ability, namely irradiation power, filler carbon amount and graphitic orientation. Herein, effect of irradiation power was investigated by calculating the increased temperature via certain irradiation time ($\Delta T=T_t-T_0$, $t_{(irradiation\ time)}$=200 s). Fig. 4.25 (a) displays the relationship between increased temperature difference and irradiation power of CNT-0.1 wt%-CPA. It is noticed that the temperature difference is direct proportional to irradiating power. And the linear fit of them is y=0.14x+21.7 (y means temperature difference whose unit is °C and x means irradiation power whose unit is W), which means that microwave absorbability of tested sample increases with irradiation power. Similar situation can be arrived for CPA (Fig. 4.25 (b)) and the fit linear-ship of CPA is y=0.13x+3.44.

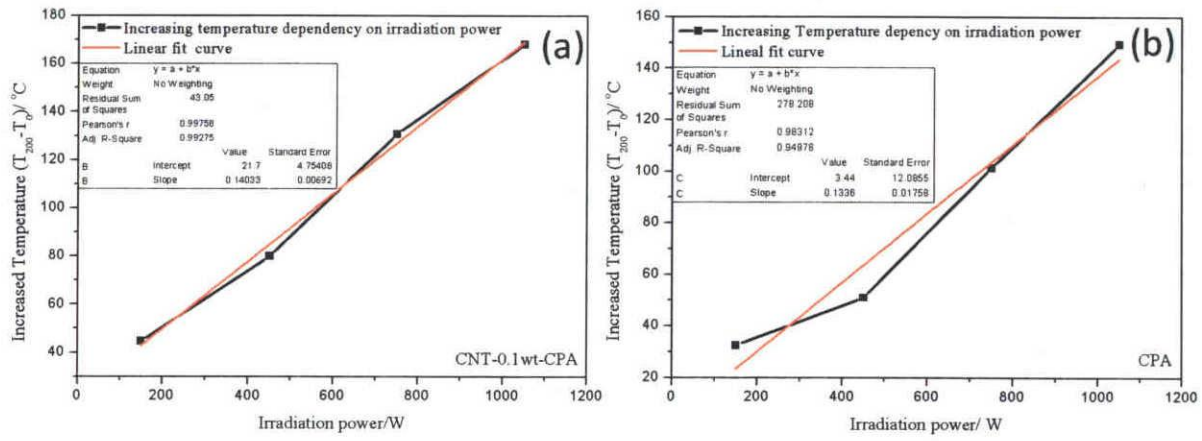

Fig. 4.25. Temperature difference (T_{200}-T_0)-irradiation power of (a) CNT-0.1 wt%-CPA and (b) CPA

4.3.3. Effect of CNT amount

4.3.3.1.Physico-chemical property of CNT/CPA with varied CNT amount

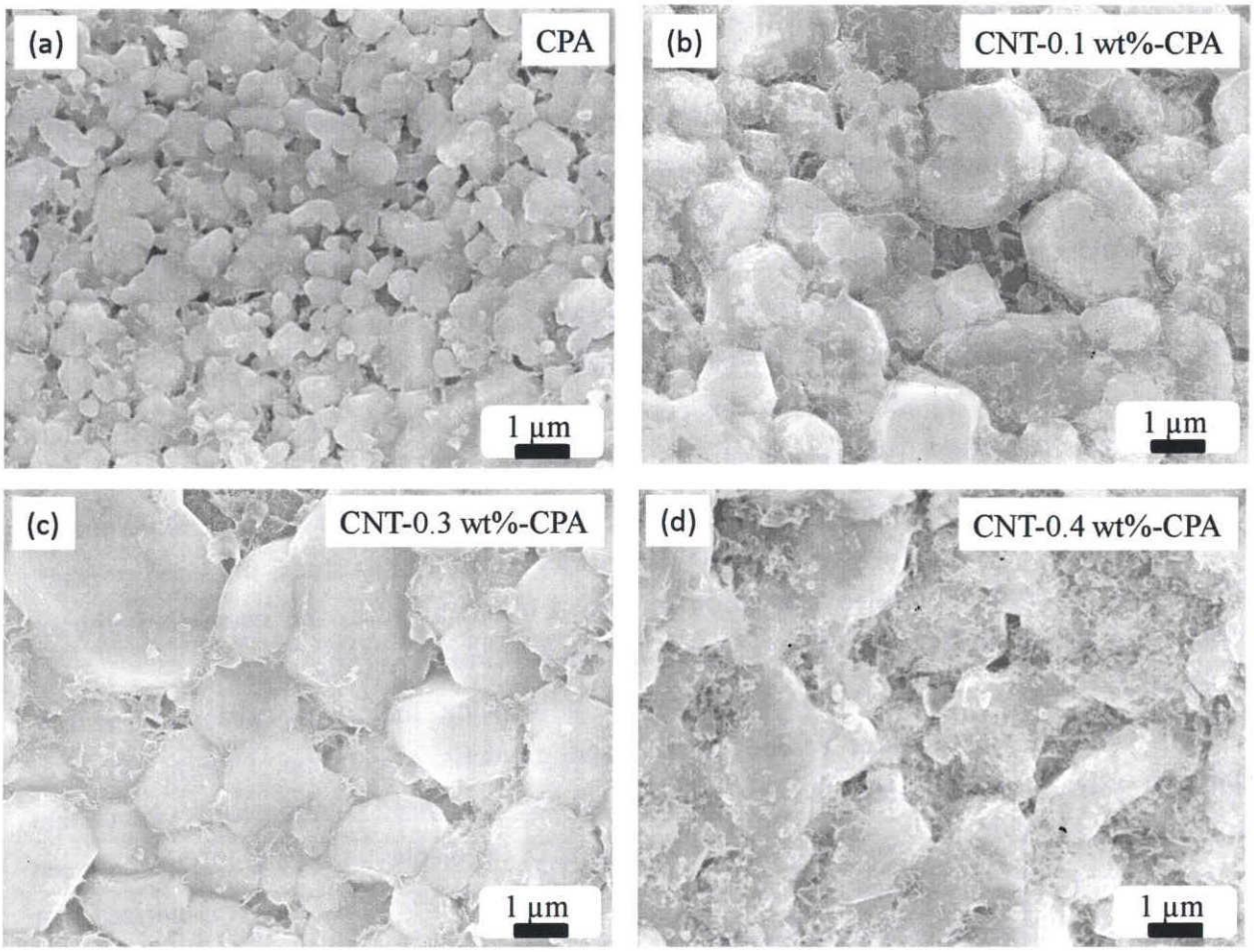

Fig.4.26. FE-SEM images of (a) CPA, (b) CNT-0.1 wt%-CPA, (c) CNT-0.3 wt%-CPA and (d) CNT-0.4 wt%-CPA

Fig.4.26 uncovers the effect of CNT amount on micro-structure of composites. It is understood that addition of CNT attributes to the increased alumina grain sizes comparing CNT-0.1 wt%-CPA, CNT-0.3 wt%-CPA and CNT-0.4 wt%-CPA with CPA. Similar with CNT-0.1 wt%-CPA, the increased ceramic grain size is attributed to the decreased binder networks (BN) on the surface of Al_2O_3 grains, which leads to the decreased hinder effect on grain growth. More, it is necessary to claim that the maximum CNT in 1000 g alumina slurry is 0.4wt %. And as shown in Fig. 4.26, it is noticed that much more CNT appears on the surface of Al_2O_3 grains as increased CNT additive amount [49].

Fig. 4.27 confirms that no contribution of CNT on carbon amount in composites. Generally, carbon in composite is around 0.75 wt%. More, comparing with CPA, the increased hydrolysis temperature of CNT-added composites as displayed in Fig.4.27 (b) is attributed to CNT, which

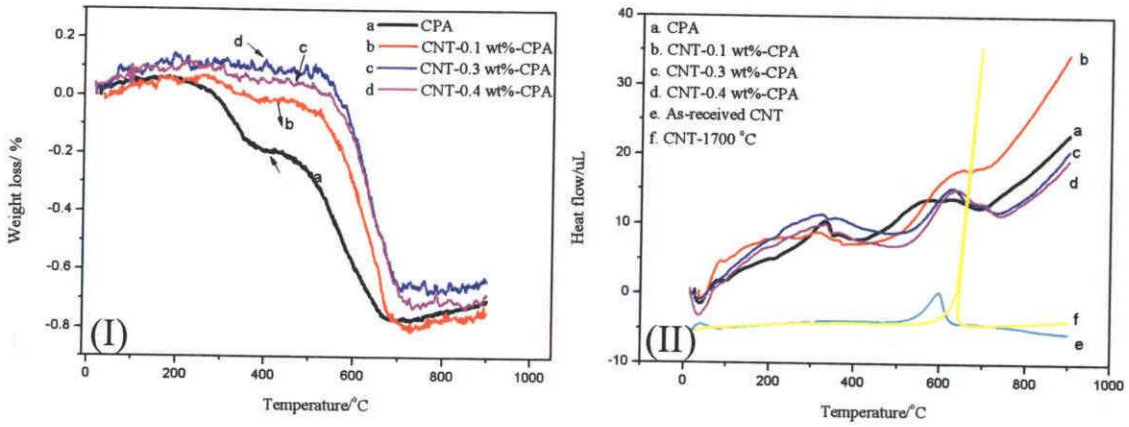

Fig. 4.27. (I) TG and (II) DTA analysis results conducted in oxygen atmosphere

Table 4.4. Density and porosity analysis results by Archimedes method

Materials	Bulk Density ($g \cdot cm^{-3}$)	Apparent Density ($g \cdot cm^{-3}$)	Real Density ($g \cdot cm^{-3}$)	Open Porosity (%)	Close Porosity (%)	Total Porosity (%)
CPA	1.32	3.65	3.91	63.85	2.38	66.23
CNT-0.1 wt%-CPA	1.44	3.78	3.90	61.89	1.24	63.13
CNT-0.3 wt%-CPA	1.32	3.76	3.88	64.97	1.05	66.02
CNT-0.4 wt%-CPA	1.36	3.85	3.88	64.64	0.28	64.92

can be verified by as-received CNT and CNT-1700 °C DTA analysis as shown in Fig.4. 27.

Table 4.4 clarifies that CNT mainly influences apparent density of sintered body and results in the decreased close porosity, which is a good proof of densification process during HTRS. As supported by Fig.4.26, CNT attributs to the increased alumina grains leading to apparent density growth.

In order to investigate the effect of CNT on as-resulted composites, green body of CNT-0.3 wt%-CPA was firstly degreased at 400 °C for 10 h (Experimental program setting is shown in Fig. 4.2.) and followed by HTRS at 1700 °C for 2 h. Because the well gelled polymer networks can be consumed around 450 °C (Fig. 4.21), while CNT was pyrolysized around 550 °C. Therefore,

as shown in Fig. 4.28 (a), it is understood that carbon content in PA is around 0.15 wt%, but the carbon content of CNT-0.3 wt%-PA is about 0.31 wt%. The detected carbon content in degreased specimens implies that it is difficult to thoroughly remove gel networks by thermal treating in oxygen atmosphere. More, comparing with CPA, the increased carbon consumptive temperature in degreased samples (PA and CNT-0.3 wt%-PA) indicates the improved crystallization degree of carbon in composites, which benefits from the added CNT with high graphitilization degree and tube-like form. Furthermore, comparing with CNT and CNT-1700 °C DTA curves as shown in Fig. 4.28 (b), not only graphitic structure of carbon in composites are proven by exothermic peak around 600 °C, also increased crystal structure of carbon meriting from CNT is concluded. This summary is proven by high-temperature shift of different composites as displayed in TG/DTA analysis results in Fig. 4.28.

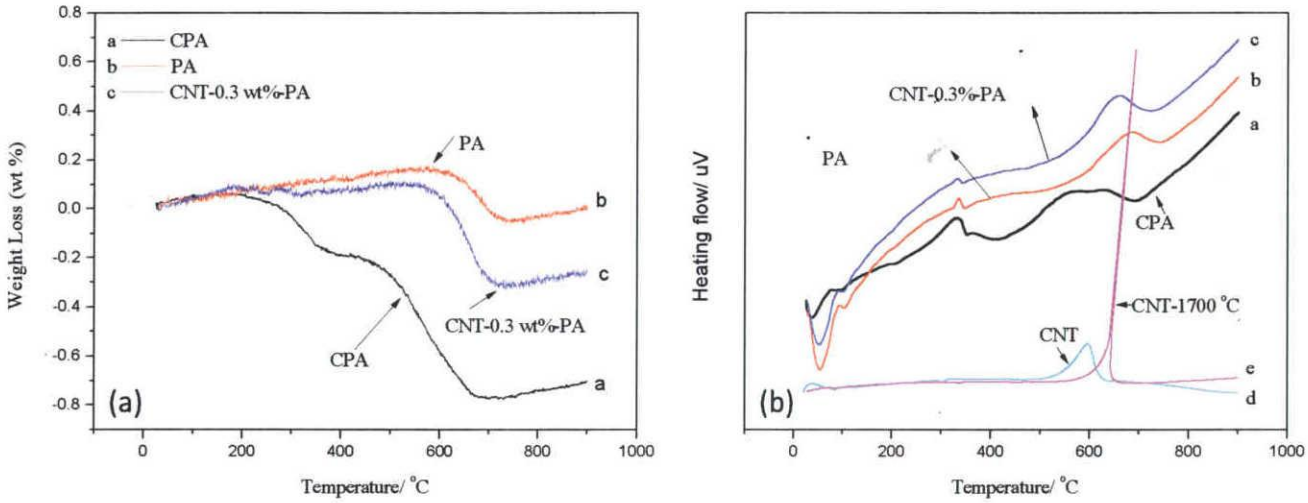

Fig.4.28. (a) TG and (b) DTA analysis results of degreased composites conducted in oxygen atmosphere

Then, it is necessary to investigate the effect of carbon structure in degreased specimens. As shown in Fig. 4.29, appearance of D band and G band proves the graphitic structure of carbon in PA and CNT-0.3 wt%-PA. This is attributed to non-thoroughly removed NCN by thermal pre-treating as confirmed by TG/DTA analysis (Fig. 4.28). Furthermore, even though the maintained PA and CNT-0.3 wt%-PA ash after TG analysis were employed to make Raman spectroscopy evaluation, graphitic typical peaks (D band and G band) implies the still existence of carbon in ash, by which it is feasible to get a conclusion that it is impossible to totally remove the carbon in composites. While even though it is impossible to totally degreasing only by thermal treating in air, as-prepared composites are useful for investigation effect of carbon amount on physic-chemical property and microwave absorptive performance.

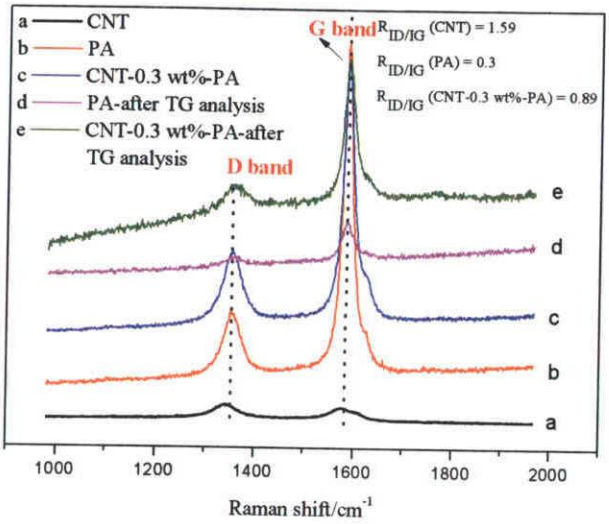

Fig. 4.29. Raman spectroscopy of (a) CNT; (b) PA; (c) CNT-0.3 wt%-PA; (d) PA-after TG analysis and (e) CNT-0.3 wt%-PA-after TG analysis

More, it is noticed that graphitic orientation of degreased specimens ($R_{ID/IG}$ (PA)=0.3 and $R_{ID/IG}$ (CNT-0.3wt%-PA)=0.89) are better than that of CPA ($R_{ID/IG}$=0.48) and CNT-0.3 wt%-CPA ($R_{ID/IG}$=0.91). This is in accordance with TG analysis results. Furthermore, the difficulty in removing NCN also supports its thermal stability.

Structures change of PA and CNT-0.3 wt%-PA were shown in Fig. 4.30. Comparing with/without degreasing samples each other,

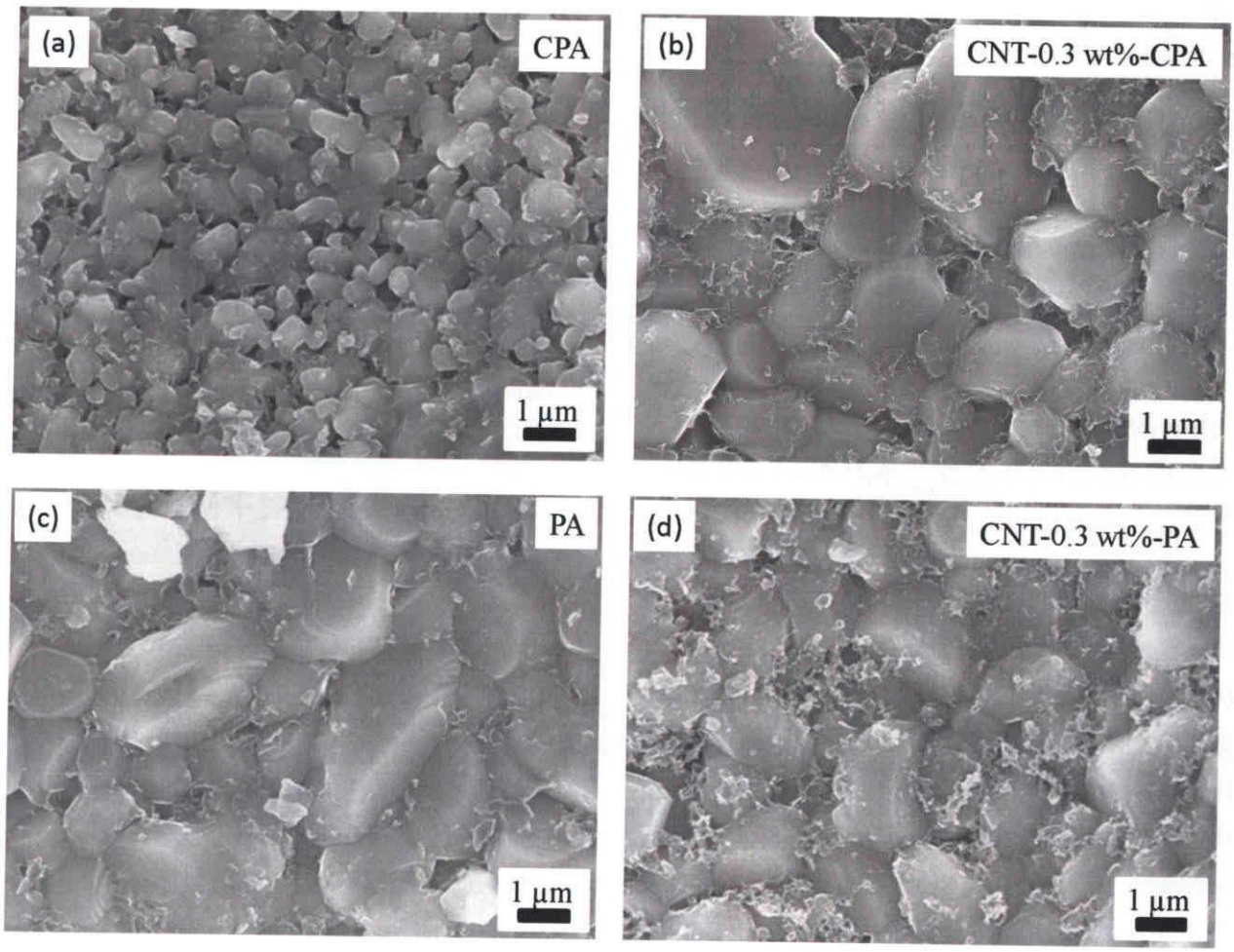

Fig. 4.30. FE-SEM images of (a) CPA; (b) CNT-0.3 wt%-CPA; (c) PA and (d) CNT-0.3 wt%-PA

the decreased amount of binder networks (BN) permits to the increased alumina grain size [48], which is consist with Fig.4.26.

4.3.3.2. Electromagnetic wave absorbability of CNT/CPA with varied CNT amount

As confirmed in 4.3.3.1, it is impossible to thoroughly remove the NCN in gel-casted bodies by thermal-treatment and HTRS. However, it supplies some useful information about microwave activities comparing them each other.

Influence of increased CNT amount for ternary composites is analyzed by Fig. 4.31. All of

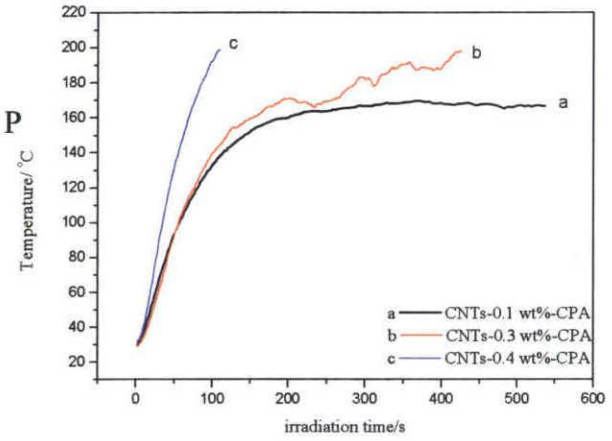

Fig. 4.31. Temperature-irradiation time curves of (a) CNT/CPA (CNT-0.1 wt%-CPA), (b) CNT-0.3 wt%-CPA and (c) CNT-0.4 wt%-CPA

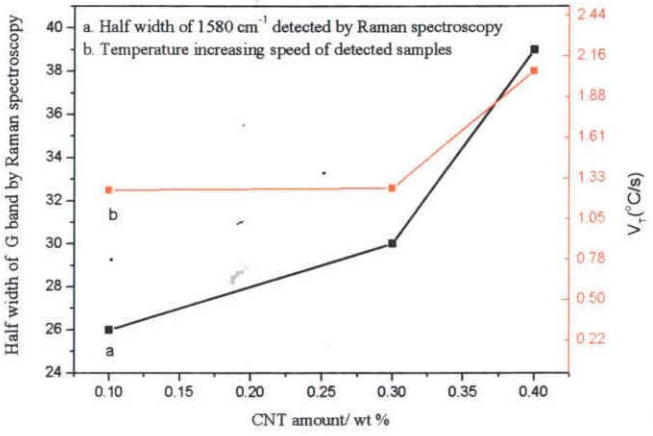

Fig. 4.32. Correlation plot among half width of G band in raman spectroscopy, CNT amount in ternary composite and temperature increasing speed (υ_T (°C/s))

these samples were irradiated at 750 W. As shown in Fig. 4.31, comparing CNT/CPA (CNT-0.1wt%-CPA), CNT-0.3 wt%-CPA and CNT-0.4 wt%-CPA each other, it is accessible to get a conclusion that microwave absorbability increases with added CNT amount. However, for this investigation, the maximum amount of added CNT is 4g per 1000g CNT/Alumina slurry. At the same irradiation power 750 W at 2.45 GHz, from initial temperature to 100 °C, linear-ship between temperature and irradiation time can be arrived. And the υ_T (°C/s) (Temperature increasing speed of irradiated specimens) of detected samples are listed in Table 4.5.

In chapter 3, we have confirmed that the microwave-induced heat performances are mainly affected by NCN graphitization degree, which can be evaluated by half width of G band ($\Delta\upsilon_{1580}/cm^{-1}$) and surface defects obtained from Raman spectroscopy. In Fig. 4.32, relationship

between carbon orientation, CNT amount and microwave-induced thermal properties of detected specimens has been discussed. CNT-induced graphite orientation decreases with CNT amount. Insteadly, microwave irradiated capacity of composites increase with accelerated CNT mass in ternary composite.

Table 4.5. Physical property of CNT/CPA with different CNT amount

Materials	υ_T (°C/s)
CNT-0.1 wt%-CPA	1.25
CNT-0.3 wt%-CPA	1.26
CNT-0.4 wt%-CPA	2.06

υ_T (°C/s): Temperature increasing speed of irradiated specimens at 2.45 GHz 750 W

Even though it is impossible to remove all of the NCN in CPA, it is expected to discuss the role of CNT in ternary composite for microwave-related heat performance. In Figure 4.33, microwave performance of PA is as good as CPA except for the initial increasing step. When irradiating time is longer than 530 s, the same temperature is arrived. Comparing CPA, PA, CNT-0.1wt%-CPA, CNT-0.3wt%-CPA and CNT-0.3 wt%-PA, absorptive behaviors are little direct relative with carbon amount (NCN for CPA and PA, NCN+CNT for CNT-0.1 wt%-CPA and CNT-0.3 wt%-PA). This conclusion is in agreement with chapter 3 discussion results. Simultaneously, the same microwave performance of CNT-0.3 wt%-PA and CPA is observed.

Table 4.6. Physical property of evaluated samples

Materials	C (mg/mm^3)	ΔT (T_{400}-T_0)/°C	Size (mm)	$\Delta\upsilon$1580cm^{-1}	$R_{ID/IG}$
Al_2O_3	0	18.1	------	------	------
CPA	0.009	110	9.03×9.19×10.19	25	0.48
PA	0.003	100	9.52×10.52×10.08	23	0.30
CNT-0.1 wt%-CPA	0.012	139	11.03×8.46×8.06	27	0.58
CNT-0.3 wt%-CPA	0.009	159	11.61×9.60×9.27	30	0.91
CNT-0.3 wt%-PA	0.004	107	10.36×10.61×9.44	26	0.89

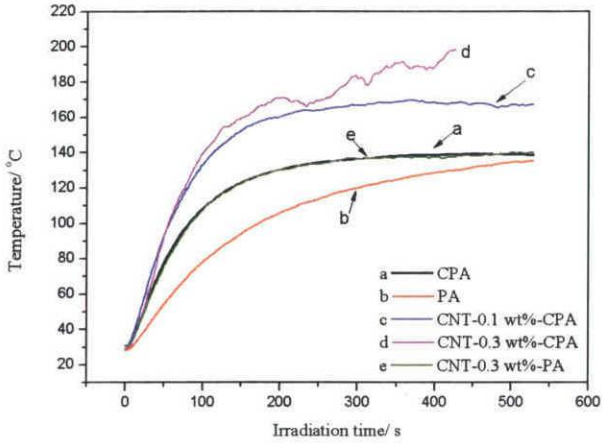

Fig.4.33. Temperature-irradiation time curves of (a) CPA, (b) PA, (c) CNT-0.1 wt%-CPA, (d) CNT-0.3 wt%-CPA and (e) CNT-0.3 wt%-PA

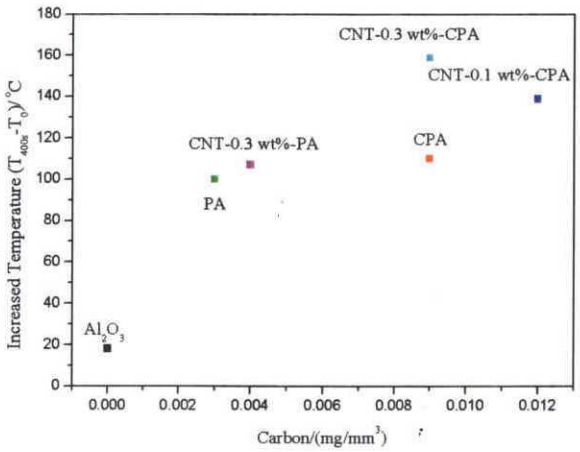

Fig.4.34. Correction of Increased Temperature (T_{400s}-T_0) and carbon amount

Table 4.6 displays the physico-chemical property of CA irradiating with 750 W at 2.45 GHz. It is noticed that several factors are involved for detected absorbents, namely, carbon mount, carbon graphitic orientation, CNT amount etc., which are discussed as follows:

a) Effect of carbon amount

As shown in Fig. 4.34, the relationship between increased temperature ($\Delta T=T_t-T_0$, $t_{(irradiation\ time)}$=400 s) and amount of carbon in investigated composites cubic with dimension (10 mm × 10 mm × 10 mm) are investigated. Microwave absorbability of CA merits from the polarization of 3-dimensional NCN. And the microwave-induced polarization ability is independent with carbon amount in composites.

b) Effect of carbon orientation

One of the key factors of carbon with graphitic structure is graphite orientation, which is usually evaluated by half width of G band. G band around 1580 cm^{-1} in Raman spectra arising from hex angel graphite vibration. Relationship between carbon amount and orientation is investigated in Fig.4.35. Comparing Fig.4.34 and Fig.4.35 (a), for CPA, CNT-0.1 wt%-CPA and CNT-0.3 wt%-CPA, both graphite orientation and microwave absorption induced temperature change with carbon amount and the same varying trend is observed. More, temperature change of them is direct proportional to decreased graphite orientation (Fig.4.35 (b)). Addition of CNT attributes to the decreased graphite orientation leading intensified phonon. And the enhanced absorptive performances of CNT-0.1 wt%-CPA, CNT-0.3 wt%-CPA and CNT-0.3 wt%-PA obtain

from the increased fiber-like graphitic sheet. Increased impurities induced effect of CNT for microwave absorbability was reported by Vázquez et al., which results from the concentrated localized joule heating effect of induced impurities [48].

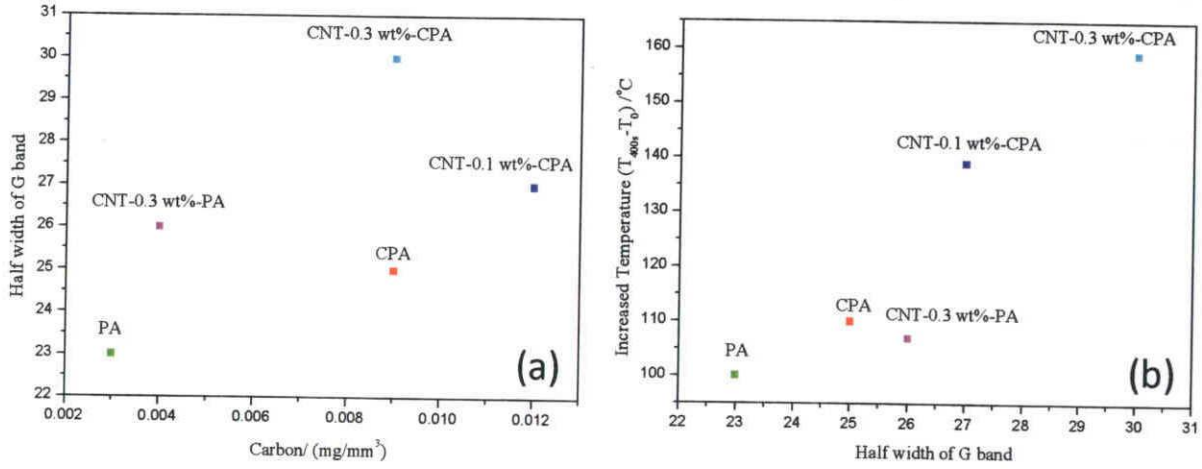

Fig.4.35. (a) Correction of half width of G band and carbon amount and (b) Correction of increased Temperature (T_{400s}-T_0) and half width of G band

c) Effect of CNT

Comparing with CPA, the enhanced absorptive behavior of CNT-0.3 wt%-CPA owing the same carbon amount in detected samples benefits from CNT leading increased surface defects. Added CNT has higher surface defects ($R_{ID/IG}$=0.98) than that of NCN in CPA ($R_{ID/IG}$=0.48). The same conclusion also has been arrived by comparing CNT-0.3 wt%-PA with PA. More, it has been proven that HTRS accelerates further graphitization of as-received CNT in 4.3.2.1 (Fig.4.16). Due to the joule heating mechanism, CNT-induced increased surface defects of as-fabricated CNT-involved composites attribute to the enhanced absorptive behaviors. This conclusion also supports that electromagnetic absorption of CNT is determined by impurities rather than orientation.

4.3.4. Effect of CNT Graphite Orientation

Based on above analysis, it is noticed that at the same irradiation condition, CNT/CPA composites with different features has been confirmed to be better absorbent than CPA. And its enhanced performances are attributed to the joule heating mechanism. More, in chapter 3, it was noticed that microwave absorbability is determined by graphitilization degree of NCN in CA. At the same HTRS condition, CDA owing better orientation has increased microwave capacity. Furthermore, in 4.3.3 section, it is reported that, due to the thermal stability of CNT in novel

atmosphere, HTRS attributes to the further graphilitization of CNT (I_D/I_G (CNT-0.1 wt%-CPA) =0.58<I_D/I_G(CNT-1700 °C)=0.98<I_D/I_G(CNT)=1.59). Therefore, it is necessary to investigate the effect of CNT graphitilization degree on CNT/CPA composite. Herein, in order to understand this point, carbon black (CB) with weak orientation and non-tube structure and highly graphitilized CNT (HGCNT, CVD method) were employed. CB is regarded as 0-tube CNT.

4.3.4.1. Physico-chemical property of CPA modified with different carbon forms owing varied graphitilization degree

Specifications of different carbon forms are listed in Table 4.7.

Table 4.7. Specifications of various carbon forms utilized in this study

Materials	Preparing method	Supplier	Size (nm)	Abbreviations
Carbon black	-------	High Purity Materials, Kojundo Chemical Labortory Co., Ltd.	66 nm	**CB**
Carbon nanotubes	Vapor grown	Showa Denko	D=20 nm	**CNT**
Highly-graphitilized carbon nanotubes	Chemical vapor deposition (CVD)	-------	D=20-30 nm	**HGCNT**

Considering the poor dispersiability of CNT in aqueous solution, as-received CNT and HGCNT were pre-treated at 60 °C for 6 h. As introduced in 4.3.1, pre-treatment resulted in the increased hydrophilic of CNT via different functional groups, which was useful for forming uniformly dispersed carbon/Al_2O_3 slurry (carbon indicates carbon black, CNT and HGCNT, carbon content in slurry is controlled to 0.1 wt%). By the combination of gelcasting and reductive sintering in novel atmosphere, CB-0.1 wt%-CPA, CNT-0.1 wt%-CPA and HGCNT-0.1 wt%-CPA were fabricated.

Structures of carbon additives are investigated by Raman spectroscopy as shown in Fig. 4.36 and Table 4.8. Two Raman active modes D band and G band in these detected samples indicate that the similarities of these carbon forms are graphitic structure.

Carbon black with layered graphite structure has weaker graphitilization degree, while tube-form (CNT and HGCNT) with large diameter-length ratio have better graphite orientation than CB. The commonly employed surface defects calculated from D band and G band intensity ratio and half width of G band ($\upsilon_{1580\ cm^{-1}}$) are shown in Table 4.8. By pre-treatment, surface defects are increased without bone structure destruction.

Table 4.8. Analysis results of various carbon forms from Fig. 4.36

Materials	$R_{ID/IG}$	$\upsilon_{1580\ cm^{-1}}$
CB	3.04	91
CNT	1.58	78
HGCNT	0.03	48
CNT-A-60 °C-6 h	1.63	73
HGCNT-A-60 °C-6 h	0.51	45

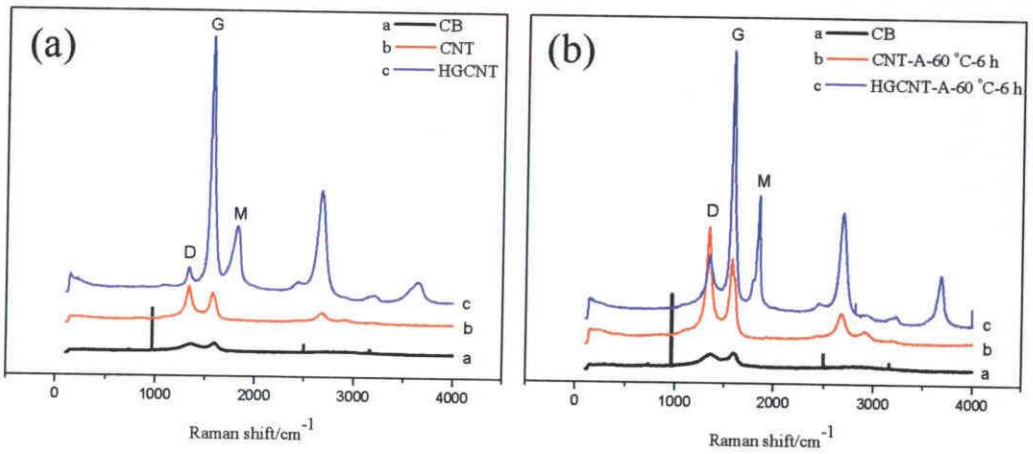

Fig. 4.36. Raman spectroscopy of various carbon forms (a) As-received and (b) with surface pre-treatment

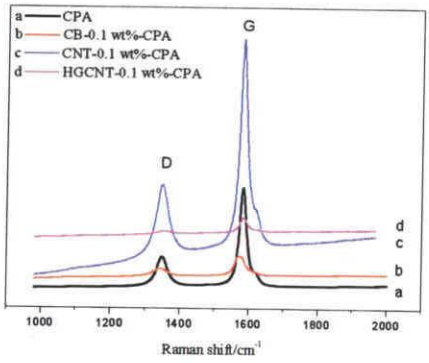

Table 4.9. Analysis results from Fig. 4.37.

Materials	$R_{ID/IG}$	$\upsilon_{1580\ cm-1}$
CPA	0.48	25
CB-0.1 wt%-CPA	0.55	36
CNT-0.1 wt%-CPA	0.58	27
HGCNT-0.1 wt%-CPA	0.47	26

Fig. 4.37. Raman spectroscopy of (a) CPA (b) CB-0.1 wt%-CPA (c) CNT-0.1 wt%-CPA and (d) HGCNT-0.1 wt%-CPA

By HTRS at 1700 °C, various carbon/CPA composites (CB-0.1 wt%-CPA, CNT-0.1 wt%-CPA and HGCNT-0.1 wt%-CPA) are arrived. In these composites, two kinds of carbon are available, that is additive carbon (CB, CNT and HGCNT) and NCN converted from polymer networks by HTRS. As shown in Fig.4.37, CNT-0.1 wt%-CPA has the highest intensity of D band and G band, while these two Raman active modes decrease with CB-0.1 wt%-CPA and HGCNT-0.1 wt%-CPA. Both CB-0.1 wt%-CPA and CNT-0.1 wt%-CPA own the same carbon orientation comparing with other composites. Half width of composite G band ($\Delta\upsilon$1580 cm^{-1}) implying graphite orientation decreases with that of carbon additives (Table 4.9). It was reported in Chapter 3, tube-like NCN form attributes to the intensified surface defects in CPA. Higher graphitilization of additives attribute to the increased graphite orientation of carbon in alumina-matrix composites. Density and porosity analysis of these composites is shown in Table 4.10.

Table 4.10. Density and porosity evaluation of composites

Samples	Bulk Density ($g \cdot cm^{-3}$)	Apparent Density ($g \cdot cm^{-3}$)	Real Density ($g \cdot cm^{-3}$)	Open Porosity (%)	Closed Porosity (%)	Total Porosity (%)
CPA	1.32	3.65	3.91	63.85	2.38	66.23
CB-0.1 wt%-CPA	1.07	3.44	3.89	68.89	3.57	72.46
CNT-0.1 wt%-CPA	1.44	3.78	3.90	61.89	1.24	63.13
HGCNT-0.1 wt%-CPA	1.22	3.79	3.95	67.94	1.30	69.24

As supported in Table 4.10, it is noticed that by adding CNT, apparent density of CNT-0.1 wt%-CPA and HGCNT-0.1 wt%-CPA are increased. More, increased porosity of carbon/CPA composites is available. Then, it is facilitated to get a conclusion that carbon additives accelerate the densification and porosity of fabricated ceramic bodies.

Structures of composites are shown in Fig. 4.38, comparing with binary composite CPA (NCN/Alumina), ternary composites (CNT-0.1 wt%-CPA, CB-0.1 wt%-CPA and HGCNT-0.1 wt%-CPA) have increased grain size (Fig.4.38 (b) (c) and (d)) proving densification of CA by adding different carbon forms. In chapter 3, it was introduced that manually degreasing attributed to the increased grain size, wherein, these carbon additives acting as monomer absorbers in carbon/alumina slurry attribute to the increased grain size.

Comparing with CPA, CB also results in the increased porosity and grain size. Existence of CB cannot be confirmed by just Fig. 4.38 (b). Contrast, the existence of CNT in both CNT-0.1 wt%-CPA and HGCNT-0.1 wt%-CPA are observed. Most of CNT covers the alumina grain surface. However, little is available for HGCNT via the same technology.

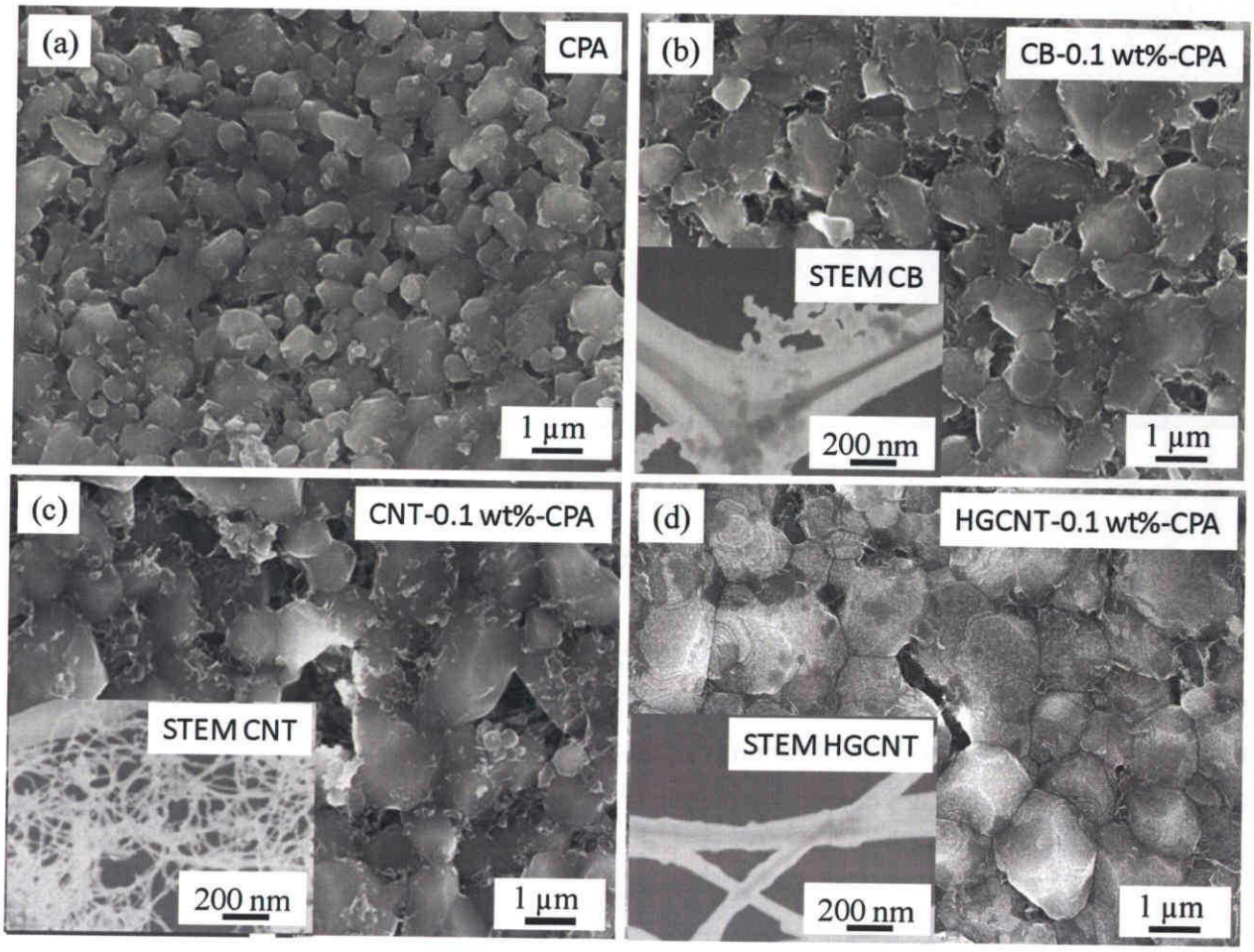

Fig.4.38. FE-SEM images of (a) CPA, (b) CB-0.1 wt%-CPA, (c) CNT-0.1 wt%-CPA and (d) HGCNT-0.1 wt%-CPA with low magnification

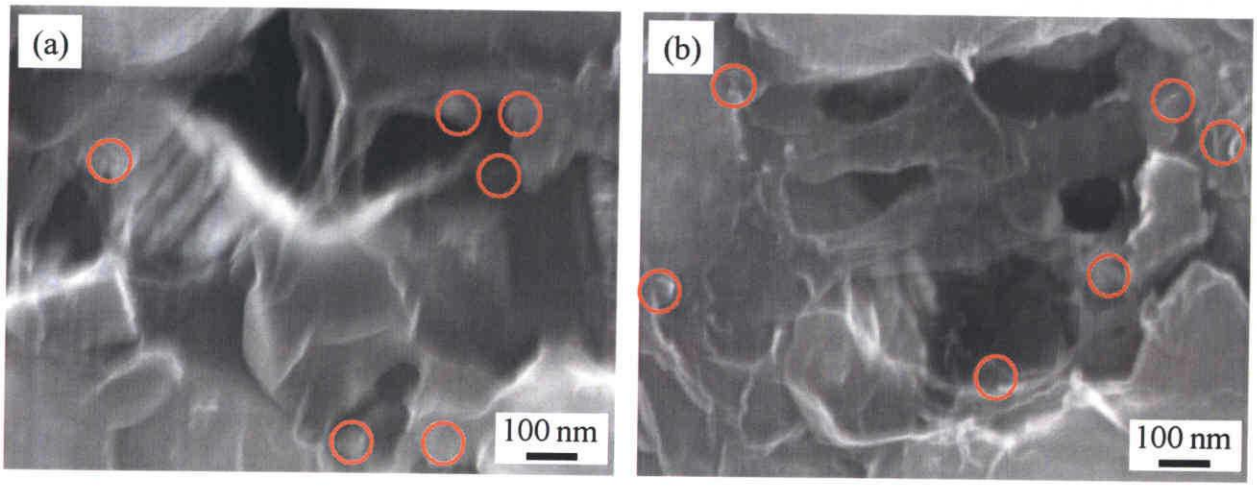

Fig.4.39. FE-SEM images of CB-0.1 wt%-CPA composite with high magnification

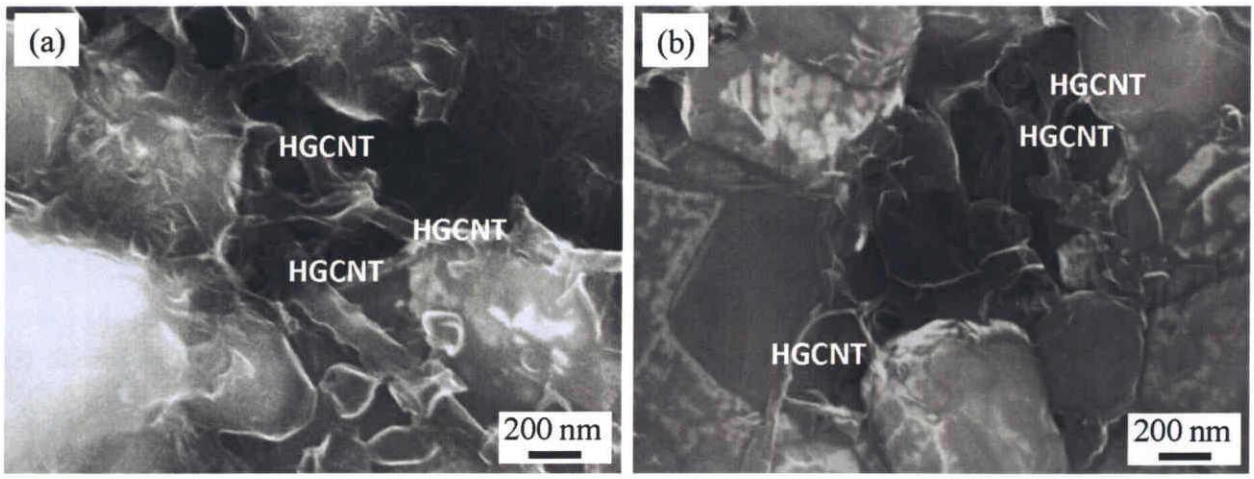

Fig. 4.40. FE-SEM images of HGCNT-0.1 wt%-CPA with high magnifications

By high magnification observation as displayed in Fig. 4.39 and Fig.4.40, it is feasible to say that NCN and carbon additives (CB, CNT and HGCNT) co-exist with alumina grains forming ternary composite. Good affinity of ceramic and carbon (NCN and additive (CB, CNT and HGCNT)) leads to high porosity and little agglomeration in composites, which indicates the good performance of them.

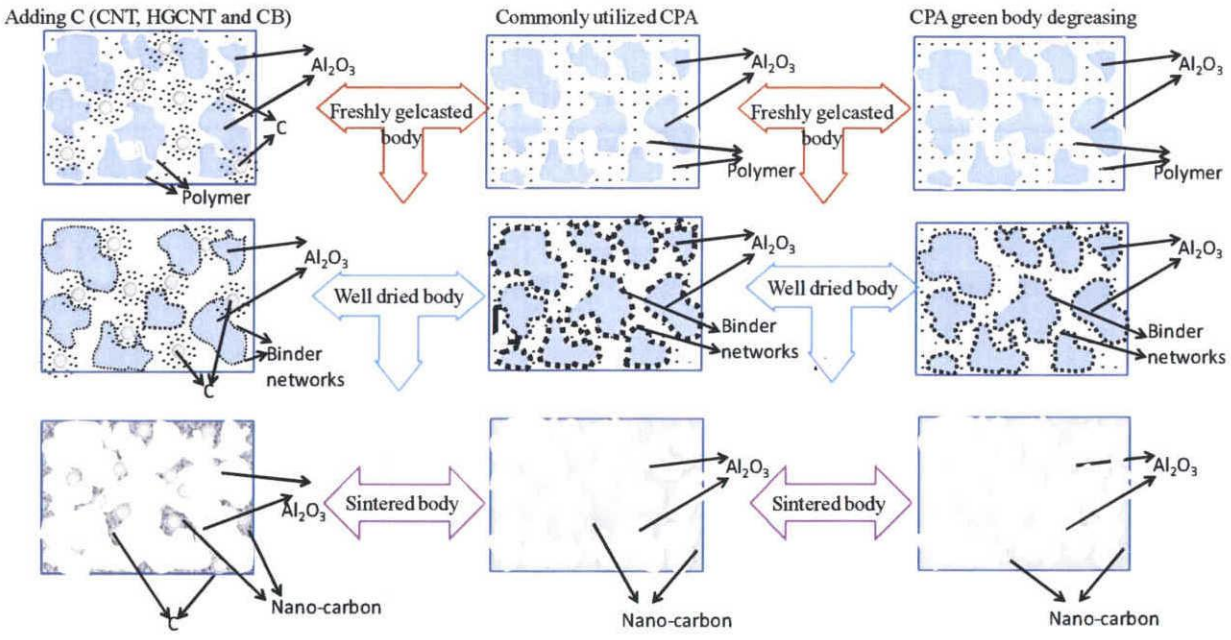

Fig. 4.41. Schematic of alumina grain size change with adding C and degreasing

It is valid that a densification procedure is available for CPA composite either by adding different carbon forms or degreasing (Fig. 3.8, Fig. 4.12, Fig.4.13, Fig. 4.26, Fig. 4.30, Fig. 4.38, Fig. 4.39, Fig.4.40, Table 4.2 and Table 4.4). Both of them have the same function for ceramic grains size increase. This function is removing the amount of binder networks on the surface of alumina grains leading to the increased alumina size at the same HTRS condition. The schematic of this is shown in Fig. 4.41.

Total carbon amount in various composites were evaluated by TG/DTA analysis, which is explained by Fig.4.42 (a) and Table 4.11. It is facilitated to get a conclusion that carbon additives except CB have no obvious contribution to the carbon amount in CPA-based composites evaluated by TG/DTA analysis in oxygen atmosphere.

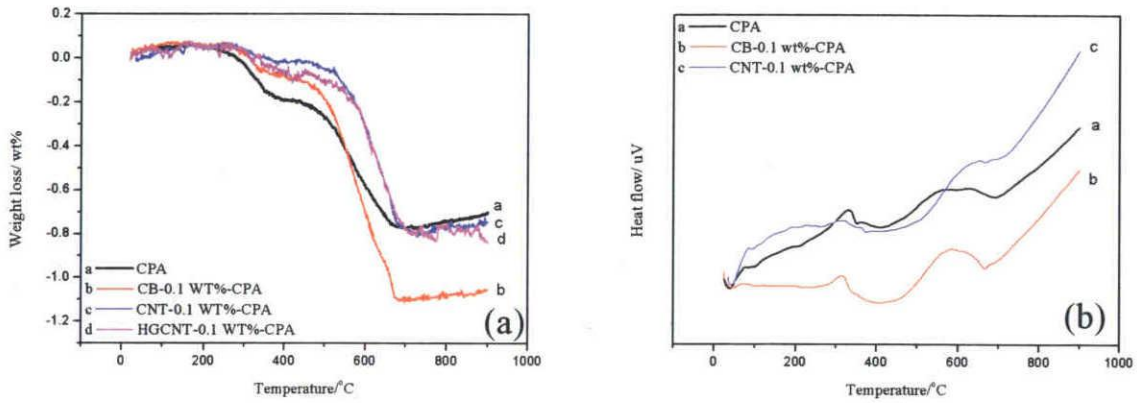

Fig. 4.42. (a) TG and (b) DTA analysis results of carbon/CPA composites conducted in oxygen atmosphere

Table 4. 11. Analysis results from TG/DTA analysis result in Fig. 4.41

Materials	Carbon content/wt%*
CPA	0.75
CB-0.1 wt%-CPA	1.11
CNT-0.1 wt%-CPA	0.80
HGCNT-0.1 wt%-CPA	0.80

**Carbon content (wt%) indicates NCN amount in CPA, various carbon additives (CB,CNT and HGCNT) and NCN in CNT-0.1 wt%-CPA, CB-0.1 wt%-CPA and HGCNT-0.1 wt%-CPA composites*

Comparing with CPA, CNT-0.1 wt%-CPA and HGCNT-0.1 wt%-CPA, CB-0.1 wt%-CPA has the highest carbon content (carbon implies NCN and CB). Because of the good thermal conductivity of carbon black, at the same HTRS condition, besides converting of NCN from binder networks (BN), part of energy is absorbed for further graphitilization of CB leading to the increased carbon amount in as-prepared CB-0.1 wt%-CPA. More, as displayed in Fig. 4.42 (b), increased pyrolysis temperature of carbon in composite implies the accelerated graphitilization degree accelerated by CNT.

4.3.4.2.Electromagnetic absorbability of CPA modified with different carbon forms owing varied graphitilization degree

In order to monitor the effect of carbon graphitilization degree on carbon/CPA composites, these composites were irradiated at different energy as shown in Fig. 4.43. As claimed by these curves, comparing with CPA, it is understood that enhanced microwave activities of CB-0.1 wt%-CPA, CNT-0.1 wt%-CPA and HGCNT-0.1 wt%-CPA are accessible. The enhanced temperature difference between carbon/CPA (carbon/CPA indicates CB-0.1 wt%-CPA, CNT-0.1 wt%-CPA and GHCNT-0.1 wt%-CPA) and CPA decrease with irradiation energy. And CNT-0.1 wt%-CPA owns the highest microwave capacity than others at the same irradiation conditions. Even though CB-0.1 wt%-CPA ($R_{ID/IG}$(CB-0.1 wt%-CPA)=0.55) has the similar surface defects with CNT-0.1 wt%-CPA ($R_{ID/IG}$(CNT-0.1 wt%-CPA)=0.58) as evaluated by Raman spectroscopy, the increased microwave absorbability of CNT-0.1 wt%-CPA is mainly attributed to the tube-like form leading to the intensified phonon by microwave irradiation. More, CNT and HGCNT owning the similar tube structure and varied graphitilization degree also have different microwave absorbability. CNT-0.1 wt%-CPA with weaker orientation than HGCNT-0.1 wt%-CPA benefits from the higher surface defects. Vázquez et al. [48] also have reported that microwave performance of CNT is attributed to thermal conductivity corresponded joule heating effect instead of polarization of graphite sheet. More, microwave capacity of CNT is non-related with its length.

Carbon additives result in the varied surface defects of composites as listed in Table 4.12. It is noticed that changed graphitilization degree attributes to the varied absorbability. Graphite orientation difference between these composites merit to the microwave capacity (CB-0.1 wt%-CPA and CPA has the same carbon amount in evaluated specimens and CNT-0.1 wt%-CPA and HGCNT-0.1 wt%-CPA has the same carbon amount). Detecting CPA and HGCNT-0.1 wt%-CPA with the same surface defects, the enhanced microwave performance of HGCNT-0.1 wt%-CPA is mainly attributed to the tube form in composite benefiting from phonon transition at the same irradiation condition.

Based on above analysis, it is facilitated to get a conclusion that additives with different graphitilization degree attribute to the increased surface defects of carbon in composites leading varied Fermi level. Under the same HTRS condition, further graphitilization of additives (CNT

and CB) results in the decreased free surface energy for ceramic densification and NCN conversion leaving increased carbon content in composite [49]. While, when a 'perfect' CNT namely HGCNT was injected into the alumina slurry, non-energy consumption for HGCNT, then, it is reasonable that the same graphite orientation and carbon content per unit (mg/mm^3) of cubic are available in this study as displayed in Table 4. 12.

Table 4.12. Physical property of evaluated samples

Materials	C (mg/mm^3)	ΔT ($T_{400s}T_0$)/°C	Size (mm)	$R_{ID/IG}$	$\upsilon_{1580\ cm}^{-1}$
CPA	0.009	110	9.03×9.19×10.19	0.48	25
CB-0.1 wt%-CPA	0.009	118	10.08×10.31×10.18	0.55	36
CNT-0.1 wt%-CPA	0.011	139	10.32×10.37×10.41	0.58	26
HGCNT-0.1 wt%-CPA	0.009	125	10.69×10.48×10.37	0.47	26

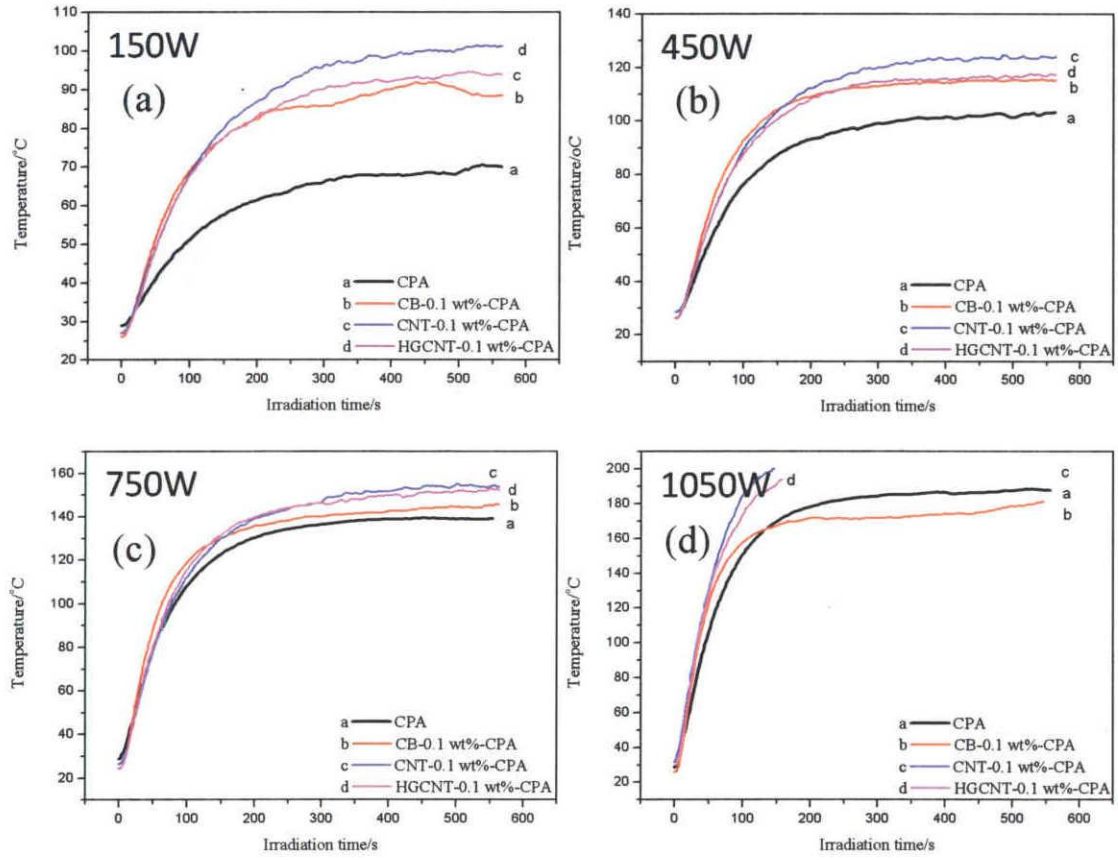

Fig. 4.43. Temperature-irradiation time curves of CPA, CB-0.1wt%-CPA, CNT-0.1wt%-CPA and HGCNT-0.1wt%-CPA at different irradiation powers (a) 150 W, (b) 450 W, (c) 750 W and (d) 1050 W

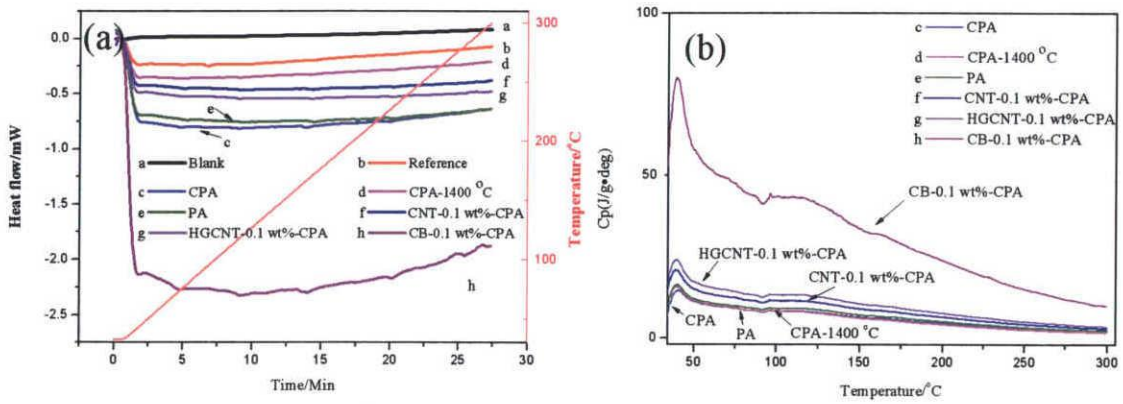

Fig. 4.44. (a) DSC analysis results of as-fabricated composites and (b) calculated specific heat capacity of composites

For varied heat performance of different composites, a general character for them is that there is an increasing step before arriving saturate temperature. In order to explain this phenomenon, specific heat capacities of materials are calculated from DSC results as shown in Fig. 4.44 (b). Benefiting from various additives, varied specific heat capacities are accessible. CB attributes to the highest value, which is attributed to the highest carbon content in as-resulted composite.

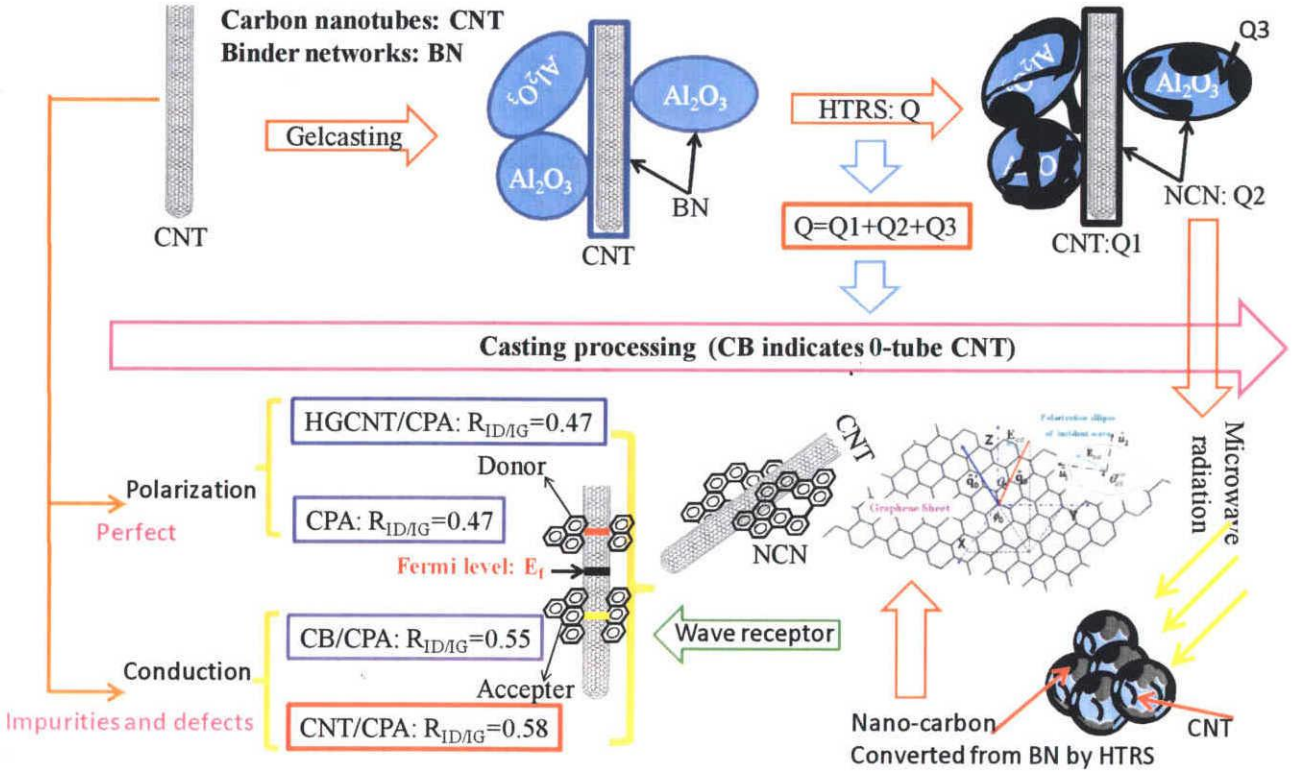

Fig. 4.45. Schematic of experimental for C-added composites and microwave irradiation mechanism proposal

Generally, two situations are concluded from above characterization results. One is HGCNT-induced increased Fermi level energy (E_f) and another is CB and CNT-resulted decreased E_f. Then, at the same irradiation powers, both CB and CNT act as electron accepter (NCN as donor) leading intensified phonon process, which leads to the increased surface defects evaluated by Raman spectra and microwave absorptive performances. Furthermore, it is noticed that even though the same amount of carbon additives were added into ceramic slurry, different carbon content per evaluated specimen cubic is calculated in Table 4.12. This phenomenon roots from varied graphitilization degree of additives.

Based on the above analysis results, it is noticed that graphite orientation plays an important role for microwave absorbance. And different with chapter 3, increased graphitilization degree does not mean the enhanced microwave capacity. More, it was reported that absorbability of CNT with 'perfect' structure is weaker than that of CNT with impurities and defects, which merits from joule heating effect permitting localized heating performance. The same schemic applies in our study. As shown in Fig. 4.45, by adding kinds of carbon additives into alumina slurry, CNT/NCN/Alumina ternary composite is available. Proposing the HTRS thermal energy as Q, further graphitilization of CNT absorbs thermal energy Q1, converting of BN to NCN needs energy Q2 and densification and coarsening of ceramic body need Q3, then, the total HTRS thermal energy Q=Q1+Q2+Q3 for various CNT/CPA composite, while Q=Q2'+Q3' is accessible for CPA. For HGCNT with high graphite orientation, the same energy distribution is possible with CPA, which can explain the same surface defects of HGCNT/CPA and CPA. Whereas, in CB/CPA and CNT/CPA, as proved in 4.3.2, it was concluded that HTRS accelerated the further graphitilization of CNT with poor orientation. More, it is believed that because of the consummated energy Q1 for them, poorer graphite orientation of NCN is reasonable ($R_{ID/IG}$ (CNT/CPA) =0.58 and $R_{ID/IG}$ (CB/CPA)=0.55). In these composites, CB, CNT, HGCNT co-exist with NCN forming C/C composite. Poorer graphitilization leads to the Fermi level decrease resulting increased microwave absorbability of CB/CPA and CNT/CPA. Both CNT and CB act as electron accepter in composite. However, good orientation of HGCNT plays as donor and the enhanced performance is attributed to induced tube-like structure in composite.

4.4. Conclusions

In this chapter, CNT/CPA ternary composite (CNT/NCN/Alumina) was fabricated by the combination of gelcasting and reductive sintering in Ar. The microwave capacity of this composite was discussed via clarifying different impact factors. Before preparing, as-received CNT was pre-treated with mixed concentrated acids with suitable condition. In order to optimum the treating condition, effects of pre-treating temperature and time have been discussed. It was concluded that increased dispersibility of as-received CNT merited from grafted functional groups. These groups induced to the minus increased ζ-potential of pre-treated CNT. The optimum treating condition was at 60 °C for 6 h. Employing pre-treated CNT at 60 °C for 6 h as

reinforcement, bending strength of as-fabricated CNT/CPA (CNT/NCN/Alumina) was 1.9 time of that of CPA (NCN/Alumina). Various co-exiting styles of main component CNT, NCN and Alumina resulted in this increased performance. By investigating the effect of added CNT amount, carbon and filler CNT orientation, it was feasible to get a conclusion that though CNT reinforce the substrate CPA, no improvement was available by increasing CNT amount. Both increased CNT amount and degreasing attribute to the increased ceramic grain size. By comparing the influence of CB, CNT and HGCNT, it was concluded that CNT with tube form and weaker graphitic orientation had the highest microwave capacity, which results from the decreased Fermi level.

References

[1]. C. Hai, H. Watanabe, T. Shirai, M. Fuji, M. Takahashi, F. Wang, Modifying the surface of the electrically conductive porous alumina, *Mater. Lett.*, 63, **2009**, 1320-1322.

[2]. C. Hai, J. Liu, H. Watanabe, M. Fuji, F. Wang, M. Takahashi, Surface Activation of Conductive Porous Alumina by Deposition Nickel Particles, *J. Am. Ceram. Soc.*, 92, **2009**, S38-S41.

[3]. J. Liu, H. Watanabe, M. Fuji, M. Takahashi, Electrocatalytic evolution of hydrogen on porous alumina/gelcast-derived-carbon network composite electrode, *Electrochem. Commun.*, 10, **2008**, 922-925.

[4]. J. Liu, R.L. Menchavez, H. Watanabe, M. Fuji, M. Takahashi, Highly conductive alumina/NCN composite electrodes fabricated by gelcasting and reduction-sintering-An electrochemical behavior study in aggressive environments, *Electrochima. Acta.*, 53, **2008**, 7191-7197.

[5]. E. Saiz, A.P. Tomsia, K. Suganuma, Wetting and strength issues at Al/α-alumina interfaces, *J. Eur. Ceram. Soc.*, 23, **2003**, 2787-2796.

[6]. H. Yang, F. Li, C. Shan, D. Han, Q. Zhang, L. Niu et al., Covalent functionalization of chemically converted grapheme sheets via silane and its reinforcement, *J. Mater. Chem.*, 19, **2009**, 4632-4638.

[7]. F. Ji, Y. Li, J. Feng, D. Su, Y. Wen, Y. Feng et al., Electrochemical performance of grapheme nanosheets and ceramic composites as anodes for lithium batteries, *J. Mater. Chem.*, 19, **2009**, 9063-9067.

[8]. J. Fan, D. Zhao, M. Wu, Z. Xu, J. Song, Preparation and Microstructure of Multi-wall Carbon Nanotubes-Toughened Al_2O_3 Composite, *J. Am. Ceram. Soc.*, 89(2), **2006**, 750-753.

[9]. Y. Hou, J. Tang, H. Zhang, C. Qian, Y. Feng, J. Liu, Functionalized Few-Walled Carbon Nanotubes for Mechanical Reinforcement of Polymeric Composite, *ACS Nano*, 3(5), **2009**, 1057-1062.

[10]. J. Xiong, Z. Zheng, X. Qin, M. Li, H. Li, X. Wang, The thermal and mechanical properties of a polyurethane/multi-walled carbon nanotube composite, *Carbon*, 44, **2006**, 2701-2707.

[11]. Y. Hou, J. Tang, H. Zhang, C. Qian, Y. Feng, J. Liu, Functionalized Few-Walled Carbon Nanotubes for Mechanical Reinforcement of Polymeric Composite, *ACS Nano*, 3(5), **2009**, 1057-1062.

[12]. J. Xiong, Z. Zheng, X. Qin, M. Li, H. Li, X. Wang, The thermal and mechanical properties of a polyurethane/multi-walled carbon nanotube composite, *Carbon*, 44, **2006**, 2701-2707.

[13]. M.J. Palmeri, K.W. Putz, T. Ramanathan, L.C. Brinson, Multi-scale reinforcement of CFRPs using carbon nanofibers, *Compos. Sci. Technol.*, 71, **2011**, 79-86.

[14]. M. Estili, A. Kawasaki, H. Sakamoto, Y. Mekuchi, M. Kuno, T. Tsukada, The homogenerous dispersion of surfacantsless, slightly disordered, crystalline, multiwalled carbon nanotubes in α-alumina ceramics for structural reinforcement, *Acta. Mater.*, 56, **2008**, 4070-4079.

[15]. V.G. Gavalas, R. Andrews, D. Bhattacharyya, L.G. Bachas, Carbon Nanotube Sol-Gel Composite Materials, *Nano. Lett.*, 1(12), **2001**, 719-721.

[16]. R Mouazer, I. Thijs, S. Mullens, J. Luyten, SiC foams produced by gel casting: synthesis and characterization, *Adv. Mater.*, 6(5), **2004**, 340-343.

[17]. Banerjee, T.H. Benny, S.S.Wong, Colvalent Surface Chemistry of single-walled Carbon Nanotubes, *Adv. Mater.*, 17(1), **2005**, 17-29.

[18]. D. Tasis, N. Tagmatarchis, A. Bianco, M. Prato, Chemistry of carbon Nanotubes, *Chem. Rev.*, 106, **2006**, 1105-1136.

[19]. H.R. Byon, H.C. Choi, Network Single-Walled Carbon Nanotube-Field Effect Transistors (SWNT-FETs) with Increased Schottky Contact Area for Highly Sensitive Biosensor Applications, *J. Am. Chem. Soc.*, 128, **2006**, 2188-2189.

[20]. H. Hu, A. Yu, E. Kim, B. Zhao, M. E. Itkis, E. Bekyarova, R. C. Haddon, Influence of Zeta Potential on the Dispersability and Purification of Single-walled Carbon Nanotubes, *J. Phys. Chem. B*, 109, **2005**, 11520-11524.

[21]. Y. Chen, L. Wei, B. Wang, S. Lim, D. Ciuparu, M. zheng et al., Dispersed Singled-walled Carbon Nanotubes Grown form Cobalt-incorporated MCM-41, *Nano*, 1(4), **2007**, 327-336.

[22]. M.T. Martínez, M.A. Callejas, A.M. Benito, W.K. Maser, M. Cochet, J.M. Andrés et al., Microwave single walled carbon nanotubes purification, *Chem. Commun.*, 9, **2002**, 1000-1001.

[23]. S.H. Tan, J.C. Goak, S.C. Hong, N. Lee, Purification of single-walled carbon nanotubes using a fixed bed reactor peaked with zirconia beads, *Carbon*, 46, **2008**, 245-254.

[24]. V.A. Sinani, M.K. Gheith, A.A. Yaroslavov, A.A. Rakhnyanskaya, K. Sun, A.A. Mamedov et al., Aqueous dispersions if single-wall and multiwall carbon nanotubes with designed amphiphilic oulycations, *J. Am. Chem. Soc.*, 127, **2005**, 3463-3472.

[25]. X. Zhang, L. Meng, Q. Lu, Cell Behaviors on Polysaccharide-Wrapped Single-wall Carbon Nanotubes: A Quantitative Study of the surface, *Nano*, 3(10), **2009**, 3200-3206.

[26]. T. Matsumoto, M. Sano, A role of van der Waals interactions in DC anhydrous electrodeposition and dielectric constant of carbon nanotubes, *Chem. Phy. Lett.*, 453, **2008**, 229-232.

[27]. D. Nepal, S. Balasubramanian, A. L. Simonian, V. A. Davis, Strong Antimicrobial Coatings: Single-Walled Carbon Nanotubes Armored with Biopolymers, *Nano lett.*, 8(7), **2008**, 1896-1901.

[28]. B. Kim, W.M. Sigmund, Functionalized Multiwall Carbon Nanotube/Gold Nanoparticle Composite, *Langmuir*, 20, **2004**, 8239-8242.

[29]. J. Ma, J. Wang, Purification of Single-Walled Carbon Nanotubes by a Highly Efficient and Nondestructive Approach, *Chem. Mater.*, 20, **2008**, 2895-2902.

[30] G. S. Tulevski, J. Hannon, A. Afzali, Z. Chem, P. Avouris, C. R. Kagan, Chemically Assisted Directed Assembled of Carbo Nanotubes for the Fabrication of Large-Scale Device Arrays, *J. Am. Chem. Soc.*, 129, **2007**, 11964-11968.

[31]. Y. Tian, D. Chassaing, A.G. Nasibulin, P. Ayala, H.Jiang, A.S. Anisimov, E.I. Kauppinen, Combined Raman spectroscopy and Transmission Electron Microscopy Studies of NanoBud Strusture, *J. Am. Chem. Soc.*, 130, **2008**, 7188-7189.

[32]. L. Chen, H. Xie, Y. Li, W. Yu, Surface Chemical Modification of Multiwalled Carbon Nanotubes by a Wet-Mechanochemical Reaction, *J. Nanomater.*, **2008**, 783981-783986.

[33]. G. Yamamoto, M. Omori, T. Hashida, H. Kimura, A novel structure for carbon nanotube reinforced alumina composites with improved mechanical properties, *Nanotechnology*, 19, **2008**, 315708/1-7.

[34]. K. Balani, A. Agarwal, Damping behavior of carbon nanotube reinforced aluminum oxide coating by nanomechanical dynamic modulus mapping, *J. Appl. Phys.*, 104, **2008**, 063517/1-063517/6.

[35]. M. Estili, H. Kwon, A. Kawasaki, S. Cho, K. Takagi, K. Kikuchi et al., Multiwalled carbon nanotube-reinforced ceramic matrix composites as s promising structural material, *J. Nucl. Mater.*, 398, **2010**, 244-245.

[36]. R.L. Menchavez. M. Fuji. M.Takahashi, Electrically Conductive dense and porous alumina with In-situ-synthesized Nanoscale carbon networs, *Adv. Mater.*, 20, **2008**, 2345-2351.

[37]. R.L. Menchavez, M. Fuji, T. Yamakawa, T. Endo, M. Takahashi, Investigation of phase composition in dense and porous gelcast alumina sintered under argon atmosphere, *Mater. Sci. Forum.*, 561-565, **2007**, 2123-2126.

[38]. Y. Yao, G. Li, K.A. Gray, R.M. Lueptow, Single-walled Carbon Nanotube-Facilitated Dispersion of Particulate TiO_2 on ZrO_2 ceramic Membrance filters, *Langmuir*, 24, **2008**, 7072-7075.

[39]. V. Skákalová, A.B. Kaiser, U. Weglikowska, K. Hrnčariková, S. Roth, Effect of Chemical Treatment on Electrical Conductivity, Infrared Absorption, and Raman Spectra of Single-walled Carbon Nanotubes, *J. Phys. Chem. B*, 109, **2005**, 7174-7181.

[40]. K.R. Moonoosawmy, P. Kruse, Amniguity in the Characterization of Chemically Modified Single-Walled Carbon Nanotubes: A Raman and Ultraviolet-Visible-Near- Infrared Study, *J. Phys. Chem. B*, 113, **2009**, 5133-5140.

[41]. H. Chu, J. Wang, L. Ding, D. Yuan, Y. Zhang, J. Liu et al., Decoration of Gold

nanoparticles on surface-grown single-walled carbon Nanotubes for decoration of Every Nanotube by Surface-Enhanced Raman spectroscopy, *J. Am. Chem. Soc.*, 131, **2009**, 14310-14316.

[42]. Jianbo Xu, Kaifeng Hua, Gengzhi Sun, Cheng Wang, Xiangyu Lv, Yujiang Wang, Electrooxidation of methanol on carbon nanotubes supported Pt-Fe alloy electrode, *Electrochem. Commun.*, 8, **2006**, 982-986.

[43]. C. Du, N. Pan, Preparation of single-walled carbon nanotube reinforced magnesia films, *Nanotechnology*, 15, **2004**, 227-231.

[44]. A. Javey, J. Guo, Q. Wang, M. Lundstrom, H. Dai, Ballstic Carbon nanotube field-effect transistor, *Nature*, 424, **2003**, 654-657.

[45]. L. An, W. Xu, S. Rajagopalan, C. Wang, H. Wang, Y. Fan et al., Carbon-Nanotube-Reinforced Polymer-derived Ceramic Composite, *Adv. Mater.*, 16 (22), **2004**, 2036-40.

[46]. J. Tatami, T. Katashima, K. Komeya, T. Meguro, T. Wakihara, Electrically Conductive CNT-Dispersed Silicon Nitride Ceramics, *J. Am. Ceram. Soc.*, 88(10), **2005**, 2889-2893.

[47]. Mao-sheng Cao, Wei-Li Song, Zhi-ling Hou, Bo Wen, Jie Yuan, The effects of temperature and frequency on the dielectric properties, electromagnetic interference shielding and microwave- absorption of short carbon firber/Silica composites, *Carbon*, 48, **2010**, 788-796.

[48]. Ester Vázquez and Maurizio Prato, Carbon Nanotubes and Microwaves: Interactions, Responses and applications, *ACS Nano*, 3(12), **2009**, 3819-3824.

[49]. M.N. Rahaman, Ceramic Processing and Sintering (Materials and Engineering, 10), *New York. Basel: Marcel Dekker INC*, **1995** Ch. 1.

[50]. S.S.Islam, Khurshed Ahmad Shah, H.S.Mavi, A.K.Shaukla, S.Rath and Harsh, Raman study on single-walled carbon nanotubes with different laser excitation energies, *Bull. Mater. Sci.*, 30 (3), **2007**, 295-299.

CHAPTER 5

SURFACE MODIFICATION OF CONDUCTIVE POROUS ALUMINA: CPA AND CNT/CPA VIA MICROWAVE-ASSISTED TECHNOLOGY

5.1. Introduction

In chapter 3 and chapter 4, by discussing the influences of different factors, physico-chemical properties and microwave-induced heat behaviors of electrically conductive ceramic CPA and CNT/CPA (CNT/CPA means CNT-0.1 wt%-CPA) had been confirmed. It was supported that nano-carbon networks (NCN) with graphite structure in CA is responsible for electrical conductivity of composite. And good orientation of NCN resulting in polarization via microwave irradiation resolves microwave transparency of Al_2O_3. Typically, in chapter 3, it was confirmed that the increased graphitization degree of NCN in CDA resulting from HTRS attributed to the improved electrical conductivity and microwave-induced heat performances. Comparing with CDA, high porosity of CPA up to 66.23 % not only supplied porous structure of ceramic, also announced good microwave absorbability of CPA. In chapter 4, Pre-treated CNT, Al_2O_3 and NCN formed high porous ternary composite. By HTRS in novel atmosphere, reinforcement CNT was further graphitilized, which is responsible for the improved electromagnetic wave absorbability of CNT/CPA. And it has confirmed that the enhanced microwave capacity of CNT/CPA was attributed to the increased surface impurities or defects, which was verified by discussing the effect of CNT amount, form and graphitilization degree.

Furthermore, as reported by Wei et al. [1], match of absorbers plays an important role for improving the electromagnetic wave absorbability and developing various potential applications in many fields. So far, kinds of ferrite/dielectric (Fe_3Al/Al_2O_3, $YBa_2Cu_3O_{7-x}/Al_2O_3$, FCC-Co/Al_2O_3, Al_2O_3- coated FeCo, $Ba_{0.65}Sr_{0.65}TiO_3$, (ZnMg)TiO_3) have been reported [1-6]. As proven by Suttisawat et al., Pt nanoparticles was not only catalyst but also good absorbents [7-9]. Up to now, various deposition methods have been reported for preparing Pt-modified composites. These methods involve conventional heating-assisted chemical reductive reaction (CRR) [7,11] and microwave-assisted chemical reductive reaction (MRR) [9,10].

Taking the good microwave activity of CPA into consideration, in this chapter, we would like to explore Pt/CPA, Pt/CNT/CPA magnetic/dielectric loss composites via one-pot MRR method. In previous studies [9-11], even though Pt nanoparticles also had been microwave-assisted deposited onto substrates, most of matrices are microwave transparent and non-porous. Herein, meriting from good microwave absorbability and high porosity resulting high accessible specific surface area of CPA and CNT/CPA, it is aimed at preparing a novel Pt/substrate composites via microwave irradiation method. For comparison, Pt/CPA prepared by conventional reductive reaction was also completed.

Taking the unique structure of substrates into consideration, in this chapter, several targets are listed as follows:

- Uniformly dispersed ultrafine Pt nanoparticles with narrow size distribution range on the surface of substrates.
- Not only outer surface but also inner pores of substrates can be modified.
- Environmentally friendly and low cost.
- Selective modification.
- High effective and efficiency.

5.2. Experimental procedures

5.2.1. Chemicals

Ethylene glycol (EG, Kanto Chemical Co., Inc) and $H_2PtCl_6 \cdot 6H_2O$ were directly utilized without any further purification.

5.2.2. Preparing of substrates

As-prepared CPA and CNT/CPA as introduced in chapter 2 and chapter 3 were cut into small cubes with desired dimension (10 mm×10 mm×10 mm).

5.2.3. Preparing of Pt/CPA and Pt/CNT/CPA composites via microwave-assisted method

Preparing procedures are listed as follows:

- 5g of CPA and CNT/CPA (CNT/CPA means CNT-0.1 wt%-CPA) cubic were immersed into 30 ml of 0.006 M H_2PtCl_6-alcohol solution at room temperature for 12h, respectively. In order to induce the Pt^{4+} into the inner pore of substrates, as-prepared systems were subjected to ultrasonication for 20 min followed by reduced pressure treating for 1 h. Then, as-resulted samples were thoroughly washed with distilled water and dried at 90 °C for one night in vacuum oven. As-received samples were denoted as Pt^{4+}/substrate, namely Pt^{4+}/CPA and Pt^{4+}/CNT/CPA.

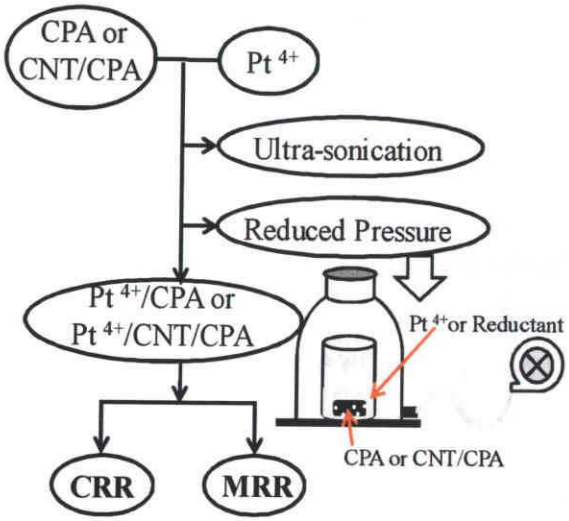

Fig. 5.1. Flowchart of experimental procedures for preparing composites

- 20 ml of EG was irradiated with different microwave powers to optimize the irradiation program for next experimental step.
- Pt^{4+}/CPA and Pt^{4+}/CNT/CPA were soaked into 20 ml EG solution followed by reduced pressure treating for 1 h. Then, as-received systems were microwave irradiated at 140 °C for different radiation time. As-resulted samples were named as Pt/CPA-MRR-I min and Pt/CNT/CPA-MRR-I min (I indicates experimental temperature holding time=1min, 5 min and 10 min). The experimental procedures involved in this section are shown in Fig. 5.1.
- For comparison, as-received Pt^{4+}/CPA was also subjected to conventional heating-assisted chemical reductive reaction (CRR) at 140 °C for 1 h (as introduced in Chapter 2). And the resulted samples were named as Pt/CPA-CRR.

5.2.4. Electromagnetic wave absorbability measurement

As-resulted Pt-decorated composites (10 mm×10 mm×10 mm) were employed for microwave absorbability evaluation. Double mode continuous microwave irradiation with 750 W was utilized to monitor microwave absorbability of detected materials on MWK-B-3.0 apparatus supplied by Takasago Industry Co., Ltd. This equipment is consisted of a 2.45 GHz microwave magnetron.

5.2.5. Characterization

To monitor the existence and morphology of Pt nanoparticles deposition on substrates, field-emission scanning electron microscopy (FE-SEM, JSM-7600R, Jeol, Corp.) equipped with Energy Dispersive X-ray Spectroscopy (EDS), Raman spectroscopy (NRS-3100, JASCO, Corp.) and X-ray diffraction (XRD, Rint, Rigaku, Japan) were employed.

5.3. Results and discussion

5.3.1. Optimization of microwave irradiation program

As introduced in references [7-13], Pt^{4+} is usually reduced to Pt metallic particles at 140 °C by both CRR and MRR methods. In our study, both reductant EG and substrates are microwave active materials. In order to optimumize the microwave irradiation program for Pt^{4+} converting to Pt particles, EG was pre-irradiated with different microwave powers as shown in Fig. 5.2.

EG has microwave absorbability as confirmed by increased temperature curves in Fig. 5.2 (a). Because the aim reaction temperature is 140 °C, then, it is necessary to find an optimum Pt deposition condition via MRR. Wherein, optimum condition indicates that the setting program equals to real temperature change in irradiated reaction systems. Fig. 5.2 (b) displays the setting temperature increasing program and real temperature curves in reaction system, which indicates the feasibility of microwave irradiation program irradiated at 2.45 GHz 300 W. The detail of

program is shown in Fig. 5.3.

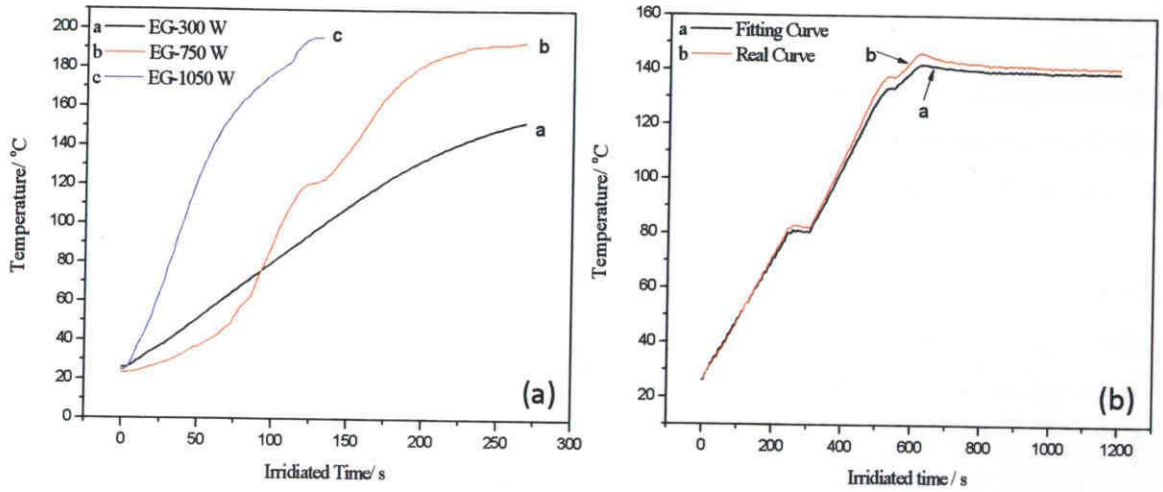

Fig. 5.2. Temperature-irradiation time curves of (a) Reductant EG with various irradiation energy and (b) Fitting curve and real curve of program for microwave-assisted Pt deposition at 300 W

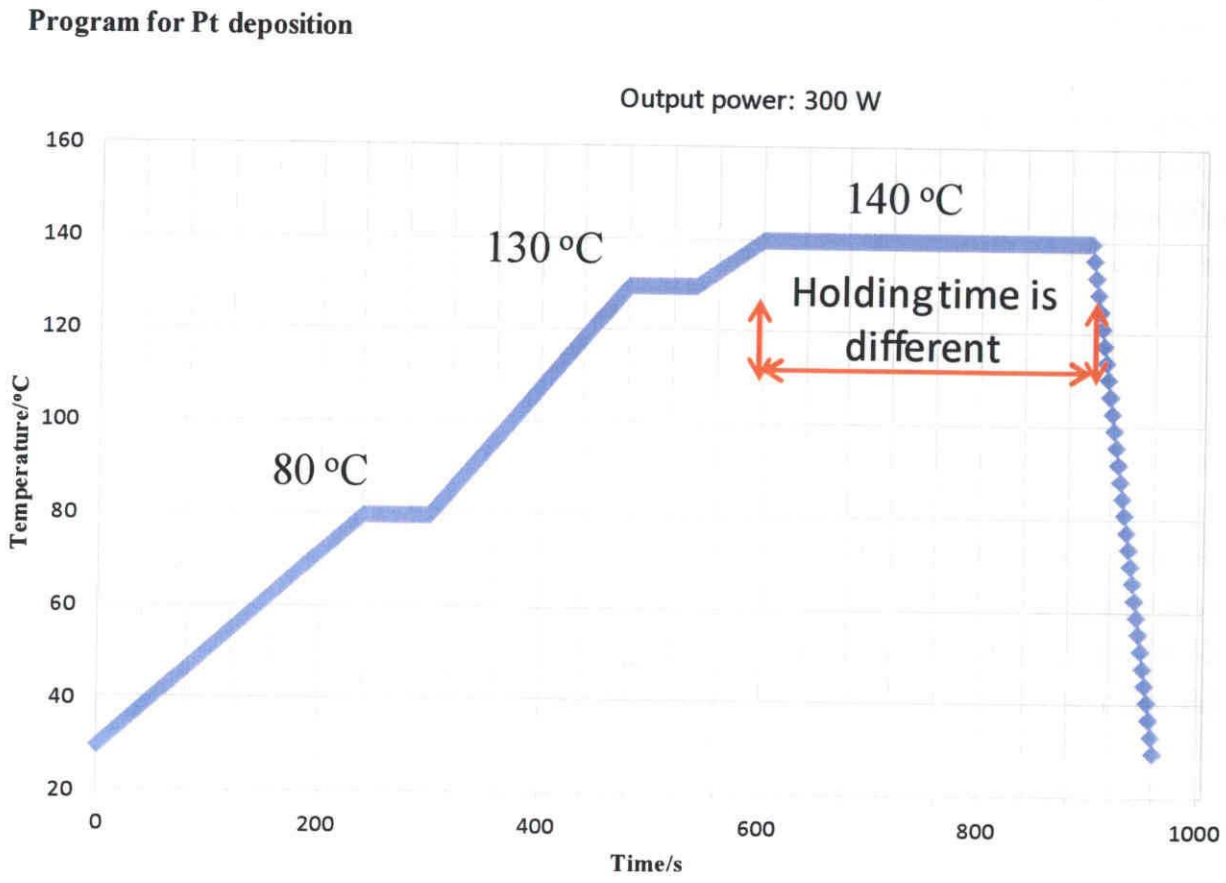

Fig. 5.3. Microwave irradiation program for Pt deposition

5.3.2. Physico-chemical property and electromagnetic wave absorbability of Pt/CPA-MRR

5.3.2.1. Physico-chemical property of Pt/CPA-MRR Composite

As shown in Fig.5.4 (I), it is noticed that electronic crystal structure of NCN in CPA belongs to graphitic structure, which was confirmed by two typical spectroscopic peaks around 1350 cm^{-1} (disorder induced D band) and 1580 cm^{-1} (tangential displacement mode named G band) [14]. Half width of G band ($\Delta\ \upsilon_{1580\ cm^{-1}}$) and calculated surface defects by intensity proportion of D band and G band ($R=I_D/I_G$) by Raman spectroscopy are universally employed to verify the graphite orientation in various carbonaceous forms (such as fullerene [15], carbon nanotubes [16] etc.). Herein, as shown in Fig.5.4 (II), good graphitic orientations of NCN in various composites are proved by half width of G band ($\Delta\ \upsilon_{1580\ cm^{-1}}$) around 25 cm^{-1}. The increased surface defects of composites also imply the success in deposition of Pt as shown in Fig. 5.4 (II), which results from metal-induced Fermi level shift of carbon (p-type doping). The same conclusion was obtained by Tarábek et al., who studied CNT (CNT means carbon nanotubes) doping [17]. It was also claimed that electron/hole doping of SWCNT attributed to the varied Raman scattering singularities, which resulted from doping-induced phonon energy renormalization [17-19]. More, it was demonstrated that, in graphene-like carbon forms, D band was related to the second-order processes involving phonons, which is explained by double resonant Raman scattering [20]. Therefore, the increased surface defects of Pt/CPA come from the enhanced electron-phonon interaction [20,21]. In a word, according to Raman spectroscopy results, comparing with as-received CPA, several conclusions can be arrived: (a) Pt deposition results in the increased surface defects, (b) Higher efficiency of MRR than CRR as evaluated by surface defects and $\Delta\ \upsilon_{1580\ cm^{-1}}$ value of samples and (c) the optimum condition for Pt/CPA-MRR is 5 min or 10 min.

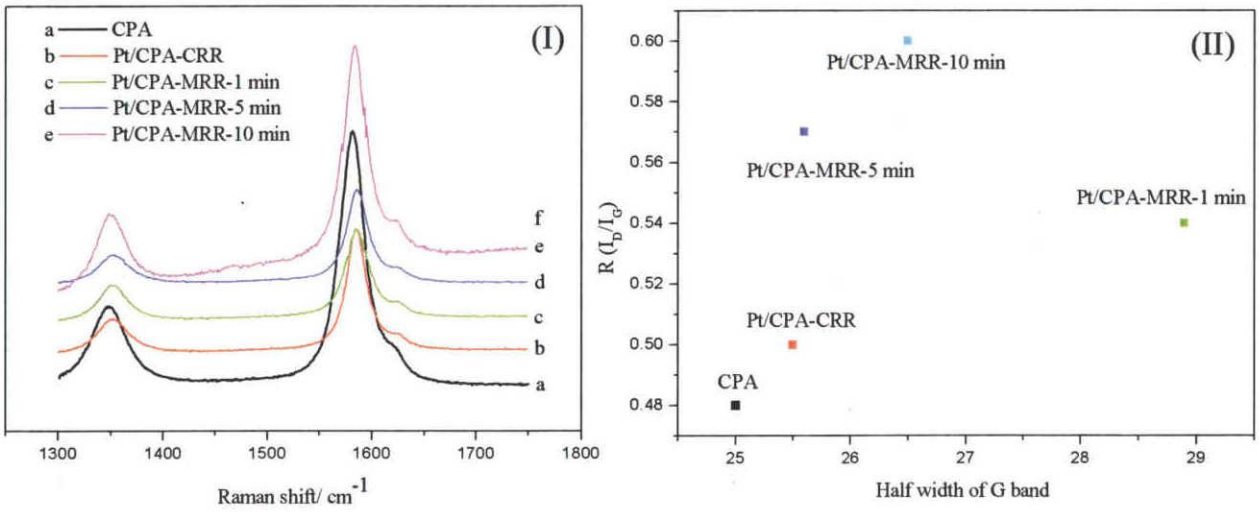

Fig. 5.4. (I) Raman spectroscopy of composites and (II) correlation plot between half width of G band and surface defects ($R(I_D/I_G)$)

Morphologies of composites are shown in Fig. 5.5. All of these images were inner fracture surface of specimens. It is facilitated to get a conclusion that Pt nanoparticles has been successfully deposited onto the surface of CPA by both CRR and MRR methods. Moreover, it is noticed that even though short irradiation time, Pt nanoparticles has been anchored onto CPA.

It is noticed that there are two surfaces in both outer and inner surface (namely cutting and fracture surface). In order to investigate the morphology differences between outer (Fig. 5.6 (a)) and inner surfaces (Fig. 5.6 (b)) of as received sample, different observation parts of one sample were taken.

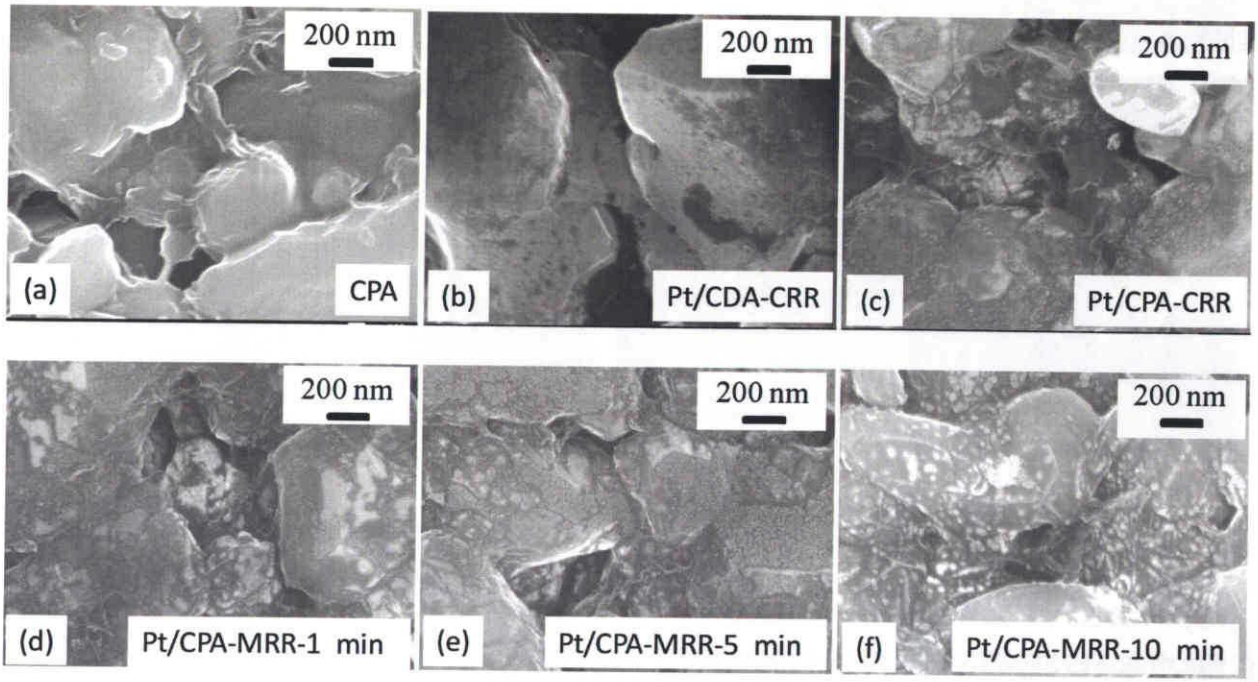

Fig. 5.5. FE-SEM images of composites (inner surface) (a) CPA; (b) Pt/CDA-CRR; (c) Pt/CPA-CRR; (d) Pt/CPA-MRR-1 min; (e) Pt/CPA-MRR-5 min and (f) Pt/CPA-MRR-10 min

By comparing with Fig. 5.5 (a), Pt nanoparticles has been obviously observed on the outer surface of as-received samples. Size of precipitated particles is around 50 nm. Contrast, the deposited Pt nanoparticles in inner surface (fracture surface, Fig. 5.7 (b) (c) and (d)) is much smaller than that of outer surface (Fig. 5.7 (a)). Then, it is facilitated to say that Pt nanoparticels grows along the NCN as displayed in Fig. 5.7 (b) forming metallic networks. The selectively deposition of Pt nanoparticles on NCN can be more clearly clarified by SEI images (Fig. 5.7 (c)) and Fig. 5.7 (d). Due to the size difference of deposited particles, it is necessary to investigate temperature difference of

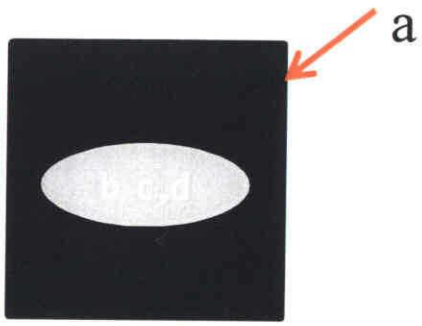

Fig. 5.6. Observation part of sample in Fig. 5.7

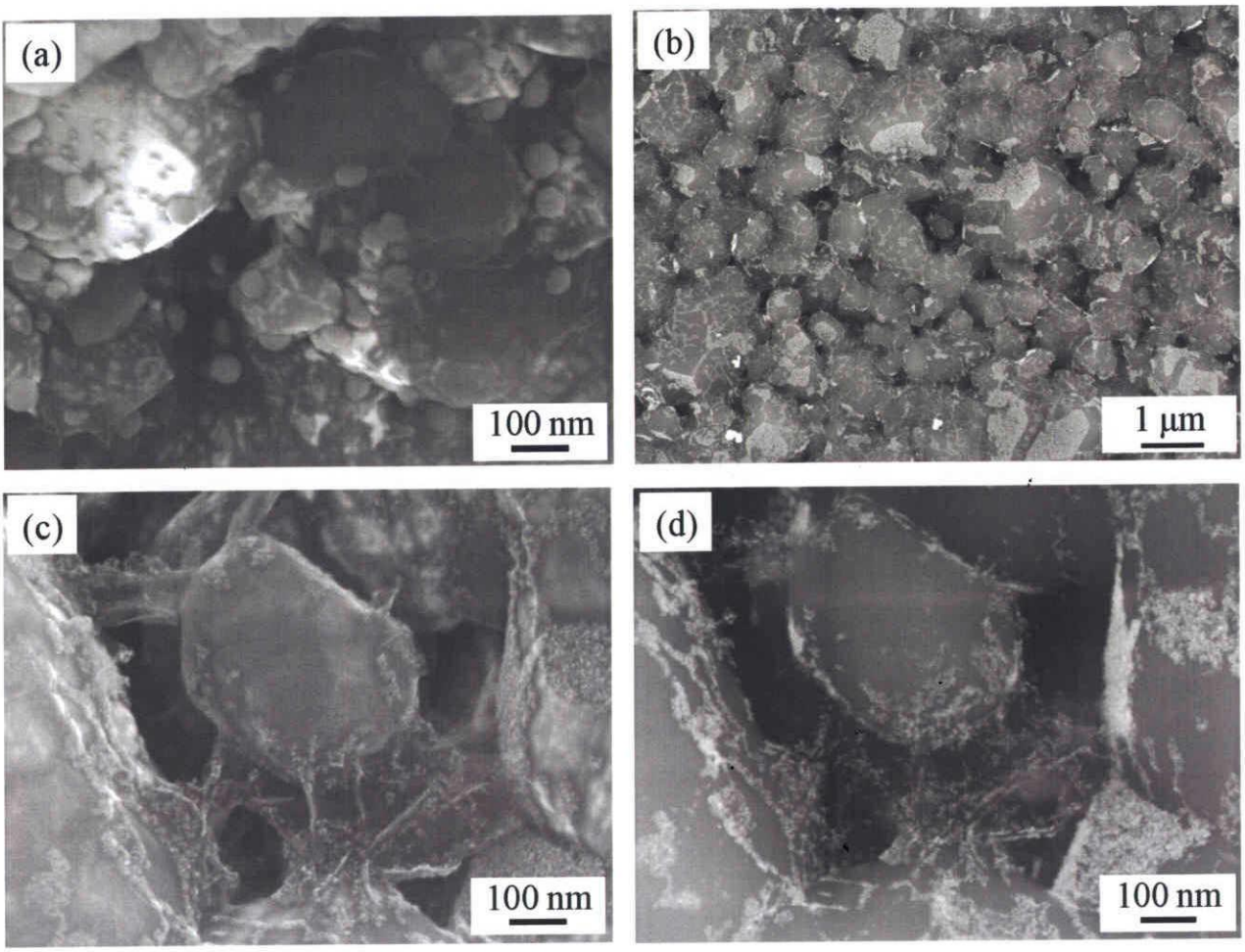

Fig. 5.7. FE-SEM images of Pt/CPA-MRR-5 min (a) outside of prepared specimen and inner surface of sample (b) low magnification and (c) and (d) high magnification (compo image)

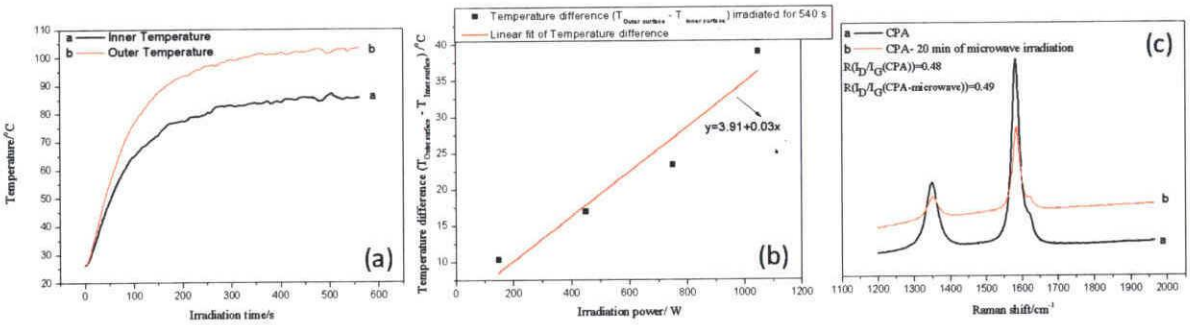

Fig. 5.8. (a) Temperature-irradiation time curves of CPA for investigating temperature difference between outer and inner surface; (b) Outer and inner surface temperature difference-Irradiation power plot of CPA at varied irradiation conditions and (c) Raman spectroscopy of CPA with/without microwave irradiation

substrate between outer and inner surfaces during microwave irradiation.

In order to monitor the temperature difference, one thermal-fiber was employed to monitor the outer surface, while another one is inserted into the opened pore to detect the inner temperature change. As shown in Fig. 5.8 (a), temperature difference between outer and inner surfaces is displayed. At the same irradiation power, obviously, outer surface temperature is higher than inner, which can effectively explain the increased particles size of Pt nanoparticles on the outer surface. By investigating the temperature difference between outer and inner surface at the same irradiation condition, temperature difference is in direct proportional to irradiation power. The fit linear equation is: y=3.91+0.03x. (y means temperature difference (the unit is °C), while x means irradiation power (unit is W)) Moreover, new defects were not generated during microwave irradiation, which can be confirmed by unvaried surface defects calculated from intensity ratio of D band (1350 cm^{-1}) and G band (1580 cm^{-1}). More, the increased surface defects of composites as shown in Fig. 5.4 also indicate the success in Pt deposition by MRR.

Deposition of Pt nanoparticles also can be confirmed by XRD pattern as shown in Fig. 5.9. A means Al_2O_3. Although high intensity of Al_2O_3 blocks detecting the Pt peaks, some small peaks around indicates the existence of Pt in this composite. Commonly, five XRD diffraction peaks are corresponded to Pt crystallite. That is 39.9 ° (111), 46.4 ° (200), 67.7 ° (220), 81.4°(311), and 86.1° (222) [22]. However, Pt (220), Pt (311) and Pt (222) are overlapped with Al_2O_3 diffraction peaks. It is difficult to detect these peaks on Pt/CPA composites.

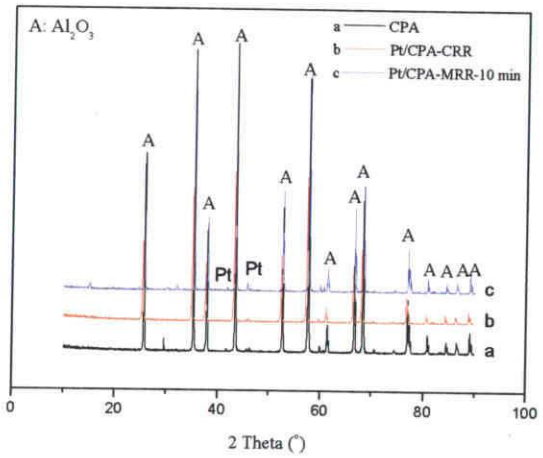

Fig. 5.9. XRD pattern of (a) CPA; (b) Pt/CPA-CRR and (c) Pt/CPA-MRR-10 min

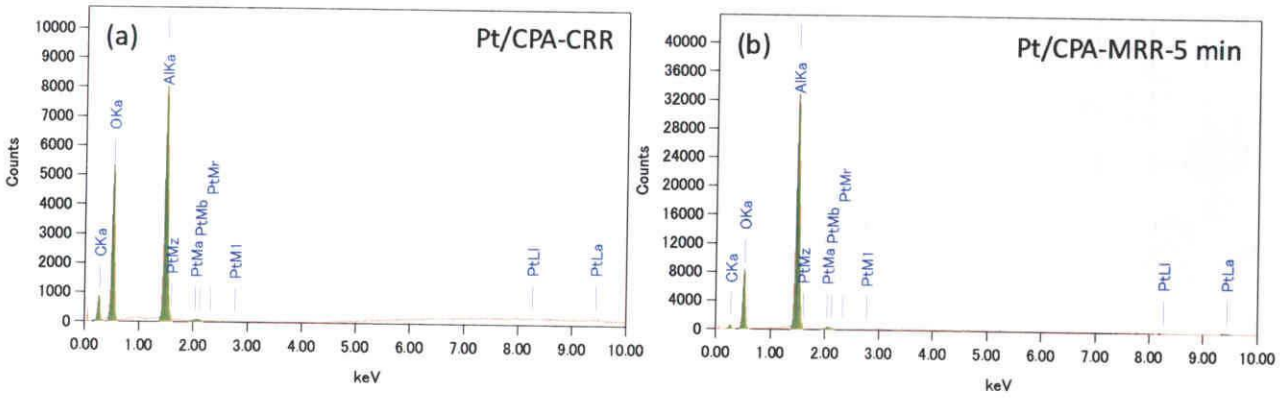

Fig. 5.10. EDS analysis results of (a) Pt/CPA-CRR and (b) Pt/CPA-MRR-5 min

Table 5.1. Calculated quality of deposited Pt nanoparticles by EDS analysis

Materials	C (wt%)	Pt (wt%)	Pt/C
Pt/CPA-CRR	39.81	0.70	0.018
Pt/CPA-MRR-1 min	43.33	3.18	0.073
Pt/CPA-MRR-5 min	13.04	2.22	**0.170**
Pt/CPA-MRR-10 min	47.91	3.41	0.071

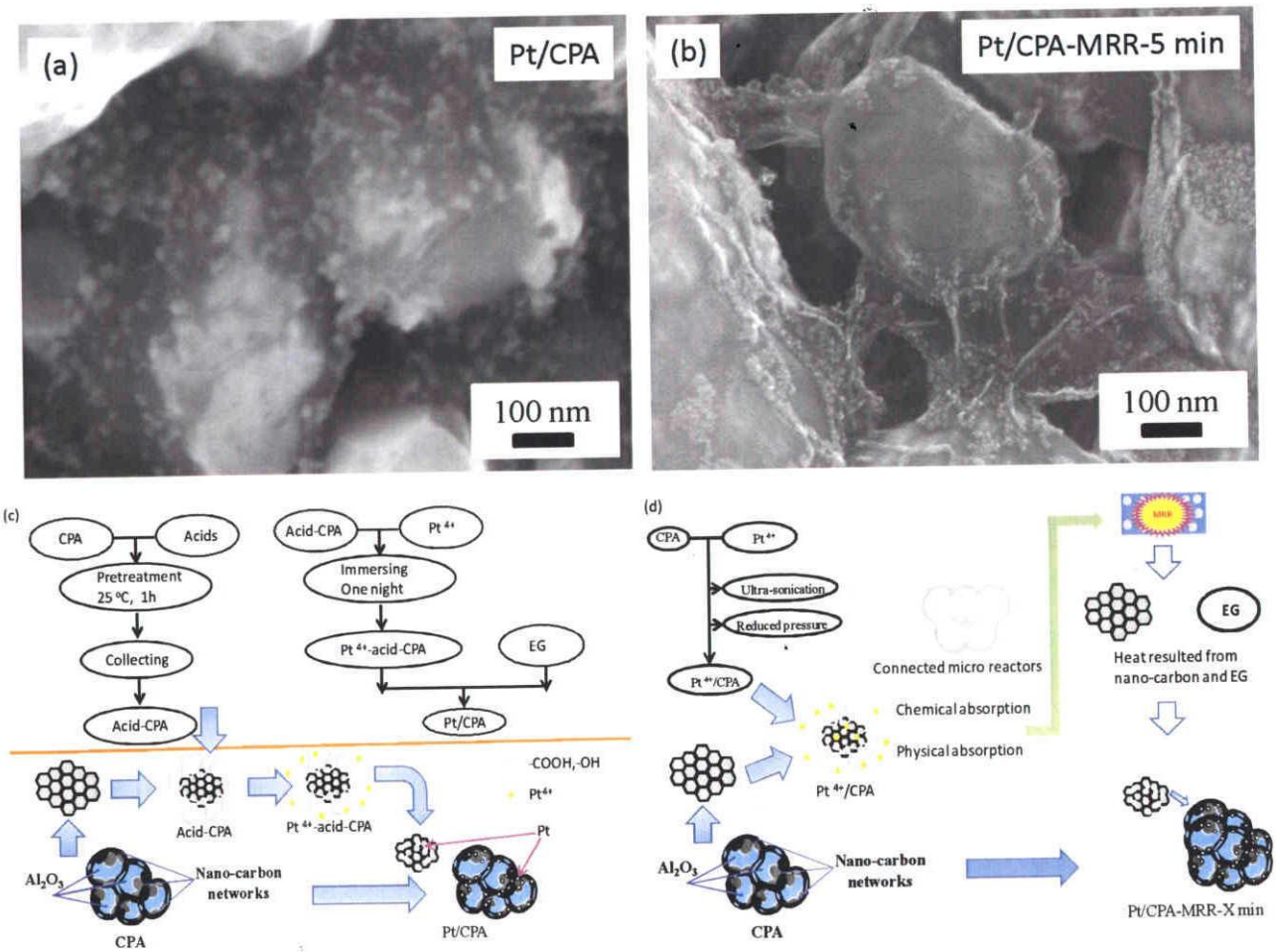

Fig. 5.11. FE-SEM images of (a) Pt/CPA-CRR and (b) Pt/CPA-MRR-5 min and proposed scheme for (c) Pt/CPA-CRR and (d) Pt/CPA-MRR-5 min

More, as shown in Fig. 5.6, Fig. 5.7, ultrafine Pt nanoaprticles with narrow size distribution range also clarifies the weak Pt crystal peak.

Fig. 5.10 displays the EDS analysis results of detected composites, by which deposition of Pt nanoparticles can be confirmed. Both CRR and MRR accelerate its precipitation. However, NCN conductive paths in substrate are not uniformly dispersed. So it is impossible to directly evaluate the loading efficiency. For comparison, the same magnification SEM images (magnification is ×30000) were taken for EDS analysis. By comparing the Pt and carbon content ratio, relative deposition ratio under various conditions can be calculated as shown in Table 5.1. In this case, based on the analysis results of Raman spectroscopy, FE-SEM images and EDS spectrum, it is facilitated to reach a conclusion that that benefiting from quick deposition, high loading efficiency and low energy consumption of MRR, the optimum deposition is Pt/CPA-MRR-5min.

As introduced in chapter 2, Pt nanoparticles also can be deposited onto the surface of pre-treated CPA [23]. Selective modification of CPA was achieved by surface pre-treatment [24]. While in this chapter, there are two components in CPA namely Al_2O_3 and nano-carbon. Only NCN is believed to be microwave active material as demonstrated in chapter 3.

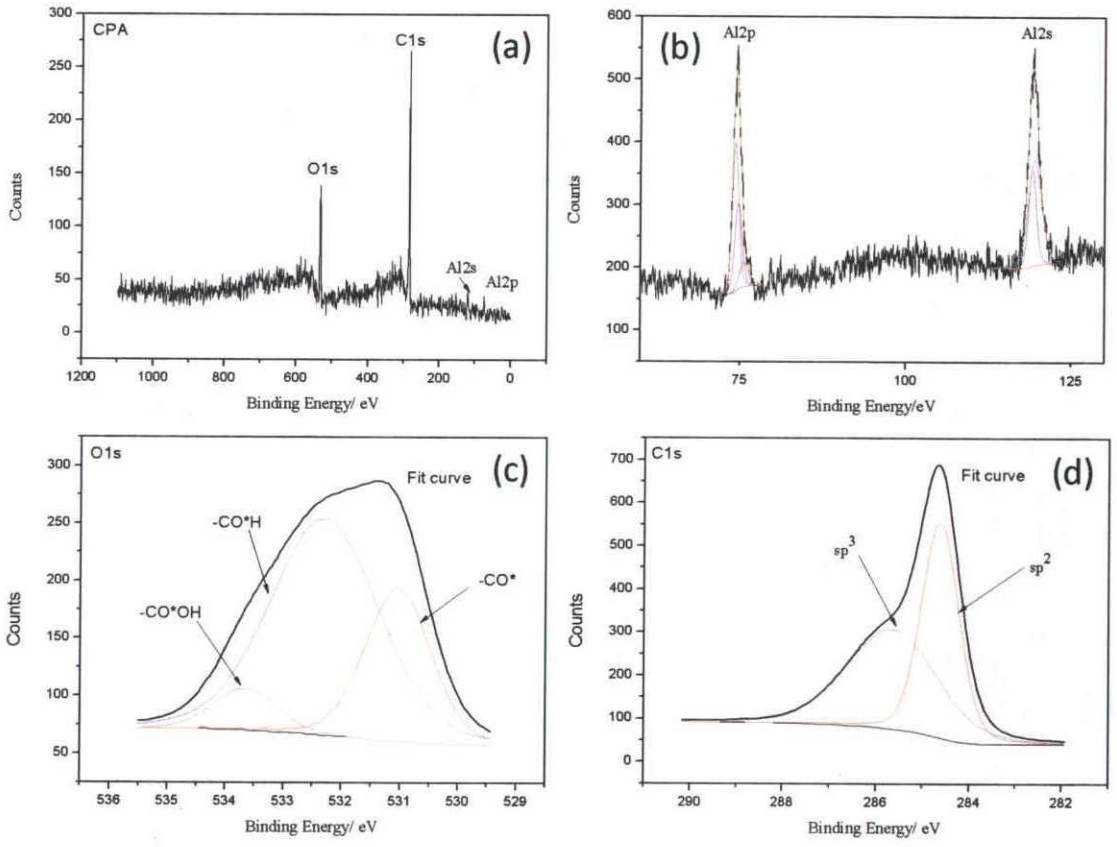

Fig. 5.12. XPS spectrum of CPA (a) all-range spectra (0~1100 eV) (b) Al2s, Al2 pregions (c) Decounted O1s regions peaks and (d) decounted C1s regions peaks

Meriting from good microwave activity of CPA, selectively depositing of nanoparticles can be controlled by microwave active material and non-active material. Moreover, during irradiation, every cross-linked pores act as linked micro-reactors resulting total modification of CPA. This scheme is shown in Fig. 5. 11(c) and (d).

It is noticed that the main component in CPA is Al_2O_3 and carbon, namely Al, O and C three elements. X-ray photoelectron spectra (XPS) is regarded as effective way for detecting components. As shown in Fig. 5.12 (a), The C (1s) signal at 284.8 eV, O (1s) at 543.1 eV, Al (2s) at 121.2 eV and Al (2p) at eV for investigated samples is well in agreement with references introduction [26-30]. The C1s core-level also indicate key feature of C1s in CPA. As shown in Fig. 5.12 (c) and (d), the deconvoluted C (1s) and O (1s) peaks of as-fabricated CPA imply the presence of C and O with different bonding structure. The C1s of as-fabricated CPA displays a maximum centered at 284.6 eV. And the deconvoluted spectrum gave two peaks which can be confirmed to be sp^2 graphitic (C=C, C-H, at 285±0.2 eV) and sp^3 (-CO-, at 286.4±0.2 eV). Moreover, the deconvoluted spectrum of O 1s also indicate oxygen-functional groups such as –CO*OH (533.4±0.2 eV), -CO*H (532.1±0.2 eV) and –CO* (530.6±0.2 eV) and defects can be expected on as-fabricated CPA, namely the well-structured 3-dimensional nano-carbon networks in CPA were partly destructed by some groups and instinctive defects [25-27].

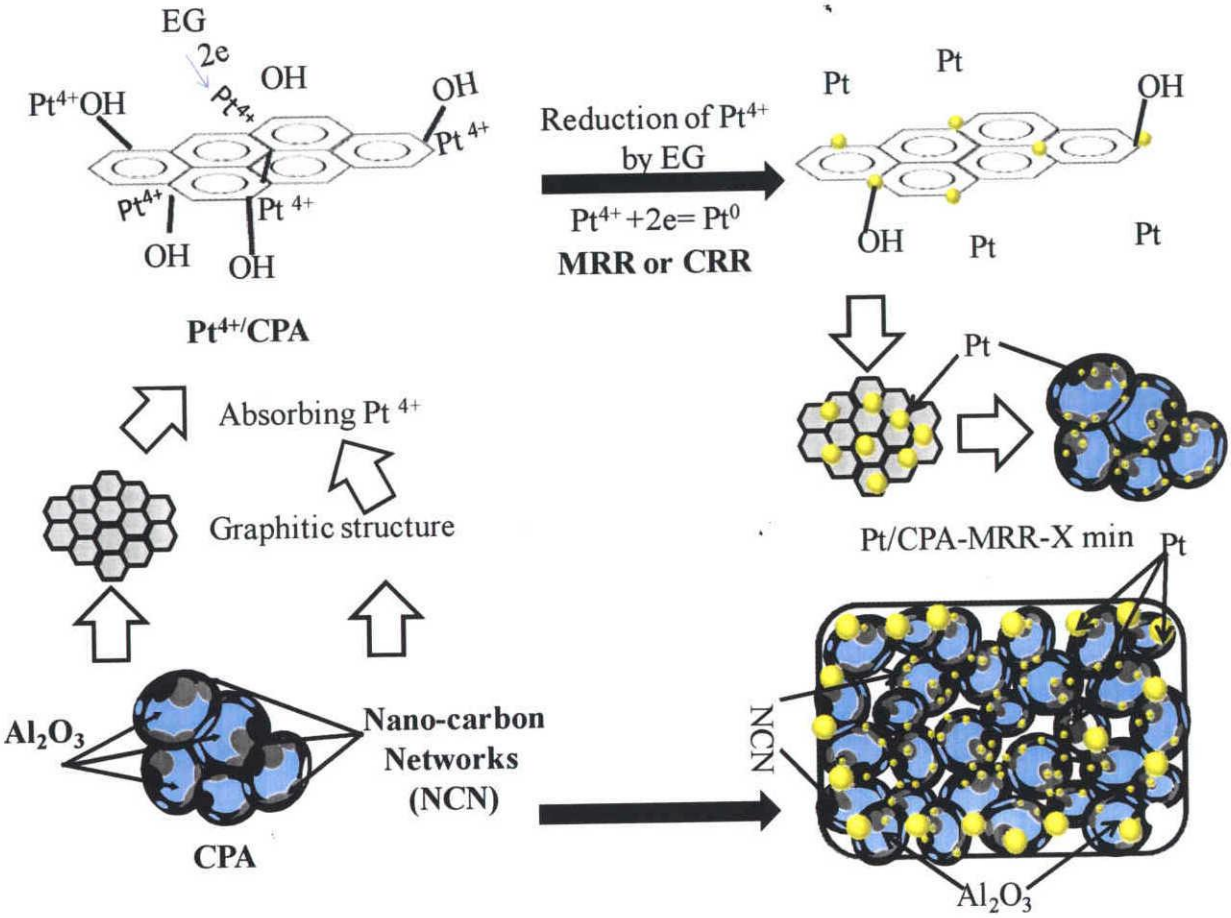

Fig.5.13. Schematic representation of synergistic reduction of Pt^{4+}

In this study, injected Pt^{4+} can be absorbed onto several sites of NCN in CPA substrate. These sites named as graphite instinctive defects include Stone-wales defects, sp^3-hybridized defects and vacancies in nano-carbon with graphitic structure. During reaction, electron donors EG sacrifice electron to the absorbed Pt^{4+} converting to Pt^0. Moreover, because of the temperature difference between outer and inner surface of substrate, Pt nanoparticles with different sizes is precipitated onto the surface. This proposal is shown in Fig. 5.13.

5.3.2.2. Electromagnetic wave absorbability of Pt/CPA-MRR Composite

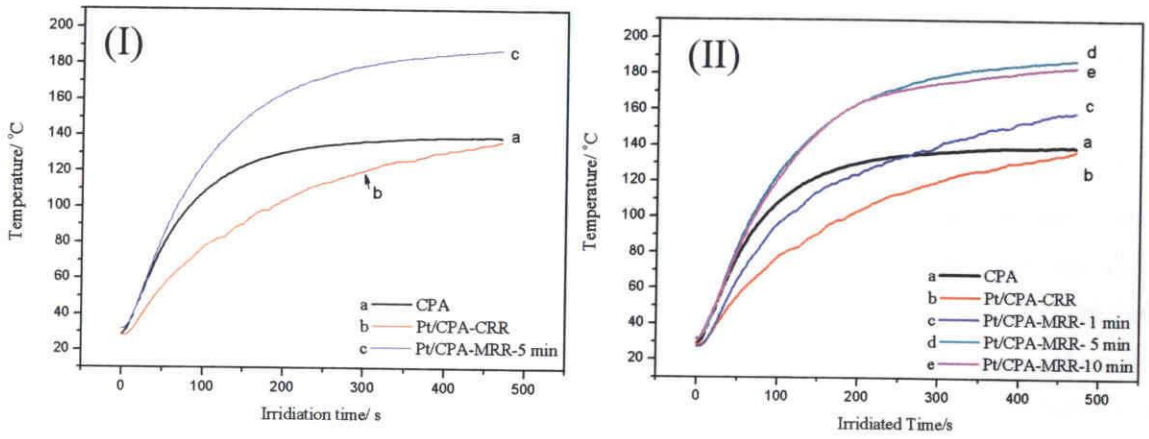

Fig. 5.14. Temperature-irradiation time curves of (I) Comparison of CPA, Pt/CPA-CRR and Pt/CPA-MRR-5min and (II) Enhanced microwave absorption of Pt/CPA-MRR-1min, Pt/CPA-MRR-5min and Pt/CPA-MRR-10min

Table 5.2. Physical property of evaluated samples

Materials	Size (mm)	NCN (mg/mm^3)	Δ T (T_{540s}-t_0)/°C	Efficiency (%)
CPA	9.03×9.19×10.19	0.009	111.1	56
Pt/CPA-CRR	9.69×10.48×10.05	0.009	113.8	84
Pt/CPA-MRR-1min	10.83×9.53×9.74	0.009	151.5	81
Pt/CPA-MRR-5min	10.73×10.50×10.11	0.009	166.0	75
Pt/CPA-MRR-10min	9.63×10.24×10.71	0.009	155.0	74

Up to now, we have fabricated Pt nanoparticles deposited composites by microwave-assisted method. Comparing with conventional heating method, rapid heating by microwave attributes to the formation of Pt nanoparticles without agglomeration. Both inner and outer surfaces of substrates can be totally modified by Pt particles. Therefore, it is interested in the contribution of Pt nanoparticles for its corresponded microwave-induced heat behaviors. For this investigation, all of specimens were irradiated at 750 W (2.45 GHz).

As shown in Fig.5.14, at the same irradiation power 750 W, different microwave absorptive abilities are confirmed by comparing with the related specimens. Meriting from the cooperation between Pt and NCN which have microwave activity in CA, Pt-deposited composites display the better absorbability.

More, it is noted that the increased behaviors of Pt/CPA-CRR and Pt/CPA-MRR-5 min result from the increased loading efficiency, which indicate that both outer and inner surface of CPA was decorated by uniformly dispersed Pt nanoparticles.

Effects of deposition time on absorbability of Pt/CPA-MRR were discussed in Fig.5.14. It is obvious that microwave absorbability of CPA have been further increased by surface modification via microwave irradiation method. And efficiency of Pt/CPA-MRR-5 min is as good as Pt/CPA-MRR-10 min, which implies that Pt nucleation can be finished in 5 min. In order to well understand this phenomenon, it is necessary to discuss the relative factors. As shown in Table 5.2, NCN amount in tested specimens (1 cm^3) is NCN amount in tested specimens is 0.009 mg/mm^3. Then, the increased efficiency is determined by Pt nanoparticles loading efficiency.

$$\text{Absorptive Efficiency} = \frac{\text{Incident power (W)} - \text{Reflective power (W)}}{\text{Incident power (W)} \times a \times b \times c} \times 100 \qquad (1)$$

a, b,c means length (cm), width (cm) and height (cm) of specimens

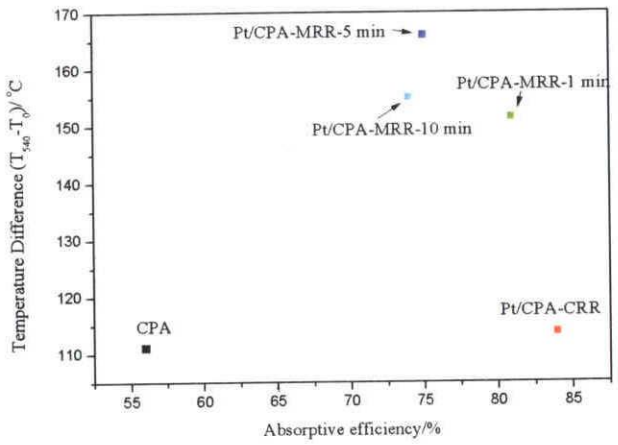

Fig. 5.15. Correction of temperature difference-absorptive efficiency of evaluated samples

Absorptive Efficiency irradiated by microwave at 2.45 GHz with different energies was calculated from equation (1).

It is noticed that Pt nano-particles deposition attributes to the increased absorptive efficiency. Fig.5.15 indicates that the increased absorptive ability is resulted from the higher temperature change at the same irradiation time (540 s) and irradiation power (750 W). By doping with Pt nanoparticles, the enhanced performance of MRR-

assisted composites benefit from the high loading efficiency as confirmed by EDS analysis (Fig. 5.10 and Table 5.1). For this performance, it was reported that carbon nanotubes (CNT) with the same graphene sheet with NCN in CPA is good microwave receptors [31]. Little relationship between length of CNT and microwave-induced heating capacity was available. Meriting from Jouel heating mechanism, impurities result in the good absorbability of CNT than 'perfect' one. In this study, the same principle applies. Pt-induced increased surface defect of 3-dimensional NCN in CPA as confirmed by Fig. 5.4 attributes to the improved performances. The decreased Fermi level of metal/carbon composite leaving intensified phonon profits the monitored heating performances in this study.

5.3.3. Physico-chemical property and electromagnetic wave absorbability of Pt/CNT/CPA-MRR Composite

5.3.3.1. Physico-chemical property of Pt/CNT/CPA-MRR Composite

Pt/CNT/CPA composite was prepared by the same method with Pt/CPA-MRR. The experimental flow-chat has been shown in Fig. 5.1.

In CNT/CPA ternary composite (CNT/NCN/Alumina), alumina grains, NCN and CNT co-exist forming reinforced composite. Benefiting from the thermal stability of CNT in novel atmosphere and NCN with good orientation, microwave activity was improved. As shown in Fig. 5.16, increased surface defects of CNT/CPA comparing with CPA indicate the poorer orientation of carbon. More, by the same preparing technology, Pt-deposited composites show the increased surface defects than substrates (CPA and CNT/CPA). More, higher defects of Pt/CNT/CPA-MRR composites are available than Pt/CPA-MRR composites as shown in Table 5.3. Furthermore, Pt nanoparticles deposition does not attribute to the change of carbon orientation but the increased surface defects meriting from electron-phonon interaction [20-21]. And the optimum depositing condition for CNT/CPA matrix is microwave irradiation 5 min at 300 W.

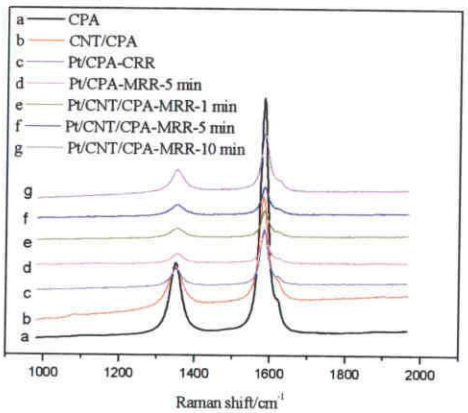

Fig. 5.16. Raman spectroscopy of composites

Table 5.3. Calculated surface defects of composites from Raman spectroscopy

Materials	I_D/I_G	$\Delta\upsilon_{1580\,cm^{-1}}$
CPA	0.48	25
CNT/CPA	0.58	27
Pt/CPA-CRR	0.50	26
Pt/CPA-MRR-5 min	0.57	26
Pt/CNTs/CPA-MRR-1min	0.66	25
Pt/CNTs/CPA-MRR-5min	0.75	25
Pt/CNTs/CPA-MRR-10min	0.65	25

Morphologies of composites have been shown in Fig. 5.17. All of these images are taken from the inner fracture surface of composites. As displayed in Fig. 5.17 (I), even though the middle part of as-fabricated composites was observed, Pt nanoparticles still can be observed, which indicates that total surface of substrates have been modified.

Co-existence style of Pt, carbon and alumina grains in composite can be confirmed by Fig. 5.17 (II). It is understood from these images that Pt nanoaprticles without agglomeration has been deposited onto the substrates. Moreover, Pt nanoparticles grows along the CNT and NCN in composite, which results from the polarization of nano-carbon by microwave irradiation.

Simultaneously, different deposition results at different observation surfaces have been discussed in Fig. 5.18. The utilized sample is Pt/CNT/CPA-MRR-1 min. Identical with Pt/CPA-MRR composite as shown in Fig. 5.7 (a), size of deposited Pt particles on outer surface is bigger than that on inner surface. Moreover, Pt nanoparticles size is also totally different on cutting and fracture surfaces. Taking outer surface for example, Pt nanoparticles around 80 nm and 30 nm is available on outer cutting and fracture surface, respectively. Instead, it is noticed that little nanoparticles is observed on inner cutting surface.

Selectively depositing of Pt nanoaprticles is further understood in Fig. 5.19. This is the SEM outer cutting surface image of Pt/CNT/CPA-MRR-1 min. Then, it is feasible to say that Pt nanoparticles is mainly deposited onto the surface of NCN rather than alumina grains in composite.

As-observed varied Pt nanoparticles size is mainly resulted from temperature difference between outer and inner surface of substrate at the same irradiation condition. High temperature at outer surface accelerates formation of bigger nanoparticles. As shown in Fig. 5.20, at the same irradiation power, CNT/CPA owns better microwave absorptive ability than CPA. And the temperature differences of outer and inner surface for different samples are almost same ($\Delta T_{(t=540s)}$ (CNT/CPA) =19.7 °C, $\Delta T_{(t=540s)}$ (CPA)=16.9 °C). Existence of Pt nanoparticles on substrates can be confirmed by EDS analysis results as shown in Fig. 5.21. The white dots in FE-SEM images are Pt particles.

Furthermore, the depositing efficiency can be roughly confirmed by Pt and carbon mass ratio as shown in Table 5.4. Moreover, the highest surface defects of composites induced by Pt deposition (Fig. 5.16) also confirm the optimum depositing condition is microwave irradiation for 5 min at 300 W. This conclusion equals to Pt/CPA composite.

Generally speaking, based on the analysis of Pt/CPA and Pt/CNT/CPA composites, it is facilitated to reach a conclusion that due to microwave-induced inner and outer surface temperature difference, Pt nanoparticles with different sizes can be deposited onto the substrates. Higher temperature of outer surface accelerates the bigger Pt size, while smaller Pt particles in the inner chamber of substrates are available. This schematic is shown in Fig.5.13.

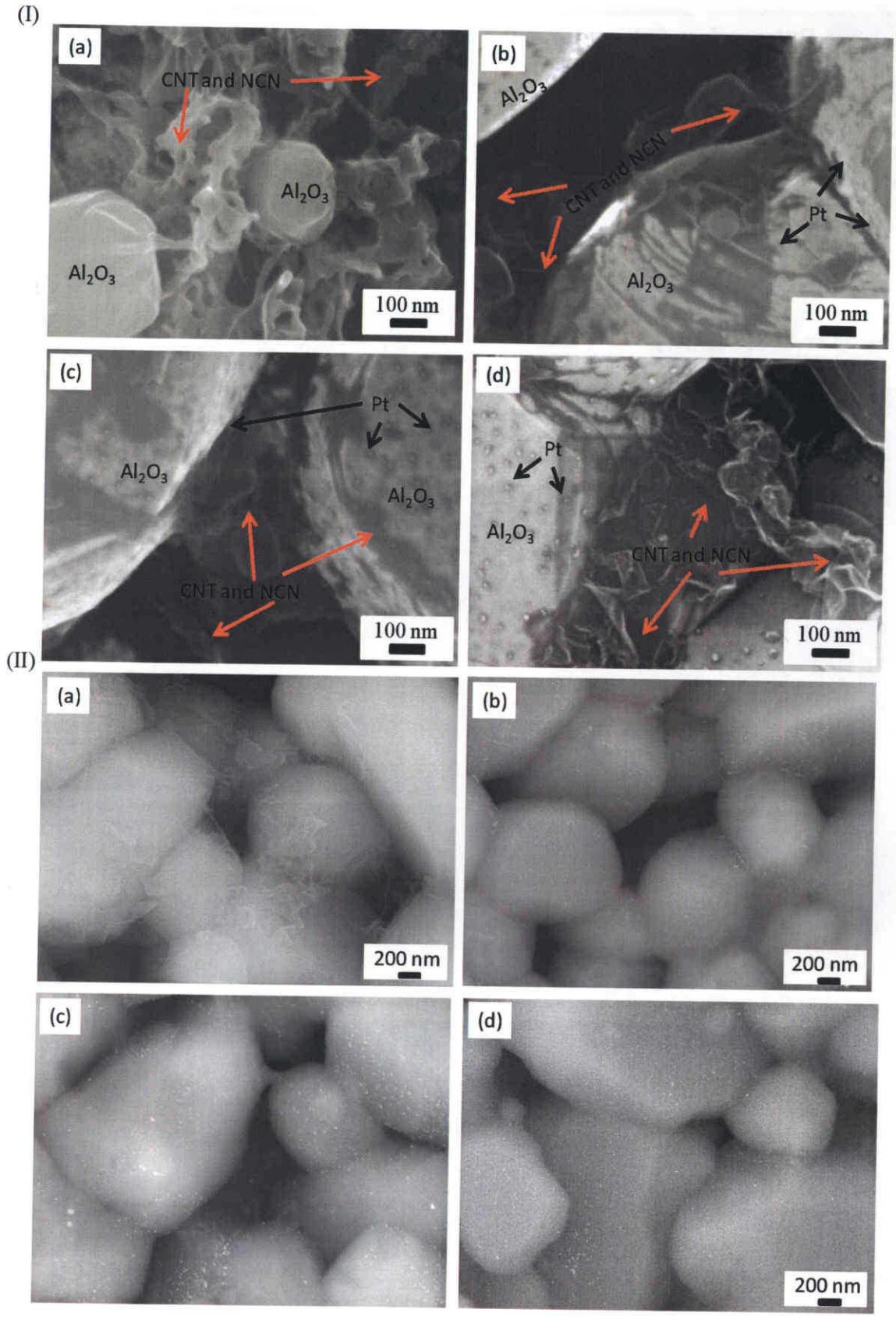

Fig. 5.17. FE-SEM images of composites (I) SEI images (a) CNT/CPA; (b) Pt/CNT/CPA-MRR-1min; (c) Pt/CNT/CPA-MRR-5min and (d) Pt/CNT/CPA-MRR-10min and (II) Compo images (a) CNT/CPA; (b) Pt/CNT/CPA-MRR-1min; (c) Pt/CNT/CPA-MRR-5min and (d) Pt/CNT/CPA-MRR-10min

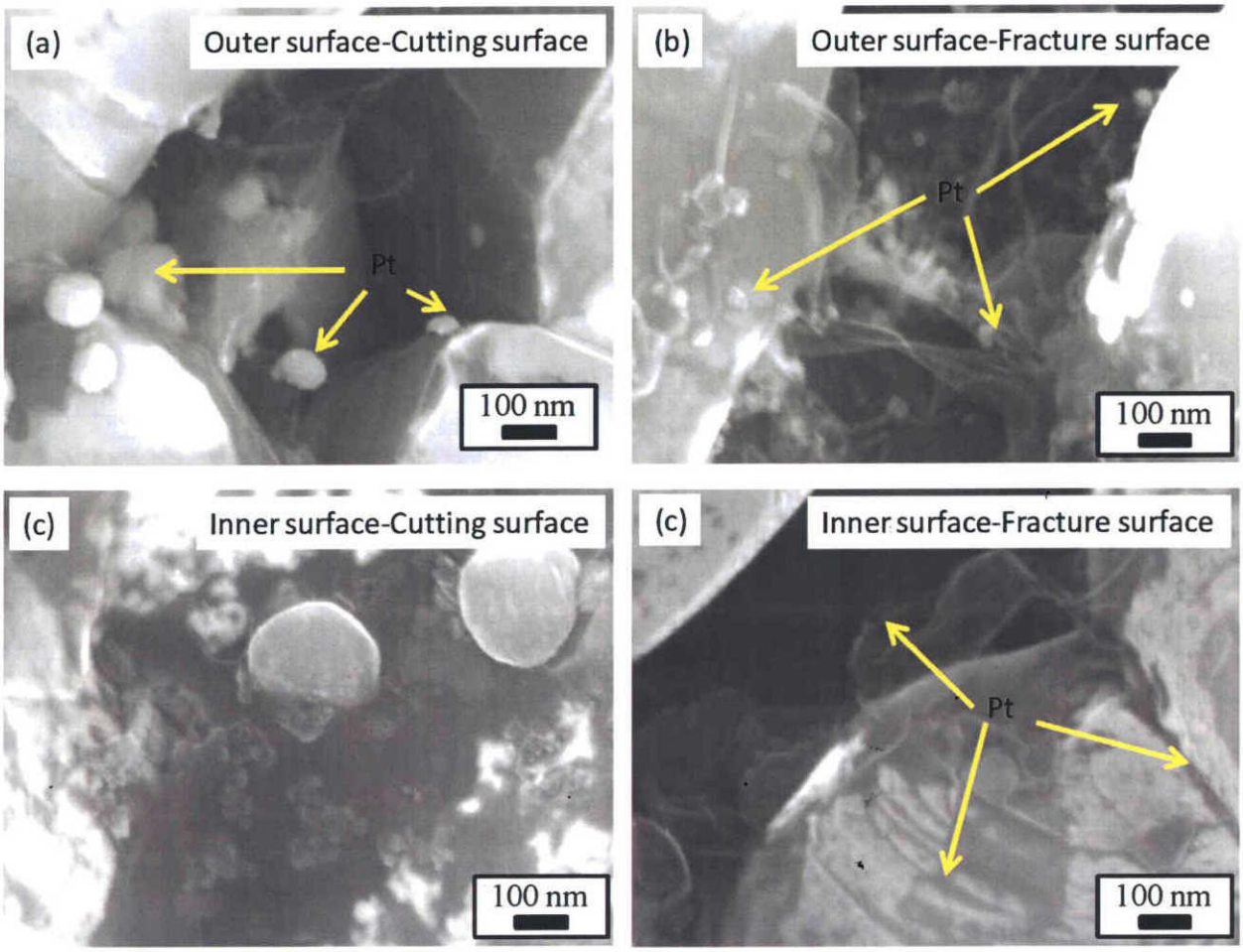

Fig. 5.18. FE-SEM images of Pt/CNT/CPA-MRR-1 min (a) cutting surface of outer surface; (b) fracture surface of outer surface; (c) cutting surface of inner surface and (b) fracture surface of inner surface

Table 5.4. Calculated quality of deposited Pt nanoparticles by EDS analysis results

Materials	C (wt%)	Pt (wt%)	Pt/C
Pt/CPA-MRR-5 min	13.04	2.22	**0.170**
Pt/CNT/CPA-MRR-1 min	39.65	0.61	0.015
Pt/CNT/CPA-MRR -5 min	31.19	3.81	**0.122**
Pt/CNT/CPA-MRR -10 min	44.72	0.4	0.001

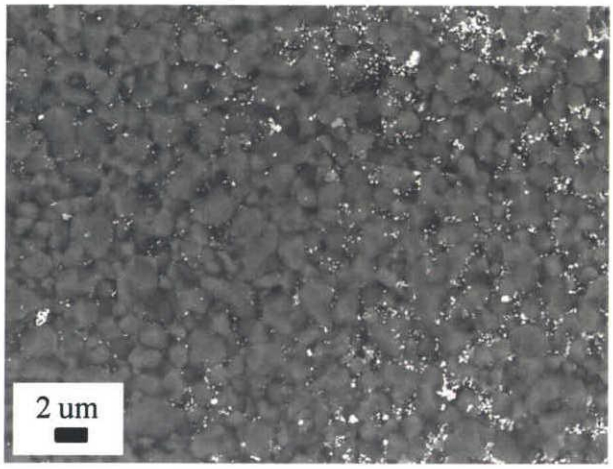

Fig. 5.19. FE-SEM Compo image of Pt/CNT-CPA-MRR-1min

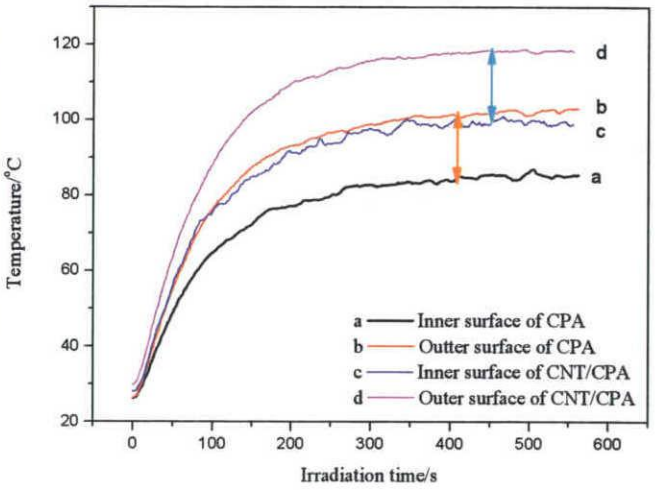

Fig. 5.20. Temperature-irradiation time curves of CPA (a) inner surface and (b) outer surface and CNT/CPA (c) inner surface and (d) outer surface

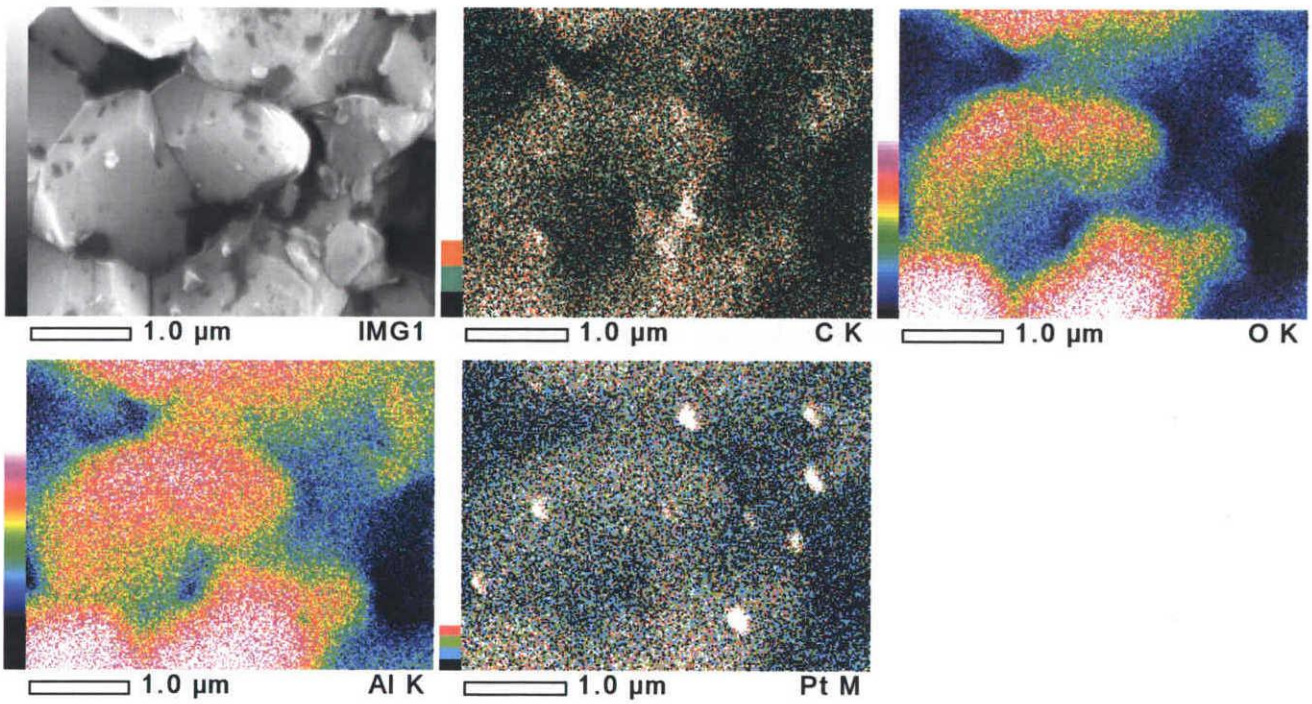

Fig. 5.21. EDS map analysis of Pt/CNT/CPA-MRR-10 min (Outer cutting surface)

5.3.3.2. Electromagnetic wave absorbability of Pt/CNT/CPA-MRR Composite

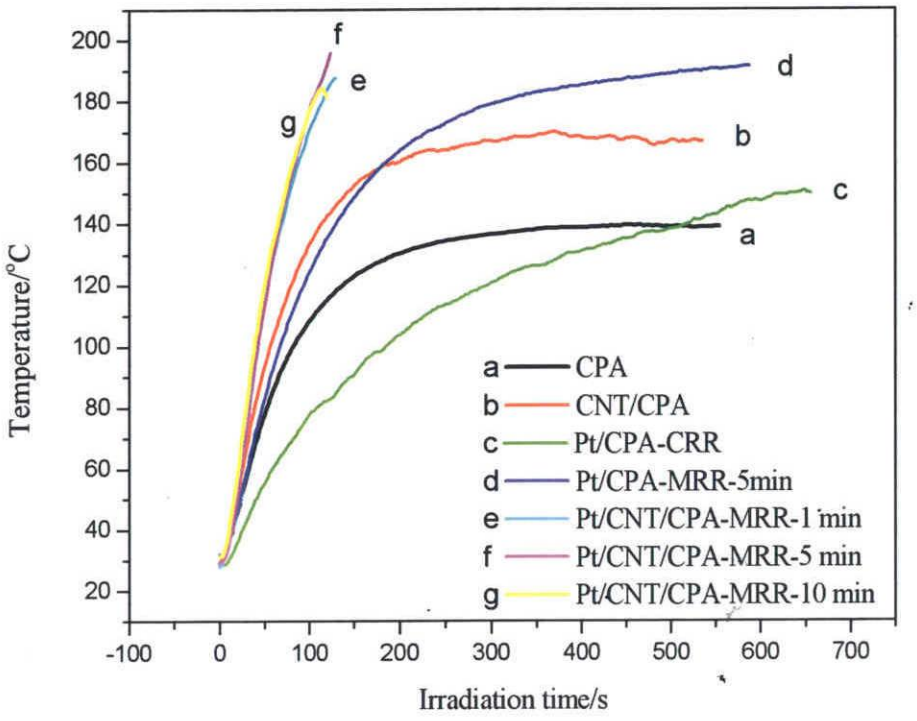

Fig. 5.22. Temperature-irradiation time curves of (a) CPA, (b) CNT/CPA, (c) Pt/CPA-CRR, (d) Pt/CPA-CRR-5 min, (e) Pt/CNT/CPA-MRR-1min, (f) Pt/CNT/CPA-MRR-5 min and (g) Pt/CNT/CPA-MRR-10min irradiating with 750 W at 2.45 GHz

Table 5.5. Physical property of evaluated samples

Materials	Size (mm)	NCN (mg/mm^3)	ΔT (T_{100s}-t_0)/°C	Efficiency (%)
CPA	9.03×9.19×10.19	0.009	79.4	56
CNT/CPA	11.03×8.46×8.06	0.012	103.8	60
Pt/CPA-CRR	9.69×10.48×10.05	0.009	49.2	84
Pt/CPA-MRR-5min	10.73×10.50×10.11	0.009	92.5	81
Pt/CNT/CPA-MRR-1min	10.29×10.85×10.64	0.012	142.4	68
Pt/CNT/CPA-MRR-5min	10.41×10.53×9.83	0.012	147.4	67
Pt/CNT/CPA-MRR-10min	9.04×10.36×10.51	0.012	145.3	65

Fig. 5.22 displays the temperature-irradiation curves of various absorbents available in our study. It is reasonable to say that Pt/CNT/CPA-MRR composites are high effective and efficiency absorbers comparing with others, which is supported by much more increased temperature with the same irradiation condition (750 W at 2.45 GHz). The highest temperature of Pt/CNT/CPA-MRR composites are attributed to the deposited Pt nanoparticles.

Physico-chemical property of evaluated specimen is listed in Table 5.5. Absorbing efficiency was calculated from equation (1).

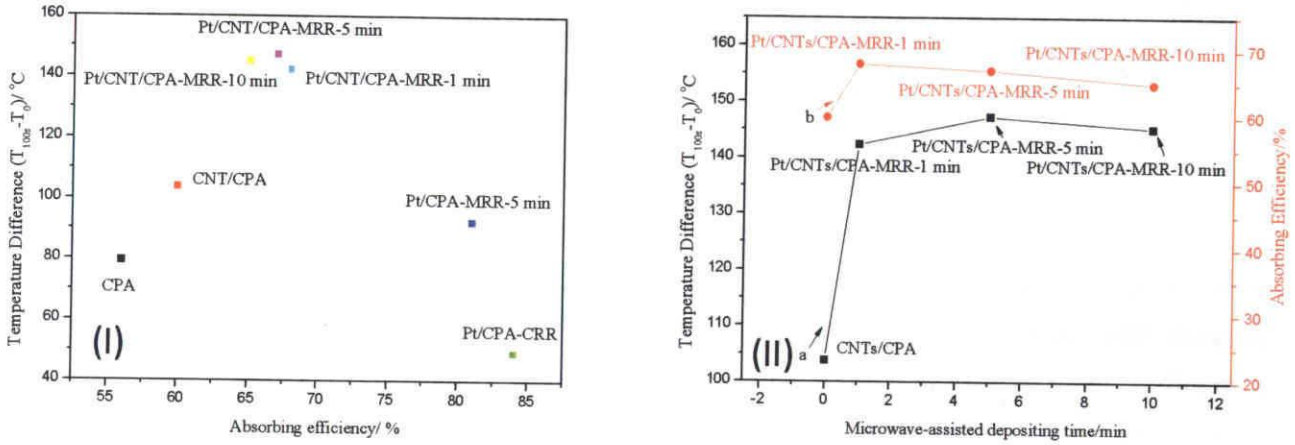

Fig. 5.23. (I) Correction plot of microwave-induced temperature difference (T_{100s}-T_0) and absorbing efficiency of different samples and (II) Correction plot of microwave-induced temperature difference (T_{100s}-T_0) and microwave irradiation time

For microwave absorbents, several factors are involved for absorbing performance:

✧ Absorbing efficiency

All of the composites were irradiated at 2.45 GHz 750W. As shown in Fig. 5.23 (I), comparing with CPA, the increased microwave absorbing efficiency of composites are attributed to either structure (by CNT) or surface modification (by Pt nanoparticles). Even though CNT/CPA composites modified by ultrafine Pt nanoparticles via microwave irradiation don't have the highest absorbing efficiency, the enhanced absorbing performances are available, which was verifieded by increased temperature-irradiation time (t=100 s) curves. This phenomenon is mainly attributed to the co-junction of Pt and CNT. Based on the physico-chemical property of Pt/CNT/CPA-MRR composites and microwave performances evaluation, the optimum absorbent is Pt/CNT/CPA-MRR-5 min.

✧ Microwave-irradiation time for preparing composites

In chapter 4, we have announced that CNT/CPA has the increased absorbability than CPA, which is attributed to tube-like CNT-induced intensified phonon. In this chapter, absorptive behaviors are further increased by surface modification via microwave-assisted irradiation method. As confirmed in Fig. 5.23 (II) curve (a), with the same irradiation time, largely increased temperature differences of composites confirm their activities. More, comparing curve (a) and (b), it is concluded that composites absorbability are related to absorbing efficiency at the same irradiation condition. More, the highest detected temperature of Pt/CNT/CPA-MRR-5 min (Fig. 5.23 (II)) also indicates the optimum experimental condition is 5 min, which is identical with Raman spectroscopy and EDS analysis results.

✧ Surface defects

As confirmed in Fig.5.16 and Table 5.3, Pt nanoparticles deposition on the surface of substrate does not attribute to the change of half width of G band ($\Delta\upsilon_{1580cm}^{-1}$) but surface defects ($R_{ID/IG}$). We have noticed that because of loading Pt nanoparticles on CNT/CPA or CPA, intensified electron-phonon interactions between carbon in matrix and Pt results in the increased defects value. The relationship between surface defects of composites and microwave induced heat performances are shown in Fig. 5.24, by which it is facilitated to get a conclusion that, at the same irradiation condition (2.45 GHz, 750 W), microwave capacity of composites increases with increased surface defects.

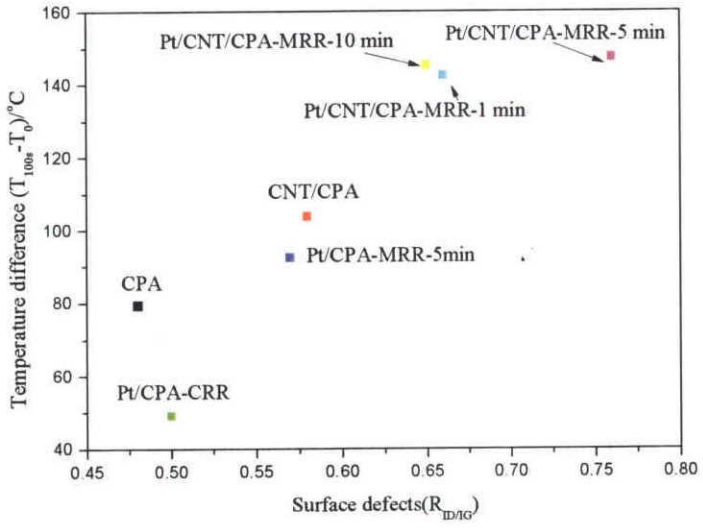

Fig.5.24. Correction plot between microwave-induced temperature difference (T_{100s}-T_0) and surface defects ($R_{ID/IG}$) of composites irradiated at 2.45 GHz 750 W

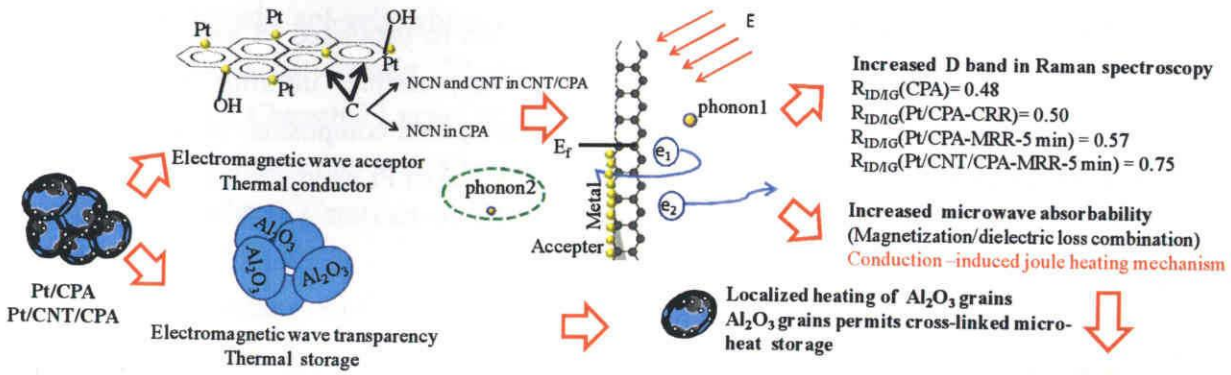

Fig. 5. 25. Mechanism discussion of Pt/CA composites with enhanced electromagnetic wave absorbability

Generally speaking, Pt acting as electron accepter with irradiation leads to the intensified phonon flow in composites. These accumulated phonons attribute to the enhanced microwave capacity [28-31].

According to the above analysis results, it is facilitated to get some conclusions as follows for as-prepared Pt/CA composites (Pt/CPA and Pt/CNT/CPA):

- ✧ Both metallic particles Pt and carbon (NCN in CPA, CNT and NCN in CNT/CPA substrate) are microwave receptors.
- ✧ Electrical and thermal insulator Al_2O_3 grains play as heat storage.
- ✧ Deposition of Pt nanoparticles leads to the decreased E_f (Energy of fermi level) resulting increased phonon at the same irradiation condition.
- ✧ Pt induced enhanced microwave absorbability of carbon is believed to conduction mechanism leading joule heating effect.
- ✧ Pt/C-induced localized joule heating allows Al_2O_3 grains as micro-heaters, which is reasonable to explain the detected outer and inner surface temperature difference at the same radiation condition.

This schematic is proposed in Fig.5.25.

5.4. Conclusions

In this chapter, ultrafine Pt nanoparticles without agglomeration had been selectively deposited onto the surface of two kinds of substrates CPA and CNT/NCN/CPA making Pt/CPA-MRR and Pt/CNT/CPA-MRR multi-element composites. Selective deposition of Pt nanoparticles on substrate was achieved by polarization of graphitic carbon in CA under microwave irradiation. By investigating the influence of depositing time at the constant radiation condition, the optimum precipitate time for both of two substrates was 5 min. The enhanced

microwave absorptive ability of composites were attributed to deposited Pt nanoparticles. The merits of microwave irradiation technique are selectivity, simple, ultrafine and low cost. Moreover, the enhanced microwave absorbability of as-prepared composites were attributed to the decreased Fermi level energy of NCN due to the deposition of Pt nanopartiles.

References

[1]. Jianqiang Wei, Jianbo Wang, Qingfang Liu, Liang Qiao, Tao Wang and Fshen Li, Enhanceed microwave absorption properties of Fe_3Al/Al_2O_3 fine particle composites, *J. Phys. D: Appl. Phys.*, 43, **2010**, 115001/1-115001/5.

[2]. Robert Janes, Kaushai K. Singh, Jane Blunt and Peter P. Edwards, Low-field microwave absorption in mechanical mixes of superconducting $YBa_2Cu_3O_{7-x}$ with Al_2O_3 and $BaPbO_3$, *J. Chem. Soc. Faraday Trans.*, 86(22), **1990**, 3829-3830.

[3]. X.G. Liu, D.Y. Geng, H. Meng, W.B. Cui, F. Yang, D.J. Kang, Z.D. Zhang, Microwave absorption properties of FCC-Co/Al_2O_3 and FCC-Co/Y_2O_3, *Solid State Commun.*, 149, **2009**, 64-67.

[4]. X.G. Liu, D.Y. Geng and Z.D. Zhang, Microwave-absorption properties of FeCo microspheres self-assembled by Al_2O_3-coated FeCo nanocapsules, *Appl. Phys. Lett.*, 92, **2008**, 243110/1-243110/3.

[5]. T. Mazon, M. A. Zaghete, J. A. Varlea, E. Longo, Barium strontium titanate nanocrystalline thin films prepared by soft chemical method, *J. Eur. Ceram. Soc.*, 27, **2007**, 3799-3802.

[6]. Bo Li, Shuren Zhang, Ying Yuan, Xiaohua Zhou, Longcheng Xiang, Dielectric properties and microstructure of TiO_2 modified $(ZnMg)TiO_3$ microwave ceramics with Cao-B_2O_3-SiO_2, *J. Mater. Sci.*, 44 , **2009**, 4993-4998.

[7]. Yindee Suttisawat, Satoshi Horikoshi, Hideki Sakai, Masahiko Abe, Hydrogen production from tetralin over microwave-accelerated Pt-support activated carbon, *Int. J. Hydrogen Energy*, 35, **2010**, 6179-6183.

[8]. Volker Derdau, Jens Atzrodt, Jochen Zimmermann, Carsten Kroll, and Francois Brückner, Hydrogen-Deuterium Exchange Reactions of Aromatic Compounds and Heterocycles by $NaBD_4$-Activated Rhodium, Platinum and Palladium Catalysts, *Chem. Eur. J.*, 15, **2009**, 10397-10404.

[9]. Maria Jose Gracia, Juan Manuel Campelo, Elia Losada, Rafael Luque, Jose Maria Marinas and Antonio Angel Romero, Micro-assisted versatile hydrogenation of carbonyl compounds using supported metal nanoparticles, *Org. Biomol. Chem.*, 7, **2009**, 4821-4824.

[10]. Alina Mariana Balu, JuAN Manuel Campelo, Rafael Luque and Antonio Angel Romero, One-step microwave-assisted asymmetric cyclisation/hydrogenation of citronellal to menthols using supported nanoparticles on mesoporous materials, *Org. Biomol. Chem.*, 8, **2010**, 2845-2849.

[11]. Minghui Yang, Yunhui Yang, Yanli Liu, Guoli Shen, Ruqin Yu, Platinum

nanoparticles-doped sol-gel/carbon nanotubes composites electrochemical sensors and biosensors, *Biosens. Bioelectron.*, 21, **2006**, 1125-1131.

[12]. Wenzhen Li, Changhai Liang, Weijiang Zhou, Jieshan Qiu, Zhenhua Zhou, Gongquan Sun and Qin Xin, Preparation and Characterization of Multiwalled carbon Nanotube-Supprted Platinum for Cathode Catalysts of Direct Methanol Fuel Cell, *J. Phys. Chem. B*, 107, **2003**, 6292-6299.

[13]. Takashi Kyotani, Li-fu Tsai and Akira Tomita, Formation of platinum nanorods and nanoparticles in uniform carbon nanotubes prepared by a template carbonization method, *Chem. Commun.*, **1997**, 701-702.

[14]. Kevin R. Moonoosawmy and Peter Kruse, Ambiguity in the Characterization of Chemically Modified Single-walled Carbon Nanotubes: A Raman and Ultraviolet-Visible-Near-Infrared Study, *J. Phys. Chem. C*, 113, **2009**, 5133-5140.

[15]. Piotr Pieta, Emilia Grodzka, Krzysztof Winkler, Magdalena Warczak, Andrzej Sadkowski, Grazyna Z. Zukowska, Ganesh M. Venukadasula, Francis D'Souza and Wlodzimierz Kutner. Conductive, Capative and Viscoelastic Properties of a new Composite of the C_{60}-Pd Conducting Polymer and Single-wall Carbon Nanotubes, *J. Phys. Chem. B*, 113, **2009**, 6682-6691.

[16]. Vladimir A. Sinani, Muhammed K. Gheith, Alexander A. Yaroslavov, Anna A. Rakhnyanskaya, Kai Sun, Arif A. Mamedov, James P. Wicksted, and Nicholas A. Kotov, Aqueous Dispersions of single-wall and Multi-wall carbon Nanotubes with Designed Amphiphilic Polycations, *J. Am. Chem. Soc.*, 127, **2005**, 3463-3472.

[17]. Ján Tarábek, Laduslav Kavan, Lothar Dunsch and Martin Kalbac, Chemical states of electrochemically doped single wall carbon nanotubes as probed by Raman spectroelectrochemistry and ex situ X-ray photoelectron spectroscopy, *J. Phys. Chem. C*, 112, **2008**, 13856-13861.

[18]. P.W. Ruch, L.J. Hardwick, M. Hahn, A. Foelske, R. Kötz, A.Wokaun, Electrochemical doping of single-walled carbon nanotubes in double layer capacitors studied by in-situ Raman spectroscopy, *Carbon*, 47, **2009**, 38-52.

[19]. Haibin Chu, Jinyong Wang, Lei Ding, Dongning Yuan, Yan Zhang, Jie Liu and Yan Li, Decoration of gold nanoparticles on surface-grown single-walled carbon nanotubes for decoration of every nanotubes by surface-enhanced Raman spectroscopy, *J. Am. Chem. Soc.*, 131, **2009**, 14310-14316.

[20]. C. Thomsen and S. Reich, Double resonant Raman scattering in Graphite, *Phys. Rev. Lett.*, 85(24), **2000**, 5214-5210.

[21]. Jinyong Wang, Rongli Cui, Yu Liu, Weiwei Zhou, Zhong Jin and Yan Li, Abnormal Raman Intensity of Single-Walled carbon nanotubes grown on silica sphere, *J. Phys. Chem. C*, 113, **2009**, 5075-5080.

[22]. Yanhui Xu, Xiangqin Lin, Selectivity attaching Pt-nano-clusters to the open ends and defects sites on carbon nanotubes for electrochemical catalysis, *Electrochim. Acta*, 52, **2007**, 5140-5149.

[23]. Chunxi Hai, Masayaoshi Fuji, Feng Wang, Hideo Watanabe, Takashi Shirai, Ikuko Yamada, Minoru Takahashi, Synthesis and Electrochemical Characterization of Electrically Conductive Porous Alumina Composite Modified By Nickel and Platinum Nanoparticles, *IOP Materials Science and Engineering*, 18, **2011**, 062009/1-062009/4.

[24]. C. Hai, H. Watanabe, T. Shirai, M. Fuji, M. Takahashi and F. Wang, Modifying the surface of the electrically conductive porous alumina, *Mater. Lett.*, 63, **2009**, 1320-1322.

[25]. Paromita Kundu, C. Nethravathi, Parag A. Deshpande, M. Rajamathi, Giridhar Madras and N. Ravishankar, Ultrafast Microwave-Assited Route to Surfactant-free Ultrafine Pt Nanoparticles on Graphene: Synergistic Co-reduction, *Chem. Mater.*, 23, **2011**, 2722-2780.

[26]. Z. Tang, N. A. Kotov, One-Dimensional Assembilies of Nanoparticles: Preparation, Properties, and Promise, *Adv. Mater.*, 17(8), **2005**, 951-962.

[27]. Gregory G. Wildgoose, Craig E. Banks, and Richard G. Compton, Metal Nanoparticles and related Materials Supported on Carbon Nanotubes: Methods and Applications, *Small*, 2(2), **2005**, 182-193.

[28]. R. Loscutova and A.R. Barron, Coating single-walled carbon nanotubes with cadmium chalcogenides, *J. Mater. Chem.*, 15, **2005**, 4346-4353.

[29]. N.M. Rodriguez, P. e. Anderson, A. Wootsch, U. Wild, R. Schl o¨gl, Z. Paál, XPA, EM, and Ctalytic Studies of the Accumulation, *J. Catal.*, 197, **2001**, 365-377.

[30]. J.T. Titantah, D. Lamoen. Sp2/sp3 characterization of carbon materials from first-principles calculations: X-ray photoelectron versus high energy electron energy-loss spectroscopy techniques, *Carbon*, 43, **2005**, 1311-1316.

[31]. Ester Vázquez and Maurizio Prato, Carbon Nanotubes and Microwaves: Interactions, Responses and applications, *ACS Nano*, 3(12), **2009**, 3819-3824.

CHAPTER 6

CONCLUDING REMARKS AND POTENTIAL DIRECTIONS FOR FUTURE RESEARCH

6.1 Concluding Remarks

This thesis successfully developed the electrochemical and microwave activities of electrically conductive alumina (CA). Taking the unique structure of CA into consideration, it was aimed at developing enhanced performances of CA as energy convertor with high effective and efficiency. Due to the 3-dimensional cross-linked NCN with graphitic structure, enhanced electrochemical performances of CA were achieved by suitable surface modification. We also claimed microwave absorbability of CA by investigating the basic physico-chemical properties of CA. Furthermore, microwave-induced heat behavior of CA was enhanced via various modifications. The involved modification methods included structure modification with CNT and surface modification with uniformly dispersed ultrafine Pt nanoparticles. As-received composites were confirmed to be good microwave-absorbents. The summary and conclusions of this thesis study are itemized as the followings.

In chapter 1, merits and limits of energy transfers via various methods (such as electrochemical evaluation (EE) and microwave-assisted heating) as reported so far were demonstrated. It was clarified the necessary and significant of exploring a novel composite with good electrical conductivity, mechanical strength and microwave absorbability in order to meet the difficulty we are facing now. Based on these advantages, disadvantages and features of substrate, aim of this study was formulated.

In chapter 2, meriting from the good isotropic electrical conductivity, electrochemical activity of CA as electrode was reported. It was noticed that ceramic insulation was effectively overcome by nano-carbon networks (NCN). Enhanced performance was completed by pre-treating and functional particles precipitation. Wherein, pre-treating not only allowed introducing various functional groups on NCN as active sites for particles growth, but also made it feasible to selectively surface modification. Pt/CPA was proven to be the highest electro-catalyst toward ORR in alkaline electrolyte. In terms of relative study, merits and disadvantages of CA as cell candidate were concluded.

In chapter 3, CA with two forms: dense/porous (CDA or CPA) were confirmed to be good microwave absorbents. Considering the unique structure of CA (cross-linked Al_2O_3 grains and NCN with graphitic structure), influences of high-temperature reductive sintering (HTRS), porosity and NCN amount on physico-chemical property and microwave absorbability of CA were well discussed. Comparing CDA-1400 °C and CDA-1700 °C with the same carbon amount (0.7 wt%), increased graphitilization degree of NCN in CDA-1700 °C attributed to increased electromagnetic wave absorbability of CA. Improved microwave absorption benefited from

polarization of NCN in CA, by which the microwave transparency of Al_2O_3 was overcome. Increased HTRS temperature also accelerated increased Al_2O_3 grain size. Simultaneously, CPA with high porosity up to 66.23 % was supported to good absorbent. High Porosity results in the existence of tube-like NCN in CPA. Comparing CPA-1700 °C (carbon content is 0.7 wt%) and PA-1700 °C (carbon content is 0.15 wt%), it was confirmed that absorptive performance was little related with carbon content. Briefly, graphitization degree of NCN in CA briefly attributed to the enhanced electromagnetic wave absorptive behaviors. Therefore, passive heating elements (PHEs) performances of CA-1700 °C for non-polar paraffin liquid announce their potential applications as microwave-assisted heating elements.

In chapter 4, electrically conductive porous alumina composite structurally modified with CNT was fabricated. As-received composite was denoted as CNT/CPA (CNT/NCN/Alumina ternary composite). In order to improve the dispersability of CNT in aqueous solution, before making uniformly dispersed CNT/Al_2O_3 slurry, as-received CNT was pre-treated with mixed acids. Treating condition was optimized by discussing temperature and time. Good affinity of Al_2O_3 grains and CNT in ternary composite CNT/CPA (CNT/NCN/Al_2O_3) was confirmed by various characterization methods. Meriting from the co-existence of Al_2O_3, NCN and CNT in composite, increased bending strength of CNT/CPA was available. Furthermore, benefiting from CNT in composite, comparing with CPA, the enhanced microwave absorbability of CNT/CPA was available, which were attributed to co-junction of NCN and CNT in specimen. Effect of CNT amount (Increasing CNT amount), CNT form (comparing with CPA and CB) and CNT graphitilization degree (Comparing with CNT and HGCNT) for varied performances of CNT/CPA were discussed. It was concluded that different filler attributed to the varied Fermi level of composites, which are responsible for the different microwave-induced heat behaviors of as-fabricated composites. Therefore, CNT tube structure, surface defect and good affinity of components attribute to the enhanced behaviors.

In chapter 5, CA-based composites deposited with uniformly dispersed Pt nanoparticles were prepared. Two kinds CA substrates (CPA and CNT/CPA) were employed. Taking graphitic structure of carbon into consideration, Pt/CA composites were prepared via microwave irradiation technique. Polarized carbon in CA via microwave radiation attributed to selective deposition of Pt nanoparticles. In order to optimum the depositing condition at the same irradiation condition, different characterization ways were employed. Even though it was difficult to direct evaluate depositing efficiency by characterization methods resulting from unique structure of substrates, the best depositing condition was selected by evaluating relative coating efficiency via calculating detected Pt and carbon weight ratio by EDS analysis. Eventually, enhanced microwave absorptive abilities of as-resulted composites were attributed to deposited Pt nanoparticles. The mechanism of these results also has been proposed.

Based on above discoveries, it is concluded that novel microwave-assisted high efficiency heater employing CA as substrate was fabricated.

6.2 Potential directions for future research

In this study, several methods have been attempted to investigate the microwave absorptive ability of conductive alumina composites, which merits from nano-carbon networks (NCN) with graphitic structure. By modifying with CNT and Pt nanoparticles, the increased performances were achieved. Further research should be focused on several items as follows:

- *Increasing graphitization degree of carbon in CA.*

It was confirmed that both electrical and microwave absorbability of CA were related with NCN. Then graphitilization degree of carbon in CA should be enhanced by other methods. One of the ways is adding catalyst for graphitic acceleration during HTRS.

- *Microwave-assisted heating investigation of conductive ceramic (CC).*

NCN with graphitic structure in CA announces it's electrochemical and microwave activity. More, these performances are also related with matrix alumina. The future design of this study should focus on employing other ceramic powders such as SiO_2, SiC, ZrO_2, ZnO and TiO_2 etc.

Besides changing ceramic matrix of CPA, for CNT-CPA composite with increased microwave absorptive ability, it should attempt several sizes of Al_2O_3 as matrix.

- *Increasing carbon amount in CA*

It was noticed that main potential applications of CA as described in this study are influenced by carbon amount and structure. More, in this study, we also have claimed that additive carbon nanotubes (CNT) was no contribution to carbon in CA. Then, it is proposed that carbon amount in CA can be increased by adding some polymer having the same structure with polymer networks (PN) in green body.

More, it was concluded that both degreasing and adding various additives attributed to varied Al_2O_3 grain size and carbon orientation. Herein, in order to change the carbon content and orientation in composites, it is necessary to realize this aim via changing Al_2O_3 matrix with different sizes.

- *Dielectric loss of various absorbents*

Although the heat performances of microwave absorbents have been discussed in this study by thoroughly discussing various factors, monitoring the dielectric loss of CA accelerates the further understanding of mechanism.

LIST OF PUBLICATIONS

Publishes in Journals

[1]. **Chunxi Hai**, Hideo Watanabe, Takashi Shirai, Masayoshi Fuji, Minoru Takahashi, Feng Wang, Modifying the surface of the electrically conductive porous alumina, Materials Letters, 63, **2009**, 1320-1322.

[2]. **Chunxi Hai**, Jingjun Liu, Hideo Watanabe, Masayoshi Fuji, Feng Wang and Minoru Takahashi, Surface Activation of Conductive Porous Alumina by Deposition Nickel Particles, J. Am. Ceram. Soc., 92[S1], **2009**, S38-S41

[3]. **Chunxi Hai**, Hideo Watanabe, TakashI Shirai, Masayoshi Fuji, Feng Wang, Jingjun Liu and Minoru Takahashi, Chemical reductive preparation of Ni decorated conductive porous alumina composite and its electro-performance in alkaline solution, Ceramic transactions, 219, **2009**, 249-254.

[4]. **Chunxi Hai**, Masayoshi Fuji, Hideo Watanabe, Feng Wang, Takashi Shirai, Minoru Takahashi, Evaluation of Surfactant-free stabilized vapor grown carbon fibers ζ-potential and Raman spectroscopy, Colloids and Surface A: Physicochemical and Engineering Aspects, 381 (1-3), **2011**, 70-73.

[5]. **Chunxi Hai**, Masayaoshi Fuji, Feng Wang, Hideo Watanabe, Takashi Shirai, Ikuko Yamada, Minoru Takahashi, Synthesis and Electrochemical Characterization

of Electrically Conductive Porous Alumina Composite Modified By Nickel and Platinum Nanoparticles, IOP Conference Series: Materials Science and Engineering, 18, **2011**, 062009/1-062009/4.

[6]. **Chunxi Hai** , Takashi Shirai, Masayoshi Fuji and Feng Wang, Selectively depositing Pt nanoparticles on pre-treated electrically conductive porous alumina and its electrochemical studies, Ceramic international, **2012**, 38, 3149-3153.

[7]. **Chunxi Hai,** Takashi Shirai, Masayoshi Fuji and Chika Takai, Microwave-induced heat performance of conductive alumina with in situ nano-carbon networks, Applied Energy, **2012,** under review.

[8]. **Chunxi Hai**, Takashi Shirai, Masayoshi Fuji, and Feng Wang, Fabrication of High Porosity Composite nano-carbon networks/alumina (NCN/alumina) reinforced with carbon nanotubes (CNT), Microporous and mesoporous materials, **2012**, under review.

[9]. **Chunxi Hai**, Takashi Shirai, Masayoshi Fuji, Microwave-assisted one-pot in situ surface modification of electrical conductive porous alumina cubic with ultrafine Pt nano particles and heat performance studies, Journal of Materials Chemistry, **2012**, Under review.

Presentations in conferences

International conferences

1). **Chunxi Hai**, Jingjun Liu, Hideo Watanabe, Masayoshi Fuji, Feng Wang and Minoru Takahashi, Surface activation of conductive porous alumina by depositing Nickel particles, 10th International Conference on Ceramic Processing Science (ICCPS-10), May. 2008, Inuyama, Japan. **Oral**.

2). **Chunxi Hai**, Hideo Watanabe, Masayoshi Fuji, Feng Wang, Jingjun Liu, Minoru Takahashi, Fabrication of Pt-deposited Conductive porous alumina by using Electroless method, The 3th international symposium on integrated Molecular/Materials Engineering (ISIMME-3), Nov. 6th-8th , 2008, Xi'an, China. **Oral**.

3). **Chunxi Hai**, Hideo Watanabe, Takashi Shirai, Masayoshi Fuji, Feng Wang, Jingjun Liu, Minoru Takahashi, Decorating Conductive Porous Alumina with Pt nanoparticles, The 9th International Symposium on Ceramic Materials and Components For Energy and Environmental Applications (CMCEE-9), Nov. 10th-14th, 2008, Shanghai, China. **Oral**.

4). **Chunxi Hai**, Hideo Watanabe, Takashi Shirai, Masayoshi Fuji, Feng Wang, Jingjun Liu and Minoru Takahashi, Chemical Reductive preparation of Ni

decorated conductive porous alumina composite and its electro-performance in alkaline solution, The third International Conference on the Characterization and control of interfaces for high quality Advanced Materials, and Joining Technology for New Metallic Glasses and Inorganic Materials (ICCCI-2009), Sep. 6^{th}-9^{th}, Kurashiki, Japan. **Oral**.

5). **Chunxi Hai**, Hideo Watanabe, Masayoshi Fuji, Takashi Shirai, Feng Wang, Minoru Takahashi, A novel composite of conductive porous alumina and Pt nanoparticles with a highly-dispersed deposition, The 4^{th} international symposium on integrated Molecular/Materials Engineering (ISIMME-4), Oct. 25^{th}-29^{th} , 2009, Chengdu, China. **Poster**.

6). **Chunxi Hai**, Hideo Watanabe, Takashi Shirai, Ikuko Yamada, Masayoshi Fuji, Feng Wang and Minoru Takahashi, Effects of MWCNTs on graphitic/alumina Nano-composite fabricated by gel-casting technology, The 5^{th} international symposium on integrated Molecular/Materials Engineering (ISIMME-5), Sep. 19^{th}-22^{th} , 2010, Changzhou, China. **Oral**.

7). **Chunxi Hai**, Masayoshi Fuji, Feng Wang, Hideo Watanabe, Takashi Shirai, Yamada Ikuko, Minoru Takahashi, Synthesis and Electrochemical Characterization of Electrically conductive porous alumina Composite Modified by Nickel and Platinum Nanoparticles, The 3^{rd} International Congress on Ceramics (ICC-3),

Nov.14th-18th, Osaka, Japan. **Oral**.

8). **Chunxi Hai**, Hideo Watanabe, Takashi Shirai, Masayoshi Fuji and Minoru Takahashi, Fabrication of electrically conductive porous alumina reinforced with uniformly dispersed CNTs, The 6th international symposium on integrated Molecular/Materials Engineering (ISIMME-6), Jun. 6th-9th , 2011, Beijing, China. **Oral**.

9). Synthesis of electrically conductive porous alumina based composites by decoration with uniformly dispersed Ni and Pt nanoparticles, **Chunxi Hai**, Takashi Shirai, Masayoshi Fuji, Feng Wang and Minoru Takahashi, The 9th International Meeting of Pacific Rim Ceramic Societies (PacRim 9), Jul. 10th-14th, 2011, Cairns, Queensland Australia. **Oral**.

10). **Chunxi Hai**, Masayoshi Fuji, Takashi Shirai and Chika Takai, Property and application of conductive porous alumina prepared by the combination of gelcasting and reductive sintering, The 13th International Symposium on Eco-materials processing and Design (ISEPD 2012), Jan. 7th-10th,2012, Guilin, China. **Oral**.

Domestic conference

1). **Chunxi Hai**, Hideo Watnabe, Masayoshi Fuji, Minoru Takahashi, Preparation of Ni-deposited conductive porous alumina electrocatalyst for methanoloxidation, **東海若手セラミスト懇話会**, 2008 年 7 月, **岐阜**. **Oral.**

2). **Chunxi Hai**, Hideo Watanabe, Takashi Shirai, Masayoshi Fuji, Minoru Takahashi, Feng Wang, Functionalization of Electrical Conductive porous Alumina, The 46th symposium on powder Science and Technology (**第 46 回 粉体に関する討論会**), Dec. 2nd-4th, 2008, Nara, Japan. **Oral**.

3). **Chunxi Hai**, Hideo Watanabe, Takashi Shirai, Masayoshi Fuji, Feng Wang, Minoru Takahashi, Aqueous dispersions of multi-wall carbon nanotubes with surface modification, The 48th symposium on powder Science and Technology (**第 48 回 粉体に関する討論会**), Oct. 20th-22th, 2010, Japan. **Oral.**

4). **Chunxi Hai**, Takashi Shirai, Masayoshi Fuji, Hideo Watanabe, Feng Wang and Minoru Takahashi, Investigation of the electrochemical properties of electrically conductive porous alumina (CPA), **第４６回技術討論会**, Jun. 14th-15th, 2011, Kyoto, Japan. **Oral**.

5). Chunxi Hai, Takashi Shirai, Masayoshi Fuji, Feng Wang, Minoru Takahashi, Insight on the effects of multi-walled carbon nanotubes in electrically conductive porous alumina, **第 42 回東海若手セラミスト懇話 2011 年夏期セミナー**,

Jun.30th -Jul. 1st , 2011, Japan, **Poster**.

6). Chunxi Hai, Takashi Shirai, Masayoshi Fuji, Feng Wang, Minoru Taskahashi, Insight into the electrochemical property of electrically conductive porous alumina with surface modification, 24th Fall Meeting of the ceramic Society of Japan (第 24 回秋季シンポジウム), Sep. 7th-9th, Hokkaido, Japan. **Oral**.

7). **Chunxi Hai**, Masayoshi Fuji, Feng Wang, Hideo Watanabe, Takashi Shirai, Ikuko Yamada, Minoru Takahashi, Synthesis and Electrochemical Characterization of Electrically conductive porous alumina Composite Modified by Nickel and Platinum nanoparticles, 日本学術振興会、先進セラミックス第 124 委員会第 137 回、11 月 25 日. 2011. 東京. 日本. **Oral**.

8). **Chunxi Hai**, Takashi Shirai, Masayoshi Fuji, Selective modification of porous nano-carbon network/Alumina (NCN/Al_2O_3) composite by ultrafine Pt nanoparticles, 21st MRS-J Academic Symposium, Dec. 19th-21th, 2011, Yokohama, Japan. **Oral**.

9). **Chunxi Hai**, Takashi Shirai, Masayoshi Fuji, Surface modification of electrical conductive porous alumina with uniformly dispersed Pt nanoparticles, Annual Meeting of the Ceramic Society of Japan, Mar. 19th -21th, 2012, Kyoto, Japan. **Oral**.

Research Foundation

[1]. Oct. 2009-Sep. 2012, Financial supported by Ministry of Education, Culture, Sports, Science and Technology (MEXT), Project "Cooperation for Innovative Technology and Advanced Research in Evolution Area"

[2]. April, 2011, Finical support from the Hori Science and Arts Foundation (公益財団法人堀科学芸術振興財団　**研究者育成のための助成金**)

Awards

[1]. July, 2011 Best presenter in 42th the association of Tokai Yong Ceramists (第42回**東海若手セラミスト懇話** 2011 **年夏期セミナー**)

[2]. 2011、**名古屋工業大学基金学生研究奨励金**

[3]. Nov., 2011, Presented an outstanding work (Work Scientist) in 21st Symposium of Materials Research Society of Japan

ACKNOWLEDGEMENTS

This study focused on various initial attempts of potential applications of novel composite electrically conductive alumina via different methods. However, I am afraid I cannot reach the peak of success without guidance, help, support and efforts of many people.

Firstly, I would like to express my appreciation to my supervisor Prof. Masayoshi Fuji. During my study in Japan, I always think that it would be impossible to smoothly finish my dissertation without the expert guidance, significant discussions and constructive suggestions from Prof. Masayoshi Fuji. He always pointed out the key to my study and gives valuable insights. I admire him not only for his profound knowledge, but also for his work attitude. I would also like to thank Prof. Masayoshi Fuji for his kindness and moral help besides study during my stay in Japan.

I would also like to express my deepest gratitude and sincere thank to Prof. Feng Wang, who is a professor in Beijing University of chemical Technology (BUCT). Without the help of Prof. Masayoshi Fuji and Prof. Feng Wang, I am worried I would not have this precious chance of study in Japan, which not only highlights my education background, but also permits much more chance for my

perspective future. During my study from Master to Doctor Courses, besides the professional guidance, he also taught me how to construct a positive attitude to study, life and difficulty.

I would like to express my great thank to Prof. Minoru Takahashi, president of Nagoya Institute of Technology, for his attention and help during my study in Japan.

I wish to thank Dr. Takashi Shirai and Dr. Hideo Watanabe for their good suggestions and warm-hearted supports for my study.

I am grateful to all of my dear lab mates in Japan. Dr. Tomoaki Kato, Dr. Chika Takai and Mr. Seiji Yamashita are so warm-hearted that I am always touched by their unselfish support. I am very impressed by every Japanese student who is so active, hardworking and positive in study. The same thanks are also extended to Mr. Jin Li and Mr. Wanghui Chen for their kindness and favor.

I am very much grateful to my parents Shixiong Hai and Yingwa Wei and younger sister Jing Hai for their love and patience during my study in Japan. At the accompany of their love and wish, I can finish my study in Japan.

Finally, I would like to thank everybody again and wish we can have more perspective future.

Chunxi Hai